TRANSPORTATION RESEARCH RECORD **1089**

Geotechnical Engineering

TRB
TRANSPORTATION RESEARCH BOARD
NATIONAL RESEARCH COUNCIL
WASHINGTON, D.C. 1986

Transportation Research Record 1089
Price $19.80
Editor: Naomi Kassabian
Compositor: Lucinda Reeder
Layout: Betty L. Hawkins

modes
1 highway transportation
3 rail transportation
4 air transportation

subject areas
24 pavement design and performance
61 soil exploration and classification
62 soil foundations
63 soil and rock mechanics
64 soil science

Transportation Research Board publications are available by ordering directly from TRB. They may also be obtained on a regular basis through organizational or individual affiliation with TRB; affiliates or library subscribers are eligible for substantial discounts. For further information, write to the Transportation Research Board, National Research Council, 2101 Constitution Avenue, N.W., Washington, D.C. 20418.

Printed in the United States of America

Library of Congress Cataloging-in-Publication Data
National Research Council. Transportation Research Board.

Geotechnical engineering.

(Transportation research record, ISSN 0361–1981 ; 1089)
1. Soil mechanics–Congresses. 2. Rock mechanics–Congresses. 3. Road construction–Congresses.
I. National Research Council (U.S.). Transportation Research Board. II. Series.
TE7.H5 no. 1089 380.5 s 87–5694
[TA710.A1] [624.1'51]
ISBN 0–309–04109–0

Sponsorship of Transportation Research Record 1089

GROUP 2—DESIGN AND CONSTRUCTION OF TRANSPORTATION FACILITIES
David S. Gedney, Harland Bartholomew & Associates, chairman

Pavement Management Section
R. G. Hicks, Oregon State University, chairman

Committee on Flexible Pavements
Joe P. Mahoney, University of Washington, chairman
James A. Sherwood, Federal Highway Administration, secretary
Chris A. Bell, James L. Brown, Stephen F. Brown, R. N. Doty, David C. Esch, C. R. Freeme, Wade L. Gramling, Douglas I. Hanson, Newton C. Jackson, W. N. Lofroos, Carl L. Monismith, Leon M. Noel, Adrian Pelzner, William A. Phang, John L. Rice, James A. Scherocman, James F. Shook, Herbert F. Southgate, Marshall R. Thompson, Harry H. Ulery, Jr., Cecil J. van Til, Loren M. Womack

Stabilization Section
Donald G. Fohs, Federal Highway Administration, chairman

Committee on Lime and Lime-Fly Ash Stabilization
Raymond K. Moore, University of Kansas, chairman
Alvin H. Meyer, University of Texas-Austin, secretary
Mehmet C. Anday, John J. Emery, James H. Gumn, Kenneth A. Gutschick, C. W. Heckathorn, Thomas W. Kennedy, Harold W. Landrum, Dallas N. Little, Eugene B. McDonald, W. C. Ormsby, Thomas M. Petry, Marshall R. Thompson, Mumtaz A. Usmen, Paul J. Wright

Committee on Soil-Portland Cement Stabilization
Wayne S. Adaska, Portland Cement Association, chairman
Ara Arman, K. P. George, William O. Hadley, J. M. Hoover, Lynne H. Irwin, Robert W. Israel, Thomas W. Kennedy, Joakim G. Laguros, Dallas N. Little, James L. Melancon, Raymond K. Moore, George A. Munfakh, Robert G. Packard, Lutfi Raad, Sam I. Thornton, Daniel R. Turner, Mumtaz A. Usmen, W. Wilk, Anwar E. Z. Wissa, David C. Wyant

Geology and Properties of Earth Materials Section
Wilbur M. Haas, Michigan Technological University, chairman

Committee on Exploration and Classification of Earth Materials
J. Allan Tice, Law Engineering Testing Company, chairman
Robert K. Barrett, P. J. Beaven, John A. Bischoff, Martin C. Everitt, H. Allen Gruen, Robert K. H. Ho, Robert B. Johnson, Jeffrey R. Keaton, C. William Lovell, B. Sen Mathur, Donald E. McCormack, Jim McKean, Olin W. Mintzer, R. L. Nanda, Zvi Ofer, Harold T. Rib, Lawrence C. Rude, Surendra K. Saxena, James Chris Schwarzhoff, Berke L. Thompson, Sam I. Thornton, A. Keith Turner, Gilbert Wilson, Duncan C. Wyllie

Committee on Soil and Rock Properties
C. William Lovell, Purdue University, chairman
Robert C. Bachus, S. S. Bandyopadhyay, Robert K. Barrett, Roy H. Borden, Carl D. Ealy, William H. Highter, Robert D. Holtz, Robert B. Johnson, Ernest Jonas, Gerald P. Raymond, Surendra K. Saxena, James J. Schnabel, J. Allan Tice, Mehmet T. Tumay, John L. Walkinshaw, Gary C. Whited

Committee on Physicochemical Phenomena in Soils
Thomas F. Zimmie, Rensselaer Polytech Institute, chairman
Larry Canter, John B. Haegler, Jr., Richard H. Howe, Don H. Jones, Joakim G. Laguros, C. William Lovell, Milton W. Meyer, Thomas M. Petry, Marion R. Scalf, Mumtaz A. Usmen, Anwar E. Z. Wissa

Committee on Frost Action
David C. Esch, Alaska Department of Transportation and Public Facilities, chairman
Stephen A. Cannistra, Barry J. Dempsey, Paul J. Diethelm, Albert F. Dimillio, Wilbur M. Haas, James W. Hill, Gary L. Hoffman, William P. Hofmann, Newton C. Jackson, Thaddeus C. Johnson, Ronald H. Jones, Hiroshi, Kubo, C. William Lovell, George W. McAlpin, Richard W. McGaw, Edwin C. Novak, Jr., Arvind Phukan, Stuart C. Tapp, Hisao Tomita, Ted S. Vinson, Donald M. Walker, Gary C. Whited, Chen Xiaobai

Committee on Engineering Geology
A. Keith Turner, Colorado School of Mines, chairman
Robert K. Barrett, William D. Bingham, Robert C. Deen, Jerome V. DeGraff, Martin C. Everitt, Jeffrey R. Keaton, C. William Lovell, Stephen F. Obermeier, Peter V. Patterson, Rodney W. Prellwitz, Berke L. Thompson, J. Allan Tice, Duncan C. Wyllie

Committee on Environmental Factors Except Frost
Malcolm L. Steinberg, Texas State Department of Highways & Public Transportation, chairman
S. S. Bandyopadhyay, Samuel H. Carpenter, Barry J. Dempsey, Donald G. Fohs, K. P. George, George R. Glenn, Richard L. Guthrie, Wilbur M. Haas, Donald J. Janssen, Badru M. Kiggundu, C. William Lovell, Robert L. Lytton, Said Ossama Mazen, R. Gordon McKeen, C. Robert McQuary, Gene R. Morris, James B. Nevels, Jr., Zvi Ofer, Albert C. Ruckman, Joe P. Sheffield, Shiraz D. Tayabji, T. Paul Teng, John L. Walkinshaw, William G. Weber, Jr.,Gdalyah Wiseman

Neil F. Hawks and George W. Ring III, Transportation Research Board staff

Sponsorship is indicated by a footnote at the end of each paper.
The organizational units, officers, and members are as of December 31, 1985.

Transportation Research Record 1089

The **Transportation Research Record** series consists of collections of papers on a given subject. Most of the papers in a Transportation Research Record were originally prepared for presentation at a TRB Annual Meeting. All papers (both Annual Meeting papers and those submitted solely for publication) have been reviewed and accepted for publication by TRB's peer review process according to procedures approved by a Report Review Committee consisting of members of the National Academy of Sciences, the National Academy of Engineering, and the Institute of Medicine.

The views expressed in these papers are those of the authors and do not necessarily reflect those of the sponsoring committee, the Transportation Research Board, the National Research Council, or the sponsors of TRB activities.

Transportation Research Records are issued irregularly; approximately 50 are released each year. Each is classified according to the modes and subject areas dealt with in the individual papers it contains. TRB publications are available on direct order from TRB, or they may be obtained on a regular basis through organizational or individual affiliation with TRB. Affiliates or library subscribers are eligible for substantial discounts. For further information, write to the Transportation Research Board, National Research Council, 2101 Constitution Avenue, N.W., Washington, D.C. 20418.

Contents

Compressibility of Compacted Fills Evaluated by the Dilatometer

ROY H. BORDEN, RAYMOND E. SALIBA, AND WESLEY M. LOWDER

The objective of this study was to investigate the relationship between the dilatometer modulus (E_D) and the constrained modulus (M) for compacted soils. An experimental program was designed using three natural soils encountered in North Carolina compacted at optimum moisture content. For the compacted soils studied, it was found that current methods for interpreting dilatometer data to predict compressibility, as determined from one-dimensional compression tests, significantly overestimated the values that were measured. On the basis of the combination of laboratory and field tests conducted, it would appear reasonable to accept the dilatometer modulus as an upper bound to the anticipated in situ constrained modulus, with the realization that values may actually be in the range of 50 to 80 percent of that value, depending on soil type.

The tangent drained constrained modulus (M) provides a localized one-dimensional modulus for a particular stress level. This modulus is defined as the slope of the linear stress-strain curve obtained from a conventional consolidation test. Marchetti (*1*) related the constrained tangent modulus to the dilatometer modulus by the equation $R_M = M/E_D$. This assumes isotropic, linear-elastic behavior and is a function of the drainage conditions under which the dilatometer modulus is determined. Equations for R_M in terms of the drained Poisson's ratio ($\bar{\mu}$) for both the drained and undrained cases are developed from the relationship of M to $\bar{\mu}$ and the drained Young's modulus ($\bar{E}$). If E_D is determined in a drained environment,

$$R_M = (1 - \bar{\mu})^2/(1 - 2\bar{\mu}) \quad (1)$$

If E_D is determined in an undrained environment,

$$R_M = (1 - \bar{\mu})/2(1 - 2\bar{\mu}) \quad (2)$$

Marchetti realized that both the in situ soil modulus and the dilatometer modulus are affected by the penetration of the blade. He therefore examined lateral earth pressure values (K_D) measured by the dilatometer. On the basis of the results of his analysis, Marchetti developed the following equations:

$$M = R_M E_D \quad (3)$$

$$R_M = 0.14 + 2.36 \log KD \quad \text{if } I_D < 0.6 \quad (4)$$

$$R_M = R_{M,o} + (2.5 - R_{M,o}) \log K_D \quad \text{if } 0.6 < I_D < 3.0 \quad (5)$$

with $R_{M,o} = 0.14 + 0.15\ (I_D - 0.6)$.

$$R_M = 0.50 + 2.00 \log K_D \quad \text{if } I_D > 3.0 \quad (6)$$

$$R_M = 0.32 + 2.18 \log K_D \quad \text{if } K_D > 10 \quad (7)$$

where the material index (I_D) is a function of soil type (the lower values are associated with clays and the higher—those above 3—with sands and other stiff soils). In all cases the value of $R_M > 0.85$.

Although Marchetti's data show significant scatter, Schmertmann (*2*) has indicated good agreement between M-values from the dilatometer and odometer tests.

For a more thorough discussion of these and other engineering parameters predicted by the dilatometer, the reader is referred the following sources: Marchetti (*1;3*, pp. 255–259), Bullock (*4*), and Schmertmann (*2*).

OPERATION OF THE DILATOMETER

The flat dilatometer, developed by Silvano Marchetti (*3*), is essentially a penetration device capable of obtaining an estimate of lateral soil stiffness. The dilatometer, shown in Figure 1, uses a thin, circular, flexible membrane mounted on the side of the blade to arrive at an estimate of the lateral stiffness of the soil. The body of the dilatometer has a width of approximately 3.7 in. (95 mm) and a thickness of approximately 0.6 in. (14 mm). When at rest, the external surface of the approximately 2.4-in. (60-mm) diameter membrane is flush with the surround-

FIGURE 1 Dilatometer and control unit.

R.H. Borden, Department of Civil Engineering, North Carolina State University, Raleigh, N.C. 27695-7908. R.E. Saliba and W.M. Lowder, Soil and Material Engineers, Inc., 9800-D Southern Pine Boulevard, P.O. Box 7668, Charlotte, N.C. 28217.

ing flat surface of the blade. The blade is either pushed or driven into the ground and when located at the desired test depth, the membrane is inflated by means of pressurized gas through a small control unit at the ground surface. Readings are taken of the A pressure required to just move the membrane (related to the lateral stresses existing in the ground) and of the B pressure required to move its center an additional approximate 0.04 in. (1 mm) into the soil (related to soil stiffness). The movements of the membrane are measured by extensometers behind the diaphragm within the body of the device. The movements activate a signal in the control unit that tells the operator to record the pressure when the membrane just moves away from the surface of the blade (the A reading) and again when the membrane has moved approximately 0.04 in. into the soil (the B reading).

In the usual test procedure, the dilatometer is pushed into the ground and the force required for penetration is measured and recorded. At predetermined intervals (usually about 8 in.) the penetration is stopped and the membrane is inflated. Once the second pressure reading (the B reading) has been taken and the pressure behind the membrane is vented, the blade is advanced to the next depth and the test repeated.

Dilatometer Modulus (E_D)

The first pressure reading actually corresponds to an approximate 0.002-in. (0.05-mm) displacement of the membrane and must therefore be extrapolated back to a zero membrane displacement. Also, the pressure readings must be corrected to account for the stiffness of the membrane. The following equations enable both of these corrections to be made on the A and B readings:

$$p_0 = 1.05\ (A - Zm - \Delta A) - 0.05\ (B - Zm - \Delta B) \quad (8)$$

$$p_1 = B - Zm - \Delta B \quad (9)$$

where

A = first dilatometer reading,
B = second dilatometer reading,
ΔA = free air correction to A,
ΔB = free air correction to B,
Zm = correction for a nonzero initial gauge reading,
p_0 = corrected first reading, and
p_1 = corrected second reading.

The difference between the two dilatometer readings may be used to obtain a modulus of elasticity. On the basis of penetration of a circularly loaded area into an elastic half-space, Marchetti *(1)* proposed that the lateral soil modulus be represented by the following expression:

$$E/(1 - \mu^2) = (2\Delta pD)/(\pi s_0) \quad (10)$$

where

s_0 = approximate 0.04-in. deflection of the center of the membrane,
Δp = difference in the corrected A and B readings,
D = 2.4-in. (60-mm) membrane diameter,
E = Young's modulus, and
μ = Poisson's ratio of the soil.

The expression $E/(1 - \mu^2)$ is then termed the dilatometer modulus, E_D.

Material Index (I_D)

The material index (I_D) is a unitless parameter that is the ratio of the difference in corrected pressure readings to a rough equivalent of the effective confining stress. It is defined by the following equation:

$$I_D = (p_1 - p_0)/(p_0 - u_0) \quad (11)$$

where u_0 is the pore-water pressure before the insertion of the blade.

Marchetti *(1)* noted that the material index was a function of grain size and soil permeability. Basically, sandy soils yield a high value of material index because as the membrane expands, drainage can occur and the increased resistance of the soil is measured by the dilatometer. Saturated clayey soils, on the other hand, do not allow for drainage or volume change. Their material index is lower because no increase in soil stiffness is detected. Empirical correlations have been developed that provide an estimate of soil type based on material index values. When plotted versus the dilatometer modulus, the material index values can also be used to predict soil densities.

Horizontal Stress Index (K_D)

The horizontal stress index is defined as

$$K_D = (p_0 - \mu_0)/\bar{\sigma}_v \quad (12)$$

where p_0 and u_0 are as previously defined in Equation 11 and $\bar{\sigma}_v$ is the vertical effective stress at the depth at which the dilatometer test is conducted.

It is at this point that a problem arises when one tries to apply these relationships to partially saturated soils. As it is not generally convenient to measure the magnitude of the negative pore pressures in the soil, it is not possible to define exactly the effective stress state. However, if the compressibility characteristics of the partially saturated sample are determined in the one-dimensional compression test, one may expect to be able to develop the relationship between M and E_D based on total stresses. This problem will be discussed later in more detail in conjunction with the presentation of the findings from this experimental program.

EXPERIMENTAL PROGRAM AND TESTING PROCEDURE

In order to evaluate the potential usefulness of the dilatometer for predicting the compressibility of compacted fills as defined

TABLE 1 SOIL CHARACTERISTICS

	Soil 1	Soil 2	Soil 3
Gradation (% passing)			
No. 4 sieve	88	97	100
No. 40 sieve	77	84	80
No. 200 sieve	43	65	54
Liquid limit (%)	46	37	57
Plasticity index (%)	3	15	24
Specific gravity	2.77	2.78	2.7
T-99 γd max (pcf)	102.4	111.0	105.5
W opt. (%)	20	16.8	18.6
T-180 γd max (pcf)	110.4	123.0	–[a]
W opt. (%)	16.8	12.2	–[a]
AASHTO classification	A-5	A-6	A-7-5

[a]Not determined.

by a one-dimensional compression test, an experimental program was designed utilizing the natural soils described in Table 1. These soils were chosen for their range of properties and significance as locally encountered materials in North Carolina. Soil 1 is a light brown silty sand with a high mica content and low plasticity. Soil 2 is a dark brown clay soil with medium plasticity. Soil 3 is a light reddish sandy silt with a significant mica content. The objective of this investigation was to establish correlations between E_D and M from one-dimensional compression tests for a range of soil types compacted at optimum moisture content.

In general, the test program may be characterized as having evaluated the following types of samples:

1. A range of sample sizes including cylindrical molds of 6-in. (152-mm) and 11-in. (280-mm) diameter and 2.8-in. (71.12-mm) Shelby tube field samples (6-in. samples predominated);
2. Moisture contents representing optimum for the compactive effort at T-99;
3. Dry densities achieved with 50 and 100 percent of the compactive effort specified in AASHTO T-99 at the optimum moisture content for the T-99 test; and
4. Soaked and unsoaked samples compacted in cylindrical molds of 6-in. diameter.

The standard preparation technique for all laboratory samples involved the air drying of soil followed by sieving through a No. 4 sieve. Any material retained on the sieve was broken down with a mortar and pestle and sieved again. The moisture content of the material was then increased with distilled water in a rotary mixer. The material was then stored in sealed plastic bags in a 100 percent humidity room for at least 72 hr to enhance moisture equilibration. All 6-in. diameter specimens were compacted by using an automatic drop weight device with a sector-shaped hammer.

After compaction, at least one sample was soaked at each energy level for all three soil types. The samples were immersed to a point slightly below the top edge of the mold to allow the water to flow upward from the bottom of the sample. All samples were soaked for at least 4 days with the recommended surcharge for a California bearing ratio (CBR) test. After the soaking, the dilatometer tests were conducted *(5)* and the water content distribution was determined.

The degree of saturation was calculated for both the initial (unsoaked) and final (soaked) conditions, with the results shown in Table 2. The increase in the degree of saturation was very small at higher compactive efforts for both the A-6 (S = 88.2 percent to S = 88.4 percent) and A-7-5 soils (S = 88.8 percent to S = 89.8 percent), but was much higher for the A-5 soil (S = 79.2 percent to S = 95.9 percent). This was probably the result of the higher permeability of the silty sand A-5 soil and the soaking technique. At the lower compactive effort the increase in the degree of saturation was much higher for all three soils because of the larger volume of voids and correspondingly higher hydraulic conductivity of the samples.

The specimen for the one-dimensional compression test was obtained after the sample was extruded from the compaction mold and cut to the section desired (vertical or horizontal or both). A consolidation test ring was then pushed into the section. The water content of the sample was determined before the test by using the trimmings and again after the test by using the entire sample. The initial wet and dry densities were then determined. The loading, unloading, and reloading stages were conducted with a load-increment ratio of 1 beginning with 1/8 tsf. Taylor's square-root-of-time-fitting method was adopted so that the time required for 90 percent consolidation ($T90$) could be determined without going too far beyond the time required for 100 percent primary consolidation (Tp or $T100$). Although any time-based system for evaluating the

TABLE 2 INITIAL AND AS-TESTED DEGREE OF SATURATION FOR SOAKED SAMPLES

Soil Type	Compactive Effort[a] (%)	Water Content (%) $W(c)$[b]	$W(s)$[c]	W[d]	Degree of Saturation (%) As Compacted	As Tested
A-5	50	20.0	28.7	29.24	68.4	98.2
A-6	50	17.3	21.7	23.37	73.75	92.9
A-7-5	50	19.3	21.5	24.5	78.7	87.7
A-5	100	20.0	24.0	25.0	79.2	95.9
A-6	100	17.2	17.6	19.9	88.2	88.4
A-7-5	100	19.3	19.6	21.8	88.8	89.8

[a]As specified in AASHTO T-99 test.
[b]As compacted.
[c]After soaking.
[d]From consolidation ring.

compressibility of partially saturated soils is somewhat difficult to interpret—that is, the process is not simply governed by the dissipation of excess pore pressure—the Taylor method provided a consistent and conventional format for evaluation of the data.

In order to determine the influence of sample disturbance resulting from dilatometer insertion, several one-dimensional compression tests were conducted on samples that had not been tested with the dilatometer but that had densities and water contents similar to samples that had been tested with the dilatometer.

Both soaked and unsoaked samples were prepared for each soil type. At least one soaked and one unsoaked sample at each compactive effort was tested with the dilatometer before the one-dimensional compression test was performed. The soaked samples that were not tested with the dilatometer were extruded from the mold. The moisture distribution in the sample and the corresponding degree of saturation were computed by measuring the water content of slices 1/2 in. thick. Sample heights were measured both before and after soaking.

RESULTS AND DISCUSSION

The results of the laboratory and field tests conducted in this study are presented in Tables 3 and 4. Consolidation specimens obtained from samples penetrated with the dilatometer are identified as either SFD (side facing dilatometer diaphragm) or BSD (back side of dilatometer). Dilatometer tests were performed after compaction for the unsoaked samples and after soaking for the soaked samples.

As mentioned previously in the discussion of K_D, the use of the conventional equations to predict R_M requires an estimate of the existing effective stress in order to first determine K_D. This will undoubtedly be somewhat of an inconvenience when partially saturated soils are tested in situ. In the case of the laboratory samples tested, the overburden stress is essentially zero [4 in. (102 mm) of soil cover], and the negative pore pressure accounts for the major component of the vertical effective stress. A limited study of soil suction for these soils indicated that near the optimum moisture content one might expect negative pore pressures in the range of 0.5 to 1 tsf (47.9 to 95.8 kPa). Therefore, it was determined that a reasonable

TABLE 3 DESCRIPTION OF ALL SAMPLES TESTED

Sample No. and Orientation	Soil Type	Condition as Tested	Compactive Effort[a] (%)	$W(c)$[b] (%)	$W(s)$[c] (%)	γd (pcf)	Side of Dilatometer
1-V	A-5	Soaked	50	20.0	28.6	95.5	SFD
2-V	A-5	Soaked	50	20.0	28.9	95.5	BSD
3-V	A-5	Unsoaked	50	20.0	–	95.7	BSD
4-V	A-5	Soaked	100	20.0	23.6	102.4	BSD
5-V	A-5	Soaked	100	20.0	24.2	102.1	–
6-V	A-5	Soaked	100	20.0	24.0	102.4	SFD
7-H	A-5	Soaked	100	20.0	23.8	102.1	–
8-V	A-5	Unsoaked	100	20.0	–	101.7	–
9-V	A-5	Unsoaked	100	20.0	–	101.7	–
10-H	A-5	Unsoaked	100	20.0	–	101.7	–
11-V	A-5	Unsoaked	–[d]	22.0	–	94.4	–
12-V	A-5	Unsoaked	–[d]	22.0	–	98.3	–
13-H	A-6	Unsoaked	–[e]	16.8	–	112.2	–
14-H	A-6	Unsoaked	–[e]	19.4	–	104.6	–
15-H	A-6	Unsoaked	–[e]	17.6	–	113.0	–
16-V	A-7-5	Unsoaked	50	19.3	–	100.6	BSD
17-V	A-7-5	Unsoaked	50	22.7	–	98.3	BSD
18-V	A-7-5	Unsoaked	100	19.3	–	106.3	BSD
19-V	A-7-5	Unsoaked	100	20.6	–	110.8	SFD
20-V	A-7-5	Unsoaked	100	20.6	–	110.8	SFD
21-H	A-7-5	Unsoaked	100	20.5	–	104.2	SFD
22-V	A-7-5	Unsoaked	100	20.5	–	104.2	BSD
23-V	A-6	Unsoaked	100	17.0	–	111.5	–
24-V	A-6	Unsoaked	50	16.8	–	105.9	–
25-V	A-6	Soaked	50	17.2	21.7	105.2	BSD
26-V	A-6	Soaked	100	17.2	17.6	111.6	BSD
27-V	A-7-5	Soaked	50	19.3	21.5	101.4	BSD
28-V	A-7-5	Soaked	100	19.3	19.6	106.0	SFD

Note: V = vertical orientation; H = horizontal orientation; SFD = side facing dilatometer; BSD = back side of dilatometer.

[a]As specified in AASHTO T-99 test.
[b]As compacted.
[c]After soaking.
[d]Statically compacted in 11 in. mold to density shown.
[e]Field-compacted Shelby tube sample.

TABLE 4 CONSTRAINED MODULUS AND DILATOMETER MODULUS VALUES FOR ALL SAMPLES TESTED

Sample No. and Orientation	M (tsf) by Stress Level 0.5 tsf	1.5 tsf	4.5 tsf	E_D (tsf)
1-V	30.0	36.4	68.0	45.0
2-V	23.0	27.0	86.0	45.0
3-V	95.0	95.6	108.0	107.0
4-V	45.0	55.0	109.0	107.0
5-V	50.0	53.5	95.0	–
6-V	52.0	56.5	105.0	107.0
7-H	48.0	52.0	103.0	–
8-V	61.0	61.7	110.0	103.0
9-V	60.0	75.0	100.0	–
10-H	120.0	101.0	130.0	–
11-V	76.0	55.6	88.0	111.0
12-V	80.0	69.4	80.0	118.0
13-H	140.0	210.0	304.0	200.0
14-H	130.0	188.7	275.0	189.0
15-H	150.0	227.3	325.0	200.0
16-V	135.0	125.0	150.0	176.0
17-V	73.0	87.0	120.0	118.0
18-V	122.0	157.0	215.0	205.0
19-V	100.0	160.0	225.0	233.0
20-V	138.0	172.0	220.0	233.0
21-H	220.0	160.0	150.0	205.0
22-V	80.0	130.0	200.0	205.0
23-V	140.0	125.0	145.0	223.0
24-V	125.0	55.0	85.0	161.0
25-V	110.0	67.0	76.0	52.0
26-V	140.0	100.0	110.0	132.0
27-V	50.0	75.0	125.0	132.0
28-V	68.0	105.0	175.0	212.0

Note: V = vertical orientation; H = horizontal orientation.

way to depict the data would be to evaluate the constrained modulus at several stress levels to ensure that the actual effective stress in the sample during the dilatometer test was bracketed. Table 4 is a summary of the M-values calculated at stress levels of 0.5, 1.5, and 4.5 tsf and the corresponding E_D-value for each of the samples tested. These values were used to determine the correlations between M and E_D as shown in Figures 2 through 8.

Correlations between the dilatometer modulus and the constrained modulus were developed at three different stress levels. These relationships are presented in the following groups: each of the three soil types, all unsoaked samples, all soaked samples, and all samples with vertical orientation. It should be noted that each point plotted does not represent a separate sample, but an individual one-dimensional compression test. Therefore, one E_D-value often corresponds to several M-values when more than one consolidation test specimen was trimmed from a given sample.

Duplicate Tests

A typical curve of log stress versus percent strain for each of the one-dimensional compression test specimens (Specimens 1 through 28) was plotted for loading, unloading, and reloading. To indicate the consistency of the results, duplicate specimens were taken from the same compacted mold. These results are plotted together as shown in Figures 9 through 12. The agreement is seen to be quite good, although there are some differences in the unloading-reloading stages.

Effect of Mold Size

For the A-5 soil, several one-dimensional compression tests were conducted on specimens taken a few inches away from the dilatometer blade penetration in the 11-in. diameter mold. The constrained modulus values were consistent with those obtained on specimens from the 6-in. diameter mold (+5 to 20 percent). The dilatometer moduli from Specimens 11 and 12 (E_D = 111.0 tsf and E_D = 118.0 tsf) are very close to that of Specimen 3 (E_D = 107.0 tsf). At the same time the constrained modulus values from the specimen in the 11-in. mold were slightly lower than those from the smaller mold, which is probably due to the higher water content of the specimen in the 11-in. mold [W_n = 22.0 percent in the 11-in. diameter mold as compared with W_n = 20.0 percent in the 6-in. diameter mold (see Tables 3 and 4)].

Blade Penetration Effects

In order to evaluate the effect of blade penetration in the sample, one-dimensional compression tests were performed on specimens obtained from two identical samples having the same water content and dry density. The dilatometer test (blade penetration) was conducted on one sample, whereas one-dimensional compression tests were performed on specimens from both samples. The constrained modulus values from the sample penetrated with the dilatometer were only slightly higher than those from the sample that was not penetrated. For example, Specimen 6 was tested with the dilatometer and had

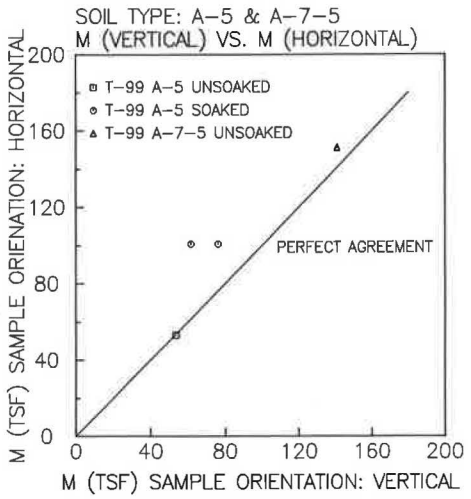

FIGURE 2 Comparison of constrained moduli from vertical and horizontal specimens.

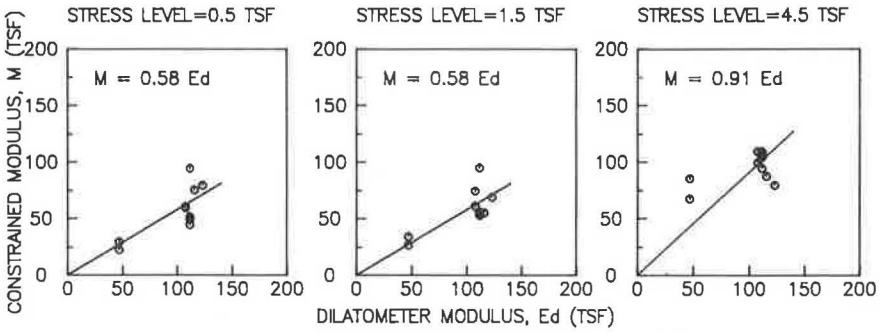

FIGURE 3 Constrained modulus versus dilatometer modulus for A-5 soil.

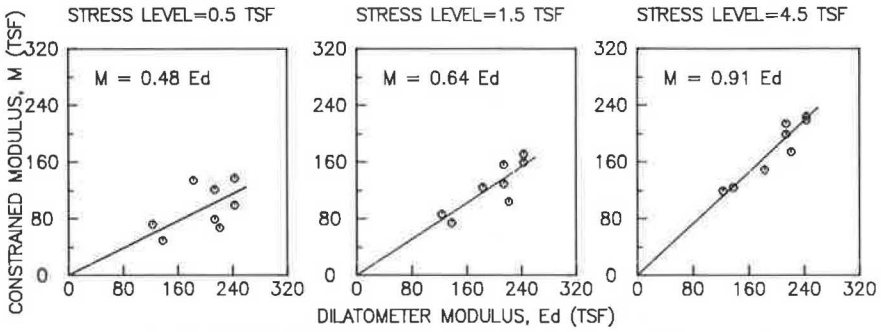

FIGURE 4 Constrained modulus versus dilatometer modulus for A-7-5 soil.

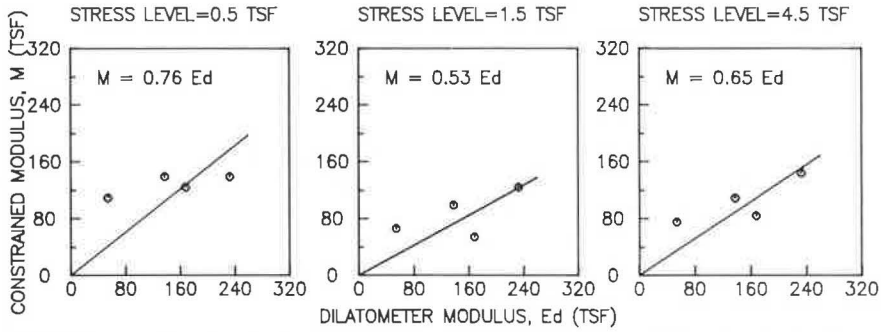

FIGURE 5 Constrained modulus versus dilatometer modulus for A-6 soil.

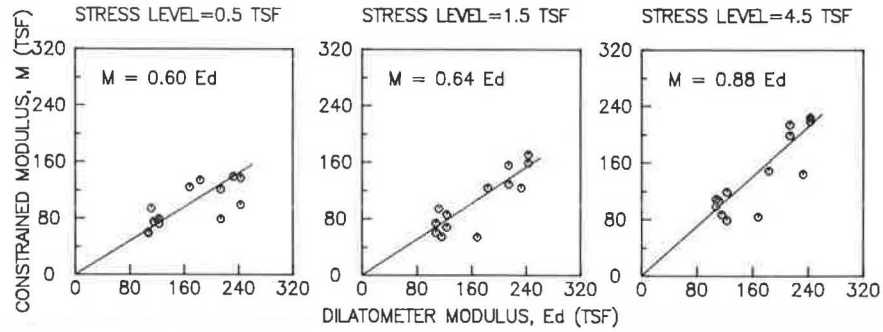

FIGURE 6 Constrained modulus versus dilatometer modulus for all unsoaked samples.

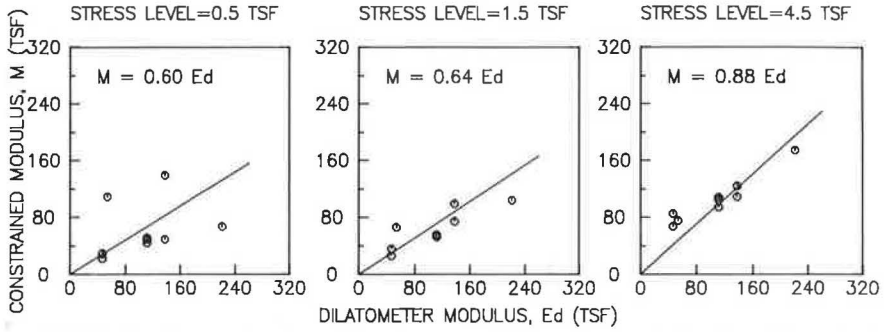

FIGURE 7 Constrained modulus versus dilatometer modulus for all soaked samples.

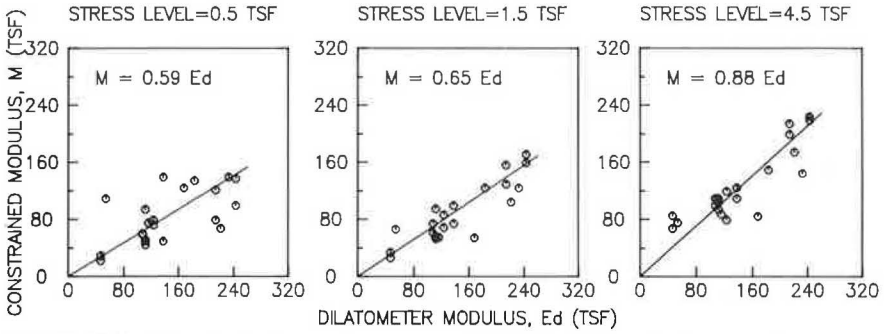

FIGURE 8 Constrained modulus versus dilatometer modulus for all samples.

an $M = 52.0$ tsf at the 0.5-tsf stress level, $M = 56.5$ tsf at the 1.5-tsf stress level, and $M = 105.0$ tsf at the 4.5-tsf stress level. Specimen 5, which was not penetrated with the dilatometer, had corresponding values of $M = 50.0$, 53.5, and 95.0 tsf. In comparison with the difference between all duplicate specimens tested, these values are not considered significantly different.

One-dimensional compression tests were also performed on samples obtained from both sides of the dilatometer to investigate the effect of the 1-mm expansion of the dilatometer diaphragm during testing. From Table 4 one can compare the data from Samples 1 and 2 and also from Samples 4 and 6. At a low stress level the constrained modulus on the sample from the side facing the dilatometer (SFD) is somewhat higher than

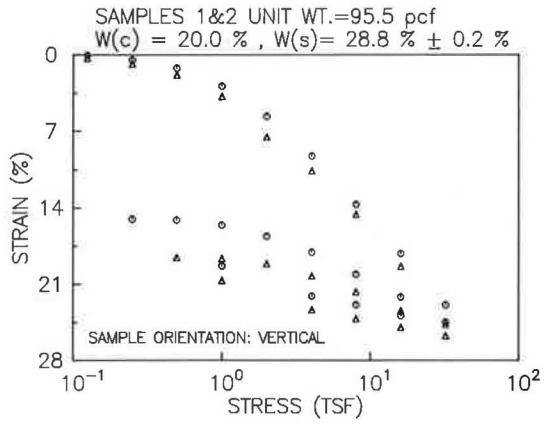

FIGURE 9 Strain versus log stress for Specimens 1 and 2.

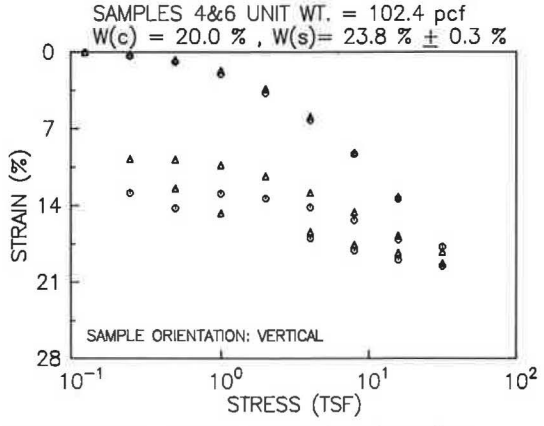

FIGURE 10 Strain versus log stress for Specimens 4 and 6.

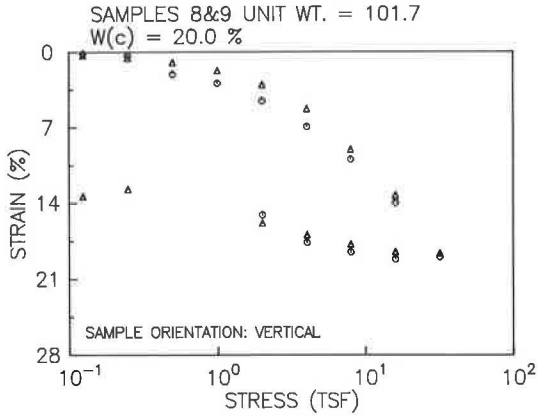

FIGURE 11 Strain versus log stress for Specimens 8 and 9.

that obtained from the sample from the back side of the dilatometer (BSD). At higher stress levels the constrained modulus on the SFD, however, is lower than that on the BSD. As the difference in constrained modulus values for specimens taken from duplicate samples ranges from 5 to 20 percent, it is not possible to conclude that a predictable difference in constrained modulus values was caused by the diaphragm expansion. This is logical because the insertion of the blade has already caused a 7-mm lateral displacement of the soil.

These test results indicate that the soil structure of the as-compacted material is stable enough that insertion of the dilatometer blade causes little change in the lateral stiffness of the soil. On this basis it was concluded that for the soils tested, the data can be used without significant concern for the influence of sample disturbance effects.

Effect of Soaking

In order to show the influence of an increased degree of saturation caused by soaking on the relationship between the constrained modulus and dilatometer response, the pertinent data from Tables 3 and 4 are reorganized and presented in Tables 5 and 6. A brief review of these tables shows that, in general, soaking causes both the resultant E_D- and M-values to be lower. However, for most of the data, the decrease in both stiffnesses is similar in magnitude, so that the ability to predict the constrained modulus from the dilatometer modulus would not be significantly limited by a lack of knowledge of the saturation state of the soil. The data contained in Tables 3 and 4 are shown in Figures 3 through 8.

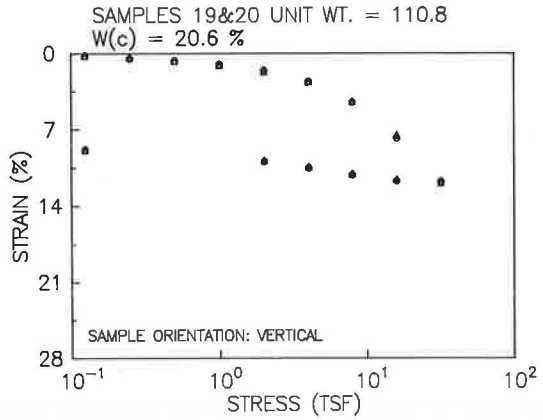

FIGURE 12 Strain versus log stress for Specimens 19 and 20.

Influence of Specimen Orientation

In Figure 2 the constrained moduli for both horizontal and vertical samples taken from the same mold are compared. These results show somewhat higher modulus values for several of the horizontal specimens when compared with those of the corresponding vertical specimens. The expansion of the dilatometer membrane measures the lateral stiffness of the soil, which is represented in this research by the vertical samples. These results indicate that the data obtained from the dilatometer may be considered a reasonable estimate of the vertical stiffness for the compacted soils tested.

Dilatometer Modulus Versus Constrained Modulus

In Figure 3 a plot of M versus E_D is presented for all tests conducted on the A-5 soil (soaked and unsoaked specimens). A straight line equation for a line passing through the origin (zero) by linear regression was used to model the relationship. Figures 4 and 5 show the relationship of the constrained modulus versus the dilatometer modulus for the A-7-5 and A-6 soils, respectively.

Figures 6 and 7 are summary plots for the unsoaked and soaked samples, respectively. A linear relation for a straight line passing through the origin was used for all data points. The resulting equations are shown on each figure.

Figure 8 is a summary plot for all the samples tested. The linear relations for straight lines passing through the origin are also given. The slopes based on data from all samples are very close to those corresponding to the unsoaked condition.

It would be of significant benefit if an initial estimate of the constrained modulus could be made directly from the field dilatometer test results without regard to soil type and moisture condition. This would be analogous to Marchetti's equation for predicting R_M when K_D is greater than 10 (Equation 7).

In order to develop this relationship, the slopes of all M-E_D relationships were plotted as a function of stress level, and the results are shown in Figure 13. In general, the coefficient relating the dilatometer modulus to the constrained modulus (R_M) is an increasing function of stress level (i.e., the slope increases with stress level). The following section presents the data generated on undisturbed field samples of the A-6 soil and aids in the interpretation of this relationship.

Field Tests and Field Samples

In order to further explore the relationship between the constrained modulus and the dilatometer modulus, three one-dimensional compression tests were conducted on specimens

TABLE 5 CHARACTERISTICS OF SOAKED AND UNSOAKED SAMPLES

Sample No. and Orientation	Soil Type	Condition as Tested	Compactive Effort[a] (%)	$W(c)$[b] (%)	$W(s)$[c] (%)	γd (pcf)	Side of Dilatometer
1-V	A-5	Soaked	50	20.0	28.6	95.5	SFD
3-V	A-5	Unsoaked	50	20.0	–	95.7	BSD
4-V	A-5	Soaked	100	20.0	23.6	102.4	BSD
8-V	A-5	Unsoaked	100	20.0	–	101.7	–
9-V	A-5	Unsoaked	100	20.0	–	101.7	–
25-V	A-6	Soaked	50	17.2	21.7	105.2	BSD
24-V	A-6	Unsoaked	50	16.8	–	105.9	–
26-V	A-6	Soaked	100	17.2	17.6	111.6	BSD
23-V	A-6	Unsoaked	100	17.0	–	111.5	–
27-V	A-7-5	Soaked	50	19.3	21.5	101.4	BSD
17-V	A-7-5	Unsoaked	50	22.7	–	98.3	BSD
28-V	A-7-5	Soaked	100	19.3	19.6	106.0	SFD
18-V	A-7-5	Unsoaked	100	19.3	–	106.3	BSD

Note: V = vertical orientation; SFD = side facing dilatometer; BSD = back side of dilatometer.

[a]As specified in AASHTO T-99 test.
[b]As compacted.
[c]After soaking.

trimmed from undisturbed Shelby tube samples of the A-6 soil obtained in a field investigation of a 15-ft (4.8-m) compacted embankment in Research Triangle Park (RTP), North Carolina. The test data were analyzed and the constrained modulus at each of the three stress levels is plotted versus the field dilatometer reading at the depth from which each of the samples was obtained. These data are shown in Figure 14, which allows the determination of an appropriate slope for each stress level, as previously discussed for Figure 13.

Figure 15 shows the R_M-values generated from Figure 14 in conjunction with those from the laboratory tests on each of the three soils. The field samples show a greater rate of increase of R_M with stress level than the laboratory-compacted specimens; however, even these values are significantly lower than those that would be predicted from Marchetti's equations. For example, the average I_D-value obtained for all tests on the A-6 soil was 1.37. Using Equation 5 and an estimate of K_D based on the existing overburden stress at a depth of 10 ft (approximately 3 m), the calculated R_M-value is around 2.3. As it is doubtful that the appropriate stress level for any of the tests would be greater than the 1.5-tsf value, it appears that using Marchetti's equations may overestimate the stiffness of compacted soils by a significant amount.

On the basis of the results of this experimental investigation, it would appear reasonable to accept the dilatometer modulus as an upper bound to the anticipated in situ constrained modulus, with the realization that values may actually be in the range of 50 to 80 percent of that value, depending on soil type.

SUMMARY AND CONCLUSIONS

In this research, the relationship between the dilatometer modulus and the constrained modulus from the one-dimensional

TABLE 6 CONSTRAINED MODULUS AND DILATOMETER MODULUS VALUES FOR SOAKED AND UNSOAKED SAMPLES

Sample No. and Orientation	M (tsf) by Stress Level 0.5 tsf	1.5 tsf	4.5 tsf	E_D (tsf)
1-V	30.0	36.4	68.0	45.0
3-V	95.0	95.6	108.0	107.0
4-V	45.0	55.0	109.0	107.0
8-V	61.0	61.7	110.0	103.0
9-V	60.0	75.0	100.0	–
25-V	110.0	67.0	76.0	52.0
24-V	125.0	55.0	85.0	161.0
26-V	140.0	100.0	110.0	132.0
23-V	140.0	125.0	145.0	223.0
27-V	50.0	75.0	125.0	132.0
17-V	73.0	87.0	120.0	118.0
28-V	68.0	105.0	175.0	212.0
18-V	122.0	157.0	215.0	205.0

Note: V = vertical orientation.

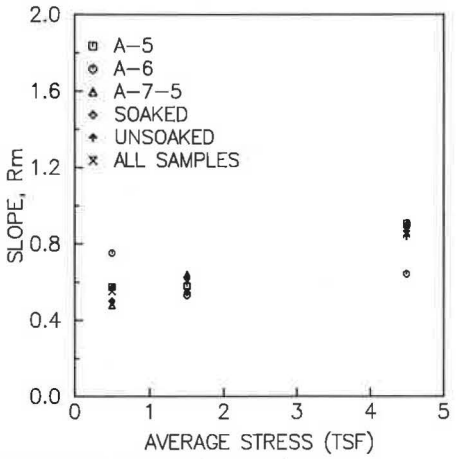

FIGURE 13 Ratio relating dilatometer modulus to constrained modulus versus stress level for laboratory samples.

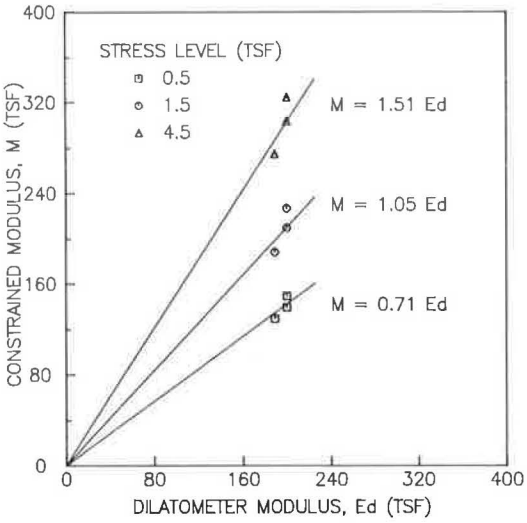

FIGURE 14 Constrained modulus versus dilatometer modulus as a function of stress level for A-6 field samples.

compression test for three different soils encountered in North Carolina has been studied.

On the basis of the results of the experimental test program reported, the following conclusions are advanced:

1. For the compacted soils studied it was found that current methods for interpreting dilatometer data to predict compressibility, as determined from one-dimensional compression

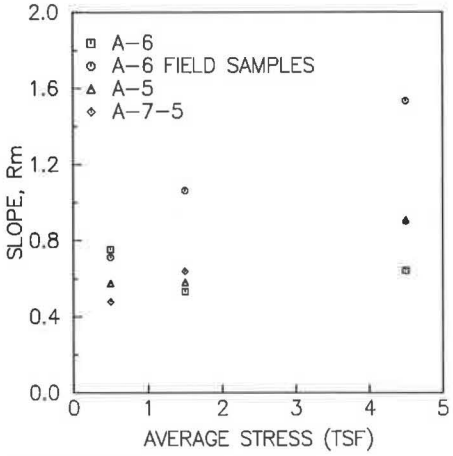

FIGURE 15 Ratio relating dilatometer modulus to constrained modulus versus stress level for laboratory and field samples.

tests, significantly overestimated the values that were measured. On the basis of the combination of laboratory and field tests conducted, it would appear reasonable to accept the dilatometer modulus as an upper bound to the anticipated in situ constrained modulus, with the realization that values may actually be in the range of 50 to 80 percent of that value, depending on soil type.

2. A laboratory technique was utilized by which dilatometer penetration tests were performed in CBR molds (6-in. diameter), after which the one-dimensional compression test specimens were obtained, so that both pieces of data were obtained from the same specimen. Although the boundary conditions appear unfavorable in the small mold, the results of the one-dimensional compression tests were consistent with those duplicate samples in which the dilatometer was not penetrated.

3. Limited one-dimensional compression tests on Shelby tube samples (field-compacted material) of the A-6 soil show a relatively higher influence of stress level on the constrained modulus for the same dilatometer modulus than on the laboratory-compacted sample. Further study should emphasize the correlation between field dilatometer tests and laboratory tests on Shelby tube or other undisturbed samples of partially saturated soils, which more closely represent in situ conditions.

ACKNOWLEDGMENTS

The research reported in this paper was sponsored by the North Carolina State Department of Transportation (NCDOT) in cooperation with FHWA, U.S. Department of Transportation.

A technical advisory committee chaired by George Wells and including Harold Landrum, John Ledbetter, Dick Reaves, and Pat Strong from the NCDOT and John Wadsworth from FHWA aided in the coordination of the research project.

Thanks are also due Billy Brantly and Njoroge Wainaina of the Materials and Test Unit and Dave Bingham, Harold Landrum, and Bill Moore of the Geotechnical Unit of the NCDOT, who made valuable contributions in the field portion of this project.

The authors wish to thank Harvey Wahls, who contributed several helpful suggestions with regard to the testing program and interpretation. The assistance of Bill Dunleavy, also of the Civil Engineering Department, who provided the technical support for all of the project instrumentation needs, is also appreciated.

REFERENCES

1. S. Marchetti. In Situ Tests by Flat Dilatometer. *Journal of the Geotechnical Engineering Division, ASCE,* Vol. 106, No. GT3, March 1980, pp. 299–321.
2. J. H. Schmertmann. In Situ Test by Flat Dilatometer—Discussion, *Journal of the Geotechnical Engineering Division, ASCE,* Vol. 107, No. GT6, June 1981, pp. 831–832.
3. S. Marchetti. "A New In Situ Test for the Measurement of Horizontal Soil Deformability." *Proc., Conference on In Situ Measurement of Soil Properties,* ASCE Specialty Conference, Raleigh, N.C., Vol. 2, ASCE, New York, June 1975.
4. P. J. Bullock. *The Dilatometer: Current Test Procedures and Data Interpretation.* Master's thesis. University of Florida, Gainesville, Fall 1983.
5. R. H. Borden, C. N. Aziz, W. M. Lowder, and N. P. Khosla. "Evaluation of Pavement Subgrade Support Characteristics by Dilatometer Test." In *Transportation Research Record 1022,* TRB, National Research Council, Washington, D.C., 1985, pp. 120-127.

Publication of this paper sponsored by Committee on Exploration and Classification of Earth Materials.

The Pressuremeter in Geotechnical Practice

ERNEST WINTER

The pressuremeter, introduced in its present form in the 1950s, has gained substantial acceptance in the United States. Typical testing procedures have for the most part not changed since the meter's introduction, but changes are being recommended by researchers to accommodate test evaluations in clay soils. The test procedure is in the process of being standardized. Typical uses of the test for foundation design, settlement analysis, and pile behavior are reviewed.

The pressuremeter as an in situ testing instrument is well known and used in the United States and is widely accepted for use in routine investigations. Since its introduction, considerable research and development have occurred and new testing methods as well as new methods of evaluation have been suggested. It is accordingly considered appropriate to trace this development from its beginning for a better overall understanding of the test of today.

ORIGINS OF PRESSUREMETER TEST

The modern use of the pressuremeter is based on the efforts of Louis Ménard, a French engineer, who developed the original concept by Kögler into a usable test instrument in the late 1950s. Ménard also recognized, however, that new empirical methods will be required to analyze foundation performance with the pressuremeter and made considerable full-scale measurements to support his empirical correlations.

At the introduction of the pressuremeter in the United States, the instrument was furnished with a whole set of new rules based on Ménard's measurements and evaluations. These evaluation methods were mostly unknown to the engineering community. The question was whether those rules would be accepted for the design or whether additional research would be necessary to produce parameters for the Ménard rules for local conditions and on correlation of the test results with known geotechnical parameters. The first category of efforts was generally pursued by consulting engineers, whereas correlations with shear parameters and compressibility were developed mostly by researchers.

After more than 20 years of use, a great number of test results are available and typical test values in particular geologic formations are known. The results of disturbance during installation are relatively well established, and experience has shown that the forming of the borehole has a significant effect on the regular pressuremeter test. Efforts to standardize the procedures of installation as well as the test have led to a new ASTM standard to be introduced in the near future.

Schnabel Engineering Associates, 4909 Cordell Avenue, Bethesda, Md. 20814.

The pressuremeter test consists of the expansion of a membrane, usually in a predrilled borehole (Figure 1). The volume change and the pressure are measured in the test, and the pressures to increase the volume are generally applied in predetermined steps. A modulus is then determined to reflect the relation between volume change and pressure, and the pressure at which failure of the soil occurs is also evaluated. It is these two parameters, the pressuremeter modulus and limit pressure, that are used in evaluations, together with the curve of pressure versus volume.

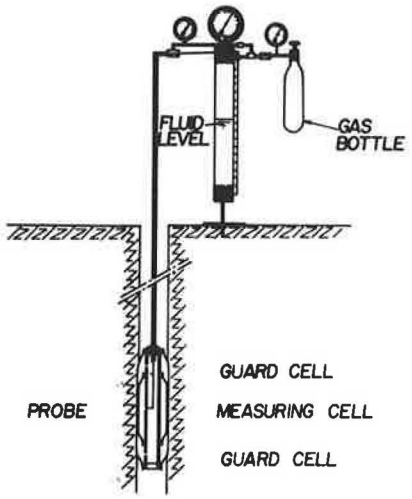

FIGURE 1 Schematic section of pressuremeter.

The performance of the test as well as methods of evaluation will be discussed in some detail in this paper; in addition some particularly well-suited and well-developed applications for the engineering design will be reviewed. The subject of this paper is the pressuremeter as an instrument in the everyday use of geotechnical engineering. With this in mind, the single most important factor affecting the quality of the tests, namely, the preparation of the borehole, is examined in some detail.

HOLE PREPARATION

Two types of disturbance occur when a borehole is drilled for the test. The first type is the result of opening the hole itself. As the borehole is drilled, a stress release occurs when material is removed from the boring. This stress release is restored during the test or reduced by performing the test as soon as possible

after drilling. The effect of this unload-load cycle will, however, exist as long as predrilling is part of the testing. An improvement is the self-boring pressuremeter, which is inserted while the original in situ stresses are maintained. This is still considered a research tool or special testing equipment and is used mostly on larger, elaborate projects in which the higher cost of such testing can be absorbed.

The second type of disturbance is caused by the drilling equipment along the walls of the borehole and can be considerably reduced by the use of the right tools and techniques. In everyday practice, some methods have been developed that are more useful in one soil than in others. Techniques vary by geography and country of origin. A tabulation has been assembled by ASTM for the upcoming standard, showing methods suited for particular subsoil conditions (Table 1). As can be readily seen, the most widely applicable method is hand augering, which causes probably the least disturbance in most soils. The soils representing the largest problems in hole preparation are the sands and gravels, especially below ground water level. In these soils good results were obtained, however, by using mud to keep the boring open.

Another factor, also related to preparation of boreholes and disturbance, is the range of tolerances to be maintained to obtain a good test. The pressuremeter generally requires a hole in which only minimal space is maintained between the probe and the walls of the borehole in order to keep the necessary expansion of the probe to the minimum. Generally a hole diameter between 3 to 20 percent larger than that of the probe should be maintained.

THE PRESSUREMETER TEST

The test itself consists of expanding a probe in a predrilled borehole and measuring volumes and corresponding pressures. The most commonly used method is to increase pressures in about 10 increments to failure. It has also been acceptable to run the test by controlling strain and measuring the corresponding stress. The principle of the test is, however, to perform the test in a relatively short period of time, thereby measuring basically undrained conditions, even where pore-pressure dissipation is significant. Because the test results are sensitive to the speed of testing, specifically in fine-grained soils, this makes standardization more important. It has been the practice of the engineering community to perform tests according to the original recommendations of Ménard in order to maintain the comparative value of the results.

As part of the testing procedure, the drill hole is advanced to the test level and cleaned of debris and cuttings. Before the probe is placed in the hole, all calibrations are completed and checked. The probe is then lowered to the test depth and pressures are applied in predetermined steps. The load incre-

TABLE 1 GUIDELINES FOR SELECTION OF BOREHOLE PREPARATION METHODS AND TOOLS

Preparation Method	Clayey			Silty		Sandy Loose			Sandy Gravel or Gravely		
	Soft	Firm–Stiff	Stiff–Hard	Above GWL	Below GWL	Above GWL	Below GWL	Medium–Dense	Sands[a] Loose	Sands[a] Dense	Weathered Rock
Rotary drilling with bottom discharge of prepared mud	2[b]	1[b]	1	1[b]	1[b]	1[b]	1[b]	1[b]	2	NR	1
Pushed thin wall sampler	2[b]	1	2	2[b]	NR	NR	NR	NR	NA	NA	NA
Pilot-hole drilling											
With subsequent sampler pushing	2	2	1	2	NR	NR	NR	NR	NA	NA	2[b]
With simultaneous shaving	2	2	1	2[b]	2[b]	2	2	2	NA	NA	NA
Continuous flight auger	NR	1[b]	1[b]	1	NR	2	NR	1	NA	NR	1
Hand auger											
In the dry	NR	1	NA	1	NR	2	NR	1	NA	NA	NA
With bottom discharge of prepared mud	1	1	NA	2	1	1	1	1	NA	NA	NA
Driven or vibro-driven sampler	NR	NR	NA	2	NR	2	NR	2	NR	NR	1
Core barrel drilling	NR	NR	2[b]	NR	NR	NR	NR	2[b]	2	2	2
Rotary percussion	NR	NR	1[b]	NR	NR	NA	NA	NR	NA	NA	2
Driven, vibro-driven, or pushed slotted tube	NR	NR	NR	NR	NR	NR	NR	NR	2	1[c]	NR

Note: GWL = groundwater level; NR = not recommended; NA = not applicable; 1 = first choice; 2 = second choice.

[a]Below GWL.
[b]Method applicable only under certain conditions (see text).
[c]Pilot-hole drilling required beforehand.

ments are estimated from testing in similar material and from experience, in order to complete the test in about 10 load increments. Readings are taken after 30 sec and 1 min during each load step. The test is complete when the probe expansion becomes excessive. The test may include cyclic loading to evaluate load-unload characteristics. The volume-pressure curve is plotted with all necessary corrections.

The test yields the pressuremeter modulus, which is the slope of the pressure-volume curve, and the limit pressure, which is the pressure at which unlimited expansion occurs. For evaluation in practice, the pressuremeter modulus is generally determined from the straight-line portion of the pressuremeter curve and the limit pressure is taken at a volume expansion that is twice the original probe volume. For all applications in general practice, these determinations are adequate and will be discussed in more detail later.

It is noted here that several pressuremeters are in use today, including the most widely accepted original Ménard type, in which three cells are used within the expandable probe. The center measuring cell is protected by two guard cells, one at the upper and one at the lower end, to prevent excessive expansion of the measuring cell in those directions. Even with this type, a relatively tight hole is advisable. Probes with feelers that measure hole diameter instead of probe volume are less sensitive to this problem but make only spot measurements at certain points of the borehole wall.

RESULTS OF THE TEST

The pressuremeter test fills a very important function in soil testing by providing information that previously was difficult to obtain with adequate accuracy. The relatively hard clays with various amounts of preconsolidation cannot be sampled and tested with ordinary methods, but once a boring has been drilled, excellent information can be obtained with the pressuremeter as to the strength and compressibility of these soils. Granular soils fall into the same category together with residual formations in various stages of decomposition. The improved understanding of strength characteristics as well as of compressibility of these formations is the result of this test.

The major parameters obtained from the test are representative of compressibility and strength. Compressibility is expressed by the pressuremeter modulus, which is determined from the following formula:

$$E_p = 2(1 + \gamma)(V_0 + V_m)\ (\Delta P/\Delta V)$$

where

E_p = pressuremeter modulus,
γ = Poisson's ratio (generally taken as 0.3 for pressuremeter applications),
$V_0 + V_m$ = volume of probe,
ΔV = volume increase in straight-line portion of test curve, and
ΔP = pressure increase corresponding to ΔV volume increase.

In Figure 2, a typical pressuremeter test curve is shown with the volume readings and pressure increments used to determine the pressuremeter modulus. Harder or denser soils will result in a flatter curve and higher pressuremeter modulus, whereas the plastic deformation represented by the right end of the curve will extend to higher pressures for these soils. Disturbance can generally be easily detected from irregularities in the shape of the curve.

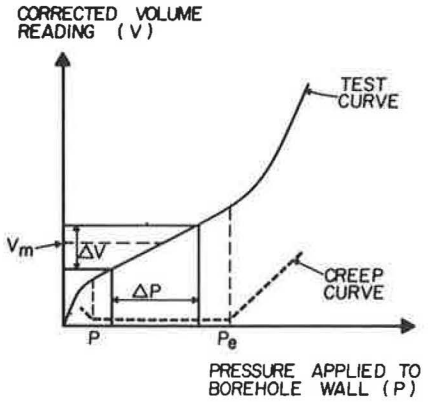

FIGURE 2 Typical pressuremeter test curve.

The limit pressure is not measured directly by this test because of limitations in the probe expansion, and an extrapolation of the last few test points must be made to obtain an estimated value. By definition the limit pressure is associated with infinite hole expansion at no additional loading and is a theoretical value. For practical purposes a hole expansion of twice the original probe volume is taken as the limit pressure. Historically this value has been used in most of the investigations to date and was adopted for the new ASTM standard. In Figure 3 the typical extrapolation is shown by using a logarithmic plot and the last few points of the test. It may be noted that the test must be carried as close as practically feasible to the limit pressure to get a reliable evaluation.

EVALUATION OF TEST RESULTS

Three typical uses of pressuremeter test results by the practicing engineer will be discussed to indicate some major applications of this test. The complete list of available uses and

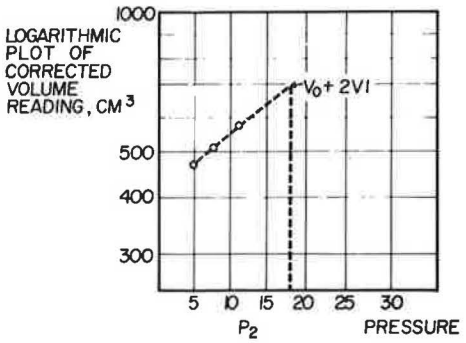

FIGURE 3 Determination of limit pressure from logarithmic plot of volume versus pressure.

applications is a long one and could not be meaningfully discussed here.

Ménard Rules for Evaluation

The complete design recommendations for the pressuremeter as introduced by Ménard were published in *Sols-Soils (1)* and include design methods for several aspects of geotechnical engineering, such as spread footing foundations, pile capacity evaluations, and settlement evaluations, with no other testing required but that done with the pressuremeter. Geotechnical consultants in the United States still use pressuremeter test data in addition to conventional analysis methods when such data are available.

The basic equation for the bearing capacity of footings or caissons has been formulated as follows:

$$q_1 - q_0 = K(P_1 - P_0)$$

where

q_1 = ultimate bearing capacity,
q_0 = overburden pressure,
P_1 = limit pressure from pressuremeter test,
P_0 = horizontal pressure at rest, and
K = bearing capacity factor varying from 0.8 to 9.

The horizontal at-rest pressure is necessary for this evaluation, which can be estimated from the pressuremeter test or can be determined by other methods.

The general formula for settlement of a foundation has been given as follows:

$$W = (1.33/3E)\, P\lambda_2^{\alpha} + (\alpha/4.5E)\, P\lambda_3 R$$

where

λ_2, λ_3 = shape coefficients, a function of the length and width of the foundation;
α = structure coefficient, generally evaluated from the ratio of pressuremeter modulus to limit pressure;
P = foundation pressure;
E = pressuremeter modulus; and
R = radius.

Values of these variables are given in Tables 2 and 3.

Bearing capacities determined by this method are generally high compared with established bearing values, and settlements are generally lower than would be expected by a static settlement calculation. As an example, the typical foundation requirements of a 6- by 6-ft spread footing are examined. This footing, when founded on high-density local gravelly sand of Pleistocene origin, would be designed for a typical soil bearing pressure of 4 tsf. The pressuremeter tests performed in this geologic formation indicate limit pressures varying between 10 and 20 tsf. An evaluation of bearing capacity using the lower value and the Ménard formulas will give an allowable bearing of 11,500 psf, considering normal embedments and a safety factor of 3. The settlements of this footing are calculated to be 0.6 in. when the pressuremeter modulus of 100 tsf on the low end of the range in this type of soil is used. Consideration of average parameters for this layer would result in high allowable bearing capacities that could not be realized in the design. Considering plate load test data available on this material used as a fill soil, settlements are believed to be in the realistic range. These formulas have been particularly useful in relatively hard soils or materials otherwise not suitable for sampling. A significant use has developed in estimating bearing capacities and settlements of caissons founded on good bearing materials. Allowable bearing capacities could be increased throughout the years as confidence develops based on performance of these foundations.

Static Settlement over Sand

In 1970 Schmertmann *(2)* published the strain distribution method to calculate settlements over sand by using the cone penetrometer. In 1978 this calculation was revised by Schmertmann *(3)* to include strip footings. The method gives good correlation with settlement of footings but requires the use of an elastic modulus *(E)*, which was evaluated from cone penetrometer tests.

For users of the pressuremeter, it came as a natural application to substitute the pressuremeter modulus in the equation. It was not clear, however, what modification to the modulus, if any, would be required. Considerable field measurements were performed, and Martin *(4)* indicated in 1977 that the pressuremeter modulus, if used directly, would give reasonable correlation with field measurements in residual soils.

A number of pressuremeter tests were analyzed by the author to evaluate the correlation between the pressuremeter modulus and the modulus of deformation as used in the strain distribution method. At this time, it is believed that the ratio in residual soils is probably somewhat higher than 1, and in sedimentary granular soils the modulus was found to be at least 2 to 3 times

TABLE 2 STRUCTURE COEFFICIENTS

Type of Material	Peat		Clay		Alluvium		Sand		Sand and Gravel	
	E/P	α	*E/P*	α	*E/P*	α	*E/P*	α	*E/P*	α
Overconsolidated	–	–	16	1	14	2/3	12	1/2	10	1/3
Normally consolidated	–	1	9-16	2/3	8-14	1/2	7-12	1/3	6-10	1/4
Weathered or altered	–	–	7-9	1/2	–	1/2	–	1/3	–	1/4

TABLE 3 SHAPE COEFFICIENTS FOR SETTLEMENT CALCULATIONS

	L/2R					
	1					
Shape Coefficient	Round Foundation	Square Foundation	2	3	5	20
λ_2	1	1.12	1.53	1.78	2.14	2.65
λ_3	1	1.1	1.2	1.3	1.4	1.5

Note: L = length of foundation.

the pressuremeter modulus. The 6- by 6-ft footing analyzed earlier by the Ménard method showed 0.8 in. settlement when this was calculated by the strain distribution method. In the sedimentary granular soils, the pressuremeter modulus is routinely used by a multiplier of 3 in these soils.

The successful use of the pressuremeter test in settlement evaluation is, however, predicated on an adequate number of tests. In many instances, the cost of adequate testing cannot be economically justified, especially in the case of smaller projects or where considerable variation in the soil profile is experienced. A logical solution appeared to be to establish a correlation with the standard penetration test that is routinely performed at frequent intervals on almost all jobs.

The evaluations were based on a great number of tests, which at first indicated no particular correlation. Then soil types were broken down by geologic origin, and correlations were attempted on that basis. Somewhat better results were obtained, and graphs (Figures 4 and 5) were developed for use with local soils.

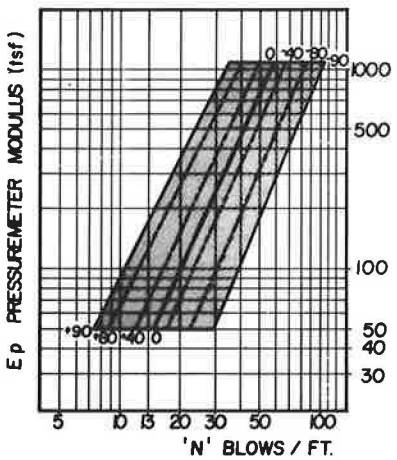

FIGURE 4 Correlation of pressuremeter versus standard penetration test for sedimentary granular soils.

The shaded areas indicate the possible correlation, which is relatively large and indicates that caution must be exercised. The percentage of tests covered above and below the weighted average, which is indicated by the center zero line, are also indicated. In practice the pressuremeter tests performed on a project are plotted on these sheets for each soil type and a typical correlation is developed. This correlation is then used for estimating modulus values between tests.

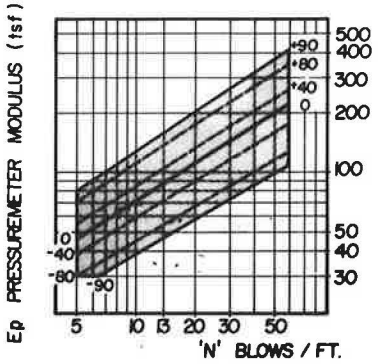

FIGURE 5 Correlation of pressuremeter versus standard penetration test for residual soils.

Various Other Uses and Applications

One of the most acceptable applications of the pressuremeter test for geotechnical design must be the horizontal capacity evaluation of piles. The analogy is obvious, considering that the pile in horizontal loading and the pressuremeter both create pressures on cylindrical holes. After closer evaluation, however, several significant differences must be considered, such as the asymmetrical loading of the pile, friction at the perimeter and the base, and so on.

Briaud et al. *(5)* in a paper on laterally loaded piles considers seven known methods of evaluating the horizontal pile capacity using the pressuremeter. In the method proposed by Briaud et al., the resistance is divided into front resistance and friction resistance at the sides. The equations as proposed are as follows:

$$Q(\text{front}) = P(\text{pmt}) \times B(\text{pile}) \times S(Q)$$

where

Q(front) = portion of soil resistance to pile movement resulting from front reaction, force per unit length of pile;
P(pmt) = net pressuremeter-test pressure;
B(pile) = the pile width or diameter; and
$S(Q)$ = shape factor = 1.0 for square piles and 0.75 for round piles.

$$y(\text{pile}) = y(\text{pmt}) \times [R(\text{pile})/R(\text{pmt})]$$

where

y(pile) = lateral deflection of pile,
R(pile) = pile radius,
y(pmt) = increase in radius of soil cavity in pressuremeter test, and
R(pmt) = initial radius of soil cavity in pressuremeter test.

$F(\text{side}) = s(\text{soil}) \times B(\text{pile}) \times S(F)$

where

F(side) = soil resistance resulting from friction, force per unit length of pile;
$S(F)$ = shape factor = 2 for square piles and 1 for round piles; and
s(soil) = soil shear stress obtained from the pressuremeter curve by the subtangent method of Palmer *(6)*.

The p-y curves are obtained by the addition of the Q-y curve and F-y curve at a particular depth, and a complete pile evaluation can be made. Briaud et al. report relatively good agreement with one instrumented horizontal pile load test.

In addition to the three applications included here, the pressuremeter is used in offshore engineering and many other specialty fields. It has proved to be a useful tool in testing before and after ground modification such as grouting and dynamic compaction, and considerable research work is still being done on use of the standard pressuremeter for evaluating clay soils. It may be noted that Schmertmann *(7)* recommends variable pressure differences between the measuring and guard cells to accommodate evaluation insensitive clays. Anderson et al. *(8)* in their research on the effects of creep on constant rate expansion during the pressuremeter test and on derivation of consolidation parameters from the test will consider special requirements on the speed and performance of the test.

For the engineering community using the regular pressuremeter, a standard procedure for performing the test is most important in order to obtain comparable and reproducible results. This need was recognized and a standard is under preparation at this time. The soon-to-be-issued ASTM standard will include the recommended procedures for preparing the borehole, calibrating the equipment, performing the test, and calculating the results. The engineering applications included here as well as the great number of other design methods available for the pressuremeter have made this instrument a valuable tool in the hands of the engineer.

REFERENCES

1. L. Ménard. Interpretation and Application of Pressuremeter Test Results. *Sols-Soils*, No. 26, 1975.
2. J. H. Schmertmann. Static Cone to Compute Static Settlement over Sand. *Journal of the Soil Mechanics and Foundation Division, ASCE*, Vol. 96, No. SM3, May 1970, pp. 1011–1043.
3. J. H. Schmertmann et al. Improved Strain Influence Factor Diagrams. *Journal of the Geotechnical Engineering Division, ASCE*, Vol. 104, No. 6T8, Aug. 1978, pp. 1131–1135.
4. R. Martin. Estimating Foundation Settlements in Residual Soils. *Journal of the Geotechnical Engineering Division, ASCE*, Vol. 103, No. 6T3, March 1977, pp. 197-212.
5. J. L. Briaud et al. "Laterally Loaded Piles and the Pressuremeter: Comparison of existing Methods." In *Laterally Loaded Deep Foundations: Analysis and Performance*. ASTM Special Technical Publication 835. ASTM, Philadelphia, Pa., 1985, pp. 97–111.
6. A. C. Palmer. Undrained Plane Strain Explansion of a Cylindrical Cavity in Clay: A Simple Interpretation of the Pressuremeter Test. *Geotechnique*, Vol. 22, 1972, pp. 451–457.
7. J. H. Schmertmann. *Pressuremeter Tests in Leda Clay*. Internal Report 450. Division of Building Research, National Research Council of Canada, Ottawa, Ontario, May 1979.
8. W. F. Anderson et al. "Pressuremeter Testing of Normally Consolidated Clays: The Effect of Varying Test Technique." *Proc., 20th Regional Meeting of the Geological Society*, University of Surrey, England, 1984, pp.21–32.

Publication of this paper sponsored by Committee on Exploration and Classification of Earth Materials.

Locating Subsurface Gravel with Thermal Imagery: Preliminary Results

DOUGLAS E. SCHOLEN, WILLIAM H. CLERKE, AND DOUGLAS E. LUEPKE

The subject of this paper is the correlation of thermal imagery with subsurface gravel deposits in vegetated areas where some ground surface is exposed. Geologic history was reviewed to select potential areas of study. An overflight was made using a thermal multispectral scanner. The data are processed with a computerized system to delineate areas showing a quartz spectral signature radiated from the ground surface. These areas were then compared with exploratory drill-hole data and found to correlate in every location where drilling had located substantial subsurface gravel. The correlation was noted during a search for gravel on national forest land in Louisiana. Processed data from an airborne scanner were compared with exploratory drill-hole logs. The correlation was noted at eight widely dispersed locations of subsurface gravel deposits. Areas without subsurface gravel showed negative correlation. It was concluded that more time and effort are needed to verify the usefulness of the correlation for locating new gravel pits.

The need for identifying and developing local sources of native road-surfacing materials for timber-haul roads has been determined by the Forest Service, U.S. Department of Agriculture (USDA), Southern Region and by the USDA Forest Service Washington Office. In the Southern Region, pits operated by the Forest Service are rare because of the high frequency of commercial aggregate pits over most of the region. A review of available geologic data has enabled the identification of areas most likely to contain usable materials. However, these areas are still too large in extent and too variable in rock content to allow cost-effective location of prospective aggregate pits.

Ample evidence attests to the extensive Pleistocene gravel deposits in the Kisatchie National Forest in Louisiana. These deposits vary in age from 800,000 to 80,000 years *(1)*. In the late 1930s units containing the gravels were mapped by Fisk *(2)*. Since that time, several large commercial gravel pits have been developed adjacent to and on national forest land under permit. This gravel was noted to be of chert origin *(2)*. Chert is a sedimentary rock consisting of a cryptocrystalline variety of quartz and amorphous silica *(3)*. A number of existing pits are in operation or have been exhausted, and continuing exploration by Forest Service engineering personnel and private operators under permit using exploratory drilling equipment has located other deposits. During the period 1982 to 1985, the Forest Service drilled more than 1,000 exploratory holes on the Kisatchie National Forest in search of gravel. This effort resulted in discovery of eight sites with a high potential for pit development and several others showing modest deposits. Commercial prospecting during that same period has yielded five sites. In spite of this effort, many square miles of the Kisatchie National Forest remain unexplored because of poor access and lack of information about likely sources. Although this tedious and often expensive trial-and-error drilling has had its intermittent successes, it is not a satisfactory method for long-range gravel resource management. Thus to obtain an improved overall understanding of the extent of gravel reserves, an investigation of the use of remote sensing was begun several years ago.

Attempts to use visible infrared and natural color aerial photography to identify subsurface gravel deposits failed completely. Publication of pertinent information *(4)* provided the inspiration for trial use of thermal imagery. In 1982 a study on the Kisatchie National Forest in Louisiana was proposed and discussions with the Earth Resources Laboratory (ERL) of the National Aeronautics and Space Administration at the National Space Technology Laboratory (Bay St. Louis, Mississippi) led to the initial acquisition of data, followed by several attempts at processing the data and correlating the obtained images with drill-hole data. The rationale and details of the effort are given in the following paragraphs.

EQUIPMENT

The thermal infrared multispectral scanner (TIMS) was developed by ERL as a definition tool for future satellite-borne, geology-oriented sensors. First flights for the completed instrument were made in summer of 1982 *(5)*. TIMS is an electro-optical line scanner currently operating in the airborne mode, sensing in six narrow bands in the range of 8.2 to 12.2 μm:

Band	*Spectral Coverage (μm)*
1	8.2-8.6
2	8.6-9.0
3	9.0-9.4
4	9.4-10.2
5	10.2-11.2
6	11.2-12.2

Average spectral sensitivity is approximately 0.1°C *(5)*. The higher sensitivity and multispectral capability of TIMS permit the detection of phenomena not detectable by commercially available devices. The sensor is flown in a Lear 23 aircraft. Instantaneous field of view (IFOV) and lateral coverage of flight lines are dependent on aircraft altitude. Within the operational limits of the Lear 23, between 2000 and 12 000 m, the altitude above terrain may be varied to provide an IFOV ranging from 5 to 30 m. For mapping aggregate deposits, an altitude of 12 000 m above the terrain provides data with 30-m pixels and a swath width of approximately 18.7 km.

USDA Forest Service, 1720 Peachtree Road, Atlanta, Ga. 30367.

DATA ACQUISITION

To acquire TIMS data for a specific location, a map of the proposed area with boundaries delineated is presented to ERL. Following a brief study, ERL provides a cost estimate and time periods available for the flight. The estimated cost must be funded before data acquisition from concurrent fiscal year funding. The use of TIMS is available only to government agencies. The actual flying time depends on weather as well as prior schedules. A 10-day period of no precipitation before the flight is necessary to prevent interference of surface moisture, and the air must be free of clouds or fog during operation of TIMS. Coordination between ERL and a ground station near the site is essential to a successful effort.

DATA PROCESSING SYSTEM

The Resource Evaluation and Monitoring Integrated Analysis System (REMIDAS) is a minicomputer-based system implemented by the Forest Pest Management (FPM) unit of the USDA Forest Service Southern Region in cooperation with the Georgia Institute of Technology Engineering Experiment Station (EES). The REMIDAS facility is located within the offices of the FPM Aerial Survey Team at the Southern Region, Doraville, Field Office. REMIDAS is designed to permit the compatible analysis of digital scanner data from collateral data such as soils and terrain. The components of the system are as follows:

1. Data General S250 integral array processor;
2. Ramtek high-resolution color display;
3. Two 1,600-byte-per-inch (bpi) tape drives;
4. Disk storage, 200-megabyte;
5. Digitized station (for input);
6. Electrostatic plotter (for output), 22 in.; and
7. Graphic camera (for output).

The current REMIDAS software was developed by EES. The bulk of this software supports the image-processing functions necessary for the display, rectification, classification, and enhancement of digital imagery. Digitizing and geographic data base capabilities are provided primarily for the integration of collateral data and to provide output compatible with user systems.

DATA PROCESSING PROCEDURES

Following acquisition, the high-density tape recorded on the aircraft is preprocessed by ERL. Computer-compatible tapes (1,600 bpi) in the standard ELAS band interleaved by line were provided to the Forest Service. This requires about a week. Once the data have been loaded into the REMIDAS system, density stretching by histogram equalization and level slicing are used for initial evaluation. The data are registered to map coordinates based on a linear transformation using the pixel coordinates of a series of readily identifiable points and nearest neighborhood resampling. Road intersections, often used as control points in registering satellite data in the visible and reflected infrared range, are more difficult to locate on thermal imagery. An enhancement procedure to separate road alignments from the remainder of the scene was developed by the authors and used to improve the location of road intersection control points.

PROPERTIES OF THERMAL IMAGES

Thermal imaging, with scanners in the thermal infrared band (8 to 13 μm), has been used successfully to identify sought-after subsurface materials with a thermal inertia substantially different from that of adjacent materials *(6,*pp.257–274). Examples are the delineation of boundaries between crystalline rocks and sedimentary rocks and the study of volcanoes *(7,*pp.275–296).

The apparent surface temperature is affected by the type of underlying material, providing an indicator of variation in subsurface materials across the landscape. This is because there is a substantial difference in thermal inertia between materials of different composition, for example, road-surfacing materials and the unusable materials generally found in association with them. High thermal inertia indicates a capacity for retaining heat. The ratio of thermal inertias of two adjacent materials provides a measure of the contrast to be expected in their thermal images. High ratios will result in greater contrast. Typical thermal inertia ratios *(6)* for dry materials of interest in road construction and surfacing are as follows:

Material	*Ratio*
Sandy gravel and sandy clay	2.0
Sandstone and shale	1.6
Granite and sandy soil	2.2
Granite and moist clay soil	1.2

The thermal inertia ratio diminishes with increasing soil moisture content because the high latent heat capacity of soil moisture can completely mask buried rock. Soil moisture can most easily be avoided during relatively dry fall weather following maximum summer heat penetration. Because the annual heating wave penetrates to depths of 20 m compared with 1.5 m for the diurnal wave, fall dates also provide periods of maximum thermal contrast between materials of different thermal inertia.

The spectral signatures of a variety of rock and clay minerals have been identified in the literature *(8,*pp.5–46). The 8- to 14-μm region is of particular interest because of the intense silicon-oxygen molecular band-stretching modes that occur and because of the minimum atmospheric absorption. The maximum silicon-oxygen stretching in quartz occurs in the 9- to 9.4-μm region, which coincides with TIMS Band 3 and results in notably low transmission on this band. This stretching also results in a moderate transmission at 8 μm (TIMS Band 1) and high transmission at 12 μm (TIMS Band 6). Other minerals have peaks and dips at different locations on the spectrum and thus can be differentiated from quartz. Figure 1 shows examples of the spectral signatures of quartz and other minerals *(8).*

In contrast to minerals, vegetation produces a nearly flat spectral signature in the thermal range, completely masking any mineral signature hidden by vegetation *(9,*pp.364–380).

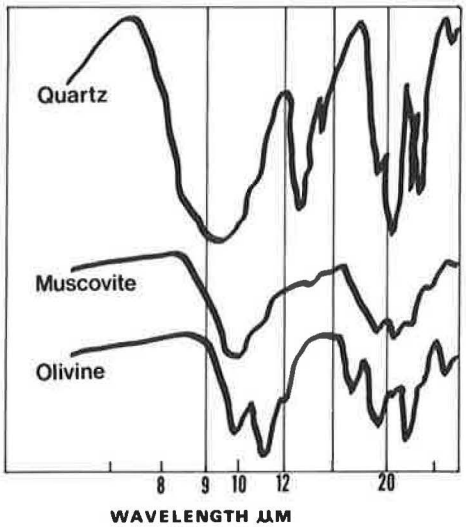

FIGURE 1 Spectral signatures of minerals.

Patches of surface soil among the vegetation must be visible from the air if the soil heat is to be recorded by TIMS.

INFLUENCE OF GEOLOGY AND VEGETATION

Thermal energy from the sun warms the earth's surface during the hot summer months. The heat flows downward toward cooler regions. Subsurface sandy gravel deposits have a higher conductivity and a lower heat capacity than overlying sands and sandy clays. These gravel deposits draw heat from the overlying materials.

By early fall when air temperatures are dropping and surface materials are losing their summer heat, the thermal conduction from these warmed gravel deposits is reaching a maximum. During the early morning hours when surface temperatures are low, heat from the warmer gravel, which consists mainly of quartz, flows upward toward the surface through the sands and clays. Thus when the radiation from the quartz layers surfaces through overlying layers of sand and is detected by the thermal sensors, it provides higher apparent temperatures than do adjacent areas without subsurface gravels. Figure 2 shows how a subsurface gravel deposit affects the surface temperature.

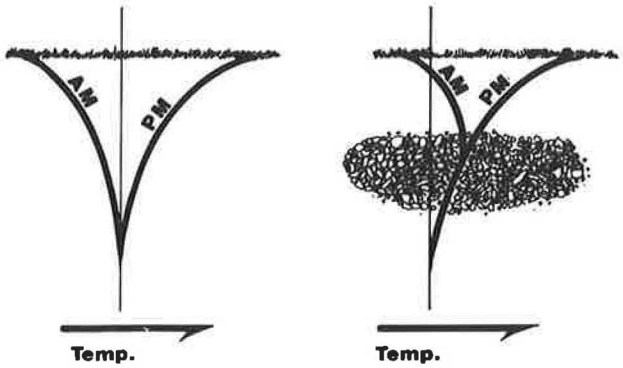

FIGURE 2 Effect of subsurface gravel deposits on surface temperature.

Because of local variations in surface temperature caused by vegetation and soil moisture, these differences in apparent temperature caused by subsurface gravels are not sufficient by themselves to identify a deposit. Geomorphic processes provide additional data required for detection. Gravels are laid down on steeper gradients than are fine-grained sediments. Over the broad areas necessary for detection by TIMS at 30-m resolution, these steeper gradients are maintained in the overburden as it is formed by deposition of finer-grained material. This results in a high velocity of flow for surface water, which carries the silt particles away and leaves a predominance of sands in contrast to the silts found on flatter adjacent areas. Thus the surface material overlying the gravel deposits has a high percentage of coarse-particled quartz sand (Figure 3).

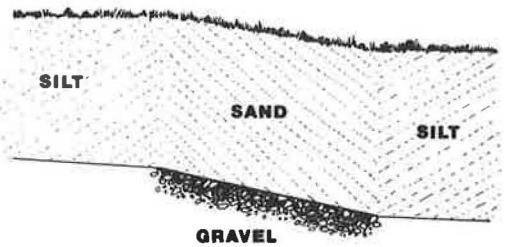

FIGURE 3 Ground slope effects.

The natural processes of silica diagenesis have the potential for enlarging the mineral grain size in surficial sands overlying chert gravel deposits. During the spring and early summer, when the water table is at the ground surface, evaporation can cause an upward flow of groundwater, bringing dissolved silica from the slightly soluble buried chert deposits and depositing opal silica overgrowths on the quartz sand crystals at the ground surface, which gradually increases their size *(10)*. Chert has a solubility that is 2 to 3 times that of igneous quartz *(10)*. Opal silica radiates a thermal signature similar to that of quartz *(8)*. Feder has discussed a similar phenomenon in which methane gas leaking from subsurface hydrocarbons caused ground surface alterations in vegetation and minerals that could be detected with thermal imagery, revealing the presence of the subsurface deposit *(11)*.

The finer-grained quartz in the silt range does not have an easily recognized spectral signature, in contrast to the sand- and gravel-sized quartz particles, which provide a pronounced spectral signature in the range covered by TIMS. Although much of the Southeast is vegetated, grass and tree cover is not continuous during the dry late summer, and frequent patches of unvegetated ground surface are visible from the air.

DATA ANALYSIS

For quartz deposits, the authors found that when Bands 6, 3, and 1 are displayed simultaneously in the red, green, and blue channels, respectively, on the REMIDAS color monitor, the surficial gravel deposits bare of vegetation show in red, and buried gravel deposits are in darker magenta because of the low reading in Band 3. However, not all dark areas are due to quartz, because certain ground conditions result in cooler tem-

peratures. To locate the quartz deposits, the spectral signature for each 30-m pixel must be inspected by reading and comparing the digital data from each of the three bands. REMIDAS software provides the capability of displaying the digital values of the three bands simultaneously on the monitor as the cursor is moved from pixel to pixel using a joystick.

To reduce the time requirements for pixel processing and to ensure that no critical pixels were missing, the authors developed a set of decision rules for detecting gravel deposits and separating buried from surficial deposits by comparing exploratory drill-hole data with the TIMS digital data. The authors noted that although areas containing surficial or shallow gravel deposits show an exaggerated quartz spectral signature, areas with deeper deposits show a more subdued signature.

For quartz identification, Bands 1, 3, and 6 are used in the decision process. In Figure 4 these bands (hatched areas) are shown superimposed on the quartz spectral signature. Signatures developed from TIMS data are shown in Figure 5 for several ground conditions. The final classification is obtained by level slicing the ratio of the differences between Bands 1 and 3 and Bands 3 and 6. To be considered for final classification, a pixel must meet three criteria. These criteria were selected by comparing the digital data with the drill-hole data from the same area.

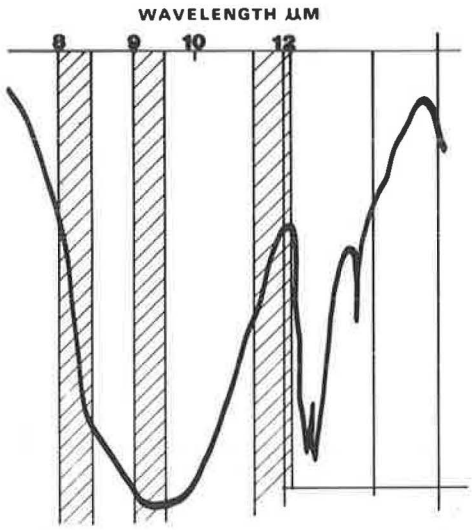

FIGURE 4 TIMS Bands 1, 3, and 6 superimposed on quartz spectral signature.

1. The digital count in Band 1 must be 4 or more counts higher than the count in Band 3. Drill-hole data examined from areas with less than this difference show only sand.
2. The digital count in Band 6 must be 9 or more counts higher than the count in Band 3. This difference was typical of areas containing gravel deposits.
3. The ratio $(6-3)/(1-3)$ must be 2 or higher as noted in all areas containing gravel deposits. Following further field study, this ratio was separated into ranges of 2.0 to 2.5, 26 to 3.0, 3.1 to 3.5, and greater than 3.5 to differentiate between the trace deposits of less than 30 cm and thicker, exploitable gravel deposits.

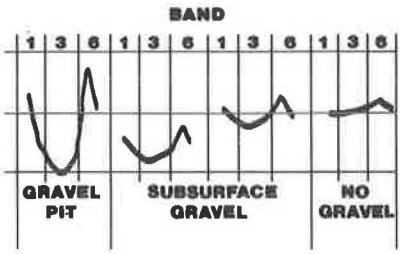

1. BAND 1 - BAND 3 › 3
2. BAND 6 - BAND 3 › 8
3. $\frac{\text{BAND 6 - BAND 3}}{\text{BAND 1 - BAND 3}}$ › 2.0, 2.5, 3.0, 3.5

FIGURE 5 Spectral signatures developed from TIMS data.

These criteria, summarized in Figure 5, were developed for a particular climate, location, and mineral and will differ in other situations.

INITIAL DEVELOPMENT PROJECT

An overflight by ERL using TIMS was programmed for October 1983 for the Kisatchie National Forest in Louisiana. The October date was chosen because at this time of the year, the earth has already soaked up the maximum solar heat for the year and surficial material is beginning to cool. The flight was made in the early morning hours between 2:00 and 4:00 a.m. to get maximum cooling of surface and maximum contrast with warm subsurface gravel deposits. A 10-day period without precipitation before the flight was noted by coordinating Forest Service personnel in the site vicinity. The October 1983 flight with TIMS was successful and usable imagery was obtained.

Following display and data analysis, areas in the imagery showing a quartz spectral signature were compared with exploratory drill-hole data and with locations of existing developed gravel pits. In every comparison (eight widely dispersed sites), locations of known deposits showed a quartz signature; surficial or shallow deposits showed the stronger signature and deeper deposits showed a more subdued signa-

FIGURE 6 Location of study area.

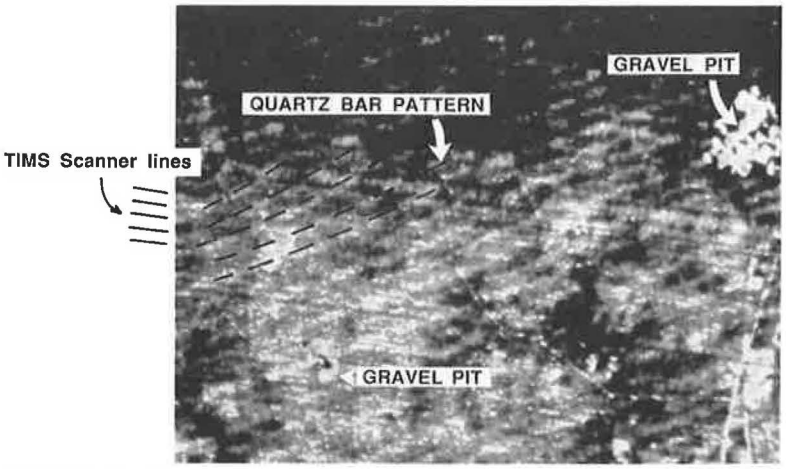

FIGURE 7 Processed thermal image scene, Evangeline District, Kisatchie National Forest.

ture. In no case did an explored area without gravel show a quartz signature of similar magnitude to that for the graveled areas. In those explored areas with very weak quartz signatures (i.e., Band 1 – Band 3 = 3 or less), the drill holes showed only sand.

The data selection criteria discussed previously were then used to code all pixels meeting the requirements for a quartz signature in a scene on the south end of the Evangeline District of the Kisatchie National Forest (Figure 6). These pixels were displayed in separate colors on the scene to show the locations of the areas emitting quartz signatures of each magnitude (Figure 7). In Figure 7 signatures of higher magnitudes are brighter shades of gray. This scene is the maximum that can be processed with currently available software.

GROUND VERIFICATION

In the initial study of the south end of the Evangeline District, the quartz spectral signature delineated a series of quartz bars running 30 degrees north of east across an area 7 mi wide (Figure 7). About 16 bars are discernible in the scene over a reach of 3 mi. Because these bars parallel the Pleistocene shoreline identified in the Louisiana geologic reports *(2)*, it is assumed that they were formed as the surf washed fines from the sand and gravel mixture and that successive bars formed as the ocean receded during the last period of glaciation. An extensive effort to correlate the images with vegetation, topography, water table, or system noise was made, but without success.

During 5 days of drilling allotted to verifying the thermal image developed in this scene, it was possible to drill at several isolated locations from the northeast corner of the scene to the west side and to drill a number of holes at a single location on the west side of the scene where a heavy concentration of quartz was indicated. Drilling sites were selected where existing roads intersected the bars of quartz signature or, for negative verification, where no quartz was indicated. A total of 13 holes were drilled; 9 were on quartz bars. Although no exploitable deposits of gravel were found during this period of drilling, trace deposits of 15 to 30 cm of gravel were noted at the same elevation in nearly every hole, which indicated that this layer is widespread across the scene. Depths vary from 8 to 18 m. Gravel particles recovered from the holes were uniformly thin, flat quartz "poker-chip" disks, suggesting prolonged erosion in the swash zones of Pleistocene beaches formed by a receding ocean shoreline as delineated in the image scene. The four holes selected for negative verification showed only sand. Although this effort was not extensive enough to prove out for the entire scene, the results were encouraging and were used as part of the criteria for differentiating between the trace deposits of 30 cm or less and the thicker exploitable gravel deposits.

Following separation of the data for the Evangeline scene into ranges, each range was assigned a different color in the resulting image to permit correlation with field data.

The resulting revised scene for the south end of the Evangeline District indicates that most of the gravel bars are trace deposits and that isolated thicker deposits are present in several areas, possibly representing accumulations from estuaries cutting through the ancient delta. Unfortunately the indicated thicker deposits are not in accessible areas. However, the procedure developed will be used to identify potential drilling sites as other scenes are processed.

CONCLUSIONS

The data obtained indicate that Bands 1, 3, and 6 of the TIMS data displayed simultaneously can be correlated with subsurface gravel deposits in vegetated areas where some ground surface is exposed. How reliable the method is for locating exploitable gravel deposits will require more time and effort to determine. Future study will concentrate on drilling indicated deposits located adjacent to proposed construction projects.

REFERENCES

1. H. A. Bernard and R. J. LeBlanc. "Resume of the Quaternary Geology of the Northwestern Gulf of Mexico Province." In H. E.

Wright, Jr., and D. G. Frey, *The Quaternary of the United States*, Princeton University Press, Princeton, N.J., 1965.
2. H. N. Fisk. Geology of Ayoyelles and Rapides Parishes. *Louisiana Geological Survey, Geological Bulletin 18*, Sept. 1940.
3. M. Gary et al. *Glossary of Geology*. American Geological Institute, Alexandria, Va., 1977.
4. B. S. and A. R. Gillespie. *Remote Sensing in Geology*. Wiley, New York, 1980.
5. F. D. Palluconi and G. R. Meeks. *Thermal Infrared Multispectral Scanner (TIMS): An Investigator's Guide to TIMS Data*. JPL Publication 85-32. Jet Propulsion Laboratory, Pasadena, Calif., 1985.
6. A. B. Kahle. "Surface Thermal Properties." In *Remote Sensing in Geology*, Wiley, New York, 1980.
7. F. F. Sabins, Jr. "Interpretation of Infrared Images." In *Remote Sensing in Geology*, Wiley, New York, 1980.
8. G. R. Hunt. "Electromagnetic Radiation: The Communication Link in Remote Sensing." In *Remote Sensing in Geology*, Wiley, New York, 1980.
9. G. L. Raines and F. C. Canney. "Vegetation and Geology." In *Remote Sensing in Geology*, Wiley, New York, 1980.
10. S. R. Aston. *Silicon Geochemistry and Biogeochemistry*. Academic Press, New York, 1983.
11. A. M. Feder. Contemporary Remote Sensing for Hydrocarbon Exploration and Development with Case Histories. *Oil and Gas Journal*, Sept. 23, 1985, pp. 160–171.

Publication of this paper sponsored by Committee on Exploration and Classification of Earth Materials.

Use of Rotational Erosion Device on Cohesive Soils

ROBERT P. CHAPUIS

Water erosion of cohesive soils is a complex phenomenon that includes different processes. A classification of erosion processes is proposed and examples are given in relation to highway construction. In the case of the scour resistance of solid clays, available prediction methods propose relationships between physical or mechanical parameters and the critical hydraulic shear stress (τc) that defines a boundary between erosion and no erosion, whereas erosion rates usually are not estimated. These methods have been questioned because it appears that the physicochemical parameters of both the clay and the eroding water control the erosion process. Subsequent research on these parameters has yet to yield reliable predictions based on indirect measurements. Consequently, it is deemed necessary to test the clay and eroding water for each case. In order to study the erodibility of solid cohesive soils, a rotational erosion device has been improved. Either intact or remolded samples can be tested, physicochemical parameters can be controlled, and the hydraulic shear stress (τ) and the erosion rate ($\dot{e}$) can be adequately determined. A relatively complete and accurate graph of $\dot{e}$ versus τ, including $\dot{e}$-values for τ-values lower than critical, can be established. The influence of water quality or of any stabilizing treatment of the cohesive soil may be quantitatively analyzed.

The erosion of cohesive soils may be an economically important problem that must be controlled in natural rivers and excavated irrigation and drainage channels, on natural and man-made slopes, and under highway pavements.

A solid cohesive soil may be eroded by the different processes shown schematically in Figure 1. They may be classified according to three criteria:

- Duration: occasional (O) or permanent (P),
- Type: steady (S) or unsteady (U), and
- Location: external (E) or internal (I).

Examples of erosion processes are given in Table 1. These processes produce sediments that are transported, sorted, and deposited and as such give rise to another problem, namely, the erosion of aqueous unconsolidated cohesive sediments.

Problems related to rain and wind erosion frequently occur in highway construction and have been covered in two TRB publications *(1, 2)*. This paper deals only with quantitative measurements of the scour resistance (external process) of cohesive soils, using a modified rotational erosion device that simulates an external erosion process.

A few researchers have attempted to use external erosion test results for predicting internal erosion *(3)* or, alternatively, pinhole test results for predicting external erosion *(4,pp.23–34)*. However, it is known that for certain clays, field observations of internal erosion do not substantiate the clay behavior during pinhole tests *(5,pp.74–93)*. Furthermore, it is believed that the internal and external erosion processes cannot be realistically compared *(6,pp.3–12;7, 8)*, even if they are influenced by many common factors.

Ecole Polytechnique, Mineral Engineering Department, P.O. Box 6079, Station A, Montreal, Quebec H3C 3A7, Canada.

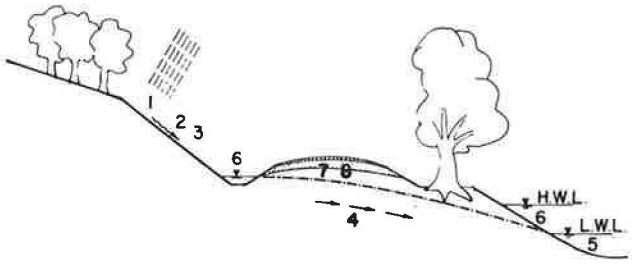

FIGURE 1 Different erosion processes involving cohesive soils (see Table 1).

BACKGROUND

For granular soils the water erosion processes are fairly well understood: they depend mainly on particle size, particle shape,

TABLE 1 EXAMPLES OF EROSION PROCESSES AND CLASSIFICATION ACCORDING TO DURATION, TYPE, AND LOCATION

Erosion Mode[a]	No., Figure 1	Example
OSE	1(2, 3)	Occasional steady rain erosion; splash, rill, and inter-rill erosions
	6	Occasional scour erosion of river above low-water line
OSI	4	Occasional internal erosion within clay foundation of road
OUE	1(2, 3)	Occasional nonsteady rain erosion
	6	Occasional scour erosion of clayey river soil caused by wave action or transported ice or debris influenced by frost action
OUI	7	Occasional dynamic erosion of clay due to traffic; end result, subbase contamination
PSE	5	Scour erosion in regulated canal
PSI	4	Internal erosion within clayey core of dam
PUE	5	Scour erosion of river under low-water line
PUI	8	Internal erosion of clay due to vibrating machine

[a]Duration: occasional (O) or permanent (P); type: steady (S) or unsteady (U); and location: external (E) or internal (I).

gradation, relative density, and the type and the amount of sediment present in the eroding fluid *(9)*. Much less is known for cohesive soils: erosion appears to be controlled by physicochemical factors. In sucessive state-of-the-art reports (*10–13*,pp.52–74) it has been concluded that the need to define the fundamental erosion processes of cohesive soils and to develop criteria and guidelines applicable to field problems is great.

Research on the erodibility of cohesive soils has been carried out by hydrotechnical and agricultural engineers and by soil scientists, who have oriented it to their needs. Hydraulic engineers use the hydraulic or tractive force defined as the shear stress induced on the soil surface by flowing water. They have defined a critical shear stress (τc) above which scour of a solid cohesive soil begins. To design a hydraulically stable channel, either a critical tractive stress or the corresponding safe water velocity (at a given depth and location) is selected to avoid undesirable erosion. Hydraulic engineers have proposed predicting τc from physical or mechanical properties.

Agricultural engineers are concerned with erosion control in permanent or temporary irrigation channels and with land erosion from rainfall in relation to damage to agricultural productivity. They take into account the influence of soil type, vegetation, and duration of rain or irrigation.

Research by soil scientists is often limited to regional aspects, and the mineralogical and chemical properties of the soil are systematically underlined.

From the available results, it appears that the erosion of cohesive soils is an interdisciplinary field and that the fundamental erosive actions are not fully understood. The electrochemical bonds between fine particles of cohesive soils have a marked influence on their erodibility. These bonds depend on many parameters, which in turn are influenced by the physicochemistry of the eroding fluid. All these factors play a great part in the complexity and the interdisciplinary character of the problem.

The external erosion of cohesive soils has been investigated with the following experimental techniques:

1. Submerged water jets perpendicular to a clay surface,
2. Open flume tests,
3. Channel tests, and
4. Rotating cylinder tests.

Techniques 1, 2, and 3 have yielded different design methods related to the physical or the mechanical properties of soils. However, their capabilities are limited: usually erosion is visually appreciated without any quantitative measurements. Furthermore, as mentioned by Berghager and Ladd *(14)*, most investigators do not adequately control the geotechnical properties of the clays.

For a better accounting of physicochemical factors, it was deemed necessary to devise new testing techniques that allow these factors to be controlled. The rotational erosion device was developed initially by Moore and Masch *(15)* at the University of Texas at Austin and has been modified by others. In the early 1960s, Epsey *(16)* and Masch et al. (*17*,pp.151–155) operated it with a mixture of water and glycerine and more recently a research team [Arulanandan et al. *(18, 19)*] at the University of California Davis Campus carried out extensive research with this technique. The research focused on remolded and reconsolidated samples of artificial clay mixes. It was shown that the critical shear stress depends on the combination of clay and eroding water and on the influence of physicochemical parameters such as the sodium absorption ratio and the concentration of pore-fluid ions. Predictive charts have been developed for certain remolded artificial soils *(20)*. No such data are available for undisturbed natural clays.

The principle of the rotational erosion device is to use an annular water flow around a stationary soil sample (Figure 2). When the outer plexiglass cylinder is rotated (at regulated speeds up to 2,500 rpm), rotation is imparted to the fluid, which in turn transmits a shear to the surface of the soil cylindrical sample. An erodibility test includes successive stages of constant revolutions per minute. For each stage, the erosion rate ($\dot{e}$) is defined as the sample loss (dry weight) per unit surface and per unit time. The shear stress acting on the soil cylinder is derived from the torque required to hold it stationary.

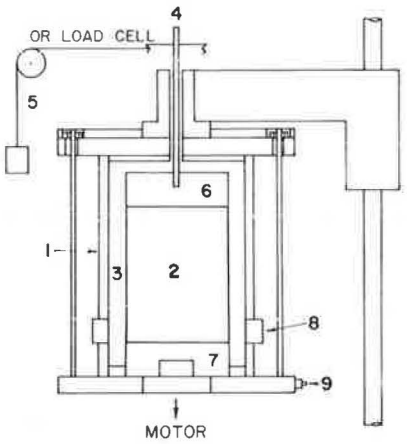

FIGURE 2 Rotational erosion device: *(1)* rotating external cylinder, *(2)* soil sample, *(3)* eroding water in annular space, *(4)* guiding shaft for installation, *(5)* torque measurement system, *(6)* head, *(7)* base, *(8)* access for cleaning, *(9)* gravity drainage.

Recent changes in the technical design and the test procedure for the rotational erosion device are discussed.

CHANGES IN TECHNICAL DESIGN

Intact or Remolded Samples

Previously only remolded cohesive soils or mixes could be tested in the rotational erosion device. In the Davis studies, a paste was prepared with distilled water, and a salt solution was then added to obtain a slurry. The salt solution consisted of predetermined amounts of Ca, Mg, K, and Na that matched as nearly as possible the chemical composition of the fluid extracted from the soil paste. The sample was then reconsolidated around a metallic shaft to which lower and upper plates were connected for support and trimming of the sample. The pro-

truding portion of the shaft was used to suspend the soil sample, which was positioned and guided only at one end.

For studies related to natural rivers or excavated channels, it is better to use intact samples. Thus, the apparatus was modified to accept either intact or remolded reconsolidated samples. The soil sample was mounted between two metallic short cylinders (base and head) of the same diameter, both guided in rotation by ball bearings (Figure 2). The shaft through the sample was eliminated. The base rotated freely relative to the bottom of the outer transparent cylinder. The torque transmitted by the eroding fluid to the soil cylinder was measured by means of an upper shaft connected to the head. Cell and sample rotations were completely independent.

The present device now allows for the study of either intact or remolded samples with an improved rotation guidance, a better alignment, a lower inherent friction, and a damped influence of end supports on the annular flow regime.

Measurement of Torque

Previously a known torque was applied to a dummy sample by means of a pulley-and-weight system, and the revolutions per minute (rpm) required to initiate the sample rotation were noted. The resulting calibration curve of the applied shear stress versus the rotation speed of the outer cylinder was used for real tests in which the clay samples were held stationary by a torsion wire. Thus, it was assumed that the clay sample was submitted to the same shear stress as that measured with the dummy sample for a given speed.

The preceding assumption was verified with the present device. Various torsion wires were tested and calibrated. None permitted a satisfactory determination of the shear stress acting on the clay surface.

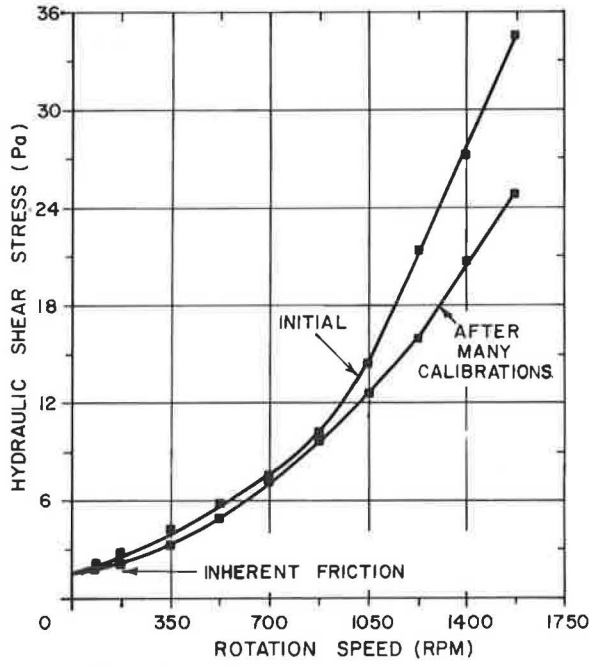

FIGURE 3 Variation of hydraulic shear stress at surface of sample of bituminous concrete versus rotation speed and number of calibrations.

The torque was then directly measured by using a pulley-and-weight system with masses ranging from 0 to 40 g at ±0.1 g. The initial tests on clays revealed that during multistage cycles of increasing and then decreasing rotation speeds, the shear stress may vary for the same rpm level. Because this phenomenon was not mentioned in the literature, different factors were considered, in particular, that of the accuracy of the measurements.

It was concluded that the shear stress acting on the soil surface depends on its roughness, in contradiction to Schlichting's equation *(21)* as presented by Arulanandan et al. *(18)*, and that this roughness is variable throughout a test because it depends on the erosive action. This conclusion became obvious after several calibrations of τ versus rotation speed had been attempted with the same sample of bituminous concrete, the surface of which became smoother as the number of calibrations increased (Figure 3).

Consequently the mean flow-induced shear stress can now be directly and continuously determined. During a stage at constant speed, the torque required to maintain the sample stationary may vary; normally it increases when particles detach and decreases when the eroded zones smooth and heal.

Measurement of Eroded Mass

Previously, before a multistage test, the sample was immersed in the eroding fluid for a period of 2 to 3 hr. At the beginning of each test stage (constant rpm), the sample with its internal shaft was immersed for 2 to 4 min to estimate the water uptake or expulsion. At the end of each 2-min stage, the sample was taken out and weighed. The difference in weight before and after each test stage, corrected for water uptake or expulsion, was considered to be the amount of eroded material. For shear stress values lower than critical, negative erosion rates were frequently calculated in the range 0 to -30 g/(m^2 · min) and down to -60 g/(m^2 · min).

This method was deemed questionable for two reasons: *(a)* the dripping sample was wiped and rapidly weighed, resulting in an approximate moist weight; thus, the small difference between two successive readings was quite inaccurate; and *(b)* repetitive manipulations disturbed the sample.

A new measuring technique was developed so that the clay sample need never be removed from the apparatus during the test. The eroding fluid was drained at the end of each test stage. The cell was then cleaned by means of a water aspiration system and rinsed with fresh eroding fluid. The amount of oven-dried eroded material was then weighed. These modifications allowed for a more accurate determination of both the shear stress and the erosion rate. In previous studies, the intercept on the τ-axis, corresponding to a zero erosion rate, was defined as the critical shear stress necessary to initiate important external erosion. With this device, the critical shear stress is defined as the point where the slope of the curve ($\dot{e}$, τ) changes abruptly.

Inherent Friction of Device

A good determination of the torque requires that the sample never be manipulated during the test: the only quantity attain-

able is the sum of the variable torque applied to the sample and that due to the inherent friction of the rotational device. The former depends on the roughness of the soil surface and on the rotation speed, whereas the latter is a mechanical rolling friction depending on the relative adjustment of the many coaxially rotating parts of the apparatus. If the cell is dismantled for sample removal at the end of each test stage, the resulting mechanical readjustments affect the inherent friction, which thus takes on as many different values as stages. However, if the sample is not manipulated, the inherent friction may be deemed constant throughout the test, and it is obtained by extrapolating the curve of τ versus rpm back toward the ordinate.

The inherent friction torque was much reduced through mechanical improvements of the rotational device and ranged from 0.05 to 0.30 N · cm. Maintaining such low values requires that some of the 10 coaxial ball bearings be replaced frequently because of abrasion by eroded sand and silt particles.

Protection of Sample Edges

In flume tests preferential erosion occurs at the contact interfaces of clay plates. Similarly, in the rotational erosion device preferential erosion frequently starts at the sample and head or base interfaces. To avoid this phenomenon, cylindrical steel foils are used to protect the contact interfaces.

SAMPLE PREPARATION

The natural clay samples must be cut from intact blocks using a template and a steel wire. The cohesive soils and the artificial mixes can be reconstituted and reconsolidated in a triaxial cell after physicochemical or mechanical treatment. In both cases, the rotational shear device allows for in situ conditions to be adequately respected.

The preparation method has a marked influence on erodibility test results. For example, the cutting of an intact sample with a thin-wall tube is not recommended: the sample surface is scaled because of surface remolding. In the case of remolded samples reconsolidated in an odometric cell, it is likely that the same surface problem would appear.

It was noted that triaxially prepared samples have a smoother and less erodible surface than samples cut from the same clay for shear stress values lower than critical. A schematic representation of this phenomenon is given in Figure 4: Curve A is for the cut intact samples, whereas Curve B is for the triaxially prepared samples of the same clay, remolded and reconsolidated at the same consolidation pressure. Generally, lower shear stresses develop at the same rotation speed on triaxially prepared samples (B): they rarely suffer from small aggregate loss before the shear stress threshold contrary to cut-sample behavior (A). This explains why Curve A is above Curve B before the critical shear stress is attained. It was also noted that the mean τc-value for the triaxially prepared samples (B) was higher than that for the cut intact samples (A). This fact may be related to the lower water content for B samples than for A samples, even if the consolidation pressure is the same. It may also be related to the horizontal consolidation pressure, which is lower for intact clays (A) than for remolded isotropically consolidated samples (B).

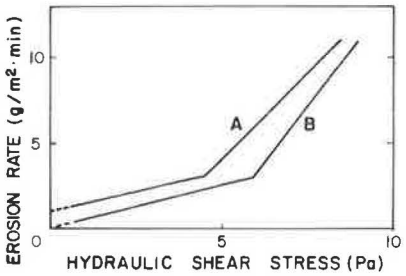

FIGURE 4 Schematized influence of sample preparation method: *(a)* intact clay samples and *(b)* triaxially prepared samples (same consolidation).

TEST PROCEDURES

A soil cylinder (75 mm in diameter and 89 mm high) is mounted coaxially on a pivoting base inside a transparent cylinder (102 mm in internal diameter) that can be rotated at a regulated speed up to 1,750 rpm. The annular space is filled with the water to be tested for its erosive properties. Rotation is imparted to the fluid by the rotating external cylinder, thereby transmitting a shear to the surface of the soil sample, which is held stationary by a pulley-and-weight system. Each test is composed of several stages at constant rotation speed, which in some respects is similar to the odometric testing procedure. A constant speed is held for 10 to 30 min and the torque is continuously recorded with a precision of 0.1 Pa for the τ-values. At the end of each stage, the fluid is drained and the cell cleaned with fresh fluid. All eroded particles thus

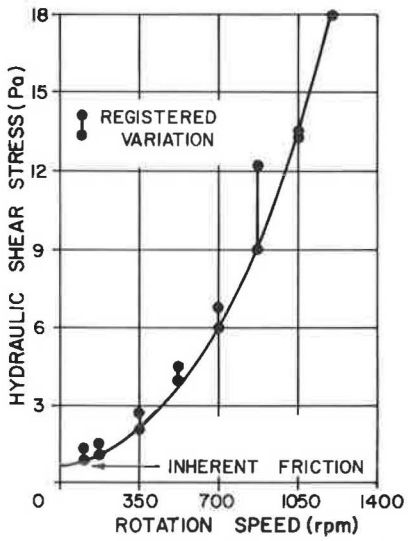

FIGURE 5 Variation of hydraulic shear stress acting on soil sample and minimum registered friction versus rotation speed.

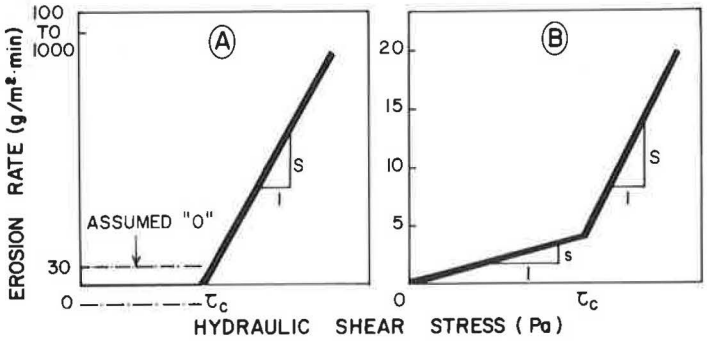

FIGURE 6 Typical results of erosion rate versus hydraulic shear stress: *(a)* earlier device (remolded samples only) and *(b)* device described in this paper (intact or remolded samples).

recovered are oven dried and then weighed at ±0.01 g. Once installed, the soil sample is never manipulated.

A test report includes a table of all measurements, a graph of the torque versus the speed (Figure 5) and a graph of the erosion rate $\dot{e}$ versus the contact shear stress τ.

For a good evaluation of the erodibility of a cohesive soil by a given eroding water, 6 to 10 samples are necessary. All test results are gathered to statistically determine *(a)* the τc-threshold above which the erosion rate $\dot{e}$ increases considerably and *(b)* the graph of the mean erosion rate [g/(m² · min)] versus the shear stress (Figure 6*b*). For natural clays, the usual range noted for $\dot{e}$ was 0 to 30 g/(m² · min) as compared with 0 to 1000 g/(m² · min) obtained by Arulanandan et al. *(18)* for artificial clayey mixes.

The influence of any treatment of the cohesive soil on its erodibility may be studied and the performance quantitatively evaluated in terms of the percentage of stabilizing agent (lime, cement, etc.). Similarly the influence of the water physicochemistry (pH, dissolved salts, cations, etc.) may be quantitatively analyzed.

APPLICATIONS

The rotational erosion device can be used for external erosion processes related to natural river diversions and excavated channels. It can also be used for erosion processes related to pumping by rigid pavements, a major contributor to their failure. If slab deflections occur, fines can be removed through pore-water pressure buildup in the subbase, or through water movements inducing surface erosion of subbase and shoulder materials. In recent research, Van Wijk *(22)* selected three testing procedures to investigate and characterize the erosion of rigid pavement subbase and shoulder materials: a brush test, a jetting test, and a rotational erosion technique with a device developed along the same lines as those used for the apparatus presented in this paper, after previous consultation with the author. The rotational erosion device gave the most useful results for cohesive and stabilized materials, according to Van Wijk *(22)*.

In the case of flexible pavements, pore-water pressure can build up in fine subgrade soils and some of the fines are removed and pumped out. This adversely contaminates the subbase aggregates: they are mechanically weakened, their permeability decreases, and their frost susceptibility increases. The performance of different geotextiles as separators has been investigated by Snaith and Bell *(23)*, Bell et al. *(24*,pp.429–434), Loubinoux et al. *(25*,pp.43–48), Salter *(26)*, Hoare *(27*,pp.423–428), Friedli and Anderson *(29*,pp.473–478), and Brochier *(30)*. According to the available results, it appears that no filter method will completely prevent fines contamination by pumping. Consequently, the erodibility of cohesive soils is still an important parameter to be evaluated for flexible pavements. This erosion is internal and of the OUI type: a reduced-scale-model method respecting physicochemical conditions is deemed more adequate than the rotational erosion device for simulating this erosion process.

CONCLUSIONS

The rotational erosion device is used for quantitative measurements of the scour resistance of cohesive soils. It has been modified to accept either intact or remolded cohesive soils, with an improved rotation guidance, a better alignment, a lower internal friction, and a reduction of the influence of end conditions of the fluid annular flow. The procedure to measure the eroded mass of soil has been modified. The major advantages of these modifications are that both the shear stress and the erosion rate can be determined more accurately and intact samples can be tested. Typical test results obtained with the improved devices are shown in Figure 6*b* and may be compared with those typically given by the previous apparatus (Figure 6*a*). This modified rotating-cylinder technique better meets the conditions required for a fundamental study of scour resistance of solid cohesive soils.

ACKNOWLEDGMENTS

This modified rotational erosion device was developed by Mon-Ter-Val Inc. for projects of the Société d'Energie de la Baie James (SEBJ). The author is indebted to J. Jacques Paré of the SEBJ for his support. The continuous support and interest shown by Roger Ethier of Mon-Ter-Val Inc. are gratefully acknowledged.

REFERENCES

1. C. E. Israelsen et al. *NCHRP Report 220: Erosion Control During Highway Construction: Research Report.* TRB, National Research Council, Washington, D.C., 1980.
2. C. E. Israelsen et al. *NCHRP Report 221: Erosion Control During Highway Construction: Manual on Principles and Practices.* TRB, National Research Council, Washington, D.C., 1980.
3. K. Arulanandan and E. B. Perry. Erosion in Relation to Filter Design Criteria in Earth Dams. *Journal of the Geotechnical Engineering Division, ASCE,* Vol. 109, No. GT5, 1983, pp. 682–698.
4. G. Lefebvre. "Geology and Slope Instability in Canadian Sensitive Clays." *Proc., 37th Canadian Geotechnical Conference,* Toronto, 1984.
5. O. Dascal, G. Pouliot, and J. Hurtubise. "Erodibility Tests on a Sensitive, Cemented Clay (Champlain Clay)." In *Special Technical Publication 623,* ASTM, Philadelphia, Pa., 1977.
6. J. L. Sherard, L. P. Dunnigan, and R. S. Decker. "Some Engineering Problems with Dispersive Clays." In *Special Technical Publication 623,* ASTM, Philadelphia, Pa., 1977.
7. R. Acciardi. Discussion: Erosion in Relation to Filter Design Criteria in Earth Dams (K. Arulanandan and E. B. Perry). *Journal of the Geotechnical Engineering Division, ASCE,* Vol. 110, No. GT7, 1984, pp. 996–999.
8. C. Kenney. Discussion: Erosion in Relation to Filter Design Criteria in Earth Dams (K. Arulanandan and E. B. Perry). *Journal of the Geotechnical Engineering Division, ASCE,* Vol. 110, No. GT7, 1984, pp. 999–1000.
9. W. H. Graf. *Hydraulics of Sediment Transport.* McGraw-Hill, New York, 1971.
10. E. Partheniades. Erosion and Deposition of Cohesive Soils. *Journal of the Hydraulics Division, ASCE,* Vol. 91, No. HY1, 1965, pp. 105–138.
11. Task Committee on Erosion of Cohesive Materials, Committee on Sedimentation. Erosion of Cohesive Sediments. *Journal of the Hydraulics Division, ASCE,* Vol. 94, No. HY4, 1968, pp. 1017–1049.
12. E. Partheniades and R. E. Paaswell. Erodibility of Channels with Cohesive Boundary. *Journal of the Hydraulics Division, ASCE,* Vol. 96, No. HY3, 1970, pp. 755–771.
13. R. E. Paaswell. "Causes and Mechanisms of Cohesive Soil Erosion: The State of the Art." In *Special Report 135: Soil Erosion: Causes and Mechanisms; Prevention and Control,* HRB, National Research Council, Washington, D.C., 1973.
14. D. Berghager and C. C. Ladd. *Erosion of Cohesive Soils.* Research Report R64-1. Department of Civil Engineering, Massachusetts Institute of Technology, Cambridge, 1964.
15. W. L. Moore and F. D. Masch. Experiments on the Scour Resistance of Cohesive Sediments. *Journal of Geophysical Research,* Vol. 67, No. 4, 1962, pp. 1437–1449.
16. W. H. Epsey, Jr. *A New Test To Measure the Scour of Cohesive Sediments.* Technical Report IIYD 01–6301. Hydraulic Engineering Laboratory, Department of Civil Engineering, University of Texas, Austin, 1963.
17. F. D. Masch, W. H. Epsey, Jr., and W. L. Moore. *Measurement of the Shear Resistance of Cohesive Sediments.* Publication 970. Agricultural Research Service, U.S. Department of Agriculture, 1963.
18. K. Arulanandan, P. Loganathan, and R. B. Krone. Pore and Eroding Fluid Influences on Surface Erosion of Soils. *Journal of the Geotechnical Engineering Division, ASCE,* Vol. 101, No. GT1, 1975, pp. 51–66.
19. K. Arulanandan, E. Gillogley, and R. Tully. *Development of a Quantitative Method To Predict Critical Shear Stress and Rate of Erosion of Natural Undisturbed Cohesive Soils.* Technical Report GL–80–5. U.S. Army Engineer Waterways Experiment Station, Vicksburg, Miss., 1980.
20. A. Alizadeh. *Amount and Type of Clay and Pore Fluid Influences on the Critical Shear Stress and Swelling of Cohesive Soils.* Ph.D. thesis. University of California, Davis, 1974.
21. H. Schlichting. *Boundary Layer Theory.* McGraw-Hill, New York, 1960.
22. A. J. Van Wijk. *Design To Prevent Pumping,* Resource Document 3: Rigid Pavement Pumping: Part 1—Subbase Erosion; Part 2—Economic Modeling. Purdue University, West Lafayette, Ind., 1985, 485 pp.
23. M. S. Snaith and A. L. Bell. The Filtration Behavior of Construction Fabrics under Conditions of Dynamic Loading. *Géotechnique,* Vol. 28, No. 4, 1978, pp. 466–468.
24. A. L. Bell, L. M. McCullough, and M. S. Snaith. "An Experimental Investigation of Sub-base Protection Using Geotextiles." *Proc., 2nd International Conference on Geotextiles,* Las Vegas, Nev., 1982, Vol. 2.
25. D. Loubinoux, Y. Faure, J. P. Gourc, and C. Machizaud. "Conservation de la Fonction Filtre des Géotextiles sous Solicitations Dynamiques et Statiques." *Proc., 2nd International Conference on Geotextiles,* Las Vegas, Nev., 1982, Vol. 1.
26. R. J. Salter. "An Experimental Comparison of the Filtration Characteristics of Construction Fabrics under Dynamic Loading." *Géotechnique,* Vol. 32, No. 4, 1982, pp. 392–396.
27. D. J. Hoare. "A Laboratory Study into Pumping Clay Through Geotextiles under Dynamic Loading." *Proc., 2nd International Conference on Geotextiles,* Las Vegas, Nev., 1982, Vol. 2.
28. P. Friedli and D. G. Anderson. "Behaviour of Woven Fabrics under Simulated Railway Loading." *Proc., 2nd International Conference on Geotextiles,* Las Vegas, Nev., 1982, Vol. 2.
29. P. Brochier. *Pouvoir Filtrant et Séparateur des Géotextiles.* M.Sc.A. thesis. Ecole Polytechnique de Montreal, Quebec, Canada, 1984.

Publication of this paper sponsored by Committee on Environmental Factors Except Frost.

Physical Properties of Southeastern Washington Loess Related to Cut Slope Design

LAWRENCE D. BEARD, JERRY D. HIGGINS, RICHARD J. FRAGASZY, ALAN P. KILIAN, AND ARTHUR J. PETERS

Loess is an aeolian soil consisting primarily of silt. The silt particles along with a lesser percentage of sand are coated by a clay binder, giving loess its unique structure. Because of the lack of development in the loessial soils of southeastern Washington, little is known about their engineering characteristics. However, recent highway construction requiring large cut slopes has prompted interest. The results of a literature review of engineering characteristics of loess and an evaluation of the physical properties of southeastern Washington loess related to design of cut slopes are presented. A map shows the general distribution of clayey, silty, and sandy loess. Results to date indicate that the basic physical properties of southeastern Washington loess are quite similar to those from deposits in the central United States. Water content tends to increase from west to east because of increasing clay content and precipitation to the east. Washington loess has a slightly lower plasticity than midwestern deposits, possibly because of greater illite and lower montmorillinite content. Based on experience in the midwestern United States and observations of existing cut slopes in southeastern Washington, design recommendations are presented. Near-vertical cuts are recommended in silty loess with low water content, and flatter cuts (approximately 2.5:1 H:V) are recommended in clayey loess and silty loess with high water content. Adequate surface drainage is a key factor of slope design.

Loess is an aeolian soil consisting primarily of silt-sized particles. The word "loess" is derived from the German word *lösen*, which means "to loosen or dissolve" and is descriptive of the structure associated with loessial soils. Major deposits of loess are located in China, Europe, and the United States. Although the most extensive deposits in the United States are located in the Midwest, a substantial portion of southeastern Washington is covered by loess. Loess is characterized by its loose structure of silt and fine sand particles coated by a clay binder. This structure allows vertical or near-vertical cuts exceeding 50 ft in height to perform exceptionally well, provided the water content remains low. Conversely, upon wetting, loess becomes relatively unstable and slope failures can occur in slopes as flat as 2:1 (H:V) *(1)*. In addition to slope failures, excessive settlement of foundations upon wetting (termed hydroconsolidation) is a well-known phenomenon associated with loessial soils.

When the structure of loess is considered, its adverse reaction to increased water content is easily understood. Because of the clay coating on the silt and sand particles, there is little intergranular contact, particularly at low confining pressures. Thus, most of the strength is attributable to the clay binder. At low water content high negative pore pressures develop in the binder, which increases shear strength. However, upon wetting, the negative pore pressures are reduced as water content within the clay fraction increases to near saturation. This leads to lower effective stress in the soil and therefore lower shear strength.

Hydroconsolidation is also a result of loess structure. As previously stated, loess exhibits a loose structure, that is, a high void ratio. Upon wetting, the reduction in shear strength allows the granular fraction to reorient, which may produce a denser soil (with a substantially lower void ratio) and large settlements.

The first comprehensive investigation of the physical properties that control the engineering behavior of loessial soils was performed by the Bureau of Reclamation on Missouri River Valley loess (2,pp.9–26). Following this work, research on other loess deposits was conducted primarily within Missouri, Iowa, Kansas, Tennessee, and Mississippi (*1,3–9,* pp.13–38; *10;11,* pp.01–020;*12*,pp.C1–C45). These works examined the variation of physical properties (gradation, plasticity, specific gravity, etc.) within deposits related to distance from the source and the influence of these properties on the engineering behavior of loess.

Because of the relative lack of development within southeastern Washington, very little research had been directed toward determination of the physical properties of the loess in that area. However, recent highway construction and realignment in southeastern Washington has produced many slope cuts that have suffered from erosion and slope stability problems related to the unique properties of loess. These problems have prompted the Washington State Department of Transportation (WSDOT) to begin research on the physical properties of southeastern Washington loess to determine how these properties relate to cut slope performance *(13)*.

Some of the principal components of the investigation are presented here: a review of previous research on the physical properties of loess related to cut slope design and a description of the physical properties of southeastern Washington loess. The literature review establishes the important physical properties that control (or help predict) engineering behavior of

L. D. Beard, J. D. Higgins, and R. J. Fragaszy, Department of Civil and Environmental Engineering, Washington State University, Pullman, Wash. 99164-2902. A. P. Kilian and A. J. Peters, Materials Laboratory, Washington Department of Transportation, Olympia, Wash. 98564.

loessial soils. Also, it includes a general description of physical properties of loessial deposits in the United States, which provides a basis for defining the similarities and differences between southeastern Washington loess and deposits from other locales. Samples collected throughout southeastern Washington were tested to establish the physical properties of the deposits. The laboratory tests included grain size distribution, Atterberg limits, and specific gravity. The test results define the basic characteristics of the deposit and reveal variations in physical properties with areal extent. Recommendations for improved cut slope design are developed on the basis of experience in similar soils in the central United States.

PHYSICAL PROPERTIES OF LOESSIAL SOILS

Characterization of Properties

One of the earliest comprehensive studies of the physical properties of loess was conducted by Holtz and Gibbs *(2)*. Although they were primarily interested in consolidation, basic laboratory tests including gradation, specific gravity, Atterberg limits, and shear strength were performed on a large number of samples. Grain size analyses revealed that the majority of samples fell within gradation limits defined as silty loess. Samples found to be finer than the boundaries established for silty loess were termed clayey loess, whereas coarser samples were categorized as sandy loess. A grain size distribution chart delineating these subdivisions is given in Figure 1.

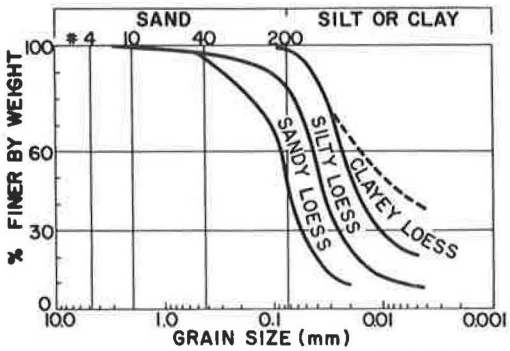

FIGURE 1 Range in grain size distribution for Missouri River Valley loess [after Holtz and Gibbs *(2)*].

Holtz and Gibbs *(2)* plotted the results of the Atterberg limits tests on a plasticity chart. A concentration of points with plasticity indexes ranging from 5 to 12 and liquid limits between 28 and 34 was found. Examination of these data in conjunction with the gradation analysis reveals that the concentration is indicative of silty loess. Furthermore, a more poorly defined grouping of higher plasticity index and liquid limits was found to coincide with gradation curves in the clayey loess range.

The investigators report that drained shear strength, as determined by triaxial testing, varies considerably with water content and to a lesser extent with dry density. Strength increased with decreasing water content and increasing density. The angle of internal friction remained fairly constant, ranging from 30 to 34 degrees, and the cohesion intercept increased rapidly as water content decreased. It is unclear to the authors whether these parameters reflect effective or total stress conditions. Gibbs and Holland *(14)* expanded the data base of the original work by Holtz and Gibbs. Additional laboratory tests as well as plate load and pile-driving tests were incorporated into the report. Results pertinent to strength properties remained essentially unchanged. The authors are currently conducting a comprehensive field and laboratory testing program including measurement of effective stress parameters for Washington loessial soils.

The relationship between water content and shear strength was more thoroughly explained by Kane *(15)*, who presented what he termed the "critical water content" concept. Unconsolidated-undrained (UU) triaxial shear tests were conducted at various water contents on undisturbed samples obtained from a site near Iowa City, Iowa. In addition, tests to measure negative pore-water pressures and volumetric strain with increasing water content were performed.

It was found that a critical water content can be determined such that an increase in water content beyond critical fills voids between particles and has little effect on the clay binder. As water content decreases below critical, negative pore-water pressures develop in the clay binder, leading to increased strength in the soil matrix. This concept has been applied by the Missouri State Highway Department as discussed in the following.

Chemical Composition

Montmorillonite or a combination of montmorillonite and illite are the dominant clay minerals for loess deposits in the central United States *(6, 8, 12, 14, 16)*. The clay fraction of Alaskan loess is predominantly chlorite with minor amounts of illite and possibly kaolinite *(17, p.67)*.

Calcite deposits in loess are generally found as discrete grains, root fillings, or nodules *(2, 14)*. In some cases a continuous layer or crust of calcite may form. This crust generally forms as the result of evaporation and has been observed on cut slopes in Mississippi *(12)*.

When present in sufficient quantities, calcite increases the dry strength of loess. However, because of the discontinuous nature of calcite accumulation, care must be taken when strength properties are determined for a specific site. If samples are obtained from a location containing a larger-than-average percentage of calcite, tests will indicate a strength higher than actually exists for the site as a whole.

Gradation and Plasticity

Figure 2 presents the combined grain size distribution for a number of locations in the United States. In general, the range in grain size distribution falls within the bounds established by Holtz and Gibbs *(2)* with the exception of Alaskan loess, which tends to be slightly coarser. The maximum grain size in loessial deposits examined within the continental United States is 2.00 mm, whereas analysis on Alaskan loess exhibits an upper limit

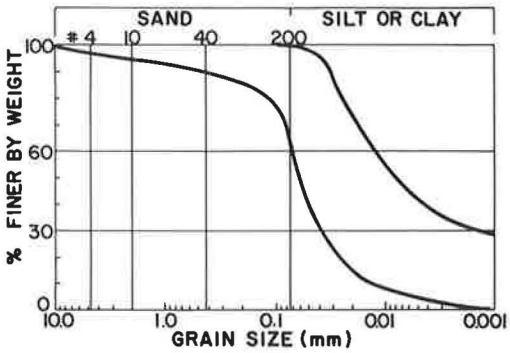

FIGURE 2 Range in grain size distribution of loess for Alaska *(18)*, Kansas *(16)*, Iowa *(17, 6)*, and Mississippi *(12)*.

of 9.53 mm. Present theory is that the particles in Alaskan loess larger than 2.00 mm may be carbonate concretions formed after deposition of the loessial unit, although testing has not been performed to substantiate this hypothesis *(19)*. The results of Atterberg limit tests from various investigations are shown in Figure 3.

Variability with Distance from Source

Although physical properties within a given deposit of loess tend to vary within narrow bounds, some trends have been noted with respect to the distance from the source. Investigations in the Midwest and South *(3, 5, 12)* indicate an increase in clay content and decrease in total thickness with distance from the source. These same studies show that in Iowa and Mississippi as clay content increases, silt content decreases and sand is a uniform, minor constituent. Variation in clay content tends to affect the engineering properties. As clay content increases, natural water content and density also increase *(4)*. Thus, natural water content and density can be expected to increase with distance from the source.

A linear relationship between thickness and the logarithm of distance from the source has been established *(5)* for midwestern loess deposits. Although this relationship is valid for some deposits, in many cases thickness is highly variable on a local scale and no clear trends are discernible. When a high degree of variability is encountered, it is usually due to hummocky terrain with maximum thicknesses near the crests of hills and minimal deposits in intervening depressions *(11)*.

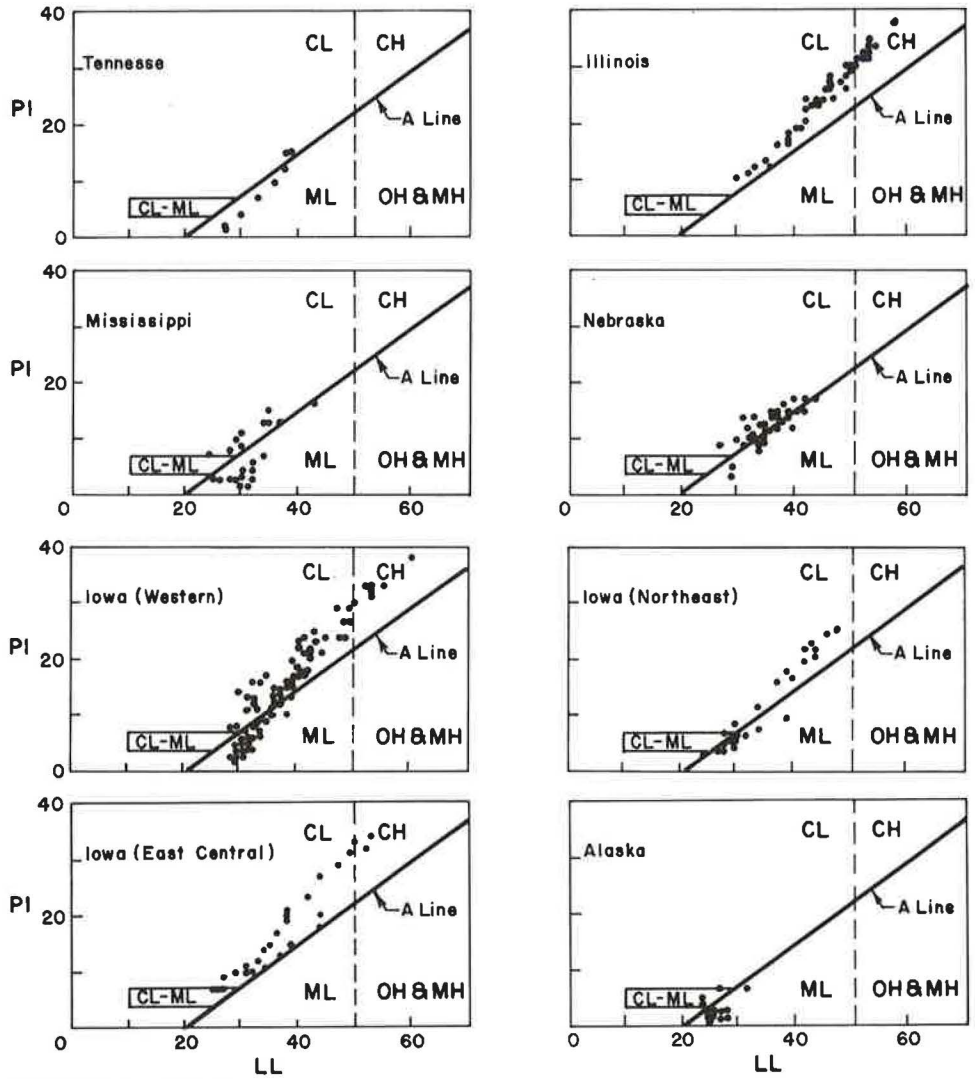

FIGURE 3 Plasticity data for loessial deposits throughout United States *(19)*.

Depth Effects

When the variation in textural composition with depth is discussed, it is not possible to generalize except to say that changes in the relative percentages of sand, silt, and clay constituents with depth are usually minor. In some areas sand content has been found to increase slightly with depth whereas clay size content remained constant or showed a minor decrease *(7)*. Conversely, some vertical sections exhibit a uniform percentage of sand with depth, whereas clay size content remains constant up to the base of the unit, where it increases slightly *(20)*. Except for isolated cases, constituent percentages do not vary more than 7 to 8 percent.

In-place density and natural water content demonstrate a more consistent trend with depth than does textural composition. Ignoring fluctuations in the upper 6 to 7 ft, both density and water content tend to increase with depth.

INDEX PROPERTIES OF SOUTHEASTERN WASHINGTON LOESS

Origin

Loessial deposits blanket the majority of southeastern Washington and extend into northern Idaho and northeastern Oregon. Traditionally the deposit has been subdivided into four loess formations: Palouse, Nez Percé, Ritzville, and Walla Walla. The earliest engineering reference to these subdivisions was by Eske (*21*, p.75) (Figure 4). The formation boundaries evidently are based on pedological classification; therefore their value with respect to engineering properties is questionable.

The source material for the southeastern Washington loess deposit is still a matter of debate. Various investigators have proposed sources ranging from northwest to southwest of the deposit; the Ringold formation, centered in the Pasco Basin west of the deposit, is the most widely accepted origin *(22)*.

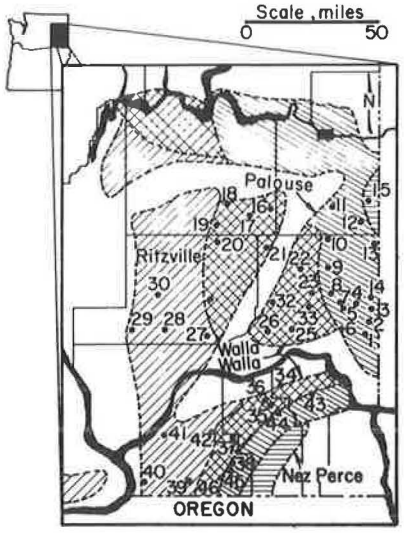

FIGURE 4 Southeastern Washington loess formations *(21)* and sample locations for field study.

Laboratory Testing Program

The primary goal of the sampling and testing program was to collect and evaluate a sufficient number of soil samples to delineate the variation in physical properties with location throughout the deposit. A total of 40 samples was collected from road cuts by hand augering. In general, samples were collected from the C horizon by augering horizontally into the road cut a minimum of 3 to 4 ft and sampling within the last foot. Samples were placed in plastic bags and immediately sealed to prevent moisture loss. An effort was made to pick sites evenly spaced throughout the study area. In this way trends in physical properties and the validity of the formation boundaries previously outlined could be evaluated. The sample locations are indicated in Figure 4.

Atterberg limits (liquid and plastic), grain size analysis, and water content were determined for 40 representative samples, and specific gravity was determined for 18 samples. All tests were performed in accordance with ASTM standards. These properties, particularly gradation and plasticity, have been found to influence engineering behavior strongly *(1, 2)* as well as to provide a basis for comparison with other deposits.

Specific Gravity

Specific gravity of southeastern Washington loess varies within narrow limits. Values range from 2.67 to 2.74 with a mean of 2.71 for the 18 samples tested. The consistency of the test results led to the decision not to conduct specific gravity tests on all samples. It was believed that the laboratory time could be better spent increasing the data base for grain size distribution and Atterberg limit tests.

Gradation

The range in grain size distribution of the 40 samples examined is shown in Figure 5 and corresponds closely with the boundaries established by Holtz and Gibbs. Of the samples tested 10 percent were classified as sandy loess, 68 percent as silty loess, and 22 percent as clayey loess.

The change in grain size distribution is a primary indicator of variation in physical properties with location for loessial soils.

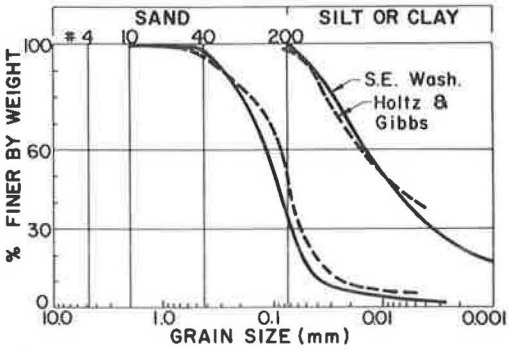

FIGURE 5 Range in grain size distribution for 40 samples of southeastern Washington loess.

As was established in the literature review, clay content, water content, and density all tend to increase with distance from the source. As the engineering behavior of loess varies with the aforementioned properties, definition of directional variation within the deposit becomes extremely important.

Although 40 samples do not constitute a large enough data base to provide a definitive answer with regard to source or distribution, they supply sufficient data to establish general

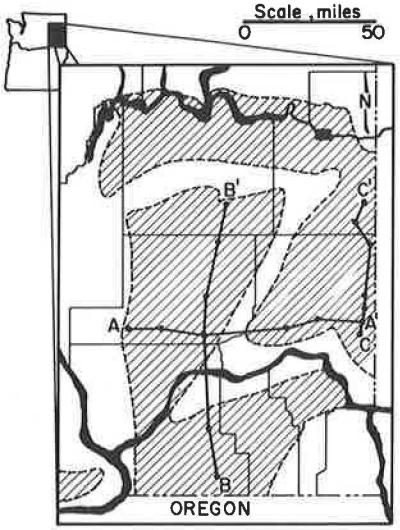

FIGURE 6 Location map for cross section *A–A′*, *B–B′*, and *C–C′*.

trends within the deposit that should be very helpful to engineering geologists and geotechnical engineers. Figure 6 shows the locations of three cross sections constructed through the deposits, one trending east-west and the other two north-south. In Figure 7, the east-west cross section *A–A′*, a general increase in clay size content and a decrease in sand to the east are

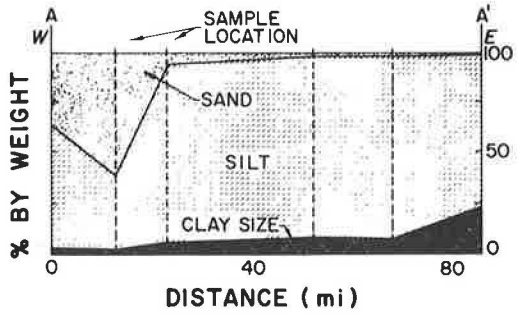

FIGURE 7 Cross section *A–A′*.

shown. In Figure 8, the westernmost north-south cross section *B–B′*, fairly constant clay-silt-sand ratios are revealed with only local fluctuations. The easternmost north-south cross section *C–C′* (Figure 9) is similar to that in Figure 8 in that the relative percentages of sand, silt, and clay size remain fairly constant. However, cross section *C–C′* has a higher clay size content and lower sand content than *B–B′*.

Clay size content (< 2 μm) was contoured for the study area

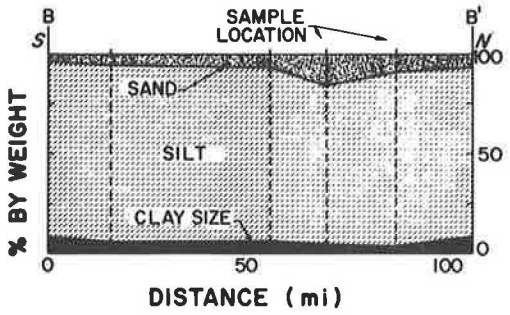

FIGURE 8 Cross section *B–B′*.

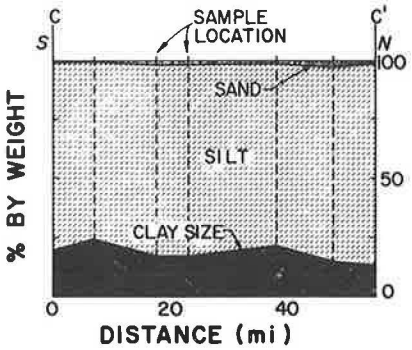

FIGURE 9 Cross section *C–C′*.

and is shown in Figure 10. Although anomalies are present, a definite trend of increasing content of clay-size material to the east is apparent. As established earlier, sand content decreases from west to east. These facts in conjunction with the cross sections suggest that the source material was to the west of the deposit with no major north or south directional component.

None of the data collected support the use as engineering units of formation boundaries shown in Figure 4. Although the subdivisions may be useful from an agricultural or pedological standpoint, the data clearly demonstrate that with regard to the

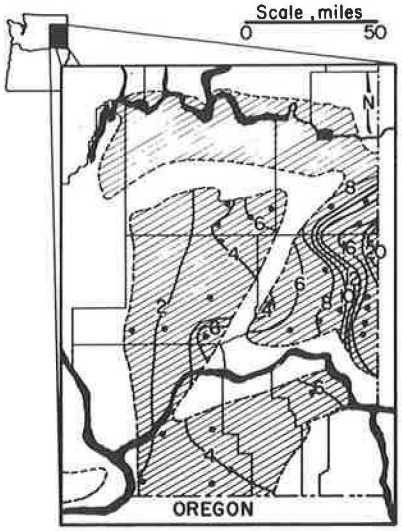

FIGURE 10 Generalized contour map of percentage content of clay-size particles for southeastern Washington loess.

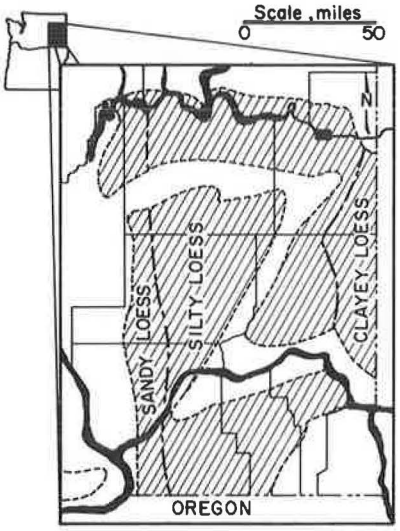

FIGURE 11 Approximate gradation boundaries for southeastern Washington loess.

properties mentioned earlier, variations can be expected to show east-west trends independent of formation boundaries. Figure 11 shows approximate gradation boundaries for southeastern Washington loess based on testing to date.

Figure 12 shows a typical vertical profile at sampling site B–25 determined from five discrete sampling points. Little variation in the relative percentages of the sand, silt, and clay fractions is shown. Although the percentage of sand-size particles varies by less than 1 percent, the clay-size material (< 2 μm) varies up to 5 percent, which is still relatively minor for a natural soil.

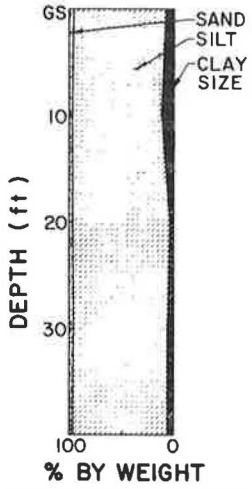

FIGURE 12 Typical variation in textural composition with depth.

Density

Although in situ densities were not measured, limited data are available from a previous investigation. Lobdell *(23)* reported dry densities ranging between 95 and 98 pcf in Palouse loess. These densities were determined from block samples in the form of 6-in. cubes from an excavation site at Washington State University. Thus, the values Lobdell reported should be an accurate indication of in situ dry density for the eastern extreme of the deposit. As discussed previously, density tends to increase with distance from the source. Because the source is to the west of the deposit, it is likely that in situ density increases from west to east. Thus, it is assumed that the density data reported by Lobdell provide an upper bound for the deposit.

Water Content

From the 40 samples tested, natural water content was obtained for 22 sites throughout the study area. From the samples tested, water content ranged from 4.5 to 27.7 percent. As might be expected, water content shows a high degree of variability from location to location. Even so, water content generally tends to increase from west to east. The directional variation in water content may be attributed to two factors. First, content of clay-size material increases from west to east as determined by the grain size analysis. As previously indicated, water content tends to increase with increasing clay size content. Second, mean annual precipitation tends to increase from west to east by as much as 100 percent.

Plasticity

Plasticity characteristics were evaluated by the Atterberg limit tests. Plastic and liquid limit tests were conducted on 40 samples and plotted on a plasticity chart (Figure 13). Examination of the plot and the grain size distributions reveals two groupings of the data. Silty loess tends to have liquid limits ranging from 14 to 32 and plasticity indexes of 0 (nonplastic) to 11. Clayey loess has liquid limits that vary between 33 and 49 with

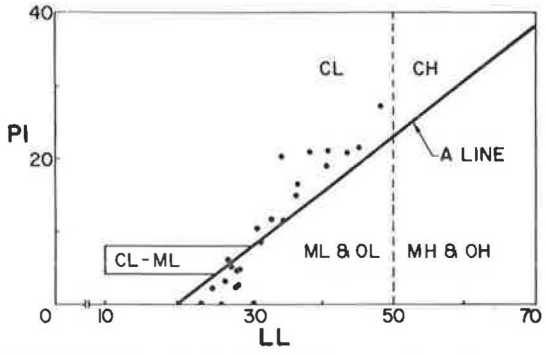

FIGURE 13 Plasticity data for southeastern Washington loess.

plasticity indexes ranging from 11 to 27. The two sandy loesses tested were nonplastic.

Calcium Carbonate

During field sampling, various forms of calcium carbonate were encountered. In most cases calcite was present as either root fillings or nodules. To a lesser extent calcite was found to exist as indurated sheets lying 6 in. to 1 ft behind the surface of a cut face. This appears to be an evaporation phenomenon similar to that noted in Mississippi *(12)*. Because of the discrete nature of most calcite deposits, the absence of calcium carbonate in an area where it might be expected does not necessarily imply that it is absent from the area as a whole.

It would appear that the presence or absence of calcium carbonate is related to mean annual precipitation. In areas averaging more than 20 in. of precipitation per year, no samples containing calcium carbonate were encountered. Conversely, a large majority of samples collected in areas where mean precipitation was less than 15 in. contained significant quantities of calcite.

Relationship Between Southeastern Washington Loess and Other Deposits

On the basis of these laboratory results, southeastern Washington loess appears similar to loessial deposits within the central United States. The range of grain size distribution is very similar to that found by Holtz and Gibbs *(2)* for Missouri River Valley loess and to the other deposits reported previously. Plasticity tends to be slightly lower in Washington loess than in other deposits, possibly because of greater illite and lower montmorillinite content *(23)*. Other properties such as calcium carbonate occurrence, variation of textural components with depth and distance from the source, as well as specific gravity appear consistent with results obtained for other deposits.

Therefore, it should be expected that the engineering behavior of southeastern Washington loess will be similar to that in the deposits in the central United States, and thus design experience from other loess areas should be helpful in the Washington deposit. Any differences in failure modes probably would be the result of the variation in climatic conditions between the Northwest and the Midwest.

CUT SLOPE DESIGN EXPERIENCE

Some of the most recent and comprehensive published data on cut slope design and performance in loess was provided by the Missouri State Highway Department (MSHD) *(1)* and the Tennessee Department of Transportation (TDOT) *(9, 10)*. The MSHD conducted an extensive study of cut slope design in loess, which resulted in correlation of the type and degree of failure, exposure, slope, moisture content, and loess type for 106 cut slopes. As a result, design specifications were developed that are based on two main criteria: *(a)* gradation boundaries similar to those established by Holtz and Gibbs *(2)* and *(b)* Kane's critical water content concept *(15)*.

The Missouri study concluded that vertical cuts perform well in silty loess if water content remains less than 17 percent (slightly higher water content is acceptable if slope exposure falls between southeastern and southwest).The cut is typically benched when the total height exceeds 25 to 35 ft, and benches 15 to 20 ft wide are placed approximately every 20 ft vertically. The benches help limit erosion of the cut face and provide increased stability of the overall slope.

Flattened slopes are recommended for silty loess with high water content and for all cuts in clayey loess. The Missouri study found that 2:1 slopes are generally flat enough from the standpoint of stability; however, slopes flattened to 2.5:1 show much less degradation by erosion. Whether vertical or flattened slopes are employed, a drainage diversion around the crest of the slope is an important design consideration.

The TDOT *(9, 10)* reported that vertical cuts in silty loess have performed better than flattened slopes. The flattened slopes experience significantly more damage from erosion of the face of the cut. Contrary to these findings, TDOT designs cut slopes 2:1 or flatter with 15- to 25-ft benches at 20- to 25-ft vertical intervals (Royster, unpublished data).

Regardless of the slope cut, Royster *(9)* and Royster and Rowan *(10)* stress the importance of surface drainage around the slope face and at the toe of the slope as well as erosion protection of the drainage channel by paving, sodding, or seeding.

WSDOT cut slope design criteria have varied somewhat over past years. Near-vertical cuts as well as many flattened slopes have been constructed; however, surface drainage structures frequently have been left out of the slope construction, or if built they often have been inadequate. WSDOT has constructed a number of near-vertical cuts (0.5:1 to 0.25:1) in silty loess in recent years, whereas the most common practice in clayey loess has been 2:1 cuts. An examination of selected cuts in eastern Washington during the spring of 1985 indicated a number of failure problems similar to those reported in Missouri. These are analyzed in detail by Higgins et al. *(13)*.

In general, vertical cuts appeared to be performing well in silty loess where the natural drainage diverted flow away from the cut face. Where surface water was allowed to accumulate near or flow over the slope face, severe damage was experienced because of erosion and piping (Figure 14). The area defined in Figure 11 as silty loess is relatively dry (generally less than 15 in. of annual rainfall). Therefore, the soils maintain a low water content, which would appear to be an ideal situation for the use of vertical cuts. The key design factor is adequate drainage.

Many slopes flattened to approximately 2:1 have been constructed in both silty and clayey loess in the eastern part of the deposit. Annual moisture in this area ranges from 15 to 20 in., much of it in the form of snowfall. In the spring, the upper few feet of soil often become saturated from snowmelt or rainfall or both, and shallow slides (or flows) of vegetation and a thin layer of soil result. These slides were very common during the spring of 1985 and ranged from small scale (1 to 10 ft wide with a depth of failure ranging between inches and 4 ft) to much

FIGURE 14 Erosion and piping damage in near-vertical cut in loess.

larger scale, involving the entire cut (Figure 15). In most cases the initial failure was followed by increased erosion due to the loss of vegetative cover with severe gully erosion a common result. A number of the cut slopes examined in the eastern part of the deposit have experienced this type of failure in the past, and as a result erosion gullies ranging up to 2 ft deep have formed on the cuts. Clearly, cuts of 2:1 in clayey loess are too steep to maintain a vegetative cover.

FIGURE 15 Shallow failure of road cut in loessial soils under melting snowdrift.

PRELIMINARY DESIGN AND MAINTENANCE GUIDELINES

Recommendations

On the basis of the similarities between the physical properties of southeastern Washington loess and loess in the central United States and the similarities in failure modes of cut slopes established in this paper, preliminary design and maintenance guidelines for routine cuts in loess slopes have been recommended. WSDOT will implement these guidelines in test sections over the next 2 years. These test sections will include some experimentation in use of slope angles, drainage ditch liners, and so on, to find the optimum design. Design of very deep cuts (much more than 50 to 60 ft) probably would require a more detailed investigation and analysis than that recommended here; that is, shear strength parameters and a slope stability analysis may be needed. The following recommendations rely heavily on the experience of MSHD *(1)*, TDOT *(9, 10)*, and observations of cut slope failures in southeastern Washington *(13)*.

Vertical Versus Flattened Slopes

If the soil at the site of the proposed cut is a silty loess with water content below critical, near-vertical cuts (0.25:1) may be considered. If vertical cuts are used they should be benched on approximately 20-ft vertical intervals when the total height of the cut exceeds 25 to 30 ft. Benches should be 15 to 20 ft wide and gently sloped toward the back of the cut. If either water content exceeds critical (17 percent can be used as an approximation based on experience in the Midwest) or the soil is a clayey loess, flattened slopes should be used. Generally 2.5:1 slopes should perform adequately, but if a water table is intercepted, flatter slopes may be required because of seepage forces. Although design criteria have not been developed for sandy loess, it is believed that content of clay-size material would be so low that vertical cuts would perform poorly.

Erosion Control

Erosion control practices similar to those reported by Royster *(9)* are suggested for Washington loess. With the possible exception of short excavations through small lobate ridges of loess, a drainage ditch approximately 10 to 15 ft behind the top of the cut should be constructed before the slope cut is made. The ditch should be seeded or lined, depending on the gradient. The drainage ditch should be constructed before the opening of the cut with as little disturbance to the surrounding vegetation as possible. Once the cut has been made, construction equipment should be kept away from the crest. If natural drainage channels are truncated by a cut, the drainage system should be adequate to transmit the flow around or over the cut face in protected channels or pipes.

Standard farming techniques in southeastern Washington entail cultivating to the edge of road cuts. This practice is not acceptable if the ditches above the slope crest are to remain operable. Continued cultivation over a drainage ditch will ultimately destroy its effectiveness. Therefore, the most desirable location for thedrainage ditch would be within a protected right-of-way.

It is suggested that for new construction, drainage ditches should be constructed approximately 10 ft away from the toe of the slope, and the ground surface should be gently sloped toward the ditch. Any material that spalls downslope between the toe and the ditch should be left in place. This practice will serve two purposes: *(a)* the spalled material will help protect and stabilize the toe of the slope, and *(b)* the location of the ditch will prevent maintenance equipment from accidentally undercutting the toe of the slope while the ditch is being cleaned.

In cases where benched cuts are required, the benches should

be seeded or sodded. If the upper drainage system is properly constructed, it should not be necessary to employ ditches on the benches or use erosion control methods in excess of vegetative cover unless extremely long cuts are made.

Side ditches offer some of the most severe erosion problems. Gradients are generally steeper than along the cut and flows tend to be higher because of the concentration from various sources. In many cases it has been necessary to pave ditches or use halved culverts to prevent erosion.

If a flattened slope is constructed, the cut should be seeded immediately following construction. In addition, a protective cover should be placed over the slope, either a straw mulch or a synthetic material. These covers serve the dual purpose of preventing raindrop erosion, a major cause of erosion on newly opened cuts, and helping to retain moisture required to initiate a vegetative cover.

Periodic Maintenance

Because of its highly erosive nature, loess slopes will deteriorate rapidly once erosion has been initiated. Thus it is important to repair any erosion damage as soon as it is discovered. Maintenance may require repairs to, enlargement of, and removal of siltation from existing ditches. Increased erosion protection, such as installation of liners or filters in ditches or in some cases construction of drainage facilities where they were previously believed to be unnecessary, may be required.

Vegetative cover requires periodic attention. In order to maintain a heavy ground cover, fertilizer must be applied every 3 to 5 years (on the basis of experience in the Midwest). In addition, some areas will not seed well the first time and may require a second and possibly a third seeding.

Removal of sediment from toe ditches on existing slopes should be done carefully to avoid undercutting of the toe of the slope. Even minor undercutting will cause at least some sloughing, and therefore the grader blade should not contact the slope cut.

CONCLUSIONS

Previous investigations have demonstrated that loessial deposits from the central United States exhibit similar physical properties. Gradation generally falls within the range reported by Holtz and Gibbs *(2)* for Missouri River Valley loess. Plasticity characteristics are similar, provided the samples fall within the same gradational subdivision (sandy, silty, or clayey).

Analysis of samples from southeastern Washington loess reveals that the deposit is similar to deposits from the central United States. Gradation curves fall within the range reported by Holtz and Gibbs *(2)* and indicate a westerly source. Grain size distribution ranges from sandy loess at the western extremity of the deposit to clayey loess near the eastern boundary. No major north-south trend was observed.

Plasticity characteristics are similar to those for midwestern deposits. However, plasticity did appear to be slightly lower for southeastern Washington loess. Lower plasticity may be due to a higher illite and lower montmorillonite content than that found in midwestern deposits. The only substantial difference between Washington loess and deposits from the central United States that may affect engineering behavior is climatic and not due to physical properties.

Design criteria for routine cuts in loess in southeastern Washington have been recommended on the basis of studies in midwestern loess and observations of cut slope failures in the Washington deposit. Near-vertical cuts are appropriate in silty loess with low moisture content. Flatter cuts (2.5:1 or less) should be most suitable in all clayey loess and silty loess with a high moisture content. No matter what slope angle is excavated, a major part of the design is diversion of surface water around the slope cut. Extremely large cuts should be designed on the basis of a detailed analysis that includes an evaluation of shear strength parameters and a slope stability analysis.

ACKNOWLEDGMENTS

This paper is the direct result of work supported by the Washington State Department of Transportation and FHWA, U.S. Department of Transportation. The authors gratefully acknowledge G. Scott Rutherford and Keith Anderson of WSDOT for their strong support and review of this work.

REFERENCES

1. *Development of Design Criteria for Cut Slopes in Loess.* Missouri State Highway Department, Jefferson City, 1978, 78 pp.
2. W. G. Holtz and H. J. Gibbs. "Consolidation and Related Properties of Loessial Soils." In *Proc., Symposium on Consolidation Testing of Soils,* Standard Technical Publication 126, ASTM, Philadelphia, Pa., 1951.
3. A. R. Dahl, R. L. Handy, and D. T. Davidson. Variation of Loess Thickness and Clay Content in Southern Iowa. *Proc., Iowa Academy of Science,* Vol. 64, 1952, pp. 393–399.
4. D. T. Davidson and R. L. Handy. Property Variations in the Peorian (Wisconsin) Loess of Southwestern Iowa. *Proc., Iowa Academy of Science,* Vol. 59, 1952, pp. 248–265.
5. R. L. Handy. Loess Distribution by Variable Winds. *Bulletin, Geological Society of America,* Vol. 87, 1976, pp. 915–927.
6. R. L. Handy, C. A. Lyon, and D. T. Davidson. Comparisons of Petrographic and Engineering Properties of Loess in Southwest, East-central, and Northeast Iowa. *Proc., Iowa Academy of Science,* Vol. 62, 1955, pp. 279–297.
7. C. A. Lyon, R. L. Handy, and D. T. Davidson. Property Variations in the Wisconsin Loess of East-central Iowa. *Proc., Iowa Academy of Science,*Vol. 61, 1954, pp. 291–312.
8. C. F. Crumpton and W. A. Badgley. *A Study of the Clay Mineralogy of Loess in Kansas in Relation to its Engineering Properties.* State Highway Commission of Kansas, Topeka, 1965, 68 pp. NTIS: PB 173038.
9. D. L. Royster. "Engineering Characteristics of Loessial Soils in Western Tennessee." In *Proc., 45th Annual Tennessee Highway Conference,* Bulletin 29. Engineering Experiment Station, University of Tennessee, Knoxville, 1963.
10. D. L. Royster and W. H. Rowan. "Highway Design and Construction Problems Associated with the Loessial Soils of West Tennessee." In *Highway Research Record 212,* HRB, National Research Council, Washington, D.C., 1968, pp. 28–32.
11. C. R. Kolb. "Physical Properties and Engineering Characteristics of Mississippi Loess." In *Field Trip Guidebook: Mississippi Alluvial Valley and Terraces,* Geological Society of America, Boulder, Colo., 1965.
12. E. L. Krinitzsky and W. J. Turnbull. "Loess Deposits of Mississippi." In *Field Trip Guidebook: Mississippi Alluvial Valley*

and Terraces, Geological Society of America, Boulder, Colo., 1967.
13. J. D. Higgins, R. J. Fragaszy, and L. D. Beard. *Development of Guidelines for Cuts in Loess Soils.* Final Report WA-RD69.1. Washington State Department of Transportation, Olympia, 1985, 96 pp.
14. H. J. Gibbs and W. Y. Holland. *Petrographic and Engineering Properties of Loess.* Engineering Monograph 28. U.S. Bureau of Reclamation, Denver Federal Center, Denver, Colo., 1960, 37 pp.
15. H. Kane. *A Mechanistic Explanation of the Physical Properties of Undisturbed Loess.* University of Iowa Research Project HR-126. Iowa State Highway Commission, Iowa City, 1968, 113 pp.
16. S. S. Bandyopadhyay. "Geotechnical Evaluation of Loessial Soils in Kansas." In *Transportation Research Record 945,* TRB, National Research Council, Washington, D.C., 1983, pp. 29–36.
17. D. T. Davidson and C. J. Roy. *The Geology and Engineering Characteristics of Some Alaskan Soils.* Bulletin 186. Engineering Experiment Station, Iowa State University, Ames, 1959.
18. L. L. Morrison. "Procedures and Problems of Highway Soils Engineering on Loessial Terrain in Alaska." In *Highway Research Record 212,* HRB, National Research Council, Washington, D.C., 1968, pp. 33–38.
19. J. B. Sheller. "Summarization and Comparison of Engineering Properties of Loess in the United States." In *Highway Research Record 212,* HRB, National Research Council, Washington, D.C., 1968, pp. 1–9.
20. J. A. Hansen, A. R. Dahl, and D. T. Davidson. Further Studies of Loess in Iowa: Thickness, Clay Content, and Engineering Classification. *Proc., Iowa Academy of Science,* Vol. 65, 1959, pp. 317–322.
21. M. Eske. "The Value of Soil Test Data in Local and Regional Road Planning." In *Proc., Symposium on Application of Soil Testing in Highway Design and Construction,* Standard Technical Publication 239, ASTM, Philadelphia, Pa., 1959.
22. R. F. Flint. Summary of Late-Cenozoic Geology of Southeastern Washington. *American Journal of Science,* Vol. 35, No. 207, 1938, pp. 223–230.
23. G. T. Lobdell. Hydroconsolidation Potential of Palouse Loess. *Journal of the Geotechnical Engineering Division, ASCE,* Vol. 107, No. GT6, 1981, pp. 733–742.

Publication of this paper sponsored by Committee on Soil and Rock Properties.

Saturation Effects on Calcareous Desert Sands

NABIL F. ISMAEL, OMAYYA AL-KHALIDI, AND MOHAMMAD A. MOLLAH

Saturation of the surface desert sands in Kuwait has caused some problems of settlement and local slope failures. The surface soils, consisting of calcareous windblown fine sand or silty sand, are sensitive to saturation. Laboratory and field testing programs were conducted to examine the effect of saturation on the shear strength parameters, settlement under load, and the ultimate bearing capacity. Laboratory testing consisted of basic properties, direct shear tests, and consolidation tests on undisturbed samples under unsoaked and soaked conditions. The samples were trimmed from block samples taken from five sites where slight interparticle cementations exist. Field tests included standard penetration, static and dynamic cone penetration tests, and plate load tests. All field tests were performed at one site on samples under unsoaked and soaked conditions. The laboratory test results indicate a reduction of the shear strength parameters due to saturation and increased compressibility or settlement under load. The field tests indicate a loss of 25 percent in both the ultimate bearing capacity and the allowable soil pressure for a given settlement criterion at the site most sensitive to saturation along a 35-km (22-mi) corridor. An average ratio of 4 was calculated between the cone penetration and the standard penetration resistance of the surface sands.

Calcareous sands exist in many parts of the world where arid or semiarid conditions prevail. These include the Arabian Peninsula *(1-3)*, southwestern United States and Mexico (*4*,pp.16–35), the Indian continental shelf (*5*,pp.113–140), South and South-West Africa (*6*,pp.296–309), and western Australia (*7*,pp.179–209). They are characterized by the presence of carbonates deposited at the points of contact between the particles *(8)* at a rate depending on local conditions and the geologic history of the deposit. As a result and depending on the grading characteristics, various degrees of cementation are produced at different locations and at different elevations at the same location. Calcareous sands encountered may be uncemented or weakly to strongly cemented *(5)*. The surface soil of Kuwait and major areas of the Arabian Peninsula usually consists of an uncemented calcareous windblown dune sand or silty fine sand to varying depths *(9, 10)*. This sand, although cohesionless, may have slight interparticle cementations in some areas, which facilitates excavation of shallow vertical cuts for temporary construction purposes.

With development and major construction in desert areas, particularly the Arabian Peninsula, interest in the properties and behavior of calcareous soils has grown. Recently, many problems of foundation and ground-floor settlement, deterioration, and local failures of slopes have occurred in Kuwait following saturation of the ground soils from heavy rain in the winter season or from the irrigation water and water leaking from underground pipelines. This pointed out the sensitivity of the local, moisture-deficient soils and the possible loss of strength and increased compressibility following saturation or soaking with water.

To examine the effect of saturation on the soil properties, a program of laboratory and field tests was carried out. Laboratory tests included basic physical properties and direct shear and consolidation tests on unsoaked and soaked undisturbed samples. All samples were trimmed from large blocks taken from five sites along a corridor 35 km (22 mi) long by 2 km (1.25 mi) wide where slight interparticle cementations existed. On the basis of the laboratory test results, a site was chosen for penetration and plate bearing tests, which were conducted at the in situ moisture conditions and after prewetting. Penetration tests included the standard penetration test (SPT) and dynamic and static cone penetration tests. All field tests were carried out at three locations within the site.

The results of the laboratory and the field tests are presented. The effect of saturation on the strength parameters, consolidation characteristics, and settlement under load is determined from laboratory test results. The reductions in both the ultimate bearing capacity and the allowable soil pressure based on a settlement criterion were determined from the results of plate bearing and penetration tests. A comparison is made between the laboratory and the field test findings.

BASIC SOIL PROPERTIES

Kuwait is located at the tip of the Arabian Gulf, as shown in Figure 1. It has an area of 17 800 km^2 (7,000 mi^2). The ground is in general a flat, gently undulating desert plain with occasional low hills, escarpments, and depressions *(11)*. A detailed examination of the soil conditions along the corridor shown in Figure 1 was carried out *(9, 10)*. The soil profile consists of a surface layer of calcareous windblown fine dune sand to a depth of 3 to 7 m (10 to 23 ft). This is underlain by a marine-deposited weakly to strongly cemented calcareous silty sand known locally as "gatch" and extending to a great depth over limestone bedrock. The Unified Soil Classification of the majority of samples in the upper layer is SP → SM, with the amount of fines passing the No. 200 sieve rarely exceeding 12 percent. The SPT values range between 15 and 35, and they generally increase in magnitude with depth. For the lower layer classified as SM → SC the SPT values generally exceed 50. In the majority of the boreholes drilled along the corridor, groundwater was encountered below the bottom of the upper layer *(9, 10)*.

N. F. Ismael, Civil Engineering Department, Kuwait University, P.O. Box 5969, Kuwait. O. Al-Khalidi and M. A. Mollah, Soils Section, Government Laboratories and Testing Station, Ministry of Public Works, Kuwait.

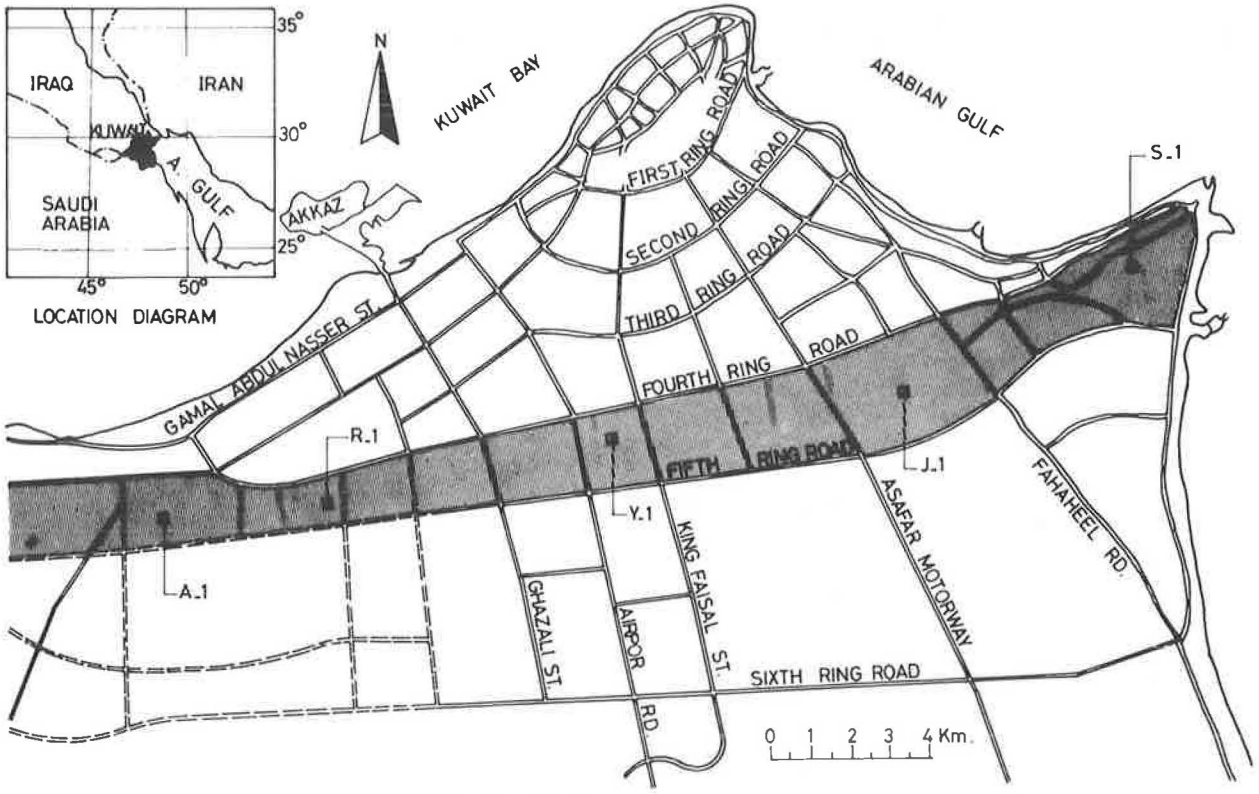

FIGURE 1 Site locations along corridor.

Five 0.5-m (1.6-ft) cubes of undisturbed block samples were cut from the bottom of excavation pits at a depth of 1.0 to 1.5 m (3.3 to 5 ft) using long knives and saws. The samples were taken from five selected sites, namely, A-1, R-1, Y-1, J-1, and S-1 (Figure 1). These samples were carefully wrapped in large plastic bags and transported to the laboratory for testing. The physical properties were determined first; they are summarized in Table 1. Indicated are the location, natural moisture content *(w)*, bulk and dry unit weights (γ_b, γ_d), specific gravity (G_s), mean diameter (D_{50}), void ratio *(e)*, degree of saturation (S_r), minimum and maximum dry densities ($\gamma_{d\ min}$ and $\gamma_{d\ max}$), relative density (R_d), the coefficient of permeability *(K)*, and the percent of fines. Examination of Table 1 reveals the similarity of the soil properties at the different sites. The subsoils are in a relatively dry condition with the natural moisture content less than 2 percent. The mean diameter is nearly constant at 0.15 to 0.16 mm and the specific gravity varies in a narrow range between 2.67 and 2.72. The relative density, averaging nearly 70 percent, indicates a compact or medium dense sand. The values of the coefficient of permeability are in the range 10^{-3} to 10^{-4} cm/sec (ft/min), indicating a free-draining sandy soil.

The complete chemical analysis on bulk samples from the different sites is given in Table 2. As indicated, quartz constitutes the principal component. The amount of carbonates varies between 10 and 20 percent, mostly in the form of calcite (calcium carbonate). The arid environment of Kuwait and the excess of evaporation over rainfall lead to upward movement of groundwater and the concentration of soluble materials at or near the ground surface, enriching the soil with carbonate and gypsum and often leading to the formation of crusts of cemented soils *(1)*.

TABLE 1 PHYSICAL PROPERTIES

Site	Natural Moisture Content, w (%)	Bulk Unit Weight, γ_b (kg/m^3)	Dry Unit Weight, γ_d (kg/m^3)	Specific Gravity, G_s	Mean Diameter, D_{50} (mm)	Void Ratio, e	Degree of Saturation, S_r (%)	Dry Density (kg/m^3) $\gamma_{d\ min}$	Dry Density (kg/m^3) $\gamma_{d\ max}$	Relative Density, R_d (%)	$K \times 10^{-3}$ (cm/sec)	Percent Passing No. 200 Sieve
A-1	1.8	1717	1687	2.72	0.15	0.612	8.0	1521	1789	65.7	2.0	15.2
R-1	1.0	1727	1710	2.69	0.14	0.591	4.6	1541	1769	76.7	1.73	6.1
Y-1	1.1	1734	1715	2.72	0.15	0.586	5.1	1574	1783	70.1	0.93	8.9
J-1	0.9	1719	1704	2.72	0.16	0.596	4.1	1564	1792	64.6	0.26	5.2
S-1	1.5	1766	1740	2.67	0.16	0.563	7.2	1577	1779	72.4	0.64	9.7

Note: Samples were from a depth of 1.0 to 1.5 m.

TABLE 2 CHEMICAL ANALYSIS OF SOIL SAMPLES

Site	pH Value	Composition (%)										
		SiO_2	Al_2O_3	Fe_2O_3	CaO	MgO	CO_3	$CaSO_4$	$CaCO_3$	MgCO3	$\overline{SO}_3$	$\overline{Cl}$
A-1	7.65	71.86	9.30	1.04	5.62	2.82	11.46	1.16	10.03	6.81	0.850	0.018
R-1	8.0	63.56	11.44	0.80	11.76	0.25	10.62	0.75	17.70	–[a]	0.44	0.021
Y-1	8.2	71.00	9.32	0.88	8.61	1.25	10.39	–[a]	15.38	2.1	0.052	0.018
J-1	–[a]	73.12	6.48	0.72	7.98	1.50	8.47	–[a]	14.26	–[a]	–[a]	0.018
S-1	8.7	76.90	5.62	0.52	6.30	1.08	9.45	1.01	11.25	3.06	0.025	0.021

Note: Samples were from a depth of 1.0 to 1.5 m.

[a]Not measured.

DIRECT SHEAR TESTS

Two sets of drained direct shear tests were conducted on samples both at in situ moisture content and after soaking (S_r = 100 percent) for 24 hr (ASTM D-3080). These tests were performed at a small rate of strain to ensure total dissipation of pore-water pressure during shear. As previously stated, all samples tested were undisturbed samples trimmed from the block samples possessing very weak cementations or bonding that could be easily crushed by a slight finger pressure.

Stress displacement curves and volume change during shear are plotted for R-1 sand in Figure 2 for samples tested under in situ moisture conditions. As shown, the stiffness and peak strength increase with an increase in the normal pressure. Volume change data indicate the development of strong dilation at small displacement, particularly with small normal pressures. The stress displacement data in Figure 2 show a ductile failure mode that has no significant drop after it reaches peak strength. However, by a comparison with the stress displacement data for soaked specimens at the same normal pressure, it will appear that soaked specimens have a much more ductile failure than the samples tested at in situ moisture content. This is shown in Figure 3, which indicates that the shear strength occurring at smaller displacement is higher for the unsoaked samples. The results are similar for other sites as well.

A summary of the peak-strength parameters under unsoaked and soaked conditions is given in Table 3 along with the residual unsoaked parameters and the predicted values based on the empirical relation between the SPT N-values and ϕ given by Peck et al. (*12*, p.310) The presence of a cohesion intercept *(C)* of about 4 to 24 kPa (0.6 to 3.5 psi) is due to the slight bond or interparticle cementation that exists at some locations. This may explain why windblown sand may stand steeply or even vertically in excavations for temporary con-

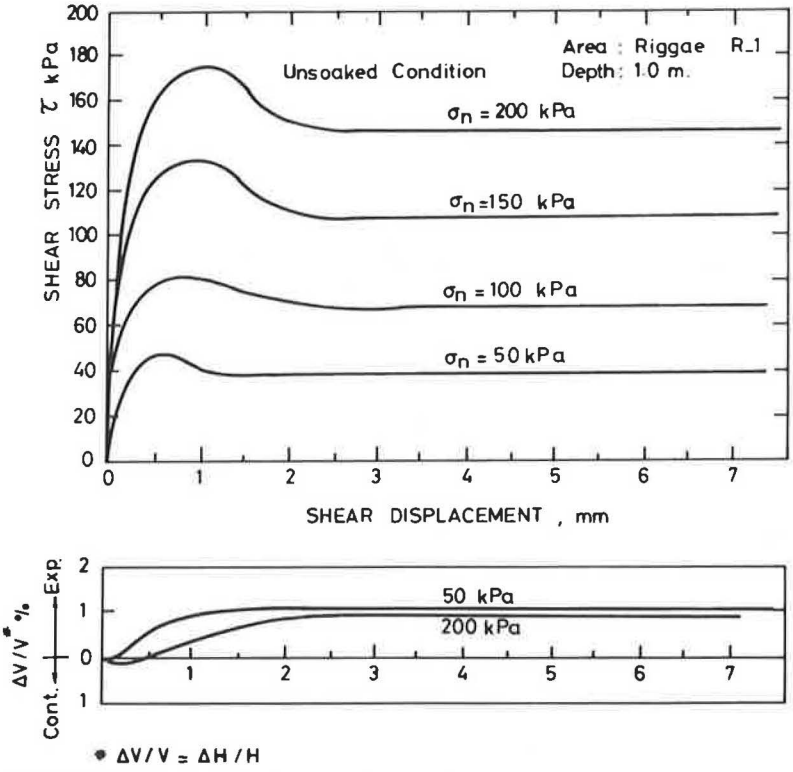

FIGURE 2 Stress displacement and volume change from unsoaked direct shear tests on R-1 soil.

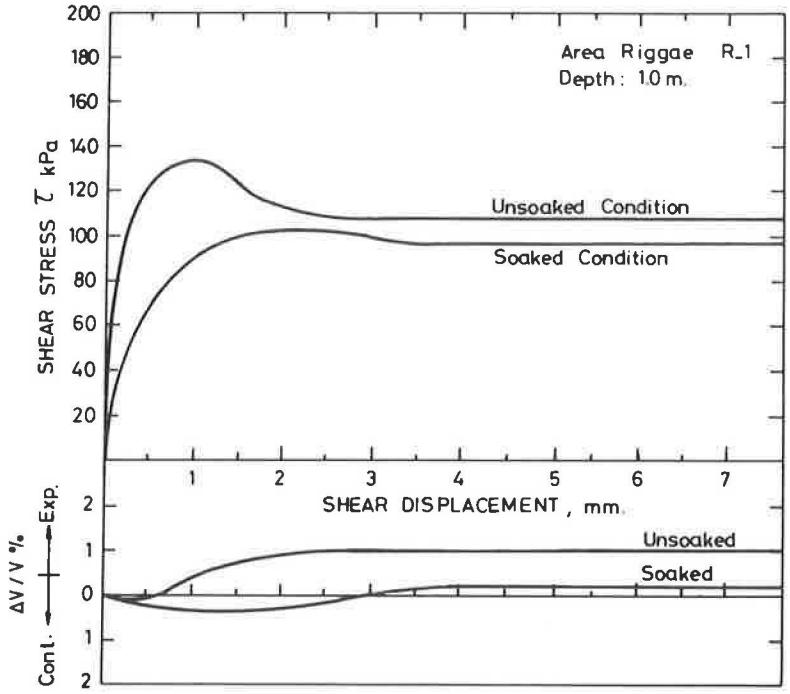

FIGURE 3 Comparison of stress displacement and volume change for unsoaked and soaked specimens (σ_n = 150 kPa).

struction. The soaked specimens have no cohesion and an angle of shearing resistance (ϕ) of 35.5 degrees compared with 40 degrees under unsoaked conditions. Plots of the shear stress versus normal stress showing the Mohr Coulomb envelopes for four of the test soils under unsoaked and soaked conditions are given in Figure 4. The fifth soil (A-1) could not be trimmed for testing because the samples crushed easily during preparation despite repeated trials. The loss of some strength because of saturation implies loss of bearing capacity and reveals the sensitivity of surface soils to excess moisture and the possible deterioration of slopes if subjected to heavy rain during the winter season.

A comparison of the residual strength parameters under unsoaked conditions with the peak soaked parameters indicates great similarity. This may be explained by noting that small interparticle cementations are destroyed once the peak strength has been reached *(13, 14)*, usually at small displacement levels, and soaking will have little extra effect, if any, in further reducing the strength.

The values of ϕ *(12)* range between 33 and 34 degrees and average 33.5 degrees. They are smaller than the measured soaked values by 2 degrees, and, as such, they are conservative lower-bound values.

CONSOLIDATION TESTS

Consolidation tests were carried out on 63.5-mm (2.5-in.) undisturbed samples. Initially the effect of soaking and the possible collapse potential were examined in a manner similar to that suggested by Knight *(15)*. A sample was loaded in the consolidation apparatus at its natural moisture content until a pressure of 200 kPa (29 psi) was reached. At the end of this loading, the specimen was flooded with water and left for a day, and the test was then continued to its maximum loading limit. The resulting curves for the test soils are shown in Figure 5. The collapse potential *(CP)* is defined as

$$CP = \Delta e_c/(1 + e_0) = \Delta H_c/H_0 \quad (1)$$

where

Δe_c = change in void ratio upon wetting,

TABLE 3 DIRECT SHEAR STRENGTH PARAMETERS FOR SURFACE SOILS

Site	SPT (N blows/0.3 m)	Peak Parameters: Unsoaked C (kPa)	Peak Parameters: Unsoaked ϕ (degrees)	Peak Parameters: Soaked C (kPa)	Peak Parameters: Soaked ϕ (degrees)	Residual Unsoaked C (kPa)	Residual Unsoaked ϕ (degrees)	Predicted ϕ' *(12)*
R-1	20	4	40.5	0	35.5	0	36	33.5
Y-1	20	0	40.9	0	35.5	0	37	33.5
J-1	18	4	41.7	0	35.8	0	36	33.0
S-1	23	24	40.4	0	35.5	0	35	34.0

e_0 = natural void ratio,
ΔH_c = change in height upon wetting, and
H_0 = initial height.

Jennings and Knight *(16)* have suggested some severity ratings for different values of the collapse potential, as follows:

CP (%)	*Severity of Problem*
0-1	None
1-5	Moderate
5-10	Normal
10-20	Severe
> 20	Very severe

From Figure 5 the collapse potential was calculated as 0.9, 1.0, 0.7, and 3.6 for Y-1, J-1, R-1, and S-1 soils, respectively. Comparing these values, which are essentially the strain caused by soaking, with the ratings of Jennings and Knight, it is concluded that there will be no problem with collapse in the first three soils, whereas the last soil (S-1) is considered to have moderate trouble with collapse. This may be explained by the fact that the surface soils consist of a relatively dry windblown dune sand—an aeolian deposit that is known to collapse *(17, 18)*. The possibility of collapse apparently increases with the presence of weak interparticle calcareous cementation bonds, which dissolve upon soaking and which vary from site to site despite the similarity of the grading characteristics.

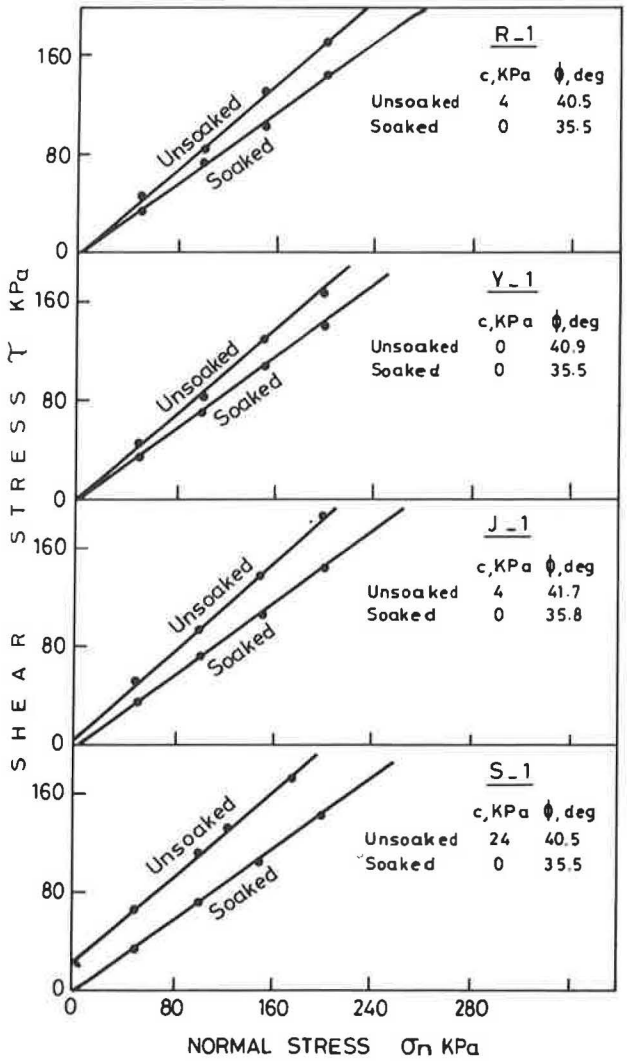

FIGURE 4 Mohr Coulomb envelopes for unsoaked and soaked specimens.

To investigate the effect of soaking on compressibility characteristics and settlement under load, double consolidation tests were performed on the four soils examined earlier *(12)* by using the method employed by Clemence and Finbarr *(17)*. Two identical undisturbed samples are placed in consolidometers under a 1-kPa (0.15-psi) load for 24 hr. At the end of this period, one sample is flooded with water, and the other sample is kept at its natural water content. Both samples are left for a further 24 hr. The test is then completed in the ordinary manner (ASTM D2435). The results of the current tests for J-1 and S-1 soils are shown in Figure 6. As is evident, the two curves do not start from the same point; the curve for the soaked samples is usually the lower one.

For settlement calculations, the total overburden pressure (P_0) at the depth of the sample is calculated and plotted on the e log p curves obtained from the two tests. The preconsolidation pressure (P_c) is found from the soaked curve and compared with P_0. For the case of normally consolidated soil in which P_c/P_0 is equal to 0.8 to 1.5, compression is considered to occur along the virgin curve and the natural moisture content curve is adjusted to the (e_0, P_0) point by drawing a curve parallel to the natural moisture consolidation curve, as shown in Figure 6 *(bottom)* for the S-1 soil. In the case of an overconsolidated soil, the adjustment to the curve follows ordinary settlement computation practice after the determination of the (e_0, P_0) point as shown in Figure 6 *(top)*.

If the load is increased by Δp, the unit settlement will consist of two components as follows:

$$S/H_0 = [\Delta e_s/(1 + e_0) + \Delta e_c/(1 + e_0)] \quad (2)$$

With reference to Figure 6, the first term is the unit settlement due to an increase in pressure (Δp) without change in the moisture content, and the second term is the unit additional settlement due to soaking. A comparison of the second term of Equation 2 for J-1 and S-1 soils under the same pressure increment of Δp = 200 kPa (29 psi) is evident from Figure 6. It indicates that settlement has nearly doubled for the S-1 soil, whereas it has increased by nearly 40 percent for the J-1 soil due to soaking. This appears to be in general agreement with what is expected in view of the results shown in Figure 5, which indicate the largest collapse potential for the S-1 soil. Each point of the curves shown in Figures 5 and 6 represents the average of two tests performed to obtain accurate results. These results indicate that the compression index is less than 0.10 and the term $C_c/(1 + e_0)$ ranges up to 0.05 for all test soils.

PENETRATION AND PLATE LOAD TESTS

To examine the effect of saturation in more detail, the site located in Salmiya (S-1), which displayed the greatest sensitivity to saturation, was selected for field testing. The site is flat, measures 100 by 200 m (330 by 660 ft), and has uniform

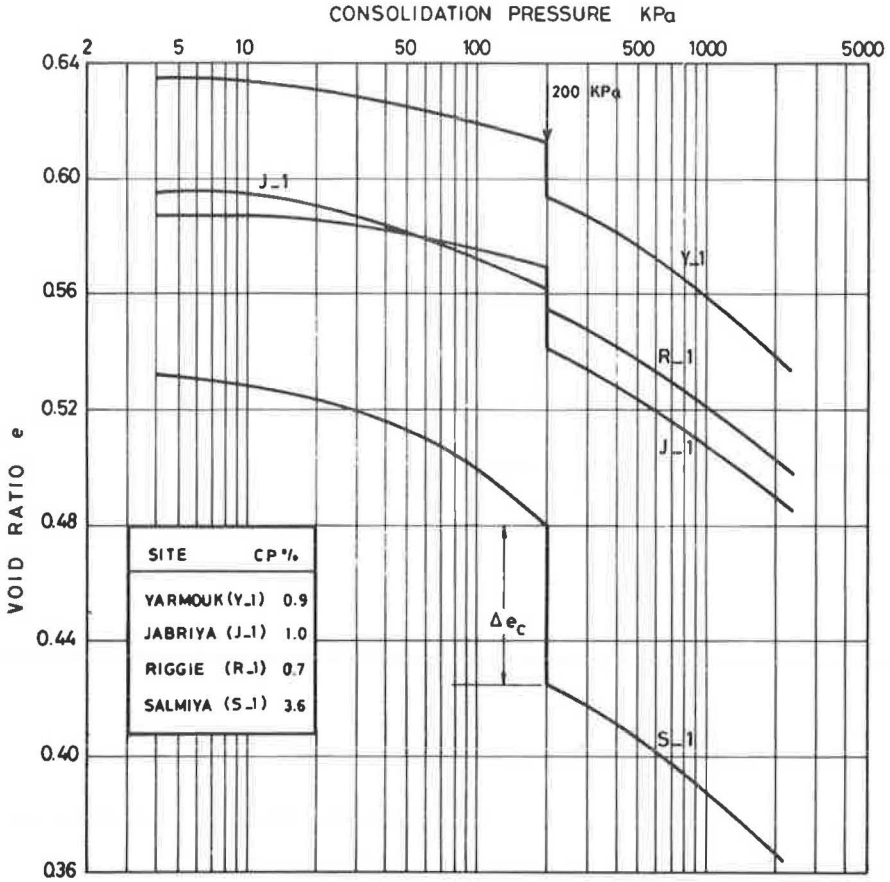

FIGURE 5 Collapse potential test results.

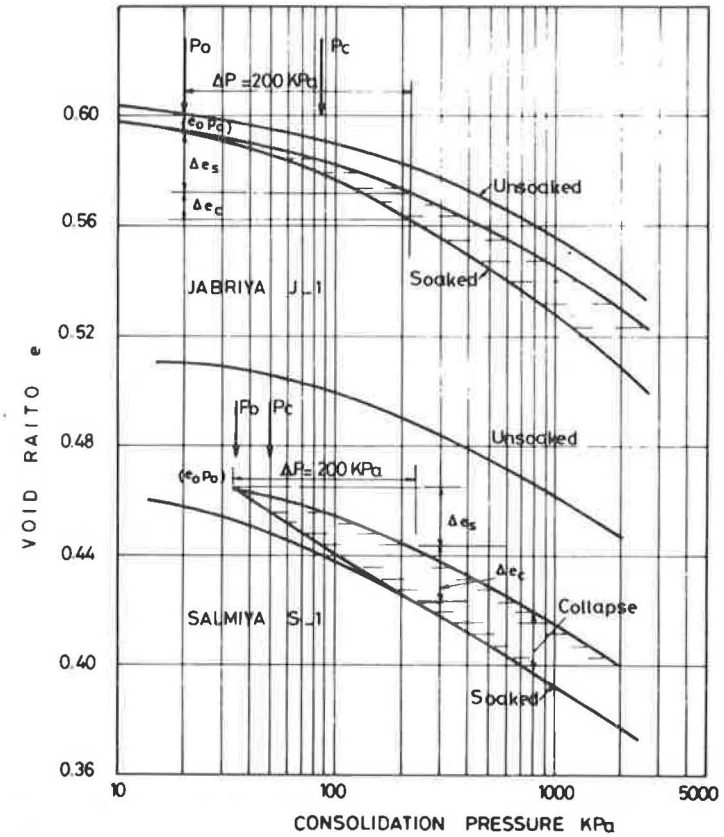

FIGURE 6 Double consolidation test results and adjustments for settlement calculations.

soil conditions. Three areas 40 m (131 ft) apart were chosen for penetration and plate bearing tests.

Penetration Tests

Standard penetration tests and dynamic and static cone penetration tests were performed in each area under in situ moisture conditions and after soaking. Wetting was achieved through four 4-m (13-ft) drill holes at the boundary of a 5 × 5-m (16 × 16-ft) area. These holes were filled with water and the surface area was saturated for 24 hr. Water was again poured before testing. Test results are summarized in Figure 7, which shows the soil profile, moisture content, and unit weight and plots of the various penetration test results under in situ moisture (unsoaked) conditions and after soaking. These results are the average of the data obtained at the three test locations.

The data in Figure 7 show that the windblown sand layer extends to a depth of 2.85 m (9.3 ft) only at this site. Within this layer the soaked penetration values are substantially reduced in comparison with the unsoaked values. By calculating the average values along the depth of the upper layer, it was found that the soaked SPT values and static cone penetration test values decreased to 62 percent of the corresponding unsoaked values. The dynamic cone penetration test values decreased to 67 percent of the unsoaked values. This shows marked consistency and implies a reduction in bearing capacity of the same order of magnitude.

To determine whether a relationship exists between the static cone penetration test values and SPT values as reported by several workers (*19; 20*,pp.473–499), the average values obtained from the three test areas under unsoaked and soaked conditions were compared. The results, summarized in Table 4, indicate a ratio of the cone penetration test values to the SPT values (q_c/N), in kilograms per square centimeter (tons per square foot), of 4.4 for the unsoaked conditions and 4.06 for the soaked conditions. This is similar to the values recommended by Sutherland *(20)* for fine sand and silty fine sand. Additional tests will be carried out at different locations along the test corridor to confirm the validity of this relationship at other sites with similar soils.

Plate Load Tests

At each of three areas selected, three plate load tests were conducted at a depth of 0.5 m (1.6 ft) in test pits 1.5 × 1.5 m (5 × 5 ft) according to ASTM D1194. The program at each area consisted of testing a 0.3-m (1-ft) plate under unsoaked conditions, soaked conditions at a pressure of 200 kPa (29 psi), and presoaked conditions in which saturation (S_r = 100 percent) was imposed before the test. The loads were applied by jacking against the rear wheel axle of a CMR 750-XL drill anchored down to 1.5 m (5 ft). Before each test was conducted, the test area was leveled properly to ensure that the plate rested on leveled, undisturbed soil. Soaking was achieved by a slow but

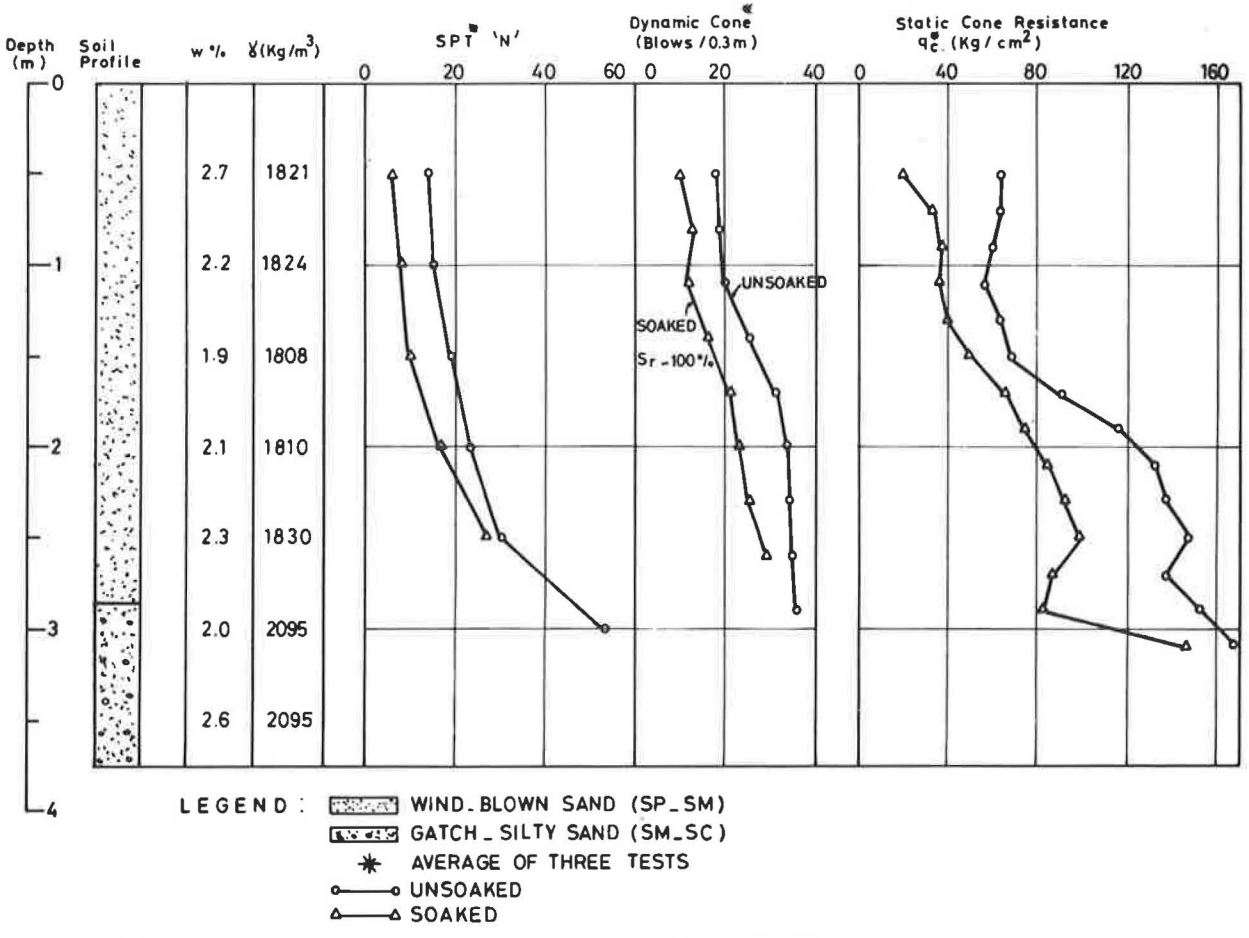

FIGURE 7 Soil conditions and penetration test data at Salmiya, Site S-1.

TABLE 4 SPT AND CONE PENETRATION TEST RESULTS AT SALMIYA (SITE S-1)

Depth (m)	Unsoaked SPT	Unsoaked CPT	Unsoaked Ratio	Soaked SPT	Soaked CPT	Soaked Ratio
0	–	–	–	–	–	–
0.5	14	64	4.572	6	20	3.334
0.7		64			34	
0.9		60			38	
1.0	15	} 58[a]	3.866	8	} 37[a]	4.626
1.1		56			36	
1.3		64			40	
1.5	19	68	3.580	10	50	5.00
1.7		90			66	
1.9		116			74	
2.0	23	} 124[a]	5.392	17	} 79[a]	4.648
2.1		132			84	
2.3		136			92	
2.5	30	148	4.934	27	98	3.630
2.7		136			84	
2.9		152			82	
3.0	39	} 159[a]	4.078	36	} 114[a]	3.166
3.1		166			196	

Note: Average ratio: unsoaked, 4.4; soaked, 4.06; therefore q_c/N = 4.4 (unsoaked), q_c/N = 4.06 (soaked). CPT = cone penetration test.

[a]Average of values enclosed in braces.

continuous pouring of water to wet the ground beneath the plate to a depth not less than twice its diameter. To do this, a 1.9-m^3 (500-gal) truck-mounted tank was employed, and the soaking period lasted for almost 2 hr after a pressure of 200 kPa (29 psi) was reached. For the tests carried out under presoaked conditions, soaking was maintained overnight before testing. The measured degree of saturation of the underlying soils (S_r) was 100 percent after soaking.

The results obtained from the three tests areas are plotted in Figure 8 in the form of pressure settlement curves for unsoaked and soaked conditions. Each curve is obtained from the average results of the three similar tests. For the tests in which partial saturation was imposed at 200 kPa, the data concided with those for the unsoaked curve before this load and were nearly identical to those for the saturated curve for loads larger than 200 kPa. Examination of Figure 8 reveals that the failure was progressive, a characteristic of local and punching shear failure. The failure load was taken at the point of maximum curvature on the pressure settlement curves as 580 kPa (84 psi) and 430 kPa (62 psi) for the unsoaked and soaked conditions, respectively. This signifies a reduction of 25 percent in the bearing capacity.

The allowable soil pressure for foundation design in sands is usually based on a permissible settlement of 25.4 mm (1 in.) *(20)*. What then would the reduction be in the allowable soil pressure due to saturation for footings of different sizes?

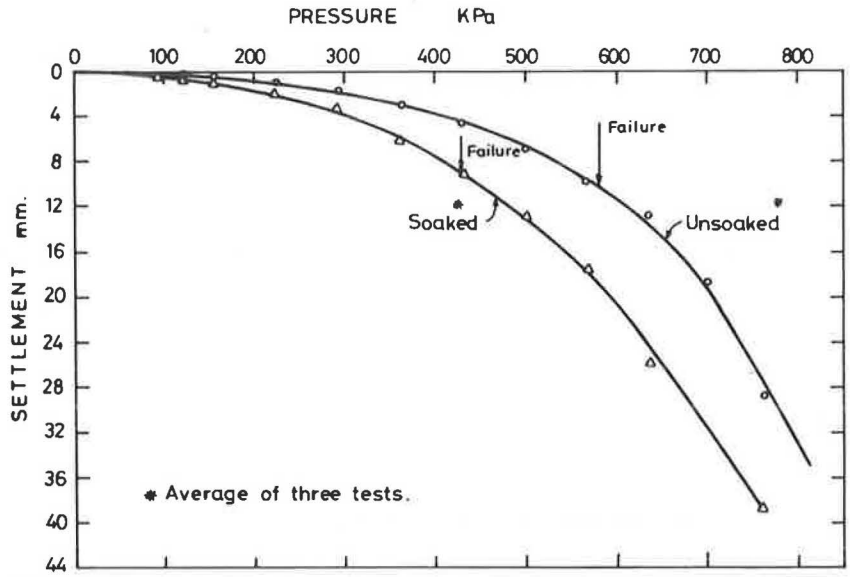

FIGURE 8 Plate load test results for unsoaked and soaked conditions.

To answer this question, one would first have to extrapolate from test-plate to full-size foundations. As explained by Parry *(21)*, this depends on how the soil stiffness (sand modulus) varies with depth. Recent field test results at seven sites in Kuwait on the same soil deposit as that examined here were in excellent agreement *(22)* with the following relationship proposed by Terzaghi and Peck (*23*, pp.494–496) between the settlement (S_B) of a footing of width B meters and the observed settlement (S_1) of a standard plate 0.3 m (1 ft) wide loaded to the same load intensity.

$$S_B = S_1 [2B/(B + 0.3)]^2 \quad (3)$$

The implication of this relationship is that the settlement of a footing of any size would never exceed four times the settlement of a 0.3-m plate. The close agreement between plate tests *(22)* and Equation 3 is not surprising in view of the analysis made by Parry *(21)* for soil conditions with a progressive increase in the relative density with depth. For such soils, which have conditions similar to those for the present soils, the analysis indicated excellent agreement with Equation 3.

Employing Equation 3, the plate settlement corresponding to 12.7-mm and 25.4-mm permissible foundation settlement was determined for different sizes of footings ranging in width from 1 to 3 m (3.3 to 10 ft). Subsequently the allowable soil pressures were determined from Figure 8 for the unsoaked and soaked conditions. The results are summarized in Table 5 in which the ratio of the soaked to unsoaked soil pressure is given. As shown, the data indicate marked uniformity with an average ratio of 0.75. On this basis the decrease in the allowable soil pressure due to saturation is 25 percent, which is the same as the reduction in the ultimate bearing capacity.

For the same applied pressure of, say, 200 or 300 kPa (29 or 43 psi) the settlement is nearly doubled because of saturation (see Figure 8). However, if the pressure is reduced by 25 percent, the settlement will be reduced by half, thus offsetting the effect of saturation. It should be emphasized, however, that a flat reduction of this magnitude applied indiscriminately at all locations where similar soils exist will be conservative. This is in view of the high sensitivity to saturation prevailing at this test site compared with the others as demonstrated by the relatively large collapse potential value in Figure 5.

COMPARISON OF FIELD AND LABORATORY TEST RESULTS

On the basis of field and laboratory tests, it is evident that saturation of calcareous windblown sands leads to a reduction of shear strength and bearing capacity and an increase in compressibility and settlement under load. Moreover, it is possible to observe some similarity between the field and laboratory test results. For example, under an applied load increment of, say, 200 kPa the settlement due to saturation for S-1 soil doubles, as shown in Figure 6. The same trend is observed if the same pressure is applied to the test plate (see Figure 8). With regard to bearing capacity, the plate tests indicate a reduction of 25 percent. However, the penetration tests indicate a decrease in penetration resistance of nearly 40 percent. The laboratory direct shear tests indicating a decrease in ϕ from 40 to 35.5 degrees correspond to a reduction of the bearing capacity factors N_q and N_γ of 40 to 50 percent.

As previously stated, the S-1 site is considered to be the most sensitive to saturation. In absence of field tests at the other sites, a simple approximate approach may be adopted to account for saturation effects. Because saturation led to a unit settlement increase of ~40 to 50 percent for the J-1, Y-1, and R-1 sites compared with 100 percent for the S-1 soil, it is possible that the same relative effect holds true for bearing capacity and allowable soil pressure. If this is true, the allowable soil pressure would be reduced by 12.5 percent for the other three sites. This needs to be confirmed, however, by additional field tests at the other sites.

CONCLUSIONS

On the basis of the laboratory and field test results presented in this paper, the following conclusions are drawn:

1. Calcareous windblown sands or silty sands cover major areas of Kuwait and other desert areas. These surface sands, consisting mainly of fine sand, are usually not cemented; however, they possess slight interparticle cementations at some locations.
2. Sensitivity to soaking was examined by laboratory direct

TABLE 5 ALLOWABLE SOIL PRESSURES FROM PLATE LOAD TEST RESULTS

Width of Footing (m)	Permissible Settlement (mm)	Equivalent Plate Settlement (mm)	Allowable Soil Pressure (kN/m^2)		Ratio: Soaked/Unsoaked
			Unsoaked Conditions	Soaked Conditions	
3	12.7	3.84	405	290	0.716
2	12.7	4.2	420	305	0.726
1.5	12.7	4.57	440	320	0.727
1	12.7	5.36	465	345	0.742
3	25.4	7.68	530	400	0.755
2	25.4	8.4	545	415	0.768
1.5	25.4	9.14	560	430	0.768
1	25.4	10.73	590	460	0.780

Note: Average ratio = 0.747-0.75.

shear tests and double consolidation tests on undisturbed samples. A decrease in the angle of shearing resistance of ~5 degrees and an increase of the unit settlement under load were recorded. The additional settlement due to collapse varies from site to site; however, at the majority of the test sites it poses no major problem.

3. Plate load test results indicate that saturation leads to a reduction of 25 percent of both the ultimate bearing capacity and the allowable pressure on the basis of a settlement criterion of 25.4 or 12.7 mm (1 or 0.5 in.). This was found for the site most sensitive to saturation. At other locations smaller reductions may be applicable.

4. Standard penetration and static cone tests show a decrease of 38 percent in the average resistance due to 100 percent saturation. This is somewhat larger than the reductions deduced from the plate tests.

5. Design of earth structures in this soil should be based on the soaked strength parameters to account for the effect of increase in the degree of saturation.

6. The ratio of the cone penetration to the standard penetration resistance in kilograms per square centimeter (tons per square foot) was found to range from 4 to 4.4 under soaked and unsoaked conditions. This is based on testing at one site only and should be confirmed by additional field testing before its use in design calculations.

REFERENCES

1. P. G. Fookes and I. E. Higginbottom. "Some Problems of Construction Aggregates in Desert Areas with Particular Reference to the Arabian Peninsula. 1: Occurrence and Special Characteristics. 2: Investigation, Production and Quality Control. *Proc., Institute of Civil Engineers,* Vol. 68, Pt. 1, 1980, pp. 39-90.
2. I. Oweis and J. Bowman. Geotechnical Considerations for Construction in Saudi Arabia. *Journal of the Geotechnical Engineering Division, ASCE,* Vol. 107, No. GT3, 1981, pp. 319–338.
3. G. Riedel and A. B. Simon. Geotechnical Properties of Kuwaiti "Gatch" and Their Improvement. *Engineering Geology,* Vol. 7, 1973, pp. 153–165.
4. G. H. Beckwith and L. A. Hansen. "Calcareous Soils of the Southwestern United States." In *Geotechnical Properties, Behavior, and Performance of Calcareous Soils,* Standard Technical Publication 777, ASTM, Philadelphia, Pa., 1982.
5. M. Datta, S. Gulhati, and G. Rao. "Engineering Behavior of Carbonate Soils in India and Some Observations on Classification of Such Soils." In *Geotechnical Properties, Behavior, and Performance of Calcareous Soils,* Standard Technical Publication 777, ASTM, Philadelphia, Pa., 1982.
6. F. Netterberg. "Geotechnical Properties and Behavior of Calcretes in South and South-West Africa." In *Geotechnical Properties, Behavior, and Performance of Calcareous Soils,* Standard Technical Publication 777, ASTM, Philadelphia, Pa., 1982.
7. F. L. Beringen, H. J. Kolk, and D. Windle. "Cone Penetration and Laboratory Testing in Marine Calcareous Sediments." In *Geotechnical Properties, Behavior, and Performance of Calcareous Soils,* Standard Technical Publication 777, ASTM, Philadelphia, Pa., 1982.
8. D. P. Krynine and W. R. Judd. *Principles of Engineering Geology and Geotechnics.* McGraw-Hill, New York, 1957.
9. N. F. Ismael, M. Mollah, and O. Al-Khalidi. *A Study of the Properties of Surface Soils in Kuwait.* Government Laboratories and Testing Station, Ministry of Public Works, Kuwait, Jan. 1985.
10. N. F. Ismael, A. Jeragh, M. Mollah, and O. Al-Khalidi. A Study of the Properties of Surface Soils in Kuwait. *Arab Journal for Science and Engineering* (in preparation).
11. S. Al-Saleh and F. I. Khalaf. Surface Texture of Quartz Grains From Various Recent Sedimentary Environments in Kuwait. *Journal of Sedimentary Petrology,* Vol. 52, No. 1, March 1982, pp. 215–225.
12. R. B. Peck, W. E. Hanson, and T. H. Thornburn. *Foundation Engineering.* Wiley, New York, 1974.
13. G. W. Clough, N. Sitar, R. Bachus, and N. Rad. Cemented Sands Under Static Loading. *Journal of the Geotechnical Engineering Division, ASCE,* Vol. 107, No. GT6, 1981, pp. 799–817.
14. S. K. Saxena and R. M. Lastrico. Static Properties of Lightly cemented Sand. *Journal of the Geotechnical Engineering Division, ASCE,* Vol. 104, No. GT12, 1978, pp. 1449–1464.
15. K. Knight. The Origin and Occurrence of Collapsing Soils. *Proc., Third Regional Conference for Africa on Soil Mechanics and Foundation Engineering,* Vol. 1, 1963, pp. 127–130.
16. J. E. Jennings and K. Knight. A Guide to Construction on or with Materials Exhibiting Additional Settlement Due to 'Collapse' of Grain Structure. *Proc., Sixth Regional Conference for Africa on Soil Mechanics and Foundation Engineering,* 1975, pp. 99–105.
17. S. P. Clemence and A. O. Finbarr. Design Considerations for Collapsible Soils. *Journal of the Geotechnical Engineering Division, ASCE,* Vol. 107, No. GT3, 1981, pp. 305–317.
18. G. T. Lobdell. Hydroconsolidation Potential of Polouse Loess. *Journal of the Geotechnical Engineering Division, ASCE,* Vol. 107, No. GT6, 1981, pp. 733–742.
19. J. H. Schmertmann. Static Cone to Compute Static Settlement Over Sand. *Journal of the Soil Mechanics and Foundation Engineering Division, ASCE,* Vol. 96, No. SM3, 1970, pp. 1011–1043.
20. H. B. Sutherland. "Granular Materials." In *Proc., British Geotechnical Society Conference,* Cambridge, England, Pentech Press, London, 1974.
21. R. H. G. Parry. Estimating Foundation Settlements in Sand From Plate Bearing Tests. *Geotechnique,* Vol. 28, No. 1, March 1978, pp. 107–118.
22. N. F. Ismael. Allowable Pressures From Loading Tests on Kuwaiti Soils. *Canadian Geotechnical Journal,* Vol. 22, No. 2, May 1985.
23. K. Terzaghi and R. B. Peck. *Soil Mechanics in Engineering Practice,* 2d ed. Wiley, New York, 1967.

Publication of this paper sponsored by Committee on Soil and Rock Properties.

Deformation Analyses of Florida Highway Subgrade Sand Subjected to Repeated Load Triaxial Tests

NORMAN D. PUMPHREY, JR., AND RODNEY W. LENTZ

Laboratory repeated load triaxial tests are conducted to estimate the effects of highway traffic on the permanent and resilient deformation of a subgrade sand commonly used as a foundation for a flexible highway pavement structure in Florida. Combinations of confining stress and cyclic principal stress difference (test variables) and of dry unit weight and moisture content (sample variables) are used for each sample and loaded to 10,000 cycles. Confining stress, cyclic principal stress difference, and dry unit weight are correlated with permanent strain and resilient modulus and thus affect deformation properties of these soils. However, moisture content correlates with neither permanent strain nor resilient modulus. Static tests are conducted on various samples similar to those used in the cyclic tests. These results are used to normalize cyclic stress and strain at 10,000 cycles. A regression model is developed for predicting cyclic strain in the sand from static tests by using a technique previously developed by Lentz. The model is compared to one for Michigan highway subgrade sand. Using a general linear test at a level of significance of 0.05, it is found that the data sets from each sand cannot be pooled to form one regression model. Values of resilient modulus after 10,000 loading cycles for the Florida sand ranged from 16,000 psi (110 240 kPa) at 5 psi (34.5 kPa) confining stress to 56,000 psi (385 840 kPa) at 50 psi (344.5 kPa) confining stress.

In many locations around the country and the world, rutting of flexible highway pavement is of major concern when useful pavement life is evaluated. One of the natural consequences of severe pavement rutting is that water will remain in puddles on the roadway, and hydroplaning—the loss of vehicle control due to excess water between tires and pavement—becomes a hazardous possibility. Yoder and Witczak *(1)* and Terrel and Rimsritong *(2)* state that rutting is due to the consolidation (densification) of one or more layers of pavement under repeated wheel loads, especially the heavier loads induced by multiaxle and multiwheel vehicles. Traffic-induced vibrations and the actual wheel load stresses are transmitted through the pavement layers, thus causing the consolidation. In many pavement design procedures, protection of the subgrade from these excess stresses and vibrations caused by traffic is a major design consideration.

Another important aspect of pavement design is the resiliency characteristics of the pavement layers, that is, the amount of deformation under a given load that is elastic. It is particularly important in design concepts using the linear elastic-layered models. The Asphalt Institute *(3)* has incorporated an elastic-layered theory model in its design by using subgrade resilient modulus as a design input.

Therefore, this investigation was undertaken to examine a Florida quartz sand commonly found as a subgrade material in parts of the Florida panhandle. The primary objectives of this study were *(a)* to investigate permanent and resilient deformation characteristics of the soil and *(b)* to analyze a technique to predict permanent deformation under repeated load laboratory tests using only static load triaxial tests. Both cyclic and static load tests were conducted on sand samples under various combinations of confining stress, cyclic principal stress difference, dry unit weight, and moisture content.

LITERATURE SURVEY

Permanent Deformation

Permanent deformation may be defined as the amount of deflection occurring under a given load that is not recoverable when the load is removed. Yoder and Witczak *(1)* state that permanent deformation is the result of two different mechanisms—densification and repetitive shear deformations (plastic flow).

Deformation due to plastic flow is the primary criterion upon which many current pavement designs are based. Two general design techniques—empirical approaches and rational methods—currently exist. Empirical approaches involve the correlation of pavement deformations to some predetermined condition of failure. Two common empirical methods are the empirical-strength procedures and the limited-subgrade-strain method. In both techniques the deformation is controlled by varying the thickness of pavement layers and by regulating the material quality based on an index test (California bearing ratio, resilient modulus, etc.). These methods involve the same basic assumptions, except that the strength approach assumes that all deformation occurs in the subgrade layer, whereas in the limited-subgrade-strain method, the deformation may occur in all layers. The major disadvantage with these methods is that neither can predict the amount of permanent strain that will occur under a given number of loadings. Purely rational design techniques have not yet enjoyed wide acceptance in practice, but interest is increasing as these methods begin to more closely model actual field conditions and as computer accessibility rises.

If empirical approaches are dominant, how might the pave-

N. D. Pumphrey, Jr., School of Civil Engineering, Purdue University, West Lafayette, Ind. 47907. R. W. Lentz, Department of Civil Engineering, University of Missouri-Rolla, Rolla, Mo. 65401.

ment design engineer predict this permanent strain (ε_p)? Cyclic or repeated load triaxial tests of soil and granular base course material have recently been the most widely accepted tests for measuring permanent deformation. Some researchers *(1, 4)* have found the relationship between permanent strain and number of load cycles *(N)* to be linear on a log-log plot. Therefore, the deformation law can be written as

$$\varepsilon_p = aN^b \quad (1)$$

where a is the ordinate intercept at $N = 1$ and b is the slope of the plot. However, Barksdale *(5)* and Lentz *(6)* found that a linear relationship exists on the ε_p -log N plot. This law can be expressed as

$$\varepsilon_p = a + b\ (\log N) \quad (2)$$

Parameter a is the ordinate intercept at $N = 1$ and b is the slope of the straight-line plot.

Diyaljee and Raymond *(4)* developed a constitutive equation relating laboratory permanent strain of a highway soil to the ratio of repeated load deviator stress, to static failure deviator stress, and to the number of cycles to which the soil is subjected.

Bouckovalas et al. *(7)* used an analogy between viscoelastic creep and strain accumulation during each cyclic loading to predict the accumulated cyclic strain on laboratory sand samples subjected to various loading and drainage conditions. Parameters used in the model development were determined from drained cyclic (viscosity parameters) and drained static (moduli parameters) tests.

McVay and Taesiri *(8)* conducted compression cyclic triaxial tests and compression-extension cyclic triaxial tests on a Florida sand and compared results from both tests on permanent and resilient strain characteristics.

Lentz *(6)* used various normalization procedures of cyclic deviator stress and permanent strain plots to develop a technique for predicting laboratory permanent strain at a particular number of loading cycles using only static triaxial tests. The basic requirement was that the dry unit weight and moisture content be the same for the static tests as that which would be analyzed in a repeated load triaxial tests. After his analysis was complete, Lentz *(6)* had selected peak static strength as the value for normalizing cyclic principal stress difference and static strain at 95 percent of the peak static strength for normalizing permanent strain. The resulting plot of normalized stress (ordinate) versus normalized strain at the end of 10,000 loading cycles (abscissa) fit a hyperbolic function with a correlation coefficient of 0.98 when least-squares regression was performed. The equation of the curve was

$$\sigma_d/S_d = (\varepsilon_p/\varepsilon_{0.95S_d})/[n + m(\varepsilon_p/\varepsilon_{0.95S_d})] \quad (3)$$

where

$\varepsilon_{0.95S_d}$ = strain at 95 percent of the peak static strength of the soil,
σ_d = cyclic principal stress difference,
S_d = peak static strength of the soil, and
n, m = regression constants,

$$n = (0.809399 + 0.003769\sigma_3) \times 10^{-4} \quad (4)$$

$$m = 0.856355 + 0.049650\ (\ln \sigma_3) \quad (5)$$

This curve could then be used by conducting a single static test to find the values of S_d and $\varepsilon_{0.95S_d}$, assuming a cyclic deviator stress that could be applied and calculating from the equation or reading from the plot the value of permanent strain to be expected in the sample.

Resilient Deformation

Resiliency is the deformational component of the soil that will be recovered after a load has been applied and removed from a sample. This resilient component can be used in the material characterization of a soil.

Laboratory testing to determine soil resiliency consists of a series of repeated load tests. The resilient modulus *(M_R)* is one method of material characterization in which the aspect of recoverable soil deflection is considered. It can be defined as follows*(1)*:

$$M_r = (\sigma_1 - \sigma_3)/\varepsilon_r \quad (6)$$

where

σ_1 = total peak vertical stress,
σ_3 = confining stress, and
ε_r = recoverable strain at a given stress repetition.

Factors Affecting Cyclic Loading Properties of Cohesionless Soils

Substantial research has been conducted to determine the effect of various variables on cohesionless soils subjected to repeated loads. These factors may be divided into the categories of test and sample variables.

Test variables can be controlled in the testing procedure and are virtually unaffected by a change in the soil sample being tested. Researchers *(5; 6-8; 9*,pp.365–383;*10-18*, pp.341–345;*19)* have identified many variables that affect both permanent and resilient deformation of a soil sample, including confining stress, number of loadings, cyclic principal stress difference, load duration and frequency, stress history, loading wave form, and sample end restraint. Most researchers agree that the first three have the greatest effect on a sample.

Sample variables affect strength and deformation characteristics of the soil because of a change in the soil sample itself. These factors include density or dry unit weight, degree of saturation, aggregate gradation or fines content, specimen size, and particle size, shape, and roughness *(1, 5, 6, 9, 12, 13, 19-22*,pp.63-74). Density of the soil sample is the most important of these variables.

SAMPLE MATERIAL, PREPARATION, AND TESTING

Highway subgrade sand was obtained from a borrow pit in Leon County, Florida. The sand had been used as subgrade fill material for an urban widening project in Tallahassee. The

classification of the material was a uniform, fine sand, or AASHTO classification A-3, with a coefficient of curvature of 0.92 and a coefficient of uniformity of 1.74. Particle sizes ranged from the No. 10 sieve to just below the No. 200 sieve, with approximately 1 or 2 percent of the material passing the No. 200 sieve.

Standard (AASHTO T-99) and modified (AASHTO T-180) compaction tests were conducted to determine maximum dry unit weight and optimum moisture content, and the results are plotted in Figure 1. The material was then compacted into a 4-in. (101-mm) diameter triaxial sample mold and prepared for testing *(23)*.

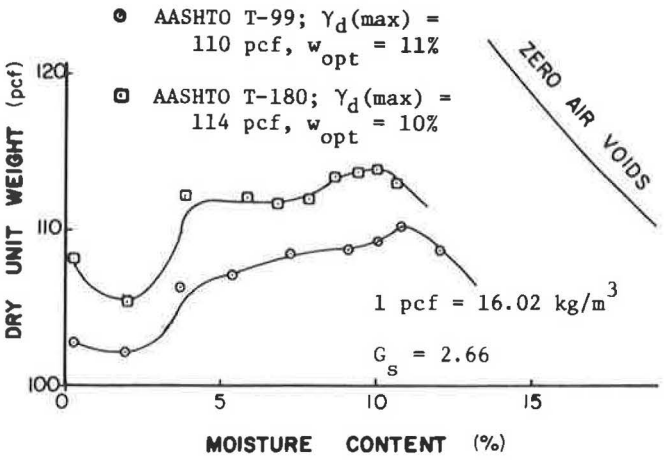

FIGURE 1 Compaction tests on highway subgrade sand, Leon County, Florida.

Several of the test and sample variables mentioned previously were selected for study. Of primary interest were confining stress, cyclic principal stress difference, dry unit weight, and moisture content. Various combinations of these factors were tested in cyclic triaxial tests. Cyclic principal stress difference was set at different percentages of the peak static soil strength (S_d) determined from samples tested at similar dry unit weight, moisture content, and confining stress combinations.

An inverted haversine wave form of 0.1-sec duration was used for all repeated load tests. This period is roughly equivalent to the time in which a vehicle traveling 30 mph (48 km/hr) affects a point in the top of the subgrade of a flexible pavement structure. The 0.1 sec was followed by a 0.9-sec rest period to allow proper damping of the load before the following load was applied. Therefore, a frequency of one load per second resulted. All cyclic tests were continued to 10,250 cycles.

RESULTS AND DISCUSSION

As stated briefly earlier in this paper, the primary objectives of this study were *(a)* to investigate the permanent deformation characteristics of the highway subgrade sand, *(b)* to examine resilient properties and particularly to determine the resilient modulus of the sand, and *(c)* to examine a technique *(6)* developed to predict permanent deformation of soil samples in cyclic triaxial tests from static triaxial test information.

Permanent Deformation

Data from cyclic triaxial loading tests were used to evaluate the permanent deformation characteristics of the highway subgrade sand under various conditions of confining pressure, cyclic principal stress difference, dry unit weight, and moisture content.

A plot of permanent strain (ε_p) versus the logarithm of the number of cycles *(N)* was constructed for each cyclic test sample. The results fit the relationship found in Equation 2. Typical plots may be found in Figure 2.

Of all the test variables that can affect the behavior of granular soil in cyclic loading tests, the confining stress (σ_3) is the most important *(5, 12, 15)*. Increasing confining stress can

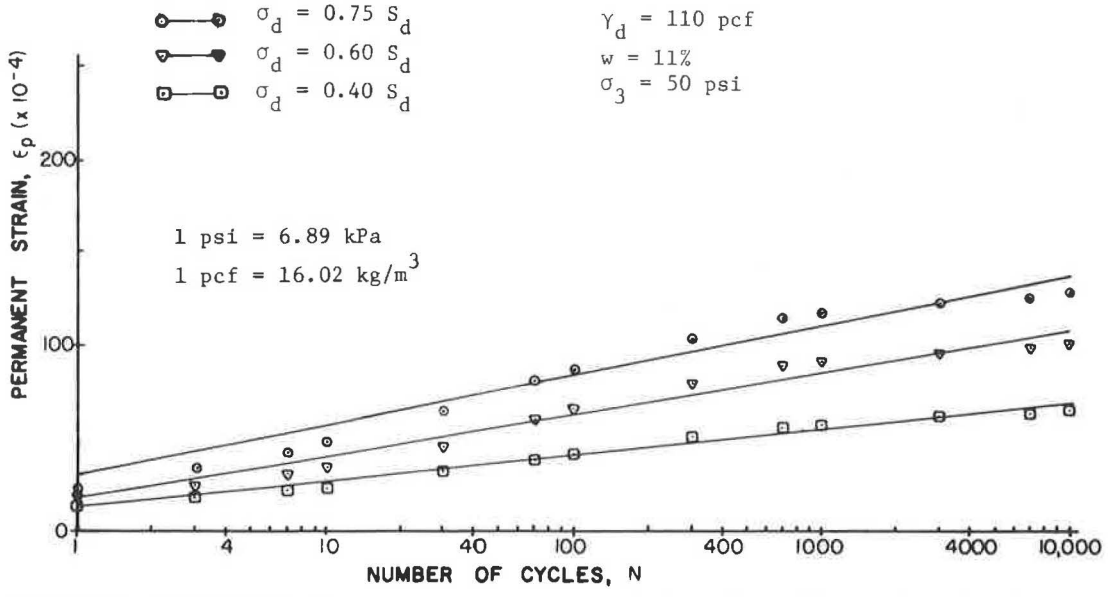

FIGURE 2 Typical plots for permanent strain versus the logarithm of the number of cycles.

greatly increase the strength and resilient modulus of a soil and decrease the permanent strain at a given level of cyclic principal stress difference. The confining stress in a pavement layer depends on the position with respect to the applied wheel load, the magnitude of wheel load, and resilient modulus. Thus, this study included testing at confining stresses of 5, 25, and 50 psi (34.5, 172.3, and 344.5 kPa) for the highway subgrade sand.

The permanent strain values for the 10,000th cycle of each sand sample were determined. The results are summarized in Figure 3 for comparison of the confining stress effects. For lower values of cyclic principal stress difference (σ_d), the permanent strain increased slightly or remained constant for larger confining stress values. However, for the σ_d of 0.75 S_d, the ε_p decreased substantially as confining pressure increased.

Cyclic principal stress difference, as would be expected, had the greatest effect on the permanent strain of the soil. Increasing σ_d results in an increase in the permanent strain for constant confining stress. Figure 3 contains a comparison of the effects on permanent strain for stress ratios of 0.40, 0.60, and 0.75. [Stress ratio is defined as the cyclic principal stress difference divided by the peak static test stress (S_d) performed on a similar sample.] At each of the confining stresses, the

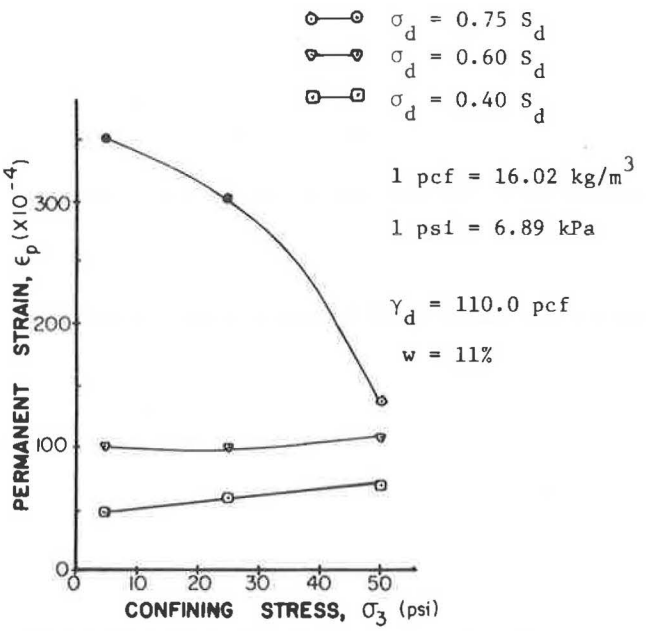

FIGURE 3 Effect of confining stress and cyclic principal stress difference on permanent strain at N = 10,000, AASHTO T-99 dry unit weight and optimum moisture content.

sample strain increased as the stress ratio increased. The difference between the strains at stress ratios of 0.40 and 0.75 was significantly less for the samples subjected to higher confining stress than for those subjected to the lower confining pressure. This observation may be explained by the fact that the higher confining stress causes increased interparticle friction and aggregate interlock, resulting in less movement under load.

Of the sample variables, density or dry unit weight (γ_d) has probably the greatest effect on the permanent strain during cyclic loading of a soil. Figure 4 shows the relationship

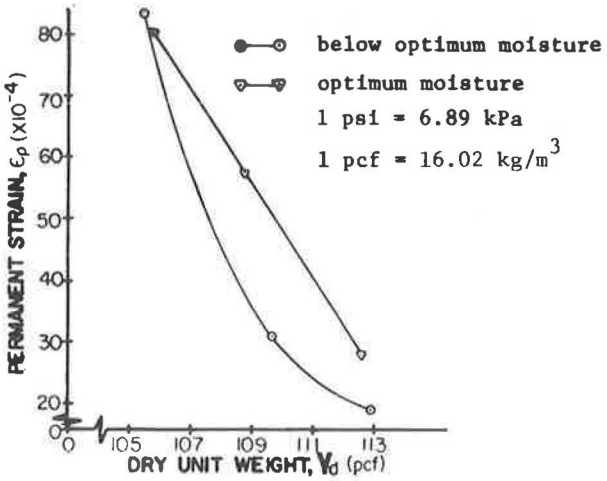

FIGURE 4 Effect of dry unit weight and moisture content on permanent strain at N = 10,000.

between density and permanent strain for the highway subgrade sand. Three dry unit weights were used in testing of the highway subgrade sand—95 percent of AASHTO T-99 (standard compaction), AASHTO T-99, and AASHTO T-180 (modified compaction). The standard and modified samples were compacted and tested at their respective optimum moisture contents. The 95 percent standard compaction samples were densified at the moisture content used as optimum for the standard method. As expected, the high soil density resulted in less permanent soil strain for both the optimum and below-optimum moisture samples. This result is reasonable because higher compactive effort decreases the volume of voids in a soil, resulting in more particle contacts and greater aggregate interlock. Thus, the soil particles are less likely to reorient themselves during loading.

Tests were conducted on two different moisture content levels (3 percent below optimum and at optimum) of the sand. Preliminary plans included testing samples at 3 percent above optimum; however, samples could not be compacted to the required density using the tamping method, so this moisture condition was eliminated from the program.

Figure 4 shows the effect of moisture content on permanent strain for the sand. At the higher densities, increased moisture in the sample appeared to cause an increase in the strain. At the lower density, the strains were virtually identical. The trend at densities outside of the range tested is not known and might be difficult to predict based on the limited results obtained during this testing program. The densities used in these tests, however, included the range that is likely to be encountered in the field.

Resilient Deformation

Another area of interest in this study program was the determination of the resilient modulus (M_R) of the subgrade sand. As with the permanent deformation discussed in the previous section, several test and sample variables and their effects on the resilient modulus were considered.

A plot of the logarithm of resilient modulus versus the logarithm of the number of cycles was constructed for each

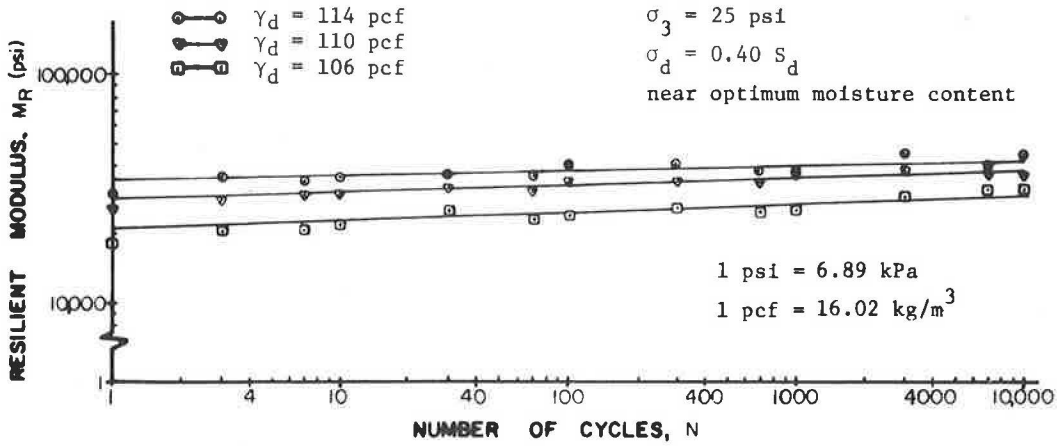

FIGURE 5 Typical plots of logarithm of resilient modulus versus the logarithm of the number of cycles.

cyclic test sample. Figure 5 contains typical plots of the data, showing a very slight increase in M_R as the number of loadings increases.

A relationship between confining stress and resilient modulus for the highway subgrade sand may be observed in Figure 6. This figure contains the values of M_R calculated from the sample regression equations for load cycle 10,000. At each

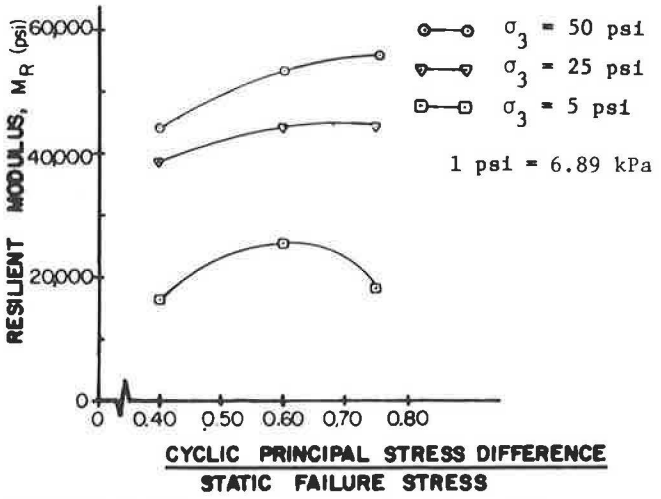

FIGURE 6 Effect of cyclic principal stress difference and confining stress on resilient modulus at N = 10,000.

cyclic principal stress difference, the effect of confining stress on M_R was the same: as confining stress increases, M_R also increases. Values of resilient modulus for the sand were found to be as low as 16,000 psi (110 240 kPa) for the 5-psi (34.5-kPa) confining stress and as high as 56,000 psi (385 840 kPa) for the 50-psi (344.5-kPa) confining stress. Thus, confining stress was shown to have a substantial effect on the value of resilient modulus. The pavement designer, then, is left with the dilemma of which value to use for design of the pavement structure. Values of M_R depend on confining pressure, but confining pressure depends on wheel load, position with respect to the wheel, and M_R.

In this research on Florida sand, conflicting results were obtained on the effect of cyclic principal stress difference on resilient modulus at the various confining stress levels. Figure 6 contains a summary of these results. For the confining stresses of 25 psi (172.5 kPa) and 50 psi (344.5 kPa), the resilient modulus continued to increase as the stress ratio on the tested samples became larger. The rate of this increase was slightly larger for the higher of these two confining stresses. However, M_R at the 5-psi (34.5-kPa) confining stress increased to a peak value and then began to decrease as the stress ratio became larger. The stress ratio at which this peak occurs could not be determined exactly from Figure 6, because only three samples were tested at this confining stress, but it appears that it occurred between stress ratios of 0.50 and 0.65. If so, the decrease in resilient modulus may have been connected with the "threshold" stress that causes a sizable increase in permanent strain on a sample. Further study is required to determine what, if any, relationship exists.

Although the exact nature of the relationship between dry unit weight and resilient modulus for the highway subgrade sand was not well defined in this study, the best-fit line tended to have a positive slope, indicating that M_R increased with increasing dry unit weight. Figure 7 contains the plot of points

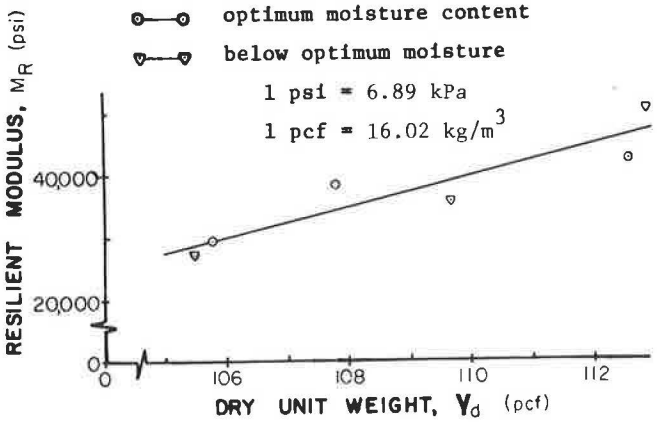

FIGURE 7 Effect of dry unit weight and moisture content on resilient modulus at N = 10,000.

obtained from the samples tested at different dry unit weights or moisture contents or both.

The effect of moisture content on resilient modulus has been a particularly elusive characteristic for researchers to examine. No definite trend has developed for all materials when this area of concern is analyzed. Figure 7 contains comparisons of highway subgrade sand samples tested cyclically at different levels of moisture content in the sand. Because of the scatter in the points, no satisfactory relationships were found between moisture content and resilient modulus.

Normalizing Effect of Static Stress and Strain

Lentz *(6)* developed a technique for predicting cumulative permanent strain in a soil sample under cyclic loads based on simple static triaxial laboratory tests on a similar sample. Because test and sample variables that affect permanent strain are essentially the same for both static and cyclic tests, static test results can be used to normalize the cyclic results. By selecting appropriate points from each test type, one may use samples tested at different densities, confining stresses, and cyclic deviator stresses to define one single curve, which may be used as a predictor of permanent strain after a given number of loading cycles.

For the cyclic tests, Lentz *(6)* selected the cumulative strain and cyclic deviator stress after the 10,000th cycle of load. This point was chosen primarily because most of the samples were loaded no higher than the 10,000th cycle, except for a few special tests on the effects of stress history. Although 10,000 cycles was considerably lower than the number of loadings that can be expected on an average highway pavement, the value was selected *(a)* because of the time required to conduct the individual tests (e.g., 24 hr would allow only 86,400 loadings at one loading per second) and *(b)* because at most cyclic deviator stress ratios, the plot of permanent strain versus log number of cycles remains linear beyond 10,000 cycles.

From the static test results, values of static stress difference and strain were required for the normalization of the cyclic values. Lentz *(6)* selected the peak deviator stress for use in normalizing the cyclic deviator stress. The cyclic stress was divided by the peak deviator stress to achieve the normalization. Thus, this ratio will normally be less than 1 for all cyclic tests. A ratio of more than 1 indicates that a cyclic load larger than the peak static load is being applied, so sample failure and plastic strain will occur after a small number of loads.

A static strain at 95 percent of the peak static deviator stress was selected for use in normalizing the cyclic permanent strain. This value was chosen because *(a)* it contained a large amount of plastic (permanent) strain because it was within only 5 percent of the peak stress and *(b)* it was a well-defined value that was readily reproduced by other testing personnel. Normalization was achieved by dividing the cyclic permanent strain by the selected static strain.

Figure 8 shows the Lentz *(6)* data plotted on the curve of normalized stress versus normalized strain. The solid line represents a hyperbolic function that was used in regression analysis to fit the data points.

Equation 3 is the equation of the hyperbolic curve. Dividing both sides of Equation 3 by $\varepsilon_p/\varepsilon_{0.95S_d}$ and reciprocating both sides gives

$$(\varepsilon_p/\varepsilon_{0.95S_d})/(\sigma_d/S_d) = n + m(\varepsilon_p/\varepsilon_{0.95S_d}) \quad (7)$$

which is a linear relationship with normalized strain as the abscissa, with the ratio of normalized strain to normalized stress on the ordinate, and with n and m the y-intercept and slope of the line, respectively.

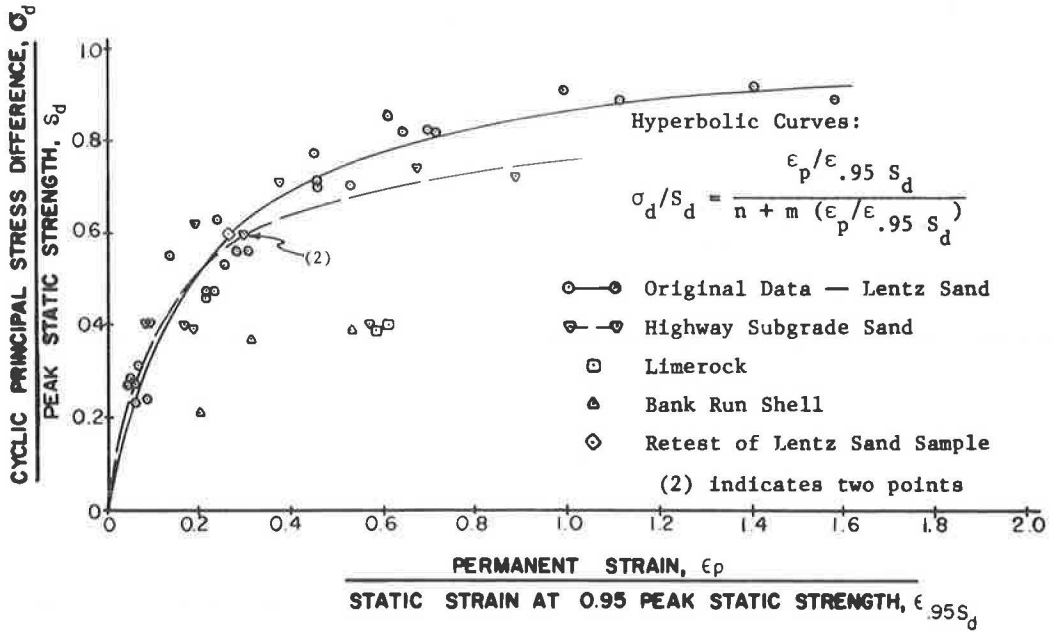

FIGURE 8 Normalized cyclic principal stress difference versus normalized permanent strain at N = 10,000.

One potential problem with the Lentz *(6)* prediction technique was that it was developed by using only one material—a subgrade sand obtained from a test site in the northern part of Michigan's lower peninsula. A primary thrust of this study was to determine whether this technique was applicable to other materials. The subgrade sand obtained from the borrow pit in Leon County, Florida, was the primary comparison material in that sufficient tests were conducted to obtain a statistical relationship between normalized stress and normalized strain. Several samples were run on two other materials, limerock and bank run shell, for an indication of applicability of the technique to other types of granular material with significantly different consistency and gradation.

Figure 8 also shows the data obtained from the testing of the Florida sand. The dashed line is the regression curve obtained for the hyperbolic function. In this same figure two points each for the limerock and bank run shell and one check point for the Michigan subgrade sand are plotted for visual comparison.

Of the 11 data points available for regression analysis on the Florida subgrade sand, 10 were logical in their graph positions, but 1 was found to be an outlier. Because the static stress-strain curve for this sample was much steeper than other curves for the sand, it was believed that some undetected problem had developed during testing. This point, therefore, was determined to be an outlier and was omitted when the best-fit regression line was determined. The remaining points provided a very suitable fit with an r^2-value of 0.977, whereas the r^2-value was reduced to 0.788 when this outlier was included.

Statistical methods provide useful tools for comparing two separate sets of data points such as the Michigan sand data from Lentz *(6)* and the Florida sand data from testing done in this study. The basis for comparing these two data sets is the *y*-intercepts *(n)* and slopes *(m)* of the lines obtained through the least-squares regression analysis, where n and m are the regression constants from Equation 7. For the Michigan sand, n = 0.1970 and m = 0.9591. Similarly, n = 0.1531 and m = 1.1941 for the Florida sand.

Neter and Wasserman *(24)* described the general linear test that allows a statistical comparison of two separate sets of data and their regression lines.

The general linear test indicated that the two regression lines are not identical. Ninety-five percent confidence interval tests were conducted for the individual parameters—slope *(m)* and *y*-intercept *(n)*—to determine whether both parameters differed for the two regression lines. It was found that the *y*-intercepts were essentially the same but that the slopes were different. Although the regression lines from Equation 7 begin at essentially the same level on the axis of normalized strain to normalized stress ratio, this value will increase more rapidly with increasing normalized strain for the Florida sand than for the Michigan sand. That is, for the higher stress ratios, the Florida sand will show significantly more normalized strain, or strain close to the sample failure values for the static tests. This fact would indicate that, of the two materials, the Michigan sand would show greater resistance to rutting in the field. Many additional sands would require testing, however, if a conclusion is desired on the rut susceptibility of these sands in the broad spectrum of sand types.

As noted previously, two samples each of limerock and of bank run shell were also normalized and plotted in Figure 8 to determine whether the relations developed for the sand were good indicators for other coarse-grained materials. Although insufficient tests were conducted to perform a reliable regression analysis, a visual inspection would suggest that the shell and limerock react completely differently from the sand material. It appears that lower stress ratios in the shell and limerock result in higher normalized strain and thus strains closer to the static test failure strain.

CONCLUSIONS

1. Increased confining stress causes a slight or no increase in permanent strain for low stress ratios but a substantial decrease in this strain for large stress ratios. The break point appears to occur somewhere between a ratio of 0.60 and 0.75. Resilient modulus increases as the confining stress becomes larger at all levels of stress ratio. The range of the increase also becomes greater as the stress ratio increases.

2. In all cases permanent strain increases with increasing number of loading cycles. Resilient modulus increases slightly as the number of cycles becomes larger.

3. At each confining stress tested, an increase in stress ratio results in an increase in permanent strain in the sample. This increase is substantial for the 5-psi and 25-psi confining stresses, but is small for the 50-psi sample group. For the 25-psi and 50-psi confining stresses, resilient modulus increases with increasing stress ratio. However, at 5 psi the resilient modulus peaks at a stress ratio between 0.50 and 0.65.

4. For both the optimum and the below-optimum moisture groups, the increase in dry unit weight causes a decrease in the permanent strain.

5. An increase in permanent strain is caused by an increase in moisture content for soil densities near the AASHTO T-99 and T-180 densities. At 96.5 percent of AASHTO T-99 density, the permanent strain is virtually the same for both water contents. Therefore, effects of moisture content on permanent strain cannot be confidently stated because of limited data and conflicting results.

6. Permanent strain on a laboratory sample may be predicted from static load tests by using a hyperbolic relationship found on a plot of normalized stress versus normalized strain. However, when separate hyperbolic relationships were compared for the Michigan sand and the Florida sand, it was statistically determined that the two sets of data produced slightly different relationships (at a 0.05 significance level) and cannot be pooled.

7. Values of resilient modulus after 10,000 loading cycles for the Florida sand ranged from 16,000 psi (110 240 kPa) at 5 psi confining stress to 56,000 psi (385 840 kPa) at 50 psi confining stress. Because confining pressure depends on wheel load and resilient modulus and resilient modulus depends on confining pressure, care should be used when the resilient modulus value to be used in pavement design is determined.

REFERENCES

1. E. J. Yoder and M. W. Witczak. *Principles of Pavement Design*, 2nd ed. John Wiley and Sons, Inc., New York, 1975.

2. R. L. Terrel and S. Rimsritong. "Pavement Response and Equivalences for Various Truck Axle and Tire Configurations." In *Transportation Research Record 602*, TRB, National Research Council, Washington, D.C., 1976, pp. 33–38.
3. *Thickness Design: Asphalt Pavements for Highways and Streets.* Manual Series No. 1. Asphalt Institute, College Park, Md., Sept. 1981.
4. V. A. Diyaljee and G. P. Raymond. Repetitive Load Deformation of Cohesionless Soil. *Journal of Geotechnical Engineering Division, ASCE*, Vol. 108, No. GT10, Oct. 1982, pp. 1215–1229.
5. R. D. Barksdale. *Repeated Load Test Evaluation of Base Course Materials.* Georgia Highway Department Research Project 7002. School of Civil Engineering, Georgia Institute of Technology, Atlanta, May 1972.
6. R. W. Lentz. *Permanent Deformation of Cohesionless Subgrade Material Under Cyclic Loading.* Ph.D. dissertation. Michigan State University, East Lansing, 1979.
7. G. Bouckovalas, R. V. Whitman, and W. A. Marr. Permanent Displacement of Sand with Cyclic Loading. *Journal of Geotechnical Engineering Division, ASCE*, Vol. 110, No. 11, Nov. 1984, pp. 1606–1623.
8. M. McVay and Y. Taesiri. Cyclic Behavior of Pavement Base Materials. *Journal of the Geotechnical Engineering Division, ASCE*, Vol. 111, No. 1, Jan. 1985, pp. 1–17.
9. F. C. Townsend. A Review of Factors Affecting Cyclic Triaxial Tests. In *Special Technical Publication 654*, ASTM, Philadelphia, Pa., 1978.
10. R. Pyke. Some Effects of Test Configuration on Measured Soil Properties Under Cyclic Loading. *ASTM Geotechnical Testing Journal*, Vol. 1, No. 3, Sept. 1978, pp. 125–133.
11. R. W. Lentz and G. Y. Baladi. "Constitutive Equation for Permanent Strain of Sand Subjected to Cyclic Loading." In *Transportation Research Record 810*, TRB, National Research Council, Washington, D.C., 1981, pp. 50–54.
12. R. G. Hicks. *Factors Influencing the Resilient Properties of Granular Materials.* Ph.D. dissertation. University of California, Berkeley, 1970.
13. G. Y. Baladi and T. D. Boker. *Resilient Characteristics of Michigan Cohesionless Roadbed Soils in Correlation to the Soil Support Values.* Final Report. Division of Engineering Research, Michigan State University, East Lansing, 1978.
14. I. V. Kalcheff and R. G. Hicks. A Test Procedure for Determining Resilient Properties of Granular Materials. *Journal of Testing and Evaluation*, Vol. 1, No. 6, Nov. 1973, pp. 472–479.
15. S. F. Brown and A. F. L. Hyde. "The Significance of Cyclic Confining Stress in Repeated Load Triaxial Testing of Granular Materials." In *Transportation Research Record 537*, TRB, National Research Council, Washington, D.C., 1975, pp. 49–58.
16. V. K. Khosla and R. D. Singh. Influence of Number of Cycles on Strain. *Canadian Geotechnical Journal*, Vol. 15, No. 4, 1978, pp. 584–592.
17. P. N. Gaskin, G. P. Raymond, and F. Y. Addo-Abedi. Repeated Compressive Loading of a Sand. *Canadian Geotechnical Journal*, Vol. 16, No. 4, 1979, pp. 798–802.
18. H. B. Seed and C. K. Chan. "Effect of Duration of Stress Application on Soil Deformation Under Repeated Loading." *Proc., Fifth International Conference on Soil Mechanics and Foundation Engineering*, Paris, 1961.
19. K. L. Lee and F. J. Vernese. End Restraint Effect in Cyclic Triaxial Strength of Sand. *Journal of the Geotechnical Engineering Division, ASCE*, Vol. 104, No. GT6, June 1978, pp. 705–719.
20. K. L. Lee, H. B. Seed, and P. Dunlop. Effect of Moisture on the Strength of a Clean Sand. *Journal of Soil Mechanics and Foundation Division, ASEC*, Vol. SM6, 1967, pp. 17–40.
21. J. H. Haynes and E. J. Yoder. "Effects of Repeated Loading on Gravel and Crushed Stone Base Course Materials Used in the AASHO Road Test." In *Highway Research Record 39*, HRB, National Research Council, Washington, D.C., 1963, pp. 82–96.
22. B. A. Vallerga, H. B. Seed, C. L. Monismith, and R. S. Cooper. "Effect of Shape, Size, and Surface Roughness of Aggregate Particles on the Strength of Granular Materials." In *Special Technical Publication 212*, ASTM, Philadelphia, Pa., 1957.
23. T. W. Lambe. *Soils Testing for Engineers.* John Wiley and Sons, Inc., New York, 1951.
24. J. Neter and W. Wasserman. *Applied Linear Statistical Models.* Richard D. Irwin, Inc., Homewood, Ill., 1974.

Publication of this paper sponsored by Committee on Soil and Rock Properties.

Construction Methods To Control Expansive Soils in South Dakota

E. B. McDonald

A review is presented of the stabilization and construction methods used by the South Dakota Department of Transportation during the past 17 years. The nature of the soils involved is discussed and a short history of the problems encountered is given along with the techniques of grading and stabilization used to control the expansive properties of the Pierre shale. The 1967 performance of the roadway surface is compared with that in 1984. The conclusion is that rideability will be better over a longer period of time at lower maintenance costs on highways placed on expansive soils when the soils have been undercut, reworked, and replaced at controlled moisture and densities than on highways placed on these soils using normal methods. Stabilizing the upper portion of the replaced soil with lime preserves the high moisture content used in placing the soils and provides added support for the prevention of rutting by the equipment used in the placement of the surfacing courses.

Swelling soils are a construction problem in many parts of the United States as well as in many areas of the world. Nearly the whole western half of South Dakota and small portions of the eastern half are composed of highly expansive Pierre shale. The liquid limit of this soil varies from 65 to 120 with plastic indices of 40 to 85. This condition is aggravated by perched water tables and associated frost problems that exist, in some areas, because of the fractured structure of the soils.

The Missouri River divides the state of South Dakota into two distinct landforms. The western half, with the exception of the Black Hills area, is composed mainly of Pierre shale. There is a small region of sand dunes near the Nebraska border and a thin Fox Hill sandstone cover in the northwest corner. The White River formation overlies a portion in the southwest central portion of the state (Figure 1).

The Pierre shale is composed of interbedded layers of highly plastic colloidal clays and silts, with some areas containing nearly pure bentonite. These deposits vary in thickness from several feet to several hundred feet. The layers are differentiated with respect to the degree of weathering, volume change, and water susceptibility. The upper portion of the deposit is weathered to a fine homogeneous till-like clay, varying in depth from 1 to 15 ft. The next portion is weathered to an open jointed condition that admits water when the upper clay mantle is removed and is susceptible to large volume changes when subjected to alternate dry and wet cycles, such as those prevalent in western South Dakota. The expansive pressure of the shale varies from 15 to 100 psi, depending on the moisture and density at which it is placed (Figures 2 and 3).

Pete Lien & Sons, Inc., 1201 W. 21st Street, Sioux Falls, S.D. 57105.

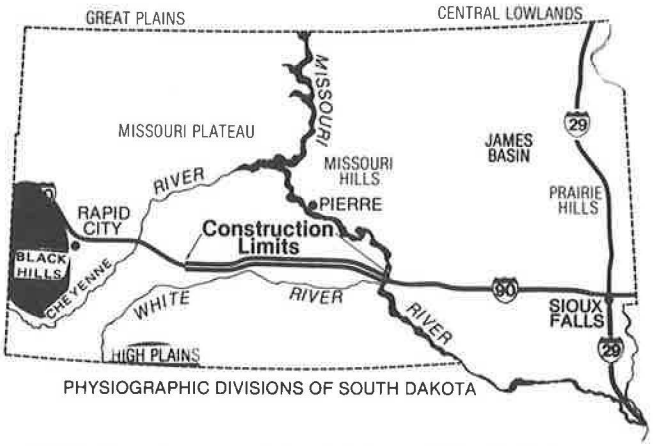

FIGURE 1 Physiographic divisions of South Dakota.

OBJECTIVE

The purpose of this paper is to briefly review the design and construction methods used by the South Dakota Division of Highways in building a 131-mi portion of I-90 through the Pierre shale and to present data on how well this length of Interstate has served in regard to rideability, deflection, and maintenance during the past 13 to 17 years.

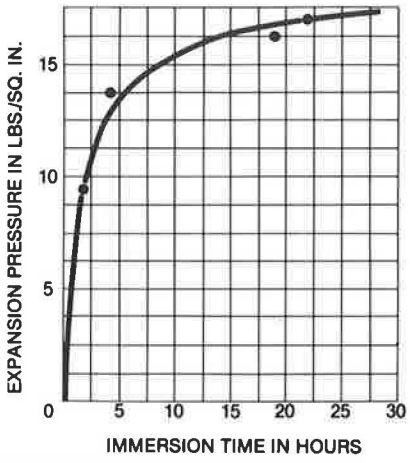

FIGURE 2 Expansion pressures of South Dakota soil: standard AASHTO compaction (T-99); moisture content, 28.9 percent.

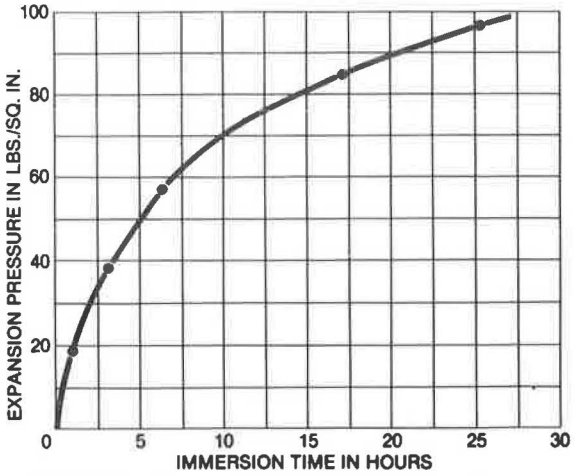

FIGURE 3 Expression pressures of South Dakota soil: modified AASHTO compaction (T-180); moisture content, 18.1 percent.

HISTORY

Before 1952 asphaltic mats of 1½ to 2-in. thickness in conjunction with 4 to 8 in. of standard base course were used as surfacing materials over the Pierre shale. Several short sections of 6 to 8 in. of concrete surfacing had been placed on the shale in and near the cities of Pierre, Winner, and Chamberlain. Both of these surfacing types distorted badly within 3 to 5 years after placement. The most dramatic failure of all of these highways was a 9-mi section east of Rapid City on I-90. It was built in 1961 with normal methods and became extremely rough in the summer of 1962. This dramatic failure provided the impetus for the Materials and Soils Section of the Division of Highways to begin a serious investigation aimed at finding methods to curtail the extreme warping of highway surfaces that occurs when they are constructed in expansive soil *(1–3)*.

A comprehensive research program involving a test project of 8.7 mi and containing several types of stabilizing agents and different types and thicknesses of surfacing materials was started in 1963. This test project was studied for a period of 4 years, concluding in 1968. A continuation study was also conducted on this project, which concluded in 1975.

Analysis of some of the early test results indicated that stabilization of the upper surface of the shale subgrade did produce, to some degree, a smoother riding surface in the same time frame as highways previously constructed without stabilization. However, because of the deep-seated nature of the moisture problems associated with the Pierre shale, a considerable amount of roughness developed in many sections of the test project.

Observations of projects built before the test project indicated that where undercutting of 6 to 12 in. was performed, an improvement of rideability was obtained. With the knowledge gained from the research project and a review of construction techniques and performance of existing highways in the Pierre shale, comprehensive laboratory tests were started in 1964. These tests included special moisture and density tests and volume change tests and freeze-thaw data on shale with and without stabilizing agents. On the basis of data obtained, a decision was made that in addition to using lime as a stabilization agent, an extreme depth of undercutting in conjunction with rigid moisture and density control would be used on the remaining portion of I-90 from Mileposts 131 to 262, which is located in the Pierre shale. The biggest factor in determining the extreme depth of undercutting was laboratory test results revealing that the swell potential of the upper mantle of Pierre shale, as well as the jointed weathered shale, could be drastically reduced when the density was held to 92 percent of AASHTO T-99 and the moisture was held at 3 percent above the optimum moisture content. The surfacing from Mileposts 131 to 198 and from 213 to 251 is composed of 8 in. of continuous reinforced concrete on a 3-in. lime-stabilized base over a 6-in. lime-stabilized subgrade. Mileposts 198 to 213 and Mileposts 251 to 262 are composed of 9 in. of asphalt concrete on a 6-in. lime-stabilized subgrade.

GRADING TECHNIQUES

Special soil inspection teams who had considerable experience in grading construction were chosen from various districts of the department. These teams were given a special course of instruction in the central laboratory that dealt specifically with construction as it related to soil selection, special moisture-density control work, soil identification, interpretation of specifications, and special provisions. These men worked directly under the resident engineer and acted in an advisory capacity to him regarding the grading operation insofar as it related to selection of soil and the identification and disposal of highly plastic soil. They were responsible for determination of undercutting that was needed in addition to the plan quantities. They were required to keep daily diaries of all phases of work within their responsibilities.

Mainline undercutting for the top 3 ft of earth subgrade was designated full roadbed width, shoulder slope to shoulder slope. The backfill material, including the upper 3 ft of the adjacent fill areas, is composed of selected subgrade topping. The undercut area below the top 3 ft to a depth of 6 ft is confined between the subgrade shoulder lines. This lower 3 ft forms a trench 52 ft wide, shoulder to shoulder (Figure 4).

In order to meet the density limits of the specifications, the energy-input method was used to control the work. It was anticipated that four uniform coverages of a sheepsfoot roller over the disked surface would meet the stipulated density requirements. Frequent moisture and pulverization tests were taken to ensure that proper moisture was adequately dispersed to obtain the required density.

Review of Special Provisions

1. Selected subgrade topping for the upper 3 ft of all roadway backfill and embankments was sufficiently processed to readily receive water with 90 percent (exclusive of rock) passing the 1-in. sieve in accordance with Test SD 212.

2. Sources of selected topping were confined to horizons and areas designated on the plans or by the soil crews and engineer. The upper 6 in. of sod was excluded.

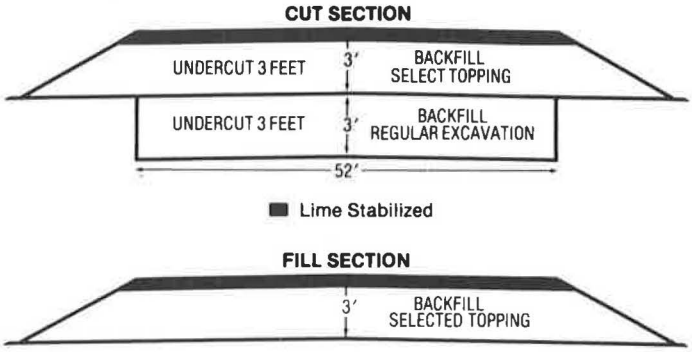

FIGURE 4 Typical grading sections: South Dakota I-90, Mileposts 131 to 262.

3. The 6-ft depth of undercutting was reduced to 3 ft or increased as necessary by the engineer.
4. Undercut or other suitable material that did not contain bentonite was used to construct the undercut area below the 3-ft selected topping zone.

Selected topping was measured and paid for on plans showing embankment volume and shrinkage. Payment was made for additional work, selection, blending, extra haul, and interim stockpiling.

Review of Requirements for Upper 6 ft of Embankment

1. The selected topping was placed in loose lifts generally not exceeding 8 in. and pulverized by disking to the satisfaction of the engineer, as determined by Test SD 113.
2. Compaction was obtained by use of controlled passes of a sheepsfoot roller. Four coverages of the sheepsfoot were normally used, with a minimum of not less than two coverages.
3. Density tests were made to guide the energy-input method; the following tests were required:

- Density minimum, 92 percent AASHTO T-99;
- Density target, 95 percent AASHTO T-99; and
- Moisture target, 3 percent above optimum,

Requirements for Embankments Below 6-ft Zone

1. Loose lifts did not exceed 12 in.
2. Each lift was leveled and pulverized by disking and properly watered and mixed.
3. Density tests to guide the energy-input method were as follows:

- Density minimum, 95 percent AASHTO T-99;
- Berm adjacent to structures, 100 percent AASHTO T-99; and
- Moisture target, 3 percent above optimum.

Review of Original Laboratory Test Data

A series of density tests was run to determine what effect higher compactive efforts would have on the shale in regard to cubic weight and moisture and what effect they would have on shale that had been stabilized with lime. The T-180 method produced a density of 96.2 pcf at an optimum of 23.5 percent for the raw shale. A density of 91 pcf at an optimum of 26.5 percent was obtained for the lime-stabilized soil. The T-99 method produced densities of 77.2 pcf at an optimum moisture of 33.6 percent for the raw soil and 70.0 pcf at an optimum of 35 percent for the lime-stabilized shale (Figure 5).

To find out how different degrees of density and moisture affected swell potential, a series of swell tests was performed on soils taken from the upper mantle of Pierre shale and from the underlying jointed shale. It was found that when this soil was subjected to lower water content and higher density, the swell potential was two to three times higher than when the soil was subjected to lower density and higher water content. The same series of tests applied to the jointed underlying shale showed that the swell potential was two to four times higher for the high-density–low-moisture condition than for the lower

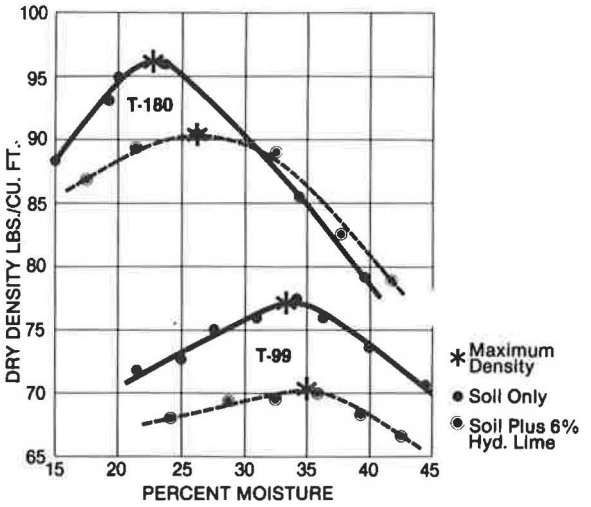

FIGURE 5 Effect of compactive effort on density of South Dakota shale.

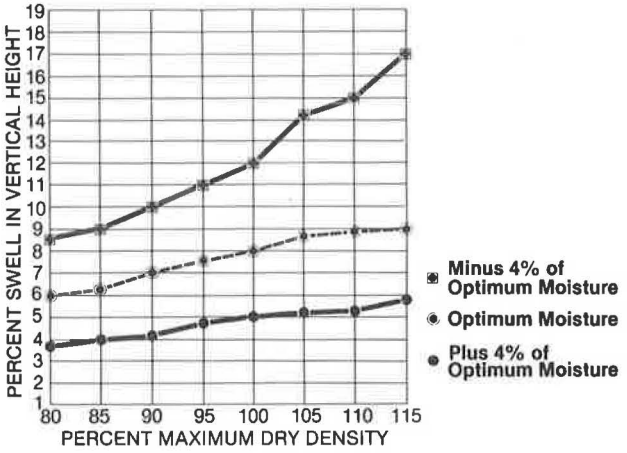

FIGURE 6 Special swell tests on weathered shale.

density and higher moisture (Figures 6 and 7). As noted earlier, it was on the basis of these tests that the decision was made to undercut the parent shale and replace it with selected topping from the upper mantle of Pierre shale.

EARLY PERFORMANCE

A review of the follow-up field tests, in which 21,851 moisture-density tests were taken, shows that the material was placed

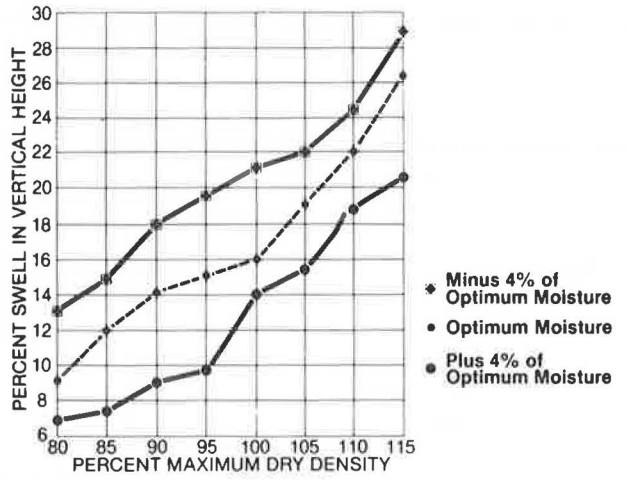

FIGURE 7 Special swell tests on jointed shale.

relatively close to the target density and moisture contents. The lower 6-ft zone of all fills was placed at 98 percent of T-99 at 2 percent above optimum moisture. The upper 6-ft zone of all undercut sections and the upper 3-ft zone of all fill sections were placed at 98 percent of T-99 at 2.1 percent above the optimum moisture content (Figure 8).

The South Dakota Division of Highways has run a comprehensive roughness and deflection program on its highways since 1970. The roughometer data are based on an index scale of 0 to 5; 5 is very good and anything below 2.5 is poor. Deflection testing is based on millimeters of deflection on a scale of 1 to 5; 1 is very good and anything over 3 is very poor.

• Total Miles Constructed—130.323
• Number of Tests Taken—21,851
• Average Density in Upper 6′ Zone—98% of T-99
• Average Moisture in Upper 6′ Zone— + 2.1% of Opt.
• Average Density in Lower 6′ Zone—98% of T-99
• Average Moisture in Lower 6′ Zone— + 2.0% of Opt.
• Number of Cubic Yards of Excavation—53,991,610
• One Test Taken for Approx. Each 2,500 Cu.Yds. of Material

FIGURE 8 Moisture-density construction data, South Dakota I-90, Mileposts 131 to 262.

The roughness index in 1975 for the asphalt surfacing was 4.22. Deep-strength asphalt has a tendency to crack at fairly close intervals, which results in faulting. Some roughness due to faulting rather than subgrade differentials resulted, which reduced the index to 3.80 by 1980. The joints were milled off in 1980 and the material was relaid, resulting in an index of 4.31 in 1984. A total of 26 mi of surfacing is composed of asphalt on this portion of the Interstate. The remaining 105 mi is composed of concrete. The roughness index for the concrete was 4.35 in 1975. In 1984 it was 4.09. It is evident that the differentials associated with surfacings built in the Pierre shale have been controlled quite well, because much of this mileage was built in 1967, 1968, and 1969 (Figure 9).

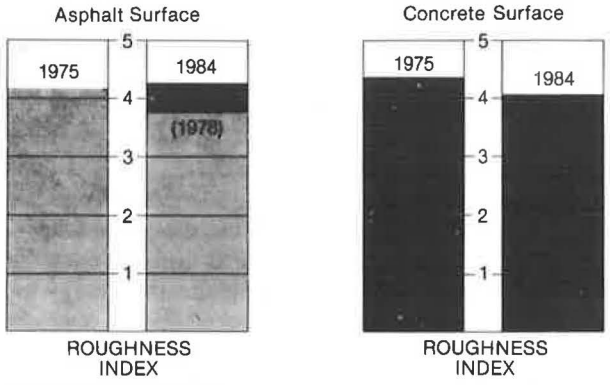

FIGURE 9 Roughometer data, South Dakota I-90, Mileposts 131 to 262.

A review of the deflection data shows that both the asphalt and concrete have slightly less deflection in 1984 than in 1975. It is possible that the overall subgrade condition had a higher moisture content in 1975 or that the lime-stabilized base or subgrade or both have higher strengths now than in 1975 (Figure 10).

The cost factor at the time that this section of highway was built is not really significant because inflation did not really begin until 1973. However, it is reasonable to believe that, all things being equal in regard to grading operations, the added cost of undercutting and lime stabilization would be in the same relative degree to the regular grading costs now as they were at the time that this grade was constructed.

A review of the surfacing, grading, undercutting, and lime

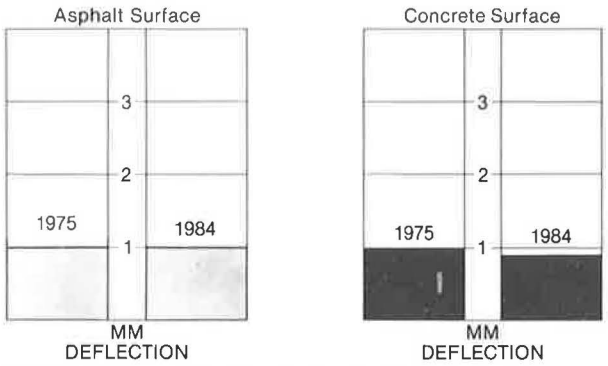

FIGURE 10 Deflection data, South Dakota I-90, Mileposts 131 to 262.

stabilization costs in Figure 11 shows that the asphalt surfacing cost about 35 percent less than the concrete, but the inflation in asphalt costs has now made these two types of surfacing about equal in cost. Grading costs in South Dakota have always been quite low in comparison with those in other areas of the country. it can be seen that the additional cost of undercutting

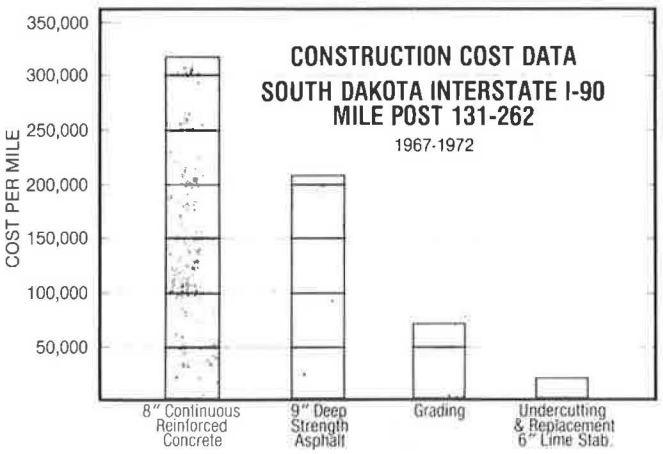

FIGURE 11 Construction cost data, South Dakota I-90, Mileposts 131 to 262, 1967–1972.

and lime stabilization increased the grading costs by about 38 percent. However, the increase was only about 5 percent of the overall surfacing and grading cost for the concrete sections and about a 9 percent increase in the overall cost for the asphalt sections.

CURRENT PERFORMANCE

Reference to the current performance in regard to rideability and deflection in 1984 is shown in Figures 9 and 10. In Figure 12 maintenance costs are compared for both asphalt and concrete surfaces that were placed on the selected lime-stabilized areas. These costs are compared with those for other similarly constructed surfaces on areas where normal grading techniques were used. It is shown that on asphalt surfaces the maintenance costs per year are approximately four times less where undercutting, lime stabilization, and moisture-density control were

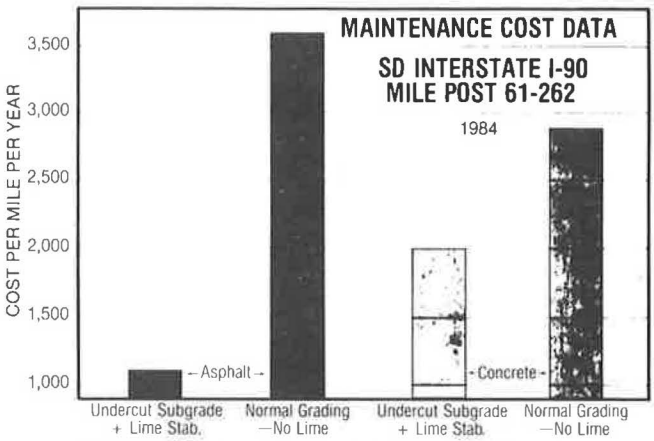

FIGURE 12 Maintenance cost data, South Dakota I-90, Mileposts 61 to 262, 1984.

used compared with costs on asphalt surfaces where these methods were not used. The maintenance costs for concrete surfaces for these same undercut and stabilized conditions are about 30 percent less than for the concrete placed on normal graded subgrades. This is a significant savings considering that most of the mileage of the highways compared is 15 years old and older.

CONCLUSIONS

The following conclusions are based on the review of the data presented.

1. Much of the objectionable differentials in the Pierre shale that have caused considerable road surface roughness in the past have been alleviated.
2. Trained crews can control undercutting and special moisture-density requirements needed to reduce the expansion of heavy plastic soils.
3. Special undercutting with special moisture-density control and replacement of soils can reduce the effects of swelling soils on highway rideability.
4. The long-term maintenance costs are less for surfacings placed on subgrades that have been undercut, reworked, or replaced at special moisture-density requirements than for surfaces placed on normal grades.

The methods discussed in this paper will not be 100 percent effective in correcting all of the differentials associated with expansive soils when highways are built in these areas. However, data given in this paper show conclusively that rideability will be better over a longer period of time at lower maintenance costs on highways placed on expansive subgrades that have been undercut and replaced using special moisture and density control methods and stabilized with lime than on highways where these procedures have not been used.

REFERENCES

1. A. W. Potter and E. B. McDonald. "Highway Design and Construction Through Expansive Soils in South Dakota." Presented at

Workshop on Swelling Soils in Highway Construction, Bureau of Public Roads, Region 9, Denver, Colo., Sept. 19-21, 1967.
2. E. B. McDonald. "Stabilization of Expansive Shale Clay by Moisture-Density Control." In *Transportation Research Record 641*, TRB, National Research Council, Washington, D.C., 1977, pp. 11–17.
3. *Treatment of Expansive Soils for Interstate Highway I-90, South Dakota.* Woodward-Clyde-Sherard and Associates, Denver, Colo., May 1965.

Publication of this paper sponsored by Committee on Environmental Factors Except Frost.

Genesis and Distribution of Colluvium in Buffalo Creek Area, Marion County, West Virginia

ROBERT B. JACOBSON

Two types of colluvium are present on the Buffalo Creek landscape, an area typical of that part of the Appalachian Plateaus underlain by rocks of the Dunkard Group. Thick deposits of entrenched, diamicton, debris-flow-generated colluvium occur as long fingers in coves (zero-order drainage basins). These deposits range up to 15 m thick but most are 5 to 8 m thick. The deposits are the product of early Wisconsinan slope processes that produced colluvium at a greater rate than it could be removed by streams. Colluvial fingers are currently well drained because they are deeply dissected by gullies; natural slopes on colluvial fingers are relatively stable. The second type of colluvium is generated as modern slope failures shear bedrock and transport material downslope. Colluvium generated by this process collects up to about 2 m thickness on bedrock benches until failure conditions are reached and the material is transferred to the next lower bedrock-controlled bench. Colluvium converges on hummocky areas at heads of gullies and is eventually delivered to streams by debris flow or fluvial erosion of failure toes. Different types of modern natural slope failures occur on different surficial geologic units, indicating that surficial geologic setting has a strong influence on failure mechanisms and relative stability of natural slopes.

The Buffalo Creek area in Marion County, West Virginia (Figure 1), is typical of much of the Appalachian Plateaus underlain by rocks of the Pennsylvanian-Permian Dunkard Group. In the Buffalo Creek area there are two distinct types of colluvium: *(a)* thick, cove-filling diamicton deposits that are relicts of the influences of a Pleistocene climate and *(b)* thin colluvium that is being generated and transported under present-day conditions. ("Diamicton" is used here to denote deposits with bimodal particle size distributions, in particular those with cobble- to gravel-size clasts mixed with a silty and clayey matrix.) The origin and occurrence of these two types of colluvial deposits and their influence on relative slope stability are discussed.

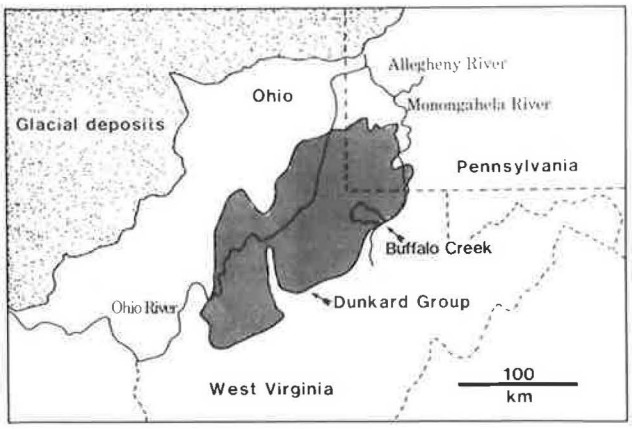

FIGURE 1 Upper Buffalo Creek study area showing outcrop area of Pennsylvania-Permian Dunkard Group and Pleistocene glacial border.

GEOLOGY OF BUFFALO CREEK AREA

The Buffalo Creek area is underlain by gently deformed sandstones, mudstones, and shales of the Pennsylvanian-Permian

Department of Geography and Environmental Engineering, Johns Hopkins University, Baltimore, Md. 21218. Current affiliation: U. S. Geological Survey, Mailstop 926, Reston, Va. 22092.

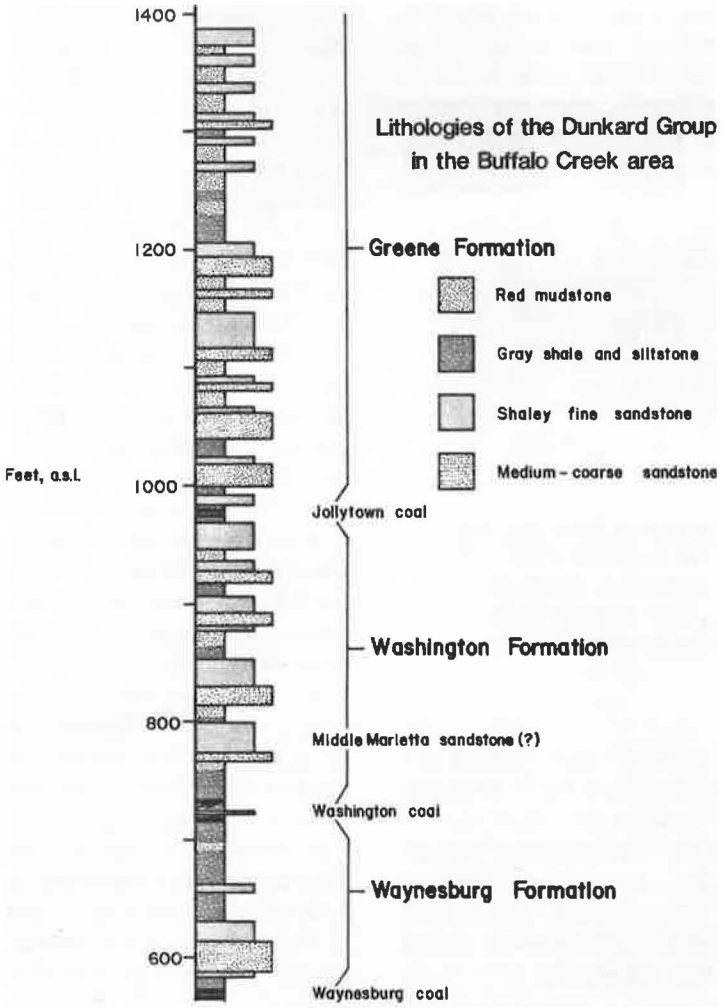

FIGURE 2 Geologic column for Buffalo Creek area from ridgetop diamond drill core log *(1)*.

Dunkard Group. Dips range from 0 to 2 degrees. A typical geologic section from a diamond drill core log is shown in Figure 2. In the Buffalo Creek area, the lower part of the Dunkard section, including the Waynesburg Formation and the lower Washington Formation [as defined by Berryhill et al. *(1)*], is composed of gray siltstone and sideritic shale interbedded with thick (15 to 30 m) sandstones. The remainder of the Washington Formation above the Middle Marietta sandstone and the entire Greene Formation are composed of repetitive cycles of interbedded sandstone and mudstone.

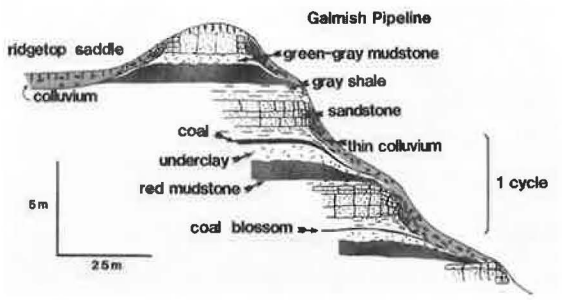

FIGURE 3 Typical hillslope stratigraphy from pipeline trench in upper Dunkard Group showing colluvial mantles on bedrock-controlled topographic benches.

Red mudstones slake readily in water and have abundant fracture porosity. These two features combine to make the mudstone much weaker than superjacent and subjacent sandstones. On typical slopes in the upper Dunkard Group, juxtaposition of these strong and weak lithologies results in distinctly stepped slope profiles with 30- to 50-degree slopes on sandstone risers and 10- to 28-degree slopes on mudstone benches. Figure 3 shows a typical Greene Formation slope profile and surficial stratigraphy in a measured section exposed in a pipeline trench in Wetzel County, West Virginia.

Topography in Buffalo Creek is characterized by deeply embayed coves (or zero-order drainage basins) that form large amphitheater-like areas at heads of drainage. Ridge-to-valley relief ranges from 150 to 180 m.

SURFICIAL STRATIGRAPHY

The Buffalo Creek basin is approximately 150 km south of the Pleistocene glacial border and was flooded with slack water at least twice during the Pleistocene when glacial ice and outwash gravel dammed the north-flowing Monongahela River (*2*, *3*).

Small isolated patches of pre-Illinoian and Illinoian lake beds can be found preserved on sandstone-protected benches on valley walls. Figure 4 shows an exposed cross section of deposits near Mannington, West Virginia, where pre-Illinoian and Illinoian clayey-silt lake sediments are overlain and underlain by thick diamicton colluvium (TDC).

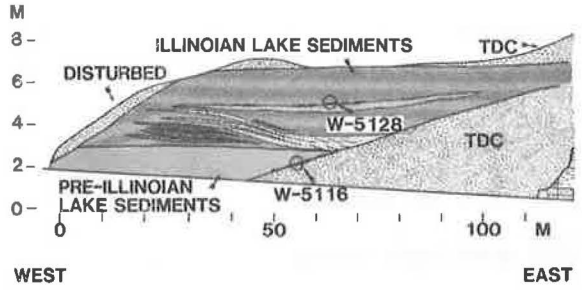

FIGURE 4 Surveyed section at Mannington, West Virginia, railroad cut showing TDC interbedded with pre-Illinoian and Illinoian lake-bed sediments. (W-prefix numbers refer to radiocarbon-dated organic samples older than 40,000 years.)

TDC consists of cobble-size sandstone clasts floating in a silty matrix. Many of the elongate clasts have rough downslope orientation. Unconformities and bedding are rare except for unusual cases from exposures on the extreme sides of deposits that have shown stacks of two to three generations of diamicton units with buried weathered soil horizons at the contacts. Most exposures of TDC show massive diamicton without internal unconformities. These observations suggest that most of the TDC that existed before the most recent pulse of TDC deposition was eroded before or during that period. Moreover, the most recent period was characterized by large debris flow events and rapid deposition rather than by smaller events and gradual deposition.

Because TDC units are found underlying pre-Illinoian lake beds as well as underlying and overlying Illinoian lake beds, it is clear that the Buffalo Creek area has experienced multiple generations of TDC deposition during the early to late Pleistocene. However, most TDC remaining on the landscape is from the most recently deposited pulse that overlies Illinoian lake beds.

TDC occurs in coves as long fingers bounded by gullies or as small eroded patches of debris fans at cove-valley junctions. The spatial distribution of remnants indicates that TDC once filled coves and was later entrenched and eroded. Remnant TDC fingers range up to 15 m thick but most are in the range of 5 to 8 m thick. TDC and other surficial geology units are shown in a three-dimensional perspective diagram in Figure 5.

Low-angle alluvial fans prograde out from TDC-entrenching gullies and grade to terraces and active floodplain of the valley bottom alluvial complex (Figure 5). Fan deposits have a noticeably higher percentage of clasts than does TDC: 70 to 90 percent by volume in fans compared with 40 to 60 percent in TDC. There is a general trend from matrix-supported debris flow sediment at fan apexes to more fluvial, clast-supported gravel and sand at fan toes. Therefore, it is concluded that most fan sediment is delivered to fans by debris flow and the sediment is then progressively reworked by fluvial processes downslope on the fans.

Alluvial fan segments grade to alluvial deposits and terraces ranging in age from Recent to late Wisconsinan, roughly 10,000 to 18,000 years old. Because the most recent TDC deposit is crosscut by the alluvial fans, it must be older than late Wisconsinan, and because the bulk of TDC overlies Illinoian lake beds, most TDC is younger than Illinoian. Comparison of iron mineralogy, clay mineralogy, and accumulated clay in TDC weathering profiles with weathering profiles from a sequence of independently dated alluvial terraces on the Ohio River indicates that the latest pulse of TDC has been weathering since the end of the early Wisconsinan glacial advance, approximately 55,000 years before the present (*3*). Correlations of weathering profiles also indicate an early Wisconsinan age for 0.5- to 2-m-thick diamicton colluvium commonly found in ridgetop saddle positions (Figure 5).

The presence of TDC deposits on ridgetops where contributing slopes are very gentle and the large volume of TDC that is apparent on reconstructing entrenched deposits show that the

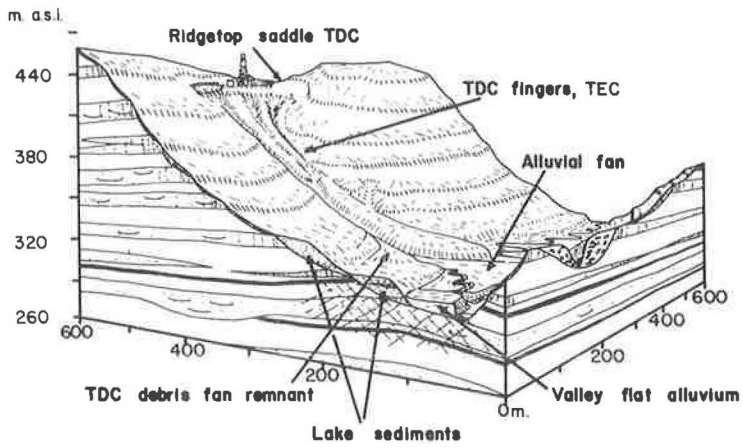

FIGURE 5 Three-dimensional perspective diagram showing morphology and stratigraphy of surficial geologic units in Buffalo Creek area.

Buffalo Creek landscape was extensively destabilized during the early Wisconsinan. Upland erosion was sufficient to strip hill-slope residual weathering profiles and form thick colluvial deposits as production of colluvium overwhelmed the transport capacity of streams. In contrast, the late Wisconsinan climate produced geomorphic processes that favored fluvial dissection of TDC. Dissection has continued to this day, leaving TDC as long fingers with 8- to 18-degree longitudinal slopes and 30- to 50-degree gully side slopes.

It should be emphasized that the spatial sequence of TDC and alluvial fan deposits described earlier is found consistently throughout this landscape (*3*). Moreover, soil cores reveal that TDC soil profiles are consistently weathered to an extent commensurate with an early Wisconsinan age.

Hill-slope area not occupied by cove-filling or ridgetop saddle TDC is covered by thin colluvium and weathered bedrock (TC/R). Figure 6 shows typical stratigraphic relations on upper Dunkard Group (upper Washington and Greene formations) TC/R hillslopes as exposed in a trench in the Buffalo Creek area. Diamicton colluvium, ranging up to 2 m thick, overlies sheared mudstone in the center of the bench and tapers to feather edges over weathered sandstone at the upper and lower ends. Shear zones and conspicuous slickensides occur at or slightly below the colluvium contact and are found on all slopes on this landscape. Movement along these zones shears mudstone and mixes in weathered sandstone to create diamicton colluvium. These observations indicate that failure in mudstone is an integral part of the process by which colluvium is created and transported on these slopes.

Weathering profiles in the TC/R complex are weakly developed. Weathered sandstone may have up to 15 cm of true residual soil over fractured and partly weathered rock. Weathering profiles in bench colluvium have cambic B horizons (weak structural development with little accumulation of clay and sesquioxides) or lack B-horizon development altogether, indicating that periods of stability are short, around several thousands of years or less.

PRESENT-DAY SLOPE PROCESSES

Slope failures on natural slopes in the Buffalo Creek area were studied by detailed mapping at 1:8000 scale in nine small drainage basins totaling 29.2 km^2. These data reveal that location, type, and density of natural slope failures are strongly influenced by surficial geology of the area. Comparison of slope-failure spatial density on the two types of colluvial units can give an indication of relative stability. However, because slope-failure temporal frequency is not considered, spatial density must be interpreted with caution.

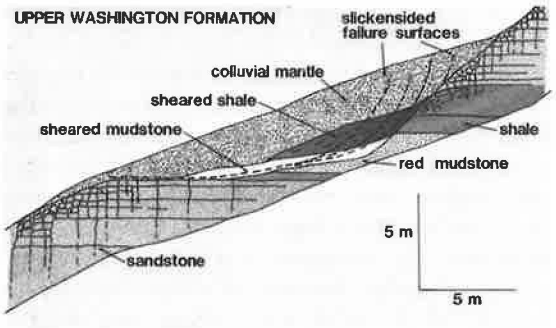

FIGURE 6 Surveyed section in trenched slope failure, upper Washington Formation, Buffalo Creek area. Rotational failure occurs in mudstone section underneath accumulating colluvial mantle.

A total of 716 slope failures was inventoried. Of that total, 561, or 78.4 percent, occurred in TC/R. Dividing TC/R failures by the area occupied by TC/R gives failure density of 28.6 failures/km^2, equal to 11 975 m^3/km^2. Among TC/R failures, 68.6 percent of the total number and 83.5 percent of the inventoried volume were rotational failures on mudstone benches like that shown in Figure 6. This amounts to 65.2 percent of the total volume of all failures regardless of surficial lithology; hence the majority of the mappable failure volume on this landscape is produced on mudstone benches.

Figure 6 shows how size and location of mudstone bench rotational failures are controlled by mudstone bedrock thickness and sandstone layer spacing; failures begin below upper sandstone layers and toe out above the next lower sandstone. Mean surface slope for mudstone bench failures is 19.8 degrees (N = 254; SD = 5.5 degrees).

Observations from the trench exposure shown in Figure 6 and from other trenched failures indicate that stability of TC/R mudstone benches is controlled by several factors. A basal slickensides shear surface starts in colluvium or weathered sandstone at the upslope end of the failure and passes downward through shale and mudstone in a near-circular arc. Older shear surfaces are often present above the basal shear surface and are often encrusted with iron and manganese oxides. About midway through the failure mass the basal shear surface flattens out, converges with the older shear surfaces, and passes to the ground surface. When a failure initiates in this setting, intact mudstone and colluvium are sheared in the circular portion of the failure surface and peak strengths of these materials are mobilized. In the flattened portion of the failure surface, where mudstone and colluvium have been previously sheared, residual or near-residual strengths are mobilized. In addition, where the failure surface intersects the root zone, typically from 0 to 1 m deep, roots can be expected to add a component of cohesive strength. Typical effective-strength values for these components were gathered from reports of geotechnical tests on similar materials in the region and are summarized in Table 1.

Using the strength values in Table 1 as representative estimates for the Buffalo Creek area and with the shear-surface geometry shown in Figure 6, Janbu static equilibrium slope-stability analyses indicate that this general class of failures requires pore pressures from a piezometric surface at least 27 cm above the ground surface in order to approach failure for the 19.8-degree mean slope condition [more details are given elsewhere (*3*)]. These calculations are consistent with field observations during periods of prolonged rainfall when artesian spouts of water up to 15 cm high have been seen issuing from root holes and faunal burrows. Excess pore pressures can develop in TC/R because the massive colluvium is much less permeable than underlying sheared and fractured mudstone and sandstone.

TABLE 1 TYPICAL EFFECTIVE-SHEAR-STRENGTH PARAMETER VALUES FOR HILLSLOPE MATERIALS IN BUFFALO CREEK AREA

Component	$\bar{\phi}$ (degrees)	$\bar{c}$ (kN/m^2)	Test	Source
Peak mudstone	18.0	10	Direct shear	Hamel and Adams (*4*)
Residual mudstone	13.0	0	Direct shear	Hamel and Adams (*4*)
Colluvium	31.5	0	Triax, CU	ASCS (*5*)
Tree roots	0	4.3	Extension device	GSA (*6*)

Note: ASCS = Agricultural Stabilization and Conservation Service; GSA = Geological Society of America.

Rotational TC/R failures tend to equilibrate at a postfailure angle of approximately 15 degrees. Each site then evolves back to failure conditions as colluvium from upslope accumulates in the failure scar. The rate of accumulation is ultimately controlled by the rate of sandstone weathering. As colluvium accumulates and loads the bench, threshold pore-water pressure values decline until the occurrence of a meteorological event of sufficient magnitude causes failure. In this manner production and accumulation of colluvium drive a cascading system of slope failures that transports colluvium downslope. Colluvium eventually converges and accumulates on benches above TDC gullies, just above the beginning of integrated drainage channels. These are common failure sites and tend to have hummocky microtopography suggestive of frequent movement. When these benches fail, colluvium is dumped directly into gullies by debris flows or fluvial erosion of failure toes. In general, colluvium generated and transported by TC/R failures completely bypasses TDC without influencing TDC stability.

The remaining 31.4 percent of TC/R failures is composed of shallow planar slides on sandstone slopes. In terms of volume, TC/R planar failures account for only 16.5 percent of the TC/R volume and 12.9 percent of total inventoried failure volume. Sandstone planar failures occur on a mean slope of 33.7 degrees (N = 157; SD = 6.1 degrees).

Slope failures on TDC compose 21.6 percent of the total inventory and 39.6 percent of the total volume. Failure density is 23.1 failures/km^2, equal to 9818 m^3/km^2. These failure density data show that TDC is somewhat more stable than TC/R under natural conditions. Planar slides on TDC gully side slopes make up 81.9 percent of TDC failures, and all appear to be the result of oversteepening by lateral stream erosion. Mean failure slope for these planar failures is 42.3 degrees (N = 110; SD = 7.7 degrees).

Simple infinite slope-failure models using typical effective Mohr-Coulomb strength parameters for colluvium and tree roots as noted in Table 1 show that slopes as steep as those found on colluvial finger side slopes should only exist under conditions of zero pore-water pressure and fully mobilized root strength. The infinite slope model for planar failures shows that a dry equilibrium slope can exist up to approximately 40 degrees. Without root strength, dry slopes should stand at the internal angle of friction, around 31.5 degrees; wet slopes, with the water table at the surface, should equilibrate near 17 degrees and wet slopes with root strength would equilibrate near 28 degrees. These simple calculations show that observed stability of natural TDC gully side slopes at inclinations exceeding 43 degrees is dependent on both tree root strength and free drainage resulting from deep dissection.

Erosion and failure of alluvial fans, valley-bottom alluvium, and old lacustrine deposits were not explicitly studied. Depositional slopes of the first two units are very stable and failures occur mainly by toppling of cut banks where lateral stream-channel migration causes local oversteepening. Remnants of old lacustrine deposits underlie only a small fraction of the Buffalo Creek area, and under natural conditions these deposits are stable because of equilibration to extreme wet conditions during the Pleistocene (*3*).

SUMMARY AND DISCUSSION

Landscape history of the Buffalo Creek area provides a model for the distribution of surficial lithologies. TDC deposits, relicts from Pleistocene-age climatic influences, exist as entrenched fingers in coves and as eroded patches of debris fans at cove-valley junctions. Late Wisconsinan to Recent entrenchment of TDC created gravelly alluvial fans that are inset against TDC and prograde onto valley bottoms.

Colluvium is being created under present-day conditions by slope failures that shear up bedrock and move colluvium downslope from bench to bench. Colluvium converges on bedrock-controlled benches just above entrenched gullies. Hummocky topography in these areas suggests that they are relatively active parts of the landscape. Failures in the hummocky areas ultimately deliver colluvium to the gullies and the rest of the fluvial system.

The genesis and spatial distribution of colluvium in the Buffalo Creek area have many similarities with other areas in the Ohio River Valley, but there are also some important differences. Slopes adjacent to major river valleys are exemplified in a study of colluvium in McMechen, West Virginia by Gray and Gardner (*7*, pp .29–32). In the McMechen area two similar processes generate colluvium: on slopes where drainage basins have been carved, colluvium accumulates in coves; on slopes with straight contours, colluvium cascades downslope from bench to bench to accumulate at the base. Because the McMechen area is in a relatively young, gorgelike section of the Ohio River [near the former divide between the preglacial Teays and Pittsburgh rivers (*2*)], slopes are uncommonly steep and surface drainage has not been developed along long sections of the valley walls. Under these conditions it appears that colluvium is being produced faster than it can be removed by streams.

In contrast, the Buffalo Creek area has been eroding steadily for a longer time and is not close to the bluffs of a major river. Hence, the topography has developed with deeply embayed coves and continuously curving convex and concave contours;

surface drainage is well developed in these small drainage basins. As a result, TC/R failures converge into coves and deliver colluvium to stream channels rather than accumulating at the foot of slopes. The modern (Holocene and Recent) balance between production of colluvium on slopes and removal by streams does not allow colluvium to accumulate in thick deposits.

In the McMechen area, the late Wisconsinan age of the thick, foot-slope colluvium (7) indicates that these steep valley-wall slopes were extensively destabilized by the late Wisconsinan climate. In contrast, the Buffalo Creek area experienced major accumulation of debris-flow-generated colluvium in early Wisconsinan time when colluvium was generated faster than streams could export it from small basins. Fluvial dissection and alluvial fan deposition occurred in this area in the late Wisconsinan.

Present-day, natural slope-failure mechanisms are strongly influenced by surficial geologic setting. Most failures occur as rotational, colluvium-generating failures on mudstone benches. Failure susceptibility of these rotational failures increases as colluvium collects on mudstone benches; the mean failure slope requires moderate artesian pore-water pressure to reach failure, an event that is not uncommon under modern conditions. A smaller proportion of failures occurs as planar failures on weathered sandstone risers.

Planar failures on TDC gully side slopes are equilibrated to fully mobilized root strength and negligible pore-water pressures. Dry conditions prevail on these slopes because deep dissection encourages rapid drainage and low groundwater tables. Sorting of failure mechanism, location, and density according to surficial geologic setting indicates that different surficial geologic units have important differences in relative stability.

The results of this study may help in geotechnical engineering problems in Dunkard Group and similar landscapes by providing a predictive model for the spatial distribution of surficial geologic materials and by showing the relative stability of these materials in their natural setting.

ACKNOWLEDGMENT

Parts of the research reported here were sponsored by the U.S. Geological Survey and the Geological Society of America.

REFERENCES

1. H. L. Berryhill, S. P. Schweinfurth, and B. H. Kent. *Coal-Bearing Upper Pennsylvanian and Lower Permian Rocks, Washington Area, Pennsylvania.* Professional Paper 621. U.S. Geological Survey, Reston, Va., 1971, 47 pp.
2. F. Leverett. Glacial Deposition in Pennsylvania. *Pennsylvania Geological Survey, Fourth Series, Bulletin G-7*, 1934, pp. 91-98.
3. R. B. Jacobson. *Spatial and Temporal Distributions of Slope Processes in the Upper Buffalo Creek Drainage Basin, Marion County, West Virginia.* Ph.D. dissertation. Johns Hopkins University, Baltimore, Md., 1985, 485 pp.
4. J. V. Hamel and W. R. Adams. "Claystone Slides, Interstate Route 79, Pittsburgh, Pennsylvania, USA." In *Proc., International Symposium on Weak Rock*, Tokyo, Japan, 1981.
5. *Geotechnical Report on Hibbs Run Flood Control Dam Site, Marion County, West Virginia.* Agricultural Stabilization and Conservation Service, U.S. Department of Agriculture, 1980.
6. M. M. Reistenberg and S. Sovonick-Dunford. The Role of Woody Vegetation in Stabilizing Slopes in the Cincinnati Area, Ohio. *Geological Society of America Bulletin*, Vol. 94, 1983, pp. 506-518.
7. R. E. Gray and G. D. Gardner. Processes of Colluvial Slope Development at McMechen, West Virginia. *Bulletin of the International Association of Engineering Geologists*, No. 16, 1977, pp. 29-32.

Publication of this paper sponsored by Committee on Engineering Geology.

The Sherman Landslide: A Case History

BERKE L. THOMPSON AND BARNEY C. STINNETT

The lower part of a massive colluvium landslide located along the Ohio River near Ravenswood, West Virginia, has affected railroad traffic for an undetermined time. The railroad had unsuccessfully attempted to stabilize it by using timber piles and railroad rails. The roadway above the railroad had not required significant maintenance before 1970. After the pool level of the Ohio was increased by the U. S. Army Corps of Engineers from elevation 551.4 ft to 560.0 ft between 1969 and 1971, the landslide movement became more active. The subsequent repair for the roadway had progressed beyond routine maintenance by 1975 with subsidence of the roadway and a near-vertical 2-ft scarp at the edge of the pavement. In a geotechnical study in 1976 to develop a correction, it was found that the movement at the roadway and railroad was but a small part of the total instability, which included the entire mountainside. The 1,000 ft of movement extended from the top of the mountain to below the pool level of the river. The methods of correction considered were a piling wall, a counter berm, and a relocation. The methods of failure ranged from shallow to deep-seated circular failures, flows, topples, and planar failures. The final correction, proposed in 1976 but constructed in 1984, that satisfactorily solved all of the instability problems was a major relocation of the roadway into the hillside.

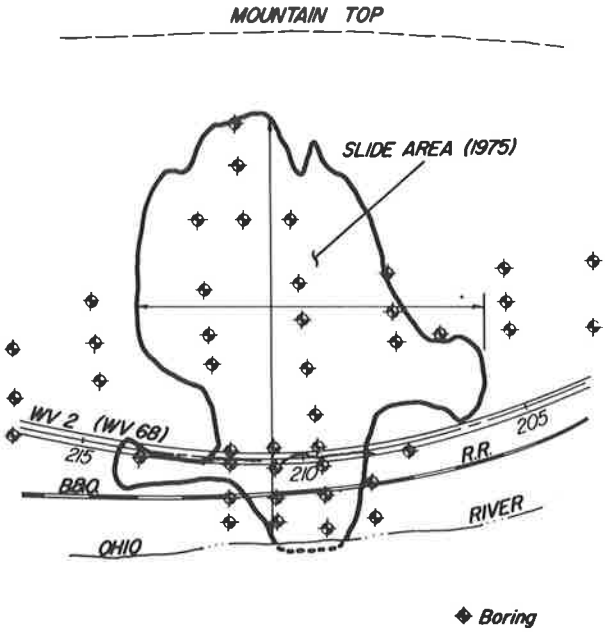

FIGURE 1 Plan view of Sherman landslide.

The Sherman landslide, so named because of a small community nearby, is located approximately 4 mi north of Ravenswood in Jackson County, West Virginia. It became a problem for the West Virginia Department of Highways in the early 1970s. A serious safety hazard resulted when a 2-ft vertical scarp occurred at the edge of the pavement. This scarp became larger as time progressed. A sag of 8 in. was apparent in the roadway, with several longitudinal tension cracks in the pavement (Figure 1).

The highway where the landslide is located was a two-lane expressway (WV-2) in the early 1970s. This highway parallels the Ohio River from Chester in the north to Huntington in the south. WV-2 is an important commercial route because of the industrial plants along the Ohio River. The entire length of approximately 235 mi has always been plagued with rockfalls and landslides that have hampered traffic flow. Because of the nearby mountainous terrain there is often no close alternative route for a detour if a portion of the route is closed.

The failures are due to weak shale bedrock and accompanying poor soil, along with fluctuating groundwater levels and high seepage forces. In addition, the pre-1950 construction of a high percentage of the roadway was by the cut-and-cast method without drainage layers.

This failure, which was surveyed in 1975 for the investigation of the landslide, involved only about 600 ft of roadway. The length of the overall failure zone transverse to the highway was almost 1,000 ft. Although the roadway had not experienced any significant problems before, the situation changed radically in the 1970s. The movement in the embankment next to the river progressed from the initial movement to such a degree that the status and size of the landslide caused it to be considered a critical one. This was one of the reasons that a 37-mi section of WV-2 containing this landslide was rerouted to Interstate 77. The classification of the bypassed section was then reduced from an expressway to WV-68, a feeder route.

The Baltimore and Ohio Railroad (B&O) has a single track 70 ft horizontally and 17 ft vertically downslope from the roadway. After the Racine Locks and Dam were built, the edge of the Ohio River at normal pool was 110 ft horizontally and 34 ft vertically downslope from the railroad. This location had apparently been a problem for the railroad for several years before 1975. During this time the railroad had tried several times unsuccessfully to stabilize their track, once with timber piles and once with railroad rails on both sides of the track. Although the highway surface had required some maintenance before 1970, the pavement thickness did not indicate that any significant leveling courses had been placed in the area before the problem in the early 1970s. The landslide activity at the roadway appeared to occur subsequent to a significant increase in the normal pool elevation of the Ohio River at this location. After the Racine Locks and Dam had been completed, approximately 20 mi downriver, the pool level was raised in stages so that the low lift wicket dams above the dam could be removed and river traffic could still be maintained. Two of these wicket dams affected the pool level at the landslide location—Number

West Virginia Department of Highways, 312 Michigan Avenue, Charleston, W. Va. 25305.

22 below and Number 21 above this location. The pool level was increased from 551.4 to 557.0 ft mean sea level (MSL) on September 20, 1969, and from 557 to 560 ft MSL on August 26, 1971, according to the Corps of Engineers, for a total increase at this site of 8.6 ft.

Although the original investigation of the slide was completed in September 1976 and a correction had been proposed, no action was taken to implement the correction until 1983 because of the cost of the correction and the lack of funds for this classification of highway.

The landslide affecting the roadway was in the lower one-third of the overall instability and continued to take more of the roadway during the 5.5 years after 1976. During this period several minor shifts of the roadway were made into the hillside in an attempt to keep it open to two-way traffic. The landslide movement by early 1982 had failed through the original alignment and had closed one lane of the relocated roadway. Any more shifts into the hillside would have required removal of a significant amount of soil, which could have precipitated a landslide into the roadway. To keep traffic moving through the failure area without any removal of soil, traffic lights were installed for one-way traffic through the landslide.

In 1983, because of continued failure, it became apparent that a permanent correction would have to be constructed to keep the roadway open. The field check in 1984 of the 1976 plans revealed that the lateral limits of the landslide had extended downriver and the instability had become deeper upslope, with much more movement near the mountaintop. The plans were modified as quickly as possible without additional geotechnical field investigation. Although some risk was inherent in this decision, the activity of the landslide and options left to maintain traffic did not allow further delay. Bids for this project were opened on October 30, 1984, and the project was awarded to Lang Brothers, Inc., of Bridgeport, West Virginia.

INVESTIGATIONS

Because of the workload of the department's Geotechnical Section in 1975, it was decided to utilize one of the geotechnical consultants who had a yearly contract to perform this type of investigation for the department. Approval by the department was required before development of any final corrective design by the consultant.

Law Engineering Testing Company was selected to perform the work. The consultant visited the site and prepared an outline of the work to be performed. This included 28 borings, laboratory testing, and a geotechnical report recommending a corrective design. Included in the 28 borings were 6 cased borings to survey subsurface movement. The department authorized the consultant to proceed with the work on September 17, 1975.

Borings

After 25 percent of the borings had been completed adjacent to the roadway, it was found that the soil depths both above and below the roadway were more than 60 ft. The consultant had originally estimated shallower depths for the soil and as a result of this initial boring data, some of the early suggested corrective methods being considered, such as piling, were found to be impractical. The consultant revised the scope of work on November 12, 1975, from 28 to 19 borings, with the approval of the department, in an effort to stay within the original approved engineering costs and still accurately define the failure planes. By January 29, 1976, it was believed that the movement data were representative of the actual landslide movement planes.

Four conclusions were reached by the department and the consultant on January 29, 1976, at the scheduled review:

1. On the basis of the subsurface data, two failure planes are located beneath the highway (Figure 2, Station 210+00). This conclusion was based on indicated movement zones in Borings C-12 and C-11. Boring C-12 above the roadway had a surface elevation of 610.6 ft and Boring C-11 below the roadway had a surface elevation of 608.6 ft. There was only one zone of movement in Boring C-12 at a depth of 19 to 22 ft. There were two zones of movement in Boring C-11, an upper zone at a depth of 9 to 13 ft and a lower zone at 25 to 30 ft. The rate of movement also varied for the two zones of movement. The upper zone, which was in Boring C-11 but not in C-12, had a

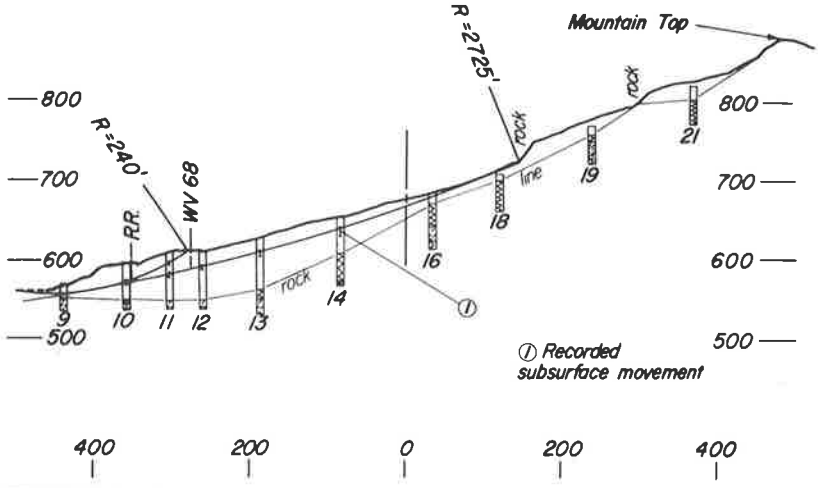

FIGURE 2 Boring locations and failure planes.

measured movement of 1.5 in. in 81 days. The lower zone in C-11 and the zone in C-12 moved 0.25 in. in 81 days. Using the movement data from Borings C-10, C-11, C-12, C-13, and C-14, it was found that the lower deep-seated movement had a scarp 400 ft to the right (east) of the roadway. The toe for this movement was below normal river pool elevation instead of above the roadway as the consultant had previously thought.

2. A berm (buttress) either between the roadway and railroad as proposed by the consultant or in the vicinity of the edge of the river, preferred by the department, will not stabilize the deep-seated lower failure zone. This conclusion was based on the evaluation of the long failure plane. The buttress would control the lower part of the failure, but a new toe for the failure could surface upslope in the vicinity of the roadway.
3. The only feasible correction is a major relocation of the roadway into the hillside and on the bedrock. This would also improve the alignment.
4. Sufficient borings should be completed to design the relocation, including the mountainside cut slope.

As a result of this review, 24 borings were added and all 43 borings were completed by April 19, 1976.

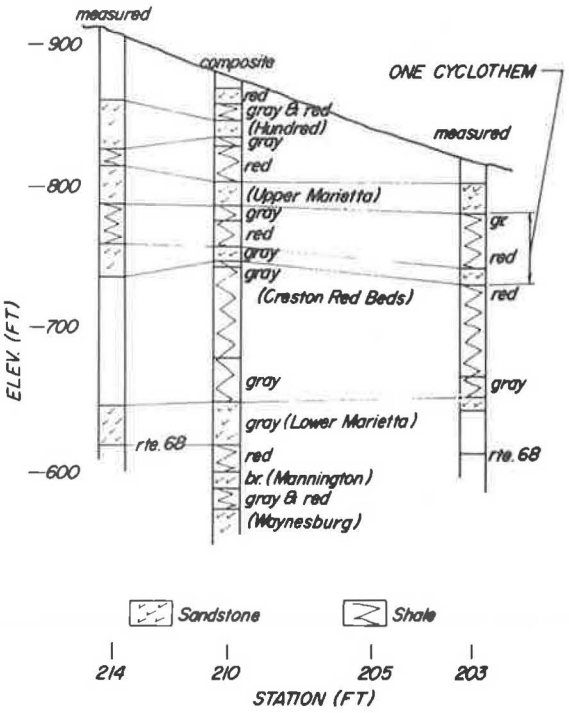

FIGURE 3 Stratigraphic columns.

Testing

The consultant performed testing and soil analyses on 38 samples from 10 of the 43 borings completed in this area (Law Engineering Testing Company, unpublished data). The following tests were performed according to ASTM on undisturbed Shelby tube samples and disturbed split spoon samples:

1. Standard Proctor, undisturbed density and natural moisture;
2. Sieve and hydrometer analysis, specific gravity, and Atterberg limits; and
3. Triaxial shear tests (consolidated-undrained, consolidated-drained, and unconsolidated-undrained).

The soil strength values from the triaxial tests were as follows (ϕ = angle of friction; c = cohesion):

	Colluvium Peak	*Colluvium from Failure Zone*	*Alluvium*
ϕ (degrees)	20–24	12	19
c (psf)	300	125	125

The soil plasticity of the colluvium was high. Using the data for consolidated triaxial tests, the permeability was estimated to be 5.1×10^{-5} ft/day.

Geology

The bedrock at the landslide site is from the Permian Period (*1*), Lower Dunkard Series, and is some of the youngest bedrock in West Virginia. It is composed of nonmarine cyclic sequences called cyclothems (*1*) of sandstone and red and gray shales.

A cyclothem is a repetitive cycle of rock types, arranged in a particular sequence (Figure 3). Normally the coal units would be used as the boundaries for each cycle. Because no coal units were present, the bases of the sandstone units were arbitrarily used for the boundaries. As with cyclothems in general, and also at this site, all the rock units in a particular cyclic sequence may not be present because of erosion or environmental conditions. This is believed to be due to the variable depositional and erosional conditions at specific sites. The theory of a cyclothem is that the bedrock members that are present will be in the same relative position in all cycles to the other members in a cycle. At this site there are at least six cycles.

The bedrock units along the face of the slope have a significant variance in thickness. Measured sections and a composite boring log for several borings were used to evaluate the bedrock for slope design of the relocated roadway. Three sections are compared in Figure 3. In the center of the 1,100-ft horizontal distance along the centerline of the project, the thickness of the sandstone units decreases by as much as 50 percent. The corresponding shale units are thickened by the amount lost from the sandstone units.

The effect of the thickening of the shale units in the cyclothems in the center of the landslide is fourfold:

1. The colluvium is more plastic;
2. The colluvium has significantly lower strength, particularly with increased moisture;
3. The quantity of colluvium is larger because of a greater mass wasting the weaker shale units of the slope; and
4. A larger weak shale unit occurs below each sandstone unit, resulting in less stability of the sandstone unit.

The well-developed joint system in the sandstone, which was opened by the erosion of the Ohio River Valley, contributes in three ways to the instability of the slope:

1. The joints provide excellent avenues for groundwater,
2. The open-joint system in the sandstone results in free-standing blocks of sandstone (some of significant size), and
3. The underlying shale units are subsequently critically weakened as a result of excess moisture and near-surface weathering, resulting in reduced foundation support for the sandstone blocks.

As a result, large blocks of sandstone become a part of the colluvium because the supporting shale is sheared off or because the blocks topple from lack of support.

Although the Parkersburg syncline is only 6.4 mi east and is almost parallel with the face of the mountainside, it does not significantly affect this location. At the site of the landslide the strike is north 7 degrees east and the dip is 0.4 degree to the southwest. The dip of the bedding plane can be considered as nearly flat and has little effect on groundwater flow or slope failure.

Soil Characteristics

There are two types of soil below the roadway (Figure 4). From the surface to a depth of approximately 30 ft is colluvium, composed of brown clayey silt and silty clay with shale and sandstone fragments.

The soil below the colluvium is alluvial, 25 to 30 ft thick, and extends to bedrock. The alluvial soil, a silty clay with no shale or sandstone fragments, is a terrace deposited by the Ohio River. The elevation of the alluvial soil indicates that it is probably the remnant of the first terrace and was deposited during or shortly after the glacial period (2).

The colluvium extends continuously up the mountainside for a horizontal distance of 630 ft from the river's edge and for a vertical height of 156 ft above the river. Upslope from this elevation, the mountainside has two exposures of weathered shale and sandstone. The remainder of the upper slope consists of a colluvium mixture of soil, weathered shale, and sandstone boulders. The slopes are in various stages and types of failure from the mountaintop down to the continuous colluvium overburden:

1. In the shale, wedge failures, flows, and shear failures;
2. In the sandstone, toppling and wedge failures; and
3. In the colluvium, shearing and flows.

This movement eventually reaches the head of the lower continuous colluvium slope that extends into the river. As it flows or shears over the lower colluvium material, it loads the upper reaches of this mass. The failure of the upper slopes thus keeps the deep-seated lower failure plane active. The rate of failure of the lower deep-seated landslide is thus somewhat dependent on the rate of failure of the upper slope.

Weather Data

Weather data for 1965 through 1984 were obtained from the National Weather Service (NWS) for Parkersburg, West Virginia, which is about 21 straightline miles north of the landslide. This is the closest weather station to the failure that maintains continuous records. Although the daily and monthly amounts of rainfall at the landslide site may or may not compare exactly with the Parkersburg data, the yearly average should be in fairly good agreement. The data were collected for 10 years before the 1975 investigation and for 10 years after the investigation (Table 1).

The data were averaged on 10-year cycles because that was one of the cycles that the NWS indicated that they had used. However, different beginning and ending years were used in this study. The NWS indicated that a variance from the average of 10 in. would be within the normally expected yearly variance from the average. There are no yearly rainfall amounts that would be considered abnormal, although the amount in 1972, 1975, and 1983 was high and that in 1981 was low.

ANALYSIS

A review of the U. S. Geological Survey topographic maps found a significant topographic expression on the river floodplain at the site of the landslide (Figure 5), which had been in evidence in all of the topographic surveys reviewed. It was apparent that this expression was made up of the continuous colluvium slope. The subsurface movement data indicated

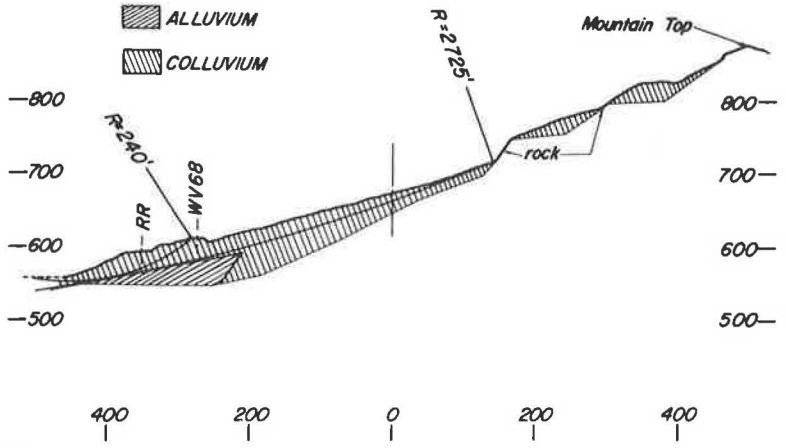

FIGURE 4 Soil types and failure planes.

TABLE 1 NATIONAL WEATHER SERVICE DATA FOR PARKERSBURG, WEST VIRGINIA

Year	Rainfall		
	Total (in.)	Avg (in.)	Departure from Avg[a] (in.)
1965	30.58	37.42	6.84–
1966	32.61	37.42	4.81–
1967	35.04	37.42	2.38–
1968	43.37	37.42	5.95+
1969	31.88	37.42	5.54–
1970	38.32	37.42	0.90+
1971	34.69	37.42	2.73–
1972	47.37	37.42	9.95+
1973	38.89	37.42	1.47+
1974	41.40	37.42	3.98+
1975	45.51	37.35	8.16+
1976	33.77	37.35	3.58–
1977	32.08	37.35	5.27–
1978	36.87	37.35	0.48–
1979	41.04	37.35	3.69+
1980	37.35	37.35	0.00
1981	28.68	37.35	8.67–
1982	36.70	37.35	0.65–
1983	45.16	37.35	7.81+
1984	36.31	37.35	1.04–

[a]A normal departure from average for this site is 10 in.

that the deep-seated (lower) failure plane was located at or near the base of the colluvium just above the alluvium–colluvium interface and was probably the cause of this expression. The shallow (upper) failure from the roadway to the river was also in the colluvium (Figure 4). The safety factor (SF) for the upper failure plane was analyzed by the consultant using the ICES LEASE I Simplified Bishop Method. (See Figure 2 for the location of the upper failure plane.)

An SF of 1.05 for a failure plane generated by the program was in the general area of the upper failure plane. The strength values used were ϕ = 12 degrees and c = 125 psf from the consolidated-undrained strength values of an undisturbed sample taken 18.6 to 19.1 ft deep in the colluvium in Boring C-12. The groundwater (piezometric surface) elevations used were measured at least 24 hr after the borings were complete. A check of the computer-developed plane was performed by using a large-scale model. The data for the model consisted of an SF of 1, the surface limits of the landslide, and the subsurface movement survey depths. The strength values determined were ϕ = 12.5 degrees and c = 125 psf; thus, the computer-developed failure surface indicated excellent agreement with the actual failure surface.

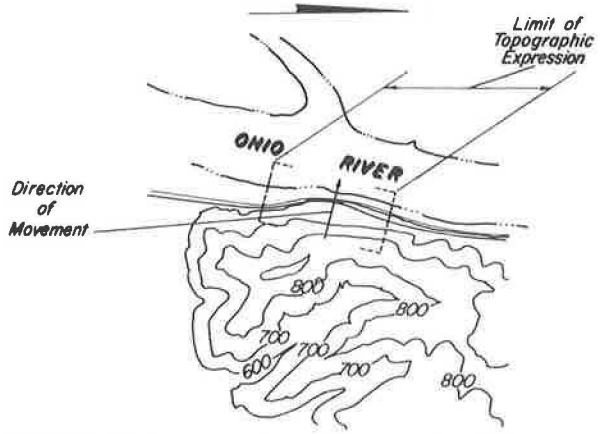

FIGURE 5 Topography of Sherman landslide.

The consultant used an infinite slope analysis to determine an SF of 0.99 for the lower, deep-seated failure plane. The input values used were a depth (d) of 25 ft on an angle of movement (B) of 17 degrees.

No further analysis of the lower slopes was necessary for the relocation correction. The excavation for the relocation at the top of the continuous colluvium slope did, however, remove some of the driving forces from the head of the lower, deep-seated failure plane. This failure plane should become less active after construction of the realignment. The relocation is not expected to create any significant improvement in the stability of the upper failure zone from the existing roadway to the river.

The department analyzed the possible reasons for the increased landslide activity after 1970. Using the ICES LEASE I Simplified Bishop Method, failure surfaces through the areas of movement indicated on the consultant's subsurface surveys were analyzed.

The analysis was conducted by using Borings C-10, C-11, C-12, C-13, and C-14 (see Figure 2), which is a cross section through the center of the landslide. A radius of 2,725 ft was used for the lower deep-seated failure plane and a radius of 240 ft was used for the upper shallow failure plane. The strength values from Boring C-12 at the depth of the failure in the colluvium were used in the analysis. The same strength values were used in the upper shallow failure (Figure 6).

The piezometric surface before 1969 to 1971 was 8.6 ft lower at the river's edge than the 1975 piezometric surface. The two surfaces were assumed to converge at the bedrock at a distance 200 ft right of the centerline of the existing roadway. This analysis indicated a reduction in SF of 10 percent for the upper shallow failure and a 5 percent for the lower, deep-seated failure plane after the pool level was raised 8.6 ft. The weight of the water in the river was considered in each analysis.

The analysis did not consider erosion of material by the river at the toe because the department could not establish whether this had occurred and, if it had, how much material had been removed.

CONTRACT PLANS AND EARLY CONSTRUCTION PROBLEMS

The consultant's final submission in 1976 provided a cut-slope design that removed only a part of the colluvium in the upper slopes. The roadway template based on borings was located on sound bedrock except at each end of the landslide. The consultant had analyzed the hardness and percentage of recovery of the bedrock core. The percentage of core recovery for both the sandstone and the shale varied from 8 to 100 percent. The sandstone generally had higher percentages of recovery than the shale. The rock quality designation (RQD) percentages were generally less than 30 percent. The recovery and RQD values indicated that the bedrock strength was poor with many

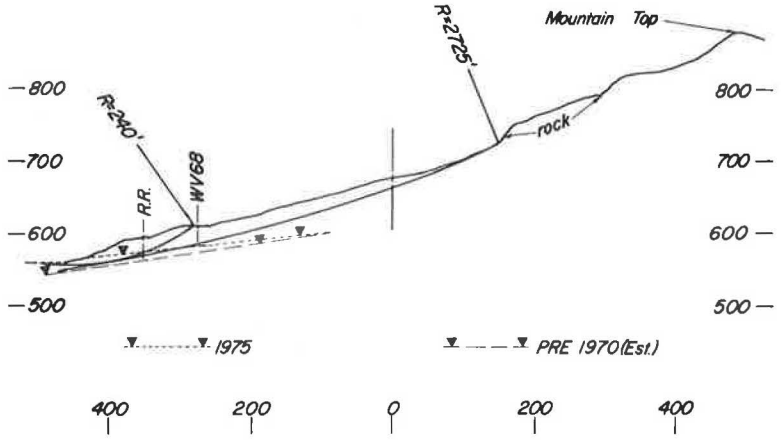

FIGURE 6 Piezometric levels and failure planes.

discontinuities. It was anticipated that there would be a considerable amount of sloughage from the design slopes in service unless gentler slope ratios were used.

The consultant's design was modified without additional boring data for the upper limits and the downriver lateral limits. The consultant's and the department's design consisted of a system of benches and backslope ratios tailored to the designer's opinion of the quality and durability of the material in the slopes. After observing the deterioration of the exposed shale and sandstone outcrops, the department decided to alter the consultant's design to reduce the risk of slope failure (see Figure 7 for the design at Station 210+00). The department's design consisted of five benches with widths from 20 to 30 ft. The backslope ratios were generally 1:1 (H:V) to 3:1 (H:V). These benches and ratios were also used for the slopes in the extended limits of the landslide. The revised design was intended to remove all unstable soil and bedrock. The first bench was located 5 ft above the roadway ditch line to reduce ditch-line maintenance. The controlling factors in the location of the benches above the first bench at 5 ft were as follows:

1. Benches were placed at the base of the sandstone units to provide good foundation support and to ensure against undercutting, and
2. Benches were placed in the shale units at maximum intervals of 40 to 45 ft for storage of sloughage from weathering of the shales. The stored colluvium should cover the shale units and reduce future weathering.

The redesign increased the excavation quantity from 441,290 yd^3, which was the amount estimated by the consultant, to 616,438 yd^3 for the department's redesign, which removed all unstable soil and bedrock, including the lateral and upslope extension of the landslide (see Figure 7).

Several slope failures occurred in the shale units and in one sandstone unit during construction. These failures were the result of the weak and highly weathered shale and the jointed sandstone supported by this shale. Failures of the 1.5:1 and 2:1 (H:V) slopes in the shale required a change of bench widths and a change in several instances to 2.5:1 (H:V) slopes in the shale. These changes increased the excavation by 26,000 yd^3.

The contract documents stated that the contractor was not to cast material downslope during the excavation. This requirement was generally adhered to. However, in constructing a haul road, which involved adding a small amount of material to the upper portions of the continuous colluvium, a landslide was created in material at the southern end of the project that had previously not shown any evidence of movement. This movement on two occasions sheared through the highway and railroad alignment with a total movement of 10 ft horizontally and

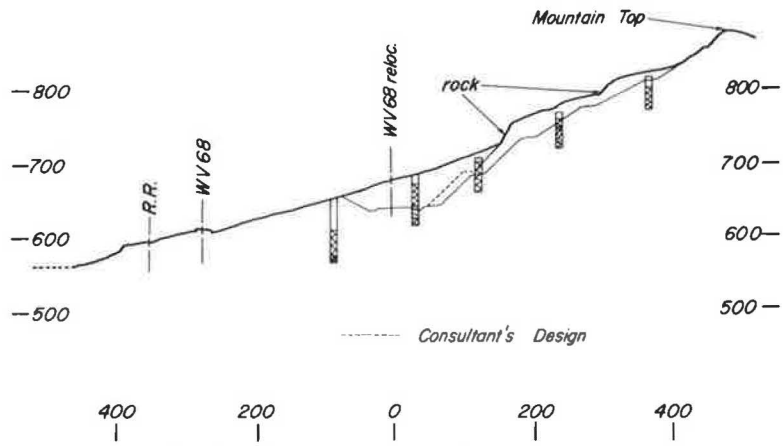

FIGURE 7 Construction cross section (1984).

1 to 2 ft vertically. A subsurface survey indicated movement at a depth of 28 ft, corresponding to the deep-seated failure plane. A toe was in evidence in the river just beyond the riverbank. Traffic has been maintained by excavation near the scarp and leveling of the roadway with aggregate.

CONCLUSIONS

This landslide exemplifies the delicate balance of the stability of colluvium soils on the mountainsides in West Virginia, and especially along the Ohio River.

The increase of the piezometric level within a landslide often lowers its stability to a critical level. The data concerning the rainfall for this general area indicate a somewhat higher amount during the early 1970s and a lower amount during the late 1970s. The yearly amounts during this time were not considered abnormal by the National Weather Service. The activity of the shallow failure surface remained nearly constant during this period. It continued to fail progressively during the 10 years after the investigation, with retrogression upslope, through the original roadway, and finally into the relocated roadway.

Analysis of the landslide indicates that the stability could have been reduced from equilibrium to below equilibrium by the change in the piezometric level as a result of the increase in the river pool elevation. Other factors may have contributed to the instability, such as some removal of material at the toe by the river. However, no man-made changes were made to the surface topography and no other major changes in conditions occurred other than the Ohio River pool change. The analysis indicates that the change in the pool level could have been the major factor causing the increase in the movement of the shallow landslide and probably affected the lower larger failure surface as well.

In studying a landslide of this magnitude, it is highly desirable to understand the mechanisms that have created the instability. This ensures that time and monies are not lost trying to develop corrective methods that will not be adequate now or at some future time.

The department's geotechnical staff recognized the delicate balance of the colluvium and bedrock failure in this landslide. As a result district personnel were advised to not make any significant changes in the topography over the years after the detailed investigation conducted in 1975 and 1976. Otherwise, the roadway and railroad might have been closed, as almost happened during the early construction phase. It was also realized that the construction work in the area could jeopardize the stability. If the landslide did endanger the highway or railroad, it was believed that construction equipment was on hand to relieve the problem.

REFERENCES

1. A. T. Cross and M. P. Schemel. *Geology and Economic Resources of the Ohio River Valley in West Virginia.* West Virginia Geological Survey, Morgantown, 1956.
2. C. E. Krebs. *County Reports for Jackson, Mason and Putnam Counties.* West Virginia Geological Survey, Morgantown, 1911.

Publication of this paper sponsored by Committee on Engineering Geology.

Dynamic Compaction of Loose and Hydrocompactible Soils on Interstate 90, Whitehall-Cardwell, Montana

TERRY L. YARGER

The use of dynamic compaction to increase bearing capacity and reduce settlement of loose foundation soils at great depths is becoming more widespread in the United States. The use of dynamic compaction on a recent Interstate highway overlay project in Montana is described. Foundation soils treated were about 20 to 25 ft (6.1 to 7.6 m) of loose dry alluvial sands and silts having low *N*-values (blows per foot) by the standard penetration test (less than 4 in some cases). Correlation has been found between known and suspected deposits of hydrocompactible soils and semiarid areas having less than about 12 in. (30 cm) of precipitation a year in Montana. A 15-ton (13.6-metric ton), 6-ft (1.8-m) diameter weight with a drop height of 60 ft (18.3 m) was used for the dynamic compaction process. The compaction was performed even in winter months through frost layers broken up by ripping equipment. Dynamic compaction was found to be a very cost-effective method for improving deep deposits of loose sand and silt. Cost savings from this method of compaction compared with feasible alternatives was estimated at $2.6 million. The average increase in *N*-value of the loose materials following compaction was 5 to 12. Some complaints of structural damage were received from local citizens even though the closest residence was 170 ft (52 m) from the compacted area.

The Whitehall-Cardwell project began as an overlay to correct several miles of bumpiness of unknown origin. The severity of the bumps demanded that a foundation investigation be performed. This was subsequently done in the fall of 1982 and spring of 1983 (*1*).

Interstate 90 in the project area is located in an intermontane basin of Cenozoic deposits overlying Archeozoic bedrock as shown in Figure 1. The area is semiarid irrigated cropland and grazing land with generally less than 12 in. (30 cm) of annual precipitation (Figure 2).

Test drilling revealed that the soils beneath the areas of distress consisted generally of loose deposits of sandy silt and silty sand with scattered channel deposits of gravels to a depth of about 20 to 25 ft (6.1 to 7.6 m). Some clayey soils were also present. The water table in the area is generally greater than 60 ft (18.3 m).

Laboratory consolidation tests were performed that indicated that some of the sands and silts exhibited a collapsing or hydrocompactible structure. This type of soil structure has been reported variously in the literature (*2*). Primarily it consists of voids between soil grains held in place by clay bonding, bubble cavities formed by air entrapment, interlaminar openings, or voids left by decaying vegetation. Its environment of deposition is typically semiarid or arid.

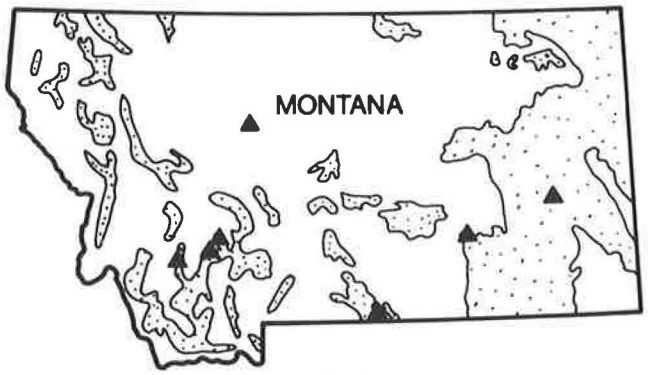

FIGURE 1 Known areas of hydrocompactible soils and Cenozoic deposits.

The most widespread deposits of collapsible soils are windblown sands and silts or loess. Deposits are also formed in alluvial fans such as the Whitehall project area, colluvial deposits, residual soils from a leaching process, and volcanic tuffs. These soils tend to settle or "collapse" from wetting, additional loading, or a combination of both.

Figures 1 and 2 show the correlation between known and suspected areas of collapsing-type soils and the areas of Cenozoic deposits and the areas of 12 in. or less annual precipitation. These correlations appear to indicate where to look or be aware of other possible deposits of collapsing-type soils.

Within the job limits, areas to be treated were delineated by mapping patched and overlaid pavement areas, and further verification was made by test drilling.

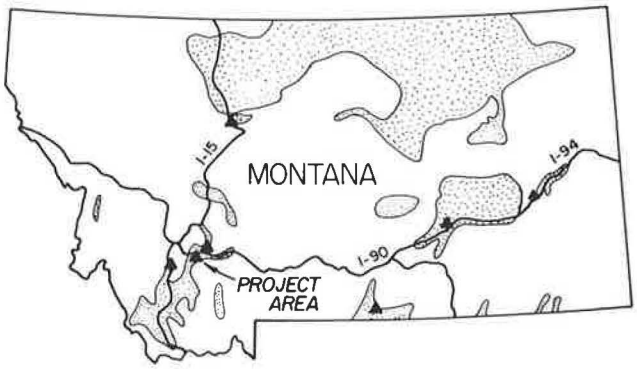

FIGURE 2 Known areas of hydrocompactible soils and areas of precipitation (12 in. or less per year).

Montana Department of Highways, 2701 Prospect Avenue, Helena, Mont. 59620.

EXAMINATION OF TREATMENT ALTERNATIVES

Various alternatives for treatment of the Whitehall project foundation soils were studied. These included vibroflotation, subexcavation, prewetting, blasting, and others. In the summer of 1983, a dynamic compaction (D.C.) test project was set up with the cooperation of a local contractor. The project consisted of dropping a 6-ft (1.8-m) diameter, 15-ton (13.6-metric ton) culvert-encased concrete weight freefall from a height of 50 ft (15.2 m). A total of 56 drops was made on five crater locations on the project. Results indicated that this method would be effective for treatment of the soils. Contract specifications for the project, such as the drop pattern shown in Figure 3, were developed from the test project. The construction specification

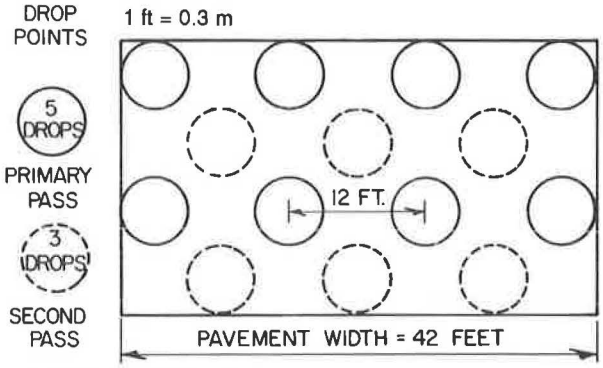

FIGURE 3 D.C. drop pattern.

developed was basically procedural, requiring a minimum of five drops of the weight per drop point for the first pass and three drops for the offset second pass following site leveling of the first-pass craters. Provision was made for additional drops if weight penetration on the final of the five- or three-drop sequence exceeded 10 percent of the total penetration up to that point (*3*). With the necessary depth of compaction known, the weight and drop height were based on the following empirical formula (*4*):

$$D = E_D (W \times H)^{1/2}$$

where

D = depth of influence (m),
E_D = efficiency (½ or 50 percent for estimating),
W = falling weight (metric tons), and
H = drop height (m).

The project design depth of influence was 20 to 25 ft. With a 15-ton weight and 60-ft drop height,

$$D = ½ (15 \text{ tons} \times 60 \text{ ft})^{1/2}$$

$$D = 26 \text{ ft } (7.9 \text{ m})$$

Because 90 to 95 percent of the soils needing treatment extended to a depth of about 20 ft (6.1 m), with the remainder extending to about 30 ft (9.1 m), the added 6 ft of treatment depth in the 26 ft was considered a good safety margin.

RESULTS

Public Relations

Before the test project was performed in 1983, letters announcing the test drops were circulated to most of the residences within about ¼ mi (0.4 km) of the project area. Some public interest was generated by these letters. One party had recently purchased an office building and house and wondered why the walls were cracked and the floors not level. The possibility that the structures had been built on poor foundation soils was explained to him.

The "production" D.C. work started at the west end of the westbound lanes on August 9, 1984, and proceeded east until completion of these lanes on September 19, 1984. After winter shut-down, work started on the east end of the eastbound lanes on February 28, 1985, and proceeded west until completion of these lanes on April 3, 1985.

Soon after the production project started in 1984, at the west end of the job, local residents complained about the contractor's working hours of 4:00 or 5:00 a.m. to 10:00 or 11:00 p.m. These complaints were generally resolved by the contractor.

Studies of available literature were made before the start of the project to determine safe distances for D.C. work to prevent structural damage (*4*). Of particular concern at the time was a large, high-pressure gas pipeline located about 75 ft (23 m) from a portion of the east end of the project area. A decision was made to perform vibration monitoring in this area during the D.C. work using the U. S. Bureau of Mines criterion for peak particle velocity of 2 in./sec (50 mm/sec) or less to prevent damage to structures. A minimum distance from the impact points to the pipeline was calculated to be about 45 ft (13.7 m). Frequency of vibration was estimated to range between 5 and 20 Hz (*5*).

Because the D.C. work was to pass fairly close to several residences on the west end during compaction of the eastbound lanes, it was decided to perform crack and damage survey and vibration monitoring near these residences. In the fall of 1984, shortly after this decision was made, a claim for damages attributed to the D.C. period for the westbound lanes was made for one of these residences.

The crack and vibration surveys were performed in March and May 1985 by Northern Engineering and Testing (*6*). Peak particle velocities were within the recommended safe level for residents, as shown in Figure 4. After D.C. work, some cracks showed an increase and some a decrease in size as compared with their measurement before D.C. A majority of the cracks measured, however, showed no change or change within what was considered an accuracy of measurement tolerance for no movement. Cracks and damage found from the field surveys appeared to be preexisting and on-going at the three residences. Damage appeared to have been caused by hydroconsolidation of the foundation soils because of poor drainage around the structures. These residences, as well as other structures in the area, appear to have undergone distress primarily from the

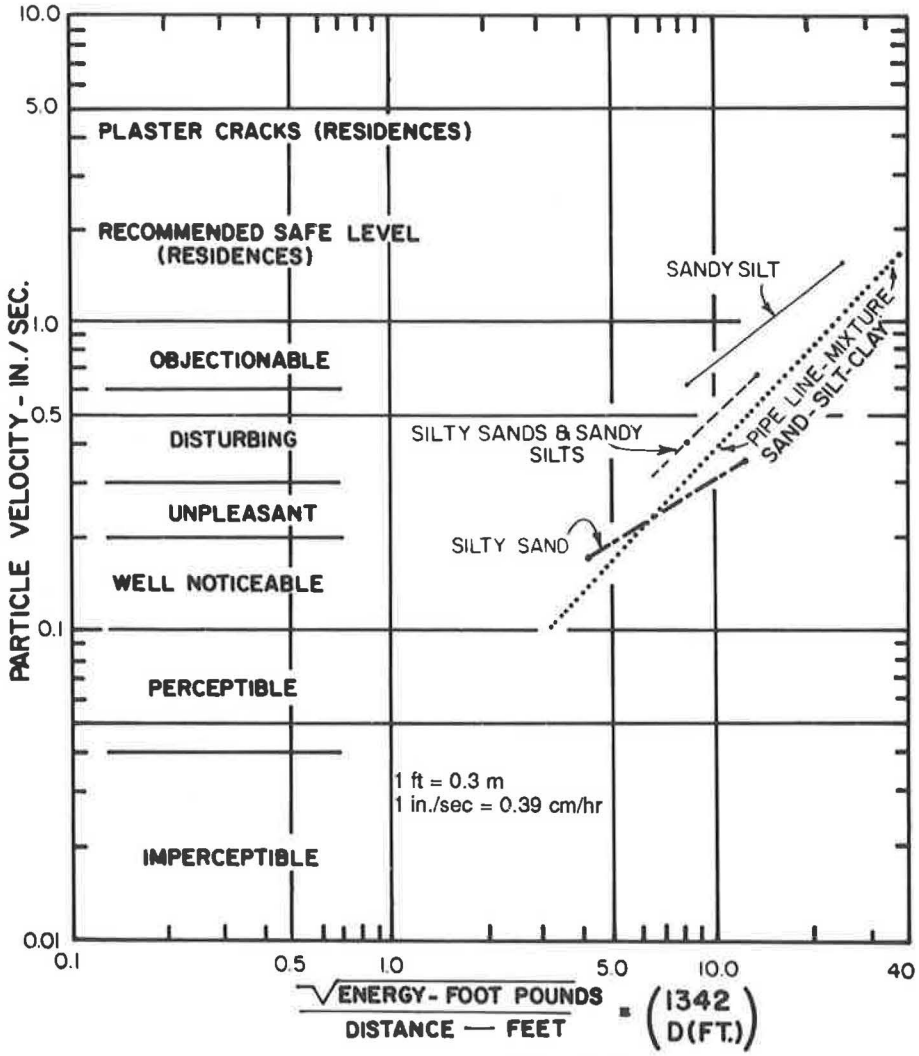

FIGURE 4 Scaled energy factor versus particle velocity.

same problems experienced by the Interstate highway in this area before the D.C. work.

Equipment Used

The D.C. equipment used on this project, with the exception of the weights, was manufactured or assembled by Neil F. Lampson, Inc., Kennewick, Washington. The two 15-ton weights were constructed by the general contractor, Hilde Construction Company.

The two compactors constructed by Lampson weighed approximately 114 tons (103 metric tons) each and were capable of lifting the weights from drop heights of almost 70 ft (21 m). The compactors moved forward and backward and turned by means of a tracked-base transporter unit. According to Lampson personnel, capacity of the transporter was 350 tons (317 metric tons) and capacity of the draw works, 500 tons (454 metric tons).

The weights were lifted by using a 1¼-in. (3.2-cm) diameter straight lay or "no spin" cable. The cable was attached to a swivel connected to two short chains, which in turn were connected to opposite sides of the top of the weight. The two connections to the weight, rather than one center connection, allow better control of the weight. The chains were threaded through several old automobile-size tires to reduce chain wear. Later it was discovered that swivel damage could be substantially reduced by threading the chains and automobile tires through a used large-diameter heavy-equipment tire. The combined weight of all the tires added approximately ¾ to 1 ton (0.7 to 0.9 metric ton) to the 15-ton compacting weight.

Craters

Craters, of course, are the immediate measurable results of D.C. Records of penetration depths and number of drops were taken for all craters on this project. Number of drops versus penetration can be plotted and indicate whether the energy input from the drops is being efficiently utilized. The D.C. was performed on 1.5 to 2.0 ft (0.3 to 0.6 m) of base-course materials left in place after removal of the existing pavement.

Figures 5 and 6 are drop curves for an area with and without 2 ft of base-course material and for an area with frost versus a frost-free area, respectively. The test area with base-course materials removed required extra drops by the special provision's 10 percent requirement, indicating the high resistance of the base-course material. Field testing, however, did not indicate any increase in the effective depth of improvement or density properties of the soils.

D.C. work on the eastbound lanes started in February 1985. Soil beneath the paved areas was frozen to depths of approximately 4 to 6 ft (1.2 to 1.8 m), whereas frost in adjacent open

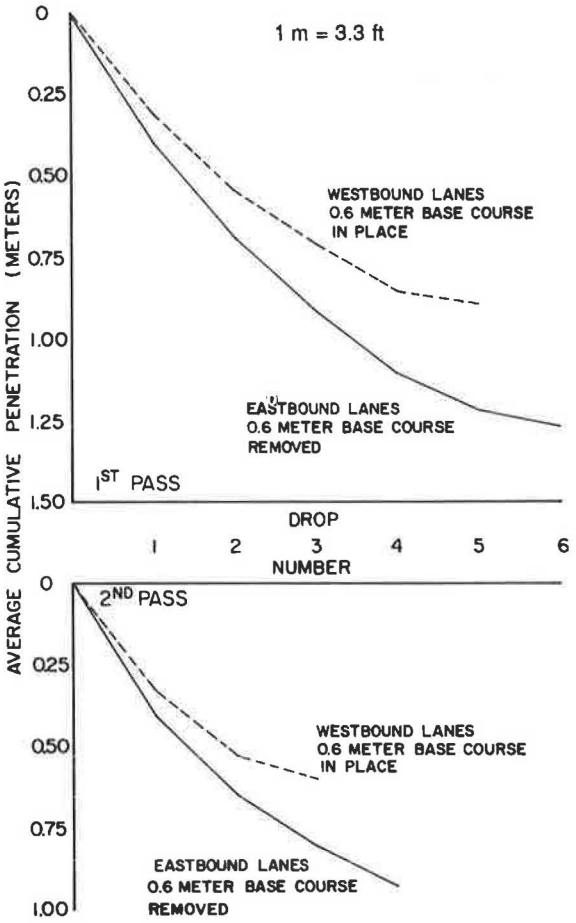

FIGURE 5 Crater depths as function of number of drops with and without 2-ft base course, Station 257± to 258±.

areas was generally less than 1 ft (0.3 m). The contractor was advised that the effects of the D.C. would be very limited in frozen ground. At the beginning of pavement removal, the contractor elected to rip the subgrade soils. This proved satisfactory, leaving only some pieces of frozen soil a maximum size of 10 to 12 in. (25 to 30 cm) nominal dimension. As pavement stripping continued and temperatures rose, the frost rapidly left the ground. The areas with frost required extra drops to meet the special provision's 10 percent requirement as compared with a frost-free area. Again, field testing did not

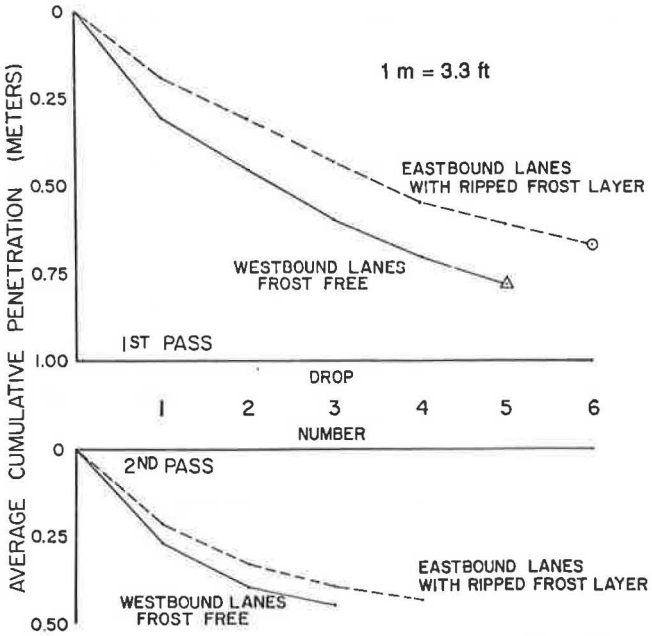

FIGURE 6 Crater depths as function of number of drops for area with frost versus a frost-free area, Station 272+00 to 272+50±.

indicate any differences in the depths of improvement or soil densities for areas with frost versus frost-free areas.

Field Testing Data

Besides the drop-penetration records, other drilling and field testing was performed. Standard penetration, dynamic cone penetration, and some Shelby tube density, as well as Dutch cone penetration tests were performed at various locations. Typical before-and-after D.C. results and qualitative statements of improvement are shown in Figure 7 and Table 1. Average increase in *N*-value for the improved soils was 5 to 12. Average lowering of the ground surface after D.C. and final compaction of the upper 2 ft (0.6 m) or so of loose material was about 0.7 ft (21 cm). A maximum of about 30 in. (76 cm) was originally projected from laboratory consolidation testing. As found during the initial drilling investigation, Shelby tube densities were very difficult to take and density results were inconclusive. Dutch cone penetration tests were also inconclusive, possibly because of the limited amount of Dutch cone testing done or types of foundation soils present, or both.

Time and Cost

A time-and-cost summary is presented in Table 2. Final treatment cost for the D.C. was $\$6.97/yd^2$. This does not include the $\pm\$0.30/yd^2$ cost for standard compaction methods used on the upper 2 ft or so of loose material left for final grading after D.C. Approximately $2.6 million was saved by using D.C. instead of other alternatives, as shown by the following cost comparisons (the actual cost per cubic yard for excavation was based on the

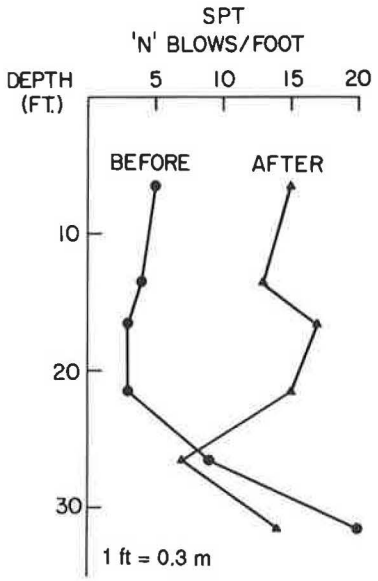

FIGURE 7 Typical field testing results before and after D.C.

cost from other jobs with similar quantities of excavation and placement):

	Engineers' Estimate	*Actual Bid or Cost*
Subexcavation (20-ft depth)	\$3,078,800 ($2.15/yd^3)	\$3,393,840 ($2.37/yd^3)
Dynamic compaction	−1,129,030 ($10.00/yd^2)	−775,130 ($6.97/yd^2)
Total savings	\$1,949,770	\$2,618,710

SUMMARY: MAJOR CONCLUSIONS AND RECOMMENDATIONS

The D.C. project in Montana was a result of technology transfer and encouragement from FHWA to try a new geotechnical procedure that apparently could be performed by almost anyone who uses the following guidelines, as well as those in the reference material (*7*). A D.C. project is particularly feasible in dry collapsible-type soils such as those found on this project.

Vibration Levels

Vibration monitoring for this project indicated that peak particle velocities were well within the recommended safe level for residences. The perceptible level of vibrations was high enough to be felt by those in the immediate project area and became a cause of concern to them.

Even though the particle velocities were within the safe range for this project, performance of vibration and crack-type surveys for any structures within the perceptible range of the D.C. work is recommended. These types of surveys would be mandatory for work in urban areas and should be done in conjunction with a general presentation to the public explaining the D.C. process, vibration perception and damage levels, and vibration and crack surveys.

Test Section

A small test section using the D.C. process in the project area proved invaluable in design of the production work. Results from this test section correlated with other examples. It is recommended that D.C. work be done on a test section unless good correlation from previous D.C. projects can be shown. This will demonstrate whether the procedure will work or not and is extremely useful in developing a procedural type of specification indicating patterns for craters and number of blows as well as weight, size, and drop heights. It is recommended that specifications allow flexible use of weight drops. For example, if five weight drops were set up and only two were used to achieve density, the remaining three would not be paid for unless used at a different location.

Resistant Layers

D.C. was effective on all but approximately 5 percent of the area compacted. The majority of materials treated on the

TABLE 1 IMPROVEMENT OF PENETRATION RESISTANCE AND SOIL PROPERTIES ON BASIS OF STANDARD PENETRATION TEST

	Silt			Sand				Clay		
	Type 1	Type 2	Type 3	Type 1	Type 2	Type 3	Type 4	Type 1	Type 2	Type 3
Initial *N*-value	0–4	4–10	10–30	0–4	4–10	10–30	30–50	4	4–8	8–15
Relative density or consistency	Very loose	Loose	Medium dense	Very loose	Loose	Medium dense	Dense	Very soft to soft	Medium stiff	Stiff
Avg increase in *N*	4	9	(−7)[a]	12	9	5	(−10)[a]	8	6	6
Improvement range	N.A.	13–19	10–18	12–16	13–19	15–30	18–23	8–12	10–14	14–19
Relative density or consistency	N.A.	Medium dense	Medium dense	Medium dense	Medium dense	Medium dense	Medium dense	Stiff	Stiff	Stiff–very stiff

Note: *N* = blows per foot.

[a]Represents data from only one test boring.

TABLE 2 TIME-AND-COST SUMMARY

	Westbound	Eastbound	Total
Starting date	08–09–84	02–28–85	08–09–84
Ending date	09–19–84	04–03–85	04–03–85
No. of working days (2- to 10-hr shifts/day)	30	25	55
Treated area (yd^2)	54,694	56,588	111,282
Total drops	29,366	31,146	60,512
Extra drops (by special provision)	1,236	1,718	2,954
Cost of extra drops ($) ($10/drop)	12,360	17,180	29,540
Cost of regular D.C. work ($) ($6.70/yd^2)	366,450	379,140	745,590
Total cost ($)	378,810	396,320	775,130
Final cost per drop ($)	12.90	12.72	12.81
Final cost per square yard ($)	6.93	7.00	6.97

project consisted of very loose to loose silty sands and sandy silts. The average increases in *N*-value for the improved soils varied between 5 and 12. Areas not improved by the actual D.C. performed included scattered pockets of loose soils located deeper than the design improvement depth, wet clay soils, and areas with scattered shallow dense gravel layers. Quality control testing did not indicate that the presence of a 2-ft thick base-course mat or a "ripped" frost layer was detrimental to the final results on this project. The weight size and drop height design appeared to overcome the resistance of these layers on this project. More energy (extra drops), however, was required at additional cost in the frost areas and in the test section where base-course gravels had been removed. It is recommended that hard layers be noted and a determination be made on the economy of removing them or designing the weight and drop height to penetrate them.

Correlation

It was determined that a correlation could be made between the semiarid unglaciated areas of Montana and the presence of known or suspected deposits of hydrocompactible soils. Improvement in the strength of these materials was accomplished on this project by the simple and economical process known as D.C.

The correlation of semiarid areas, material types, and the presence of hydrocompactible soils is known to exist in other states. As more construction projects are relegated to marginal use land, a rough land use planning map should be prepared for other states showing areas of detrimental hydrocompactible soils.

The D.C. process is available to anyone and is recommended as a safe, simple, and economical way to improve soil strengths at great depths.

ACKNOWLEDGMENT

This D.C. and overlay project was carried out under the supervision of the Butte District, Montana Department of Highways, and funded in part by the Federal Highway Administration. Almost all sections of the highway department were involved in this project and help from the personnel in these sections is appreciated. The authors also thank General Constructors, Inc., of Butte, contractor for the D.C. test project; Hilde Construction Company of Great Falls, Montana, general contractor for the final project; and Neil F. Lampson, Inc., of Kennewick, Washington, who designed and assembled the production compacting equipment. Special thanks to E. L. Predmore for presentation of graphics.

REFERENCES

1. J. E. Armstrong and T. L. Yarger. *Collapsible Soils, Whitehall-Cardwell Project IR-90-5(44)250.* Geotechnical Report. Montana Department of Highways, Helena, 1983.
2. S. P. Clemence and A. O. Finbarr. Design Considerations for Collapsible Soils. *Journal of the Geotechnical Engineering Division, ASCE*, Vol. 107, No. GT3, March 1981, pp. 305–317.
3. *Federal Aid Project IR 90-5(44)250; Grade, Gravel, P.M.S. and P.M.S. Overlay; Whitehall-Cardwell; Jefferson County: Plans and Specifications.* Montana Department of Highways, Helena, 1984.
4. R. G. Lukas. Densification of Loose Deposits by Pounding. *Journal of the Geotechnical Engineering Division, ASCE*, Vol. 106, No. GT4, April 1980, pp. 435–446.
5. L. G. O'Dell. *Report of Geotechnical Services, Vibration Monitoring, Dynamic Compaction Project, I-90 Whitehall to Cardwell, Montana.* Northern Engineering and Testing, Inc., Billings, Mont., 1984.
6. L. G. O'Dell. *Report of Vibration Monitoring and Crack and Damage Survey, Whitehall Dynamic Compaction, Whitehall, Montana.* Northern Engineering and Testing, Inc., Billings, Mont., 1985.
7. R. G. Lukas. *Dynamic Compaction Manual* (first draft). FHWA, U. S. Department of Transportation, 1984.

Publication of this paper sponsored by Committee on Engineering Geology.

Performance of Cement-Modified Soils: A Follow-Up Report

JOHN D. ROBERTS

In 1938 the Oklahoma Highway Department investigated the use of cement-modified subgrades by constructing 7 mi of test sections on US-62. Much of the subgrade consisted of expansive clay. A total of 38 test sections with 11 different cement contents was used to modify the subgrade soils. Cement contents varied from 4 to 16 percent by volume with an average cement content of 6 percent. At the time of construction the plasticity index of the subgrade was reduced from an average of 29 to 13 through cement modification. In 1983 an investigative program was conducted to determine the plasticity characteristics of the cement-modified subgrade following 45 years of service. Samples were obtained from each of the 11 different cement-content sections. The plasticity indexes ranged from nonplastic to a maximum of 13 with an average of 6. Results from these tests show that the effectiveness of cement modification of the fine-grained soils was permanent. Information on the original cement-modification work is presented and the 1983 investigative program is described in detail.

The investigation of an Oklahoma highway project constructed in 1938 where expansive clay subgrade soils were modified by the addition of portland cement is described. The purpose of a 1983 investigation was to sample the cement-modified subgrade and perform laboratory tests to determine the current characteristics of the cement-modified subgrade. Results of the investigation reveal that changes in the physical and plastic characteristics of the cement-modified subgrade have remained constant or improved in the half-century of weathering and continued service.

The technical data contained in this paper have been tabulated to provide the engineer with background information as to portland cement's long-term performance in modifying the plastic and physical characteristics of fine-grained soils. This does not imply that such modification will or should perform as well as treatments meeting the more rigid standards of soil-cement.

TERMINOLOGY

Various terms are used to describe the products made when soil and cement are mixed together. These terms are often misunderstood or used incorrectly. In this paper, the term "cement modification" or "cement-modified soil" is used to describe an unhardened or semihardened soil material with improved properties of plasticity, volume change, and bearing strength. Cement-modified soil contains less cement than that required to produce hardened soil-cement. For fine-grained soils, the degree of modification is usually judged by changes in the plasticity properties, and the normal use of the material is for subgrade modification.

Dolese Company, 20 N.W. 13th Street, Oklahoma City, Okla. 73103.

BACKGROUND OF 1938 PROJECT

A report by Ried *(1)*, published in the 1939 *Proceedings of the Highway Research Board,* describes preliminary soils survey and testing, design, construction, specifications, and field testing. Some of this information is condensed here. The 1939 report documents the physical properties of the soils both before and after the cement modificatin.

In early 1938 the Oklahoma State Highway Commission, now the Oklahoma Deparmtent of Transportation (ODOT), conducted a preliminary soil survey on an already constructed grading and drainage project. The project was located in Comanche County, southwestern Oklahoma, on US-62, in and next to the town of Indiahoma. The soil survey indicated a large portion of the subgrade to be A-4, A-6, and A-7 soils by the AASHTO Soil Classification System.

After reviewing several other types of improvements relative to costs and the long-time service value of the finished construction, ODOT authorized a research project using a cement-modified subgrade 6 in. thick and 22 ft wide. The surface pavement would be portland cement concrete 20 ft wide. Construction of the modified subgrade was to follow procedures similar to those for soil-cement.

The subgrade modification was completed during the late fall of 1938 and the concrete paving in 1939, and the project was opened to traffic.

Testing and Design

The amounts of cement required for proper reduction of the volume-change characteristics of the various soil types encountered on the project were determined by preliminary laboratory tests. The liquid limit, plastic limit, plasticity index, field moisture equivalent, shrinkage limit, and shrinkage ratio were determined on the raw soils and the cement-soil mixtures.

The guiding values recommended as desirable to obtain a subgrade with small volume changes due to moisture changes were that the "cement-modified" subgrade have a ratio of the volume at shrinkage limit to volume at field moisture equivalent of about 0.90 and a ratio of the volume at shrinkage limit to volume at liquid limit of about 0.80. The lowest percent of cement required to obtain these desired results as indicated by the tests was selected as the design mix.

On the basis of the results of the soil survey and the testing program, it was decided that the project would consist of 38 different sections using 11 different cement contents. The

cement contents ranged from 4 to 16 percent by volume. The average was approximately 6 percent by volume.

Records of Construction

To determine the compliance with pulverization specifications composite samples of the material being processed were taken from at least three points across the roadway at not greater than 300-ft intervls, or more often as appeared desirable. These samples were usually taken as pulverizing was being completed.

The original mix design requirements were reviewed as to the station limits for quantity of cement required, and the spacing of cement bags was established for spreading the cement.

As dry mixing of the cement and the soil progressed, the mixture was inspected from time to time to adjust the operation of equipment as necessary to secure a uniform mix. As dry mixing was being completed, moisture samples were taken throughout the area. From these, the amount of water to bring the mix to optimum requirement was estimated. Additional moisture tests were made during damp mixing to assure uniformity and to ascertain that the optimum requirement had been reached throughout the mixture, at which time compaction could be started.

As the rolling appeared to be completed, density tests were made at selected points at intervals not greater than 300 ft. The sand density method was used for this determination, which was compared with the standard density previously obtained for this particular mixture.

At least 7 days after processing, four samples were obtained from each day's mix for comparative information, for check tests against the original design, and for further tests for information on the effect of aging. In addition, moisture samples were taken just ahead of paving opertions in order to complete records of the project as paving was placed.

Pulverization

The first section to be processed contained some of the heavier soils on the project. It was found practically impossible to pulverize this soil to the requirement that 80 percent pass the No. 4 sieve. Much time was spent with the different pieces of equipment and special methods of manipulation in an effort to secure specification requirements under the cool weather conditions prevailing (late October). The work moved on into somewhat lighter soils and when no appreciable improvement in gradation was found, prewetting and sprinkling during pulverizing was resorted to. Gradation samples were taken before and after premoistening, during dry mixing with cement, and after final mix was at or near optimum moisture requirement with the result that no appreciable improvement was effected. However, the test data show that additional pulverization was obtained during both dry and damp mixing after cement application.

It was quite evident that in these types of soil the machinery and methods commonly used for this work could not produce a pulverization of much more than 60 percent. It was therefore found desirable and practical to change the specifications as follows: "That the gradation of the raw soil prior to addition of cement be such that 95% pass the 1-in. sieve and at least 60% pass the No. 4 sieve." The average condition, as recorded during the construction of the project, indicates 98 percent passing the 1-in. sieve and 67 percent passing the No. 4.

Soils analyses of completed cement mixtures of both coarse and fine gradings of soil were made, which showed no appreciable variation or difference. Further comparative tests were made on soil-cement cylinders with soil of the coarser or revised pulverization requirement and also of soil, all of which passed the No. 4 sieve. These were measured for volume change and absorption, one each during 26½ days and one each for 77½ days exposed to capillary moisture, and at the end of that time complete soil analysis was made. None of these results showed any apparent difference to be reflected in either the coarse or the fine-graded or pulverized soil. It appears, therefore, that the change to the requirement of only 60 percent passing the No. 4 sieve will have no detrimental effect on this subgrade treatment.

Density

In the early mixes completed and immediately compacted after the sample was mixed, it was found that densities in place were not comparable with the (regular) moisture-density curves (AASHTO T-99) determined in the laboratory. All the methods were checked for errors or discrepancies, with no results. Samples of the mixture in place compacted in Proctor molds showed lower densities, indicating that the change, or modification, of the moisture-density relation of the soil was effected over a period of several hours during wetting and mixing. A series of moisture-density tests, delayed for a period of several hours after mixing, developed the fact that the principal change in density wa attained in approximately 5 hr.

These 5-hr delayed tests were made during the remainder of the work. The mixture of soil-cement for test was slightly moistened and placed in tight buckets and stirred or agitated at intervals through a period of 5 to 6 hr, after which moisture-density tests were made by using the standard procedure. Such 5-hr delayed determinations or comparisons of density with the compacted sample of the finished road mixture should be specified for control of construction of this type.

Conclusions, 1938 Work

Grading must be accurately finished to elevation and section of subgrade before construction of the treated subgrade. Scarifying this grade to the true section and elevation at the required depth for the treatment is of the utmost importance. A scarifier or gang plow, or both, of proper design and manned by skilled operators should be used throughout so that this initial work will be carefully controlled to provide a true subbase section, or "work table," for the control of all subsequent pulverization, mixing, processing, and compacting.

The loosening of 6 in. of soil in the completed roadway provided an excess thickness of finished mix sufficient for any normal irregularities or adjustments in grade or section and

permitted the paving planer to trim surplus from the grade rather than to level or fill with untreated soil. As work progressed, this surplus was available for the few low areas that occurred in the grade. Proper care at this stage of construction is of great importance.

During the initial stages of compaction, no rubber-tired equipment or traffic was allowed and the offset tandem disk was used behind the roller to prevent surface crusting. After about an hour of rolling, the disk was replaced with a spiketooth harrow. Particularly during dry weather, it was found necessary to sprinkle the surface two or three times during the rolling operation. As rolling neared completion, the road was shaped frequently with motor patrol and final compaction was completed with a pneumatic-tired roller.

The final shaping of the completed subgrade was not difficult. The contractor had provided and used two extra sets of cutting bits for both his subgrade machine and the planer; because new bits were changed as necessary, very little delay developed on account of the hard subgrade. In general, the finished subgrade was practically perfect, as indicated by records of the yield of concrete (which averaged 99.28 percent), thickness tests, and measurements of cores in the completed concrete pavement.

It is highly desirable that proper and sufficient pieces of equipment for pulverization and processing be available on the job. There is no substitute for a gang plow (2 to 4 bottom), a regulated-depth scarifier, springtooth harrow (power lift and depth regulated), offset tandem disk harrow with at least 18- to 20-in. disks, double spiketooth drag harrow, and one-way disk plow.

An ample water supply must be available and it is recommended that application be provided by two or more pressure distributors. On this project, a protable water storage tank enabled the distributor trucks to load more quickly than would have been possible from pipeline and thus deliver water at a satisfactory rate.

All sheepsfoot rollers to be used should be of same general design as to spacing and area of feet and weight.

Results of tests during construction and the final characteristics of the modified soils indicate that the revised grading or pulverization requirement (95 percent passing 1-in. sieve and 60 percent passing No. 4 sieve) was generally satisfactory. It is recommended that such specifications be used in future pulverization projects on which modified soils are to be produced or that practical grading limits for the soil be predetermined and wider limits provided if necessary.

It is recommended that the density of the completed work be specified as the percentage of the density of 5-hr delayed compaction.

No protection or curing was specified for this work. It is believed, however, that some provision for protection of the cement mix in progress should be provided. On one section heavy rain fell on the finished mix just as rolling started. Subsequent tests indicated that the volume-change values were not as designed. Two percent additional cement was reprocessed in a portion of the section and 5 percent in the remainder.

1983 INVESTIGATION

After 34 years of service as a primary U.S. highway, this section was transferred in 1973 to Comanche County when a new alignment of US-62 was opened about 1 mi to the north. In 1983 the old project was still performing very well as a county road.

The 1983 investigation included field sampling and laboratory testing from each of the 11 different cement-content sec-

FIGURE 1 CME 750 coring the concrete pavement.

FIGURE 2 Thin-walled tube sampling the soil.

TABLE 1 SUMMARY OF FIELD INVESTIGATION: PART 1

Soil Description	Brown Silty Clay			Brown Silty Sand			Brown Silty Sand			Brown Silty Clay		
Soil Classification	A-6			A-1-b			A-2-4			A-6		
Station to Station	1044+00 to 1068+00			1087+50 to 1098+00			1098+00 to 1110+00			1110+00 to 1120+00		
Cement Content (percent by volume)	8.0			11.0			10.0			9.0		
	Raw Soil	1938 CMS	198[a] CMS	Raw Soil	1938 CMS	1983 CMS	Raw Soil	1938 CMS	1983 CMS	Raw Soil	1938 CMS	1983 CMS
Coarse Sand	7.1	7.0	7	7.0	9.6	53	9.7	10.0	26	7.0	6.8	13
Fine Sand	23.9	36.2	26	27.5	43.5	27	28.7	39.4	35	22.4	51.4	25
Silt	45.2	54.9	60	45.5	45.4	19	41.0	49.0	37	47.4	41.2	54
Clay	23.8	1.9	2	20.0	1.5	0	20.6	1.6	2	23.2	0.6	5
Colloids	10.3	1.4	5	1.2	1.5	0	7.3	1.6	0	9.8	0.6	3
Plasticity Index	24.9	13.8	13	32.4	11.8	N.P.	25.2	14.1	1	29.6	12.7	11
Shrinkage Limit	13.5	25.0	20.0	11.4	32.9	NVC	12.6	26.7	21.0	12.1	28.9	19.3
Shrinkage Ratio	1.96	1.6	1.55	2.06	1.45	NVC	2.00	1.56	1.45	2.01	1.50	1.57

Note: CMS = cement-modified soil.
[a]Average of three samples for all except 5.5 percent cement content where two samples were averaged.

tions. The 11 test sections were randomly selected to gather representative subgrade samples.

Initially the investigation was to include one sample in each of the 11 test sections. However, to avoid inconclusive results due to a nonrepresentative sample, a series of three tests was taken in each section. The center sample location was chosen at random and the other two samples were taken 50 ft on each side of the initial location. All samples were located approximately 5 ft left of the centerline.

The pavement was cored and the subgrade sampled by using a CME 750 multiuse core and auger rig (Figure 1). Cores of the asphaltic concrete patches, concrete pavement, and, in some samples, a portion of the cement-modified subgrade were cut with a 4-in.-diameter diamond-bit core barrel. Subgrade samples were obtained by thin-walled tube sampling procedures in accordance with AASHTO T207-81 (Figure 2). Following sampling, the pavement was returned to its original condition by filling the core holes with ready-mixed concrete.

The subgrade samples were wrapped to prevent moisture loss and returned to the laboratory. All samples wer visually inspected and classified. The samples first were logged and described as to color and texture; then the Atterberg limits and gradations were determined and the soils were classified.

A summary of results is given in Tables 1–3. Included are the

TABLE 2 SUMMARY OF FIELD INVESTIGATION: PART 2

Soil Description	Brown Silty Sand			Brown Clayey Silt			Reddish Brown Clayey Soil			Brown Clayey Silt		
Soil Classification	A-2-4			A-4			A-4			A-4		
Station to Station	1126+00 to 1144+50			1181+00 to 1189+00			1189+00 to 1197+25			1222+50 to 1236+50		
Cement Content (percent by volume)	9.5			7.0			6.0			5.5		
	Raw Soil	1938 CMS	1983 CMS	Raw Soil	1938 CMS	1983 CMS	Raw Soil	1938 CMS	1983 CMS	Raw Soil	1938 CMS	1983 CMS
Coarse Sand	7.7	9.0	42	14.4	16.5	16	20.1	15.4	29	17.0	16.3	15
Fine Sand	16.1	39.2	31	20.9	40.0	25	22.5	11.3	29	30.4	31.0	30
Silt	44.1	51.3	26	35.8	30.7	55	34.2	72.1	40	30.4	50.4	54
Clay	32.1	0.5	0	28.9	12.8	2	23.2	1.2	1	22.2	2.3	1
Colloids	11.7	0.5	0	11.9	9.7	3	11.0	0.8	1	9.7	2.3	0
Plasticity Index	40.8	18.0	3	25.5	12.1	8	21.5	6.6	3	18.0	14.0	6
Shrinkage Limit	10.2	27.4	21.1	14.0	29.0	22.6	15.0	28.2	15.9	14.5	21.8	20.3
Shrinkage Ratio	2.12	1.55	1.40	2.00	1.53	1.51	1.90	1.50	1.61	2.00	1.68	1.52

Note: CMS = cement-modified soil.

TABLE 3 SUMMARY OF FIELD INVESTIGATION: PART 3

Soil Description	Brown Sandy Silty Clay			Brown Sandy Silty Clay			Brown Sandy Silty Clay		
Soil Classification	A-2-4			A-2-4			A-2-4		
Station to Station	1236+50 to 1246+00			1269+00 to 1272+00			1301+50 to 1307+65		
Cement Content (percent by volume)	5.0			4.0			16.0		
	Raw Soil	1938 CMS	1983 CMS	Raw Soil	1938 CMS	1983 CMS	Raw Soil	1938 CMS	1983 CMS
Coarse Sand	18.6	16.5	32	16.2	19.9	29.0	2.0	11.6	40
Fine Sand	29.2	34.2	37	40.7	44.3	32.0	17.1	45.4	31
Silt	26.6	47.2	25	29.1	33.5	31.0	42.6	38.4	27
Clay	25.6	2.1	2	14.0	2.3	3	38.3	4.6	1
Colloids	12.8	1.3	4	1.7	1.3	5	14.5	1.6	0
Plasticity Index	26.0	13.2	6	20.8	12.8	8	50.5	15.0	4
Shrinkage Limit	13.0	23.0	13.8	15.6	24.2	18.2	10.5	34.7	22.3
Shrinkage Ratio	2.0	1.66	1.68	1.90	1.65	1.70	2.1	1.42	1.42

Note: CMS = cement-modified soil.

average plasticity indexes, shrinkage limits, shrinkage ratios, and gradations of each group of three samples. Also shown are original raw soil data and cement-modified soil tests made in 1938. A comparison of the 1938 and 1983 plasticity index data is shown in Figure 3.

SUMMARY AND CONCLUSIONS

A cement-modified soil project was built in southwestern Oklahoma in the fall and winter of 1938; 11 different cement contents were used in 38 different test sections along 7 mi of roadway. The average cement content for the total project was 6 percent by volume. Tested in 1983, the plasticity indexes ranged from nonplastic to a maximum of 17 on those sections included. The average plasticity index for these tests was 6 compared with a 1938 average of 12 for identical sections. In each section tested in 1983, the average plasticity index was less than the plasticity indexes measured in 1938. These test results show the long-term effectiveness of portland cement in reducing the plasticity indexes of fine-grained soils.

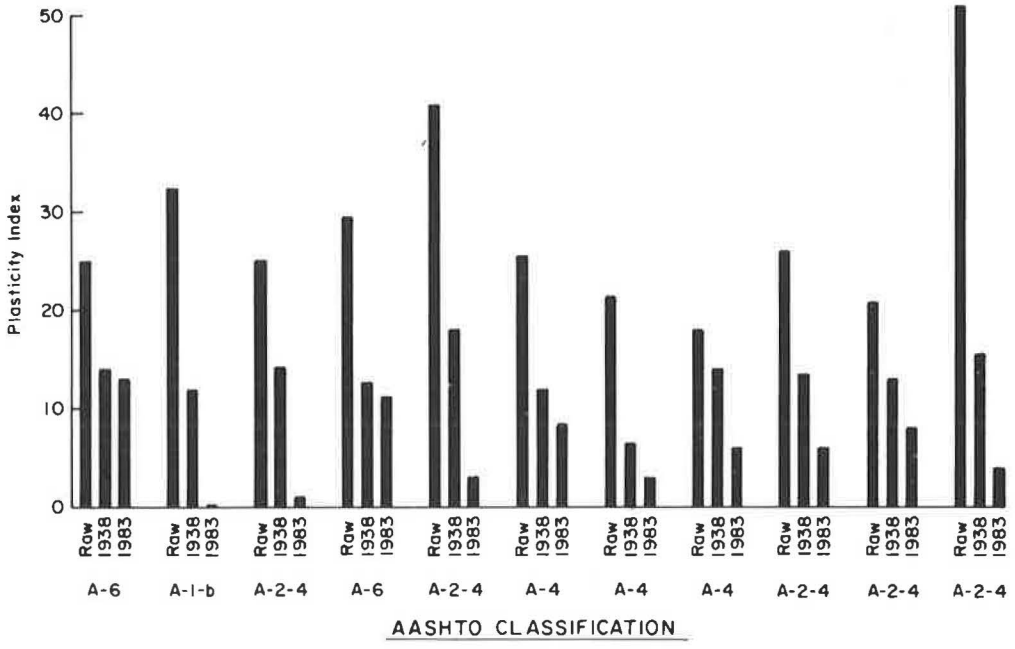

FIGURE 3 Comparison of plasticity index data for raw soil and cement-modified soil.

ACKNOWLEDGMENTS

The author wishes to thank Frank Hawthorne and the other commissioners of Comanche County for permission to core and sample their county road; Mayor Bailey and the citizens of Indiahoma for authorizing the Portland Cement Association to core and sample their street; Atlas-Truck Concrete, Inc., Duncan, for supplying the concrete and assisting in repairing the cored holes; and Shepherd Engineering and Testing Company, Norman, Oklahoma, for conducting the field and laboratory investigations.

REFERENCE

1. C. R. Reid. "Concrete Pavement Subgrade Design, Construction, Control." *HRB Proc.*, Vol. 19, 1939, pp. 541–551.

Publication of this paper sponsored by Committee on Soil-Portland Cement Stabilization.

Flexural Fatigue Strength of Lime-Laterite Soil Mixtures

P. G. BHATTACHARYA AND B. B. PANDEY

Laterite soils, which are the products of tropical or subtropical weathering, have been stabilized with lime to evaluate the dynamic modulus and the flexural fatigue strengths of the lime-soil mixtures. Tests have been carried out on four types of laterite soils compacted at three dry density ranges—light, medium, and heavy. Least-squares regression analysis was used to establish relationships between stress ratio and the logarithm of the number of stress cycles to failure. Heavily compacted lime-soil specimens were found to have considerably higher dynamic modulus and fatigue life than those having standard Proctor compaction. Increased values of dynamic flexural modulus and strength at the higher dry density favor the use of lime-laterite soil as a road base.

Highway pavements need good quality paving materials with adequate strength and durability characteristics. With petroleum prices rising sharply, bitumen is no longer a cheap material, particularly in India, and therefore asphalt-bound pavement layers cannot be considered economical road bases now. Highway activities, on the other hand, have increased manyfold and as a result quality paving materials have become scarce and costly. Under the circumstances, utilization of locally available indigenous materials may provide a solution to reduce construction costs if the characteristics of the in situ soils, otherwise unsuitable, are modified by appropriate treatment. This study is an attempt to evaluate the suitability of lime-treated laterite loams available in India.

Laterites are apparently very complex and controversial materials that defy any satisfactory geological, chemical, or pedological definition (*1*, p. 5). Essentially, they are products of tropical or subtropical weathering that includes all stages from parent rock to the surface and in which iron or aluminum content or both are higher and silicon content is lower than in merely kaolinized parent rock (*2*, pp. 1–10). Though they frequently occur in the humid tropical areas of South America, Africa, India, Indonesia, and Australia (*3*), there is an absence of adequate engineering data for highway and runway construction.

Areas of laterite soil occur in coastal India and the adjoining interior. The present study area at Kharagpur is on the east coast. These reddish-brown fine-grained laterite soils are evaluated for their suitability as a lime-bound base. Tests were carried out on four laterite soils treated with an optimum lime content of 5 percent.

The changes that take place on addition of lime to certain laterite soils are rapid amelioration effects and strength development due to hydration and increased degree of crystallinity of the reaction products formed during the first 5 to 7 days (*4*). The strength of a stabilized soil has been quantitatively assessed by unconfined and confined compressive strength tests (*5*; *6*, p. 290; *7–9*) and also by the split tensile strength test (*10*). But the shear and compressive strengths of lime-soil mixtures are not the limiting factors in their application as subbase or base-course materials (*11*). The lime-soil

P. G. Bhattacharya, B. E. College, Shibpur, Howrah, India. B. B. Pandey, Indian Institute of Technology, Kharagpur 721 302, India.

TABLE 1 LATERITE SOIL PROPERTIES

Property	Soil A	B	C	D
Gravel (>2 mm) (%)	1.02	0.78	0.75	0.40
Sand (2–0.075 mm) (%)	42.89	47.52	43.87	35.70
Silt (0.075–0.005 mm) (%)	47.40	46.22	48.54	54.00
Clay (<0.005 mm) (%)	8.69	5.48	6.84	9.90
Liquid limit (%)	30.95	23.60	23.50	38.63
Plasticity index (%)	12.58	10.35	10.54	18.07
Standard Proctor maximum dry density (kg/m^3)	1926	1945	1910	1900
Optimum moisture content (Proctor) (%)	12.78	11.50	12.50	13.50
Modified AASHTO maximum dry density (kg/m^3)	2080	2085	2040	2015
Optimum moisture content (modified AASHTO)	10.23	9.50	10.50	12.00
AASHTO classification	A–6(5)	A–4(3)	A–4(4)	A–6(9)
Textural classification	Loam	Loam	Loam	Silty loam
Unified classification	CL	CL	CL	CL

layer in a pavement is subjected to repeated flexural stresses, and therefore its flexural strength and fatigue responses are more important considerations. Published fatigue data for lime-treated soil in general and lime-laterite soil mixtures in particular are limited. Swanson and Thompson (*11*) conducted a flexural fatigue study of selected lime-soil mixtures with the primary objective of evaluating the general flexural fatigue response of the materials and determining whether the fatigue response would limit the use of these materials in subbase and base-course applications.

PURPOSE AND SCOPE

The main purpose of this investigation was to determine the dynamic and flexural fatigue response of lime-laterite soil mixtures at three levels (low, medium, and heavy) of compaction. The standard Proctor and modified AASHTO compactions are designated as low and heavy compaction, respectively, and the mean of the two is defined as medium compaction. Simply supported beam specimens of nominal size 50 mm high, 64 mm wide, and 254 mm long were tested under symmetrical third-point loading in a fatigue-testing apparatus developed in the laboratory (*12*) for the specific purpose of applying pulsating loads on lime-soil beams and similar materials. The study was limited to laterite soils described as loam and silty loam belonging to the CL group of the Unified Soil Classification System and to the A-4 to A-6 groups of the AASHTO classification.

TEST MATERIALS

Soils

Four laterite soils, air-dried and passing the 4.75-mm sieve, were designated A, B, C, and D; the samples were from the well-developed mottled zone found in and around Kharagpur, India. The soils were all reddish brown, blocky, and sticky, with iron nodules fairly well distributed. Soils A, B, and C were collected from scrub jungle and D from a paddy cultivation area. The soils ranged from loams to silty loams, with particle sizes smaller than 0.075 mm varying from nearly 52 to 64 percent and plasticity index (PI) values ranging from 10 to 18. Addition of 5 percent lime by weight of air-dried soil reduced the PI values of the lime-soil mixtures to about 40 to 50 percent of those of the untreated soils. Tables 1 and 2 give the properties of the laterite soils and the lime-laterite soil mixtures.

TABLE 2 LIME-LATERITE SOIL MIXTURE PROPERTIES

Property	Soil A	B	C	D
Lime treatment (%)	5	5	5	5
Liquid limit (%)	30.45	23.00	—	33.80
Plasticity index (%)	7.25	6.30	—	7.73
Standard Proctor maximum dry density[a] (kg/m^3)	1884	1878	1875	1870
Optimum moisture content (OMC) (Proctor)[b] (%)	14.96	13.78	13.95	14.63
Modified AASHTO maximum dry density[c] (kg/m^3)	2035	2030	2000	1980
Optimum moisture content (modified AASHTO)[d] (%)	11.97	10.60	12.00	13.20

[a]Mean = 1877 kg/m^3.
[b]Mean = 14.33 percent.
[c]Mean = 2011 kg/m^3.
[d]Mean = 11.94 percent.

Lime

Commercial-grade quick lime, slaked, dried, and sieved through a 0.075-mm sieve, was used throughout the testing program. The mean calcium oxide content of the hydrated lime was nearly 64 percent.

SPECIMEN PREPARATION

Each batch of soil was weighed and mixed with the required amount of lime. The compaction water was then added and the mixture was again hand mixed until it appeared to be uniform with an even distribution of moisture. The mean amount of compaction water needed to achieve maximum dry density for the lime-laterite soil mixtures was 14.33 and 11.94 percent for standard Proctor and modified AASHTO compaction, respectively. Dry densities of 1880, 1940, and 2000 kg/m^3 represented light, medium, and heavy compactions. The soil-lime mixture was compacted in a steel mold in three layers, each layer being subjected to 15 tamping blows of a standard Proctor hammer. The soil was then compressed to a given volume by a hydraulic jack. Next the sample was extruded from the mold and weighed. Side dimensions were measured for volume calculations, and the dry density was calculated considering the actual moisture content and the weight of the specimen.

Beam samples, after extrusion from the mold, were placed inside polyethylene bags to prevent escape of moisture from within and cured in a temperature-regulated oven at 50 ± 1°C for 3 days. In a separate study (*12*) it was found that 3 days of oven curing at 50°C is equivalent to 41 days of moist curing at the mean summer temperature of 30.50°C having a maturity of 1245 degree-days above a 0°C datum.

STRENGTH EVALUATION OF LIME-LATERITE SOIL MIXTURES

Static compression test studies were conducted in which 64 oven-cured cylindrical specimens 50.8 mm in diameter and 101.6 mm high were tested under unconfined compression to examine the variation of strength with dry density and lime content of the specimens. Lime content of 5 percent was found to be the optimum for the stabilization of laterite Soil A, because the rate of strength gain for higher lime contents was not significantly high (*13*, *14*, pp. 37–41). The least-squares regression line for the lime-soil mixture with 5 percent lime content was found to be

$$\sigma_u = -15.3158 + 9.4342 \times 10^{-3}\,\gamma_d \qquad R^2 = 0.84 \qquad (1)$$

where

σ_u = unconfined compression strength (MPa),
γ_d = dry density (kg/m^3), and
R^2 = coefficient of determination.

In order to assess the applicability of the foregoing equation to other lime-treated laterite soils in the area, cylindrical samples of Soils B, C, and D of the same size and treated with 5 percent lime were tested under identical conditions. The predicted and observed unconfined compressive strength values of all 22 samples of Soils B, C, and D, along with 32 samples of Soil A, were observed to compare favorably with respect to the 1:1 correlation line, indicating that laterite Soils A, B, C, and D treated with lime would develop comparatively equal strengths. The coefficient of determination between the predicted strength values from Equation 1 and the observed values for Soils B, C, and D was found to be 0.87.

STATIC FLEXURAL STRENGTH STUDIES

The stress ratio in the flexural fatigue test is the ratio of the applied flexural stress (σ_f) on the beam specimen to its modulus of rupture. It is therefore necessary to predict the static flexural strength of the beams for analysis of fatigue test results. Beam specimens of different densities were tested under third-point loading at a rate of 1.25 mm/min until failure. The test results yielded the following regression equation:

$$MR = -7.0361 + 4.3 \times 10^{-3}\,\gamma_d \qquad R^2 = 0.89 \qquad (2)$$

where MR is the modulus of rupture in megapascals.

EXPERIMENTAL INVESTIGATION

Figure 1 is a representative diagram of the experimental setup for the fatigue testing machine. The rate of loading is 110 cycles/min with a cycle length of 0.54 sec and the distribution of loading to unloading time adjusted to 1:1. Load and deflection of the beams were recorded on a two-channel electronic recorder. The load cell and the linear variable differential transformer were calibrated before use for the purpose.

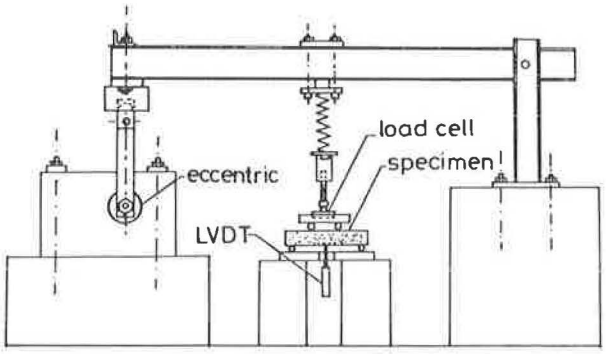

FIGURE 1 Fatigue-testing experimental setup.

Three types of beams, depending on the compaction (light, medium, or heavy), were tested under repeated flexure to study the fatigue characteristics of the material. The stress ratio varied from 0.41 to 0.68 for lightly compacted beams, from 0.47 to 0.71 for medium-compacted beams, and from 0.31 to 0.72 for heavily compacted beams. Once the dry density of the specimen had been determined, the modulus of rupture was calculated by using Equation 2, and the stress ratio was calculated by noting the applied load on the specimen obtained from

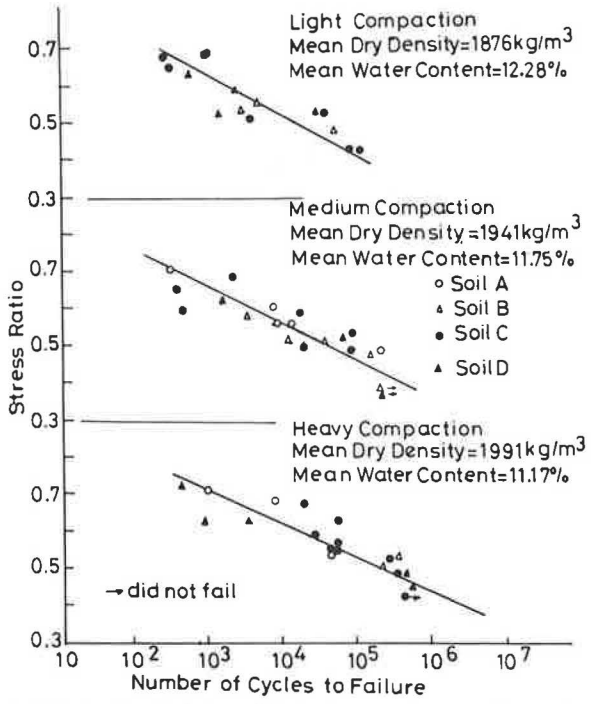

FIGURE 2 Relationship between stress ratio and fatigue life for lime-laterite soil mixtures.

the recorder. The results of the tests are shown in Figure 2. The least-squares regression lines for different dry densities are as follows:

Light compaction:

$$S = 0.96 - 0.114 \log N_f \quad R^2 = 0.76 \tag{3}$$

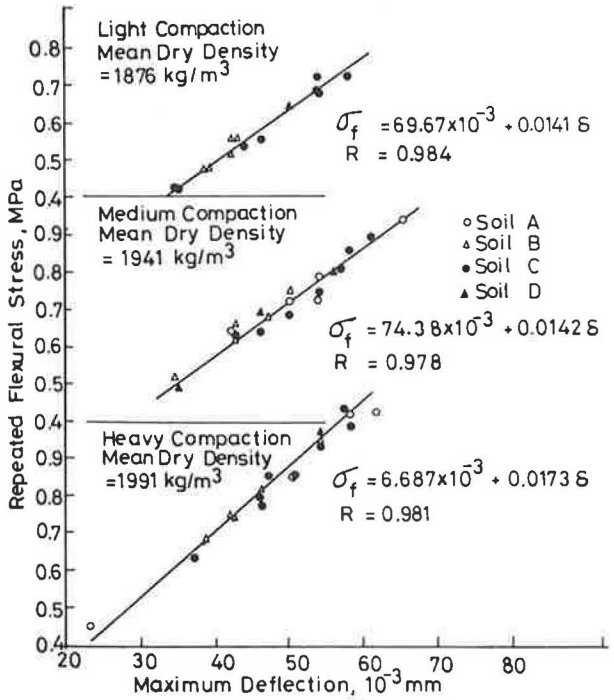

FIGURE 3 Relationship between repeated flexural stress and deflection for lime-laterite soil mixtures.

Medium compaction:

$$S = 0.95 - 0.099 \log N_f \quad R^2 = 0.77 \tag{4}$$

Heavy compaction:

$$S = 0.982 - 0.090 \log N_f \quad R^2 = 0.79 \tag{5}$$

where S is the stress ratio and N_f is number of cycles to fracture.

The applied flexural stresses have been plotted in Figure 3 against the central deflections of beams subjected to third-point loading. The scatter is very small and the coefficients of determination for linear regression for all compactive efforts are around 0.97. The lime-laterite soil beams thus display linear elastic behavior right up to the rupture stage under the cyclic loading, because deflections and loads remain constant till the specimens suddenly fail.

DYNAMIC MODULUS AND DRY DENSITY

Fifty-four beams with dry densities ranging from light to heavy were tested under repeated flexure, and for each beam the dynamic flexural modulus was calculated according to the following equation:

$$E_{DF} = 23WL^3/1296\delta I \tag{6}$$

where

E_D = flexural dynamic modulus,
W = load applied,
L = simply supported span (225 mm),
I = moment of inertia of the beam, and
δ = central deflection.

E_{DF}-values have been plotted against dry density in Figure 4

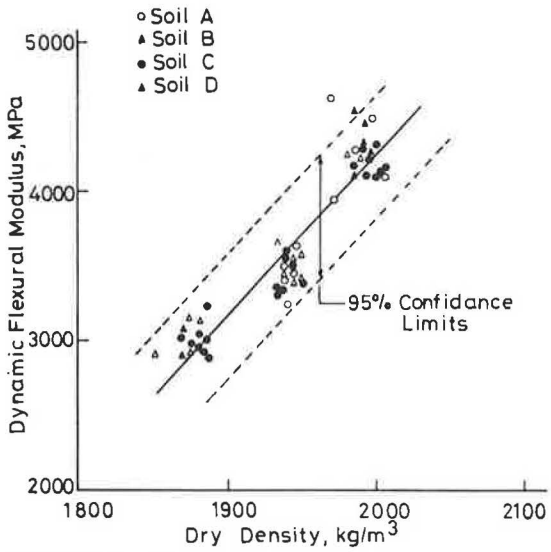

FIGURE 4 Relationship between dynamic flexural modulus and dry density for lime-laterite soil mixtures.

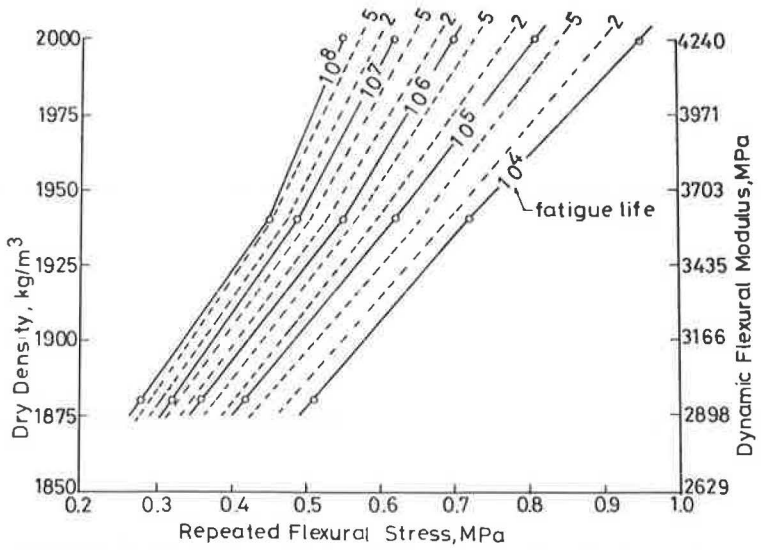

FIGURE 5 Variation of fatigue life with dry density, dynamic flexural modulus, and flexural stress for lime-laterite soil mixtures.

and the following equation relating E_{DF} in megapascals and γ_d in kilograms per cubic meter was obtained:

$$E_{DF} = -17.234 + 10.734 \times 10^{-3}\gamma_d \qquad R^2 = 0.84 \tag{7}$$

Using Equations 2 and 7, the relationship between MR and E_{DF} (in megapascals) was found to be

$$E_{DF} = 330 + 2496MR \tag{8}$$

The major findings of the investigation are combined in Figures 5 and 6, which show the relationships among various parameters that are important for design of pavements having lime-laterite soil layers.

PRACTICAL APPLICATION

The fatigue data presented in the paper can be applied to the design of pavements having lime-stabilized laterite soil. The design method essentially consists of two steps.

The first step is to select a thickness of pavement to prevent fatigue failure in the lime-soil layer. The tensile stresses computed in the lime-soil layer by elastic-layer analysis are increased by 50 percent (*15*, pp. 409–416) to account for increased stresses resulting from loading at the transverse crack that may develop after construction because of shrinkage and temperature changes.

The second step is to ascertain that the combination of load and thermal stresses will not crack the stabilized layer (*15*).

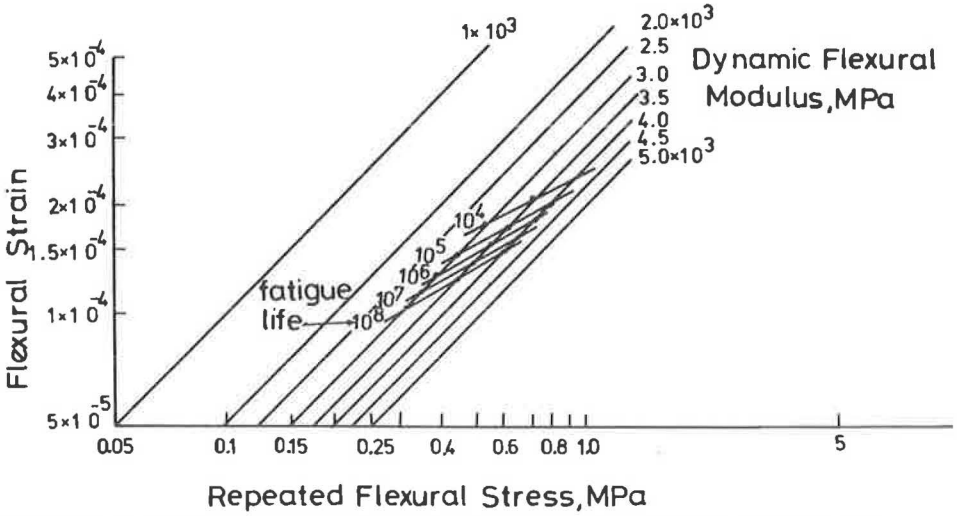

FIGURE 6 Relationship among flexural stress, strain, dynamic modulus, and fatigue life.

The design of a pavement consisting of lime-stabilized base with a thin bituminous wearing surface has been determined (*12*) for the Kharagpur region by assuming an axle load spectrum identical to that of the left-hand traffic lane of the northbound carriageway of Trunk Road A1 at Alcombury Hill in England (*16*, p. 52). Assuming the traffic growth to be 5 percent, it was found that a 45-cm lime-bound laterite soil base at modified AASHTO compaction with a thin bituminous surfacing has a life of about 20 years.

DISCUSSION OF RESULTS

The physicochemical properties of laterite soils are responsible for the strength values for the lime-soil mixture, which are different from those reported by others (*11*, *17*), though there is a similarity in the trend of the results.

The plots of S versus $\log N_f$, σ_f versus δ, and E_{DF} versus γ_d have yielded linear relationships with coefficients of determination varying from 0.74 to 0.97. The slopes of the fatigue lines in Figure 2 are higher for lightly compacted soil, indicating that fatigue damage takes place at faster rates when the dry density is low. An examination of Table 3 reveals that heavily compacted lime-laterite material will withstand flexural stresses almost twice the values sustained by the lightly compacted beams for the same number of repetitions.

Study of Figure 3 reveals that the stress-deflection relationship is strikingly linear for all the compactions and the material behavior is linearly elastic. The lightly compacted beams undergo deflections that are nearly one-and-one-half times the deflection of the heavily compacted beam at various applied stresses. The dynamic modulus, a major parameter for pavement design, can be estimated from the values of dry density spread over the three dry density ranges. The dynamic modulus at heavy compaction is one-and-one-half times that at light compaction.

Fatigue response curves relating flexural stress, dry density, dynamic modulus, and flexural strain have been developed for N_f varying from 10^4 to 10^8 repetitions to cover a wide range of traffic movement; these curves are shown in Figures 5 and 6. They show the effects of various parameters on fatigue lives of the lime-soil mixture.

TABLE 3 REPEATED FLEXURAL STRESSES AT DIFFERENT DRY DENSITIES AND AT SELECTED FATIGUE LIFE

Compaction	Dry Density (γ_d)(kg/m^3)	Dynamic Flexural Modulus (E_{DF})(MPa)	Fatigue Life (N_f)	Repeated Flexural Stress (σ_f)(MPa)
Light	1880	2952	10^4	0.51
Medium	1940	3596		0.72
Heavy	2000	4240		0.95
Light	1880	2952	10^5	0.42
Medium	1940	3596		0.62
Heavy	2000	4240		0.81
Light	1880	2952	10^6	0.36
Medium	1940	3596		0.55
Heavy	2000	4240		0.70
Light	1880	2952	10^7	0.32
Medium	1940	3596		0.49
Heavy	2000	4240		0.62
Light	1880	2952	10^8	0.28
Medium	1940	3596		0.45
Heavy	2000	4240		0.56

CONCLUSIONS

1. Good correlation exists between the flexural fatigue life and stress ratio and between dry density and dynamic flexural modulus for two stabilized laterite soils. The relationships are all linear and statistically significant.
2. Lime-laterite soil mixtures behave like linear-elastic brittle materials under pulsating loads. Hence, a lime-laterite soil layer may be considered a linearly elastic material in the stress analysis of pavements.
3. The fatigue resistance of lime-laterite soils is increased to a considerable extent at the higher dry density. Heavily compacted materials can be subjected to almost twice the flexural stresses as compared with the lightly compacted beams for the same number of repetitions to failure.
4. The dynamic flexural modulus of heavily compacted lime-soil mixtures is nearly 1.5 times that of the lightly compacted ones and the values of the moduli at light, medium, and heavy compaction are, respectively, 2952, 3596, and 4240 MPa.

REFERENCES

1. M. D. Gidigasu. *Lateral Soil Engineering*. Elsevier Scientific Publishing Company, New York, 1976.
2. W. Schellmann. "Considerations on the Definition and Classification of Laterites." *Proc., International Seminar on Laterisation Processes*, Trivandrum, India, 1979.
3. J. K. Nixon and B. O. Skipp. "Airfield Construction on Overseas Soils, 5: Laterites." *Proc., Institution of Civil Engineers*, Vol. 8, 1957, pp. 253–292.
4. J. G. Cabrera and C. A. Nwakanma. "Pozzolanic Activity and Mechanism of Reaction of Red Tropical Soil-Lime Systems." In *Transportation Research Record 702*, TRB, National Research Council, Washington, D. C., 1979, pp. 199–207.
5. M. A. Jan and R. D. Walker. "Effect of Lime, Moisture, and Compaction on a Clay Soil." In *Highway Research Record 29*, HRB, National Research Council, Washington, D. C., 1963, pp. 1–12.
6. *Laterite and Laterite Soils and Other Problem Soils of Africa.* Report AID/C8D-2164. U. S. Aid for International Development, Washington, D. C., 1971.
7. J. G. Laguros. "Lime-Stabilized Soil Properties and the Beam Action Hypothesis." In *Highway Research Record 92*, HRB, National Research Council, Washington, D. C., 1965, pp. 12–20.
8. J. W. H. Wang, M. Mateos, and D. T. Davidson. "Comparative Effects of Hydraulic, Calcitic and Dolomatic Limes and Cement in Soil Stabilization." In *Highway Research Record 29*, HRB, National Research Council, Washington, D. C., 1963, pp. 42–54.
9. M. R. Thompson. "Shear Strength and Elastic Properties of Lime-

Soil Mixtures." In *Highway Research Record 139*, HRB, National Research Council, Washington, D. C., 1966, pp. 1–14.
10. M. R. Thompson. "Split Tensile Strength of Lime Stabilized Soils." In *Highway Research Record 92*, HRB, National Research Council, Washington, D. C., 1965, pp. 69–80.
11. T. E. Swanson and M. R. Thompson. "Flexural Fatigue Strength of Lime-Soil Mixtures." In *Highway Research Record 198*, HRB, National Research Council, Washington, D. C., 1967, pp. 9–18.
12. P. G. Bhattacharya. *Static and Flexural Fatigue Strength of Lime-Laterite Soil—Plain and Fibre Reinforced.* Ph.D. thesis. Indian Institute of Technology, Kharagpur, India, July 1984.
13. P. G. Bhattacharya and B. B. Pandey. "Study of Strength and Curing of Lime-Stabilized Soil—Plain and Fiber Reinforced." *Indian Roads Congress, Highway Research Board Bulletin 24*, 1984, pp. 1–26.
14. P. G. Bhattacharya and B. B. Pandey. "Effect of Density on Strength and Modulus of Plain and Fiber Reinforced Lime-Laterite Soil Mixtures under Static and Repeated Load." Presented at Indian Geotechnical Conference, Calcutta, 1984.
15. J. K. Mitchell and C. L. Monismith. "A Thickness Design Procedure for Pavements with Cement Stabilized Bases and Thin Asphalt Surfacings." *Proc., 4th International Conference on Structural Design of Asphalt Pavements*, University of Michigan, Ann Arbor, 1977.
16. D. Croney. *The Design and Performance of Road Pavements.* Her Majesty's Stationery Office, London, 1977.
17. L. W. Locket and R. K. Moore. "Lime-Soil Mixture Design Consideration for Soils of Southeastern United States." In *Transportation Research Record 839*, TRB, National Research Council, Washington, D. C., 1982, pp. 20–25.

Publication of this paper sponsored by Committee on Lime and Lime-Fly Ash Stabilization.

Experimental Aspects of Mercury Intrusion Porosimetry

DOUGLAS N. WINSLOW

Several frequently ignored aspects of mercury intrusion porosimetry are discussed. The importance of knowing the correct contact angle between the mercury and the solid is emphasized. It is also suggested that mercury intrusion be considered in some instances when a specific surface measurement is desired. Also, a method for handling inhomogeneous samples is discussed. Finally, a possibly instructive use for the hysteresis found on depressurization is explored.

Mercury intrusion has become the predominant experimental technique for determining pore-size distributions. This is because modern instrumentation allows one to measure rapidly pores with sizes ranging over about six orders of magnitude. Much of the experimental technique and data reduction has become routine, and ASTM standard methods are beginning to appear (ASTM D 4284-83 and D 4404-84).

Nevertheless, certain experimental aspects have not received the attention that the author believes they deserve. It is the intent of this paper to discuss several of these aspects. It is assumed that the reader is familiar with the fundamentals behind the phenomenon of mercury intrusion and with the basis of the experimental technique. A general reference for experimental technique is *Surface and Colloid Science* (*1*, Vol. 13, Ch. 6).

School of Civil Engineering, Purdue University, West Lafayette, Ind. 47907.

CORRECT CONTACT ANGLE

It is necessary to know the applicable contact angle in order to accurately convert the pressures that are recorded during an intrusion experiment into their corresponding pore sizes. In some cases, the exact value of this angle is not particularly important. If tests are being conducted merely to determine whether or not a piece of porous material has the same pore structure as a companion piece of the same material, any angle will serve. Indeed, under such circumstances, one can make the comparison by using the pressure-intrusion data without bothering to convert the pressures into pore sizes.

However, when the aim is to correlate pore sizes with some other property of a material, a wrong impression may be obtained if the pores sizes are incorrectly calculated. Another case in which accurate angles are needed is in the comparison of the pore structures of different materials. This is because the contact angle is a function of the surface properties of both the

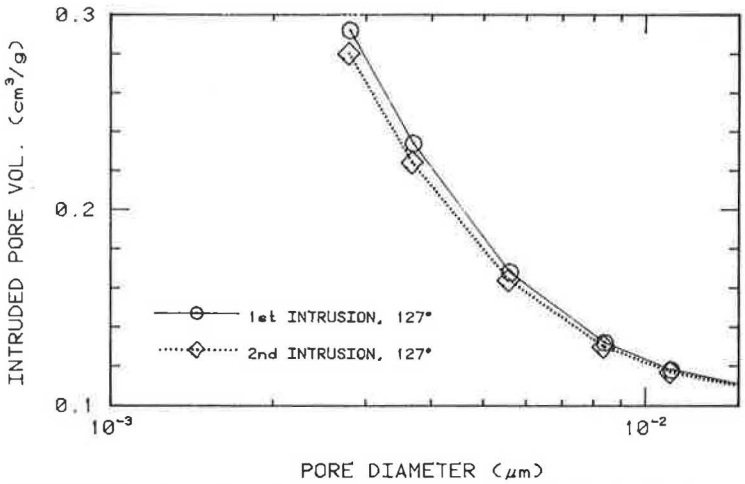

FIGURE 1 Pore-size distributions of alumina plotted with the same contact angle.

mercury and the porous solid. These latter properties can be expected to vary between different materials.

An example of a wrong impression is given in Figure 1. It shows two pore-size distributions of a sample of porous alumina. Only the distributions of the smaller pores are shown, to emphasize the point being made. The solid line is the distribution found during the first intrusion of a virgin sample. The dotted line is the distribution found on a second intrusion after removal of the mercury by distillation. Both are plotted using a contact angle of 127 degrees. This is the angle that was found to be applicable for the virgin alumina.

The obvious conclusion from Figure 1 is that the act of intruding the sample has caused some crushing and that the pore volume has been reduced. This appears to be especially true in the smallest pore size ranges where the pressure is the greatest, an apparently logical finding. However, the act of distilling the mercury from the sample has left its surface somewhat altered. A direct measurement of the applicable angle showed that it had changed to 131 degrees.

This change of 4 degrees may appear small at first glance, but it is the cosine of this angle that is used in the conversion of pressure to size. The cosines of the two angles differ by about 9 percent, and thus there is a 9 percent error in the sizes of the pores depicted by the dotted line in Figure 1. When the correct contact angle is used for each set of data, the result is as shown in Figure 2.

The conclusions from Figure 2 are different; there has been no crushing of the sample during the initial intrusion, and its pore structure has remained unchanged. This is an example of why applicable contact angles must be determined for critical research work. Measuring contact angles is a laborious operation (2), but it is necessary if wrong conclusions are to be avoided in research.

MEASUREMENT OF SURFACE AREA

A number of years ago, Rootare and Prenzlow (*3*) derived a method for obtaining a measure of the surface area of a sample directly from the curve of pressure versus intruded volume of an intrusion experiment. Basically, the technique yields the surface area of a sample by finding the amount of work (the

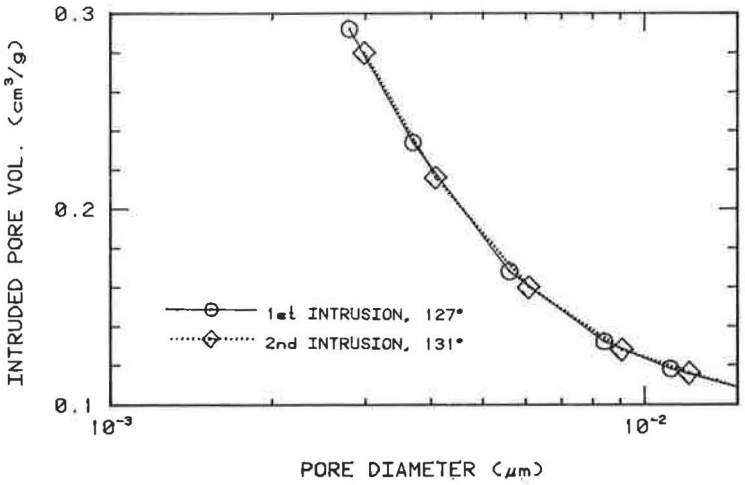

FIGURE 2 Pore-size distribution of alumina plotted with different, correct contact angles.

area under the curve of pressure versus volume) needed to cover the surface with mercury. This technique does not appear to be widely used. However, it has certain unique advantages over the more traditional vapor sorption technique and deserves more attention.

The traditional vapor sorption technique becomes experimentally difficult when the sample has a small surface area because so little vapor is adsorbed. It is precisely this class of samples for which the intrusion procedure is ideally suited, and experimenters might consider performing an intrusion experiment solely to obtain a measure of surface area. For example, several results for some samples of fly ash are as follows:

	Area	
Sample	*By Intrusion (m^2/g)*	*By Sorption (m^2/g)*
NIP 1A	1.6	1.7
NIP 2	2.3	2.1
NIP 1	4.2	4.1

Generally one is not interested in the distribution of the interparticle pores in a collection of fly-ash particles. However, mercury intrusion proved to be a rapid and accurate method of obtaining the surface area of the samples discussed here. The foregoing data indicate that the intrusion procedure gives results comparable to those obtained by vapor sorption, and these were obtained in about 1 percent of the time required for sorption.

One strong note of caution about the use of this intrusion technique: if insufficient pressure is available to intrude all the pore space and cover all the surface, this method will return an erroneously low measure of the surface area. On the other hand, if higher pressures cause a crushing of sealed pores, this method will yield an erroneously high measure. Usually, when these complications are not present, the curve of pressure versus intrusion will flatten out, and no further intrusion will be recorded for the higher pressures. Thus, if the intrusion curve is still rising at the highest pressures, the method is probably not applicable. Figure 3 demonstrates this important difference with two distributions. One shows continued intrusion, and the other shows that intrusion has stopped. Fortunately, for many materials with small surface areas such as coarse-grained soils, the intrusion curves do flatten out, and the method has considerable merit.

HANDLING HETEROGENEOUS SAMPLES

Most porosimeters can only accept samples with a bulk volume of a few cubic centimeters. This does not present a sampling problem as long as the material has a pore structure that is homogeneous within this volume. However, many construction materials are not this uniform. One obvious strategy is to perform a number of tests and to combine the results. This is the equivalent of performing a single test on a much larger sample, but it requires extensive testing.

An alternative approach is suggested here that, under the right circumstances, can be used to greatly reduce the number of tests. The procedure envisions a large sample, such as a piece of rock or brick, from which subsamples with a volume of a few cubic centimeters possess substantially different pore volumes. This is what is meant here by a heterogeneous pore structure.

The first step is to crush the material and to separate a certain size fraction, that is, material passing the No. 4 sieve and retained on the No. 8. This material is then reduced with a sample splitter until one has a sample with sufficiently few grains to permit testing. This technique allows one to test more randomly selected pieces simultaneously, which has the effect of smoothing out variations in pore structure and giving one a reasonable chance of testing a homogeneous sample.

One can assess the efficacy of this procedure by looking at the coefficient of variation of the total intruded pore volumes from repeat tests with different sizes of crushed pieces. Data for two materials are as follows:

Material	*Particle Size*	*Coefficient of Variation (%)*
Limestone	1/2–3/8 in.	28.9
Limestone	No. 4–No. 8 sieve	4.0
Masonry brick	3/8 in.–No. 4 sieve	6.8
Masonry brick	No. 4–No. 8 sieve	3.0

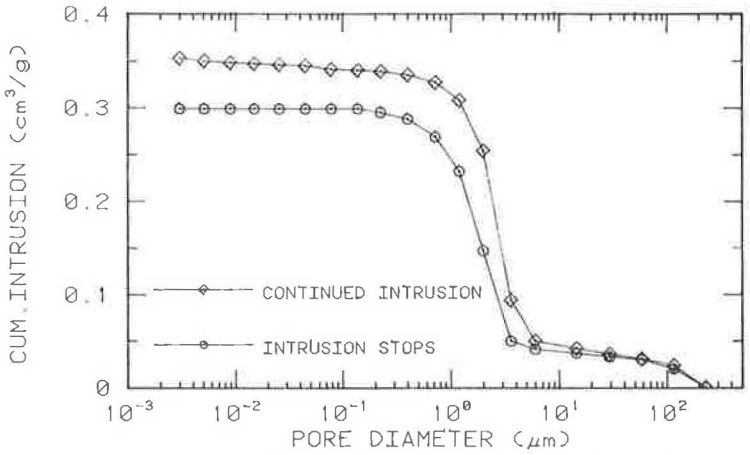

FIGURE 3 Pore-size distributions showing continuing and completed intrusions.

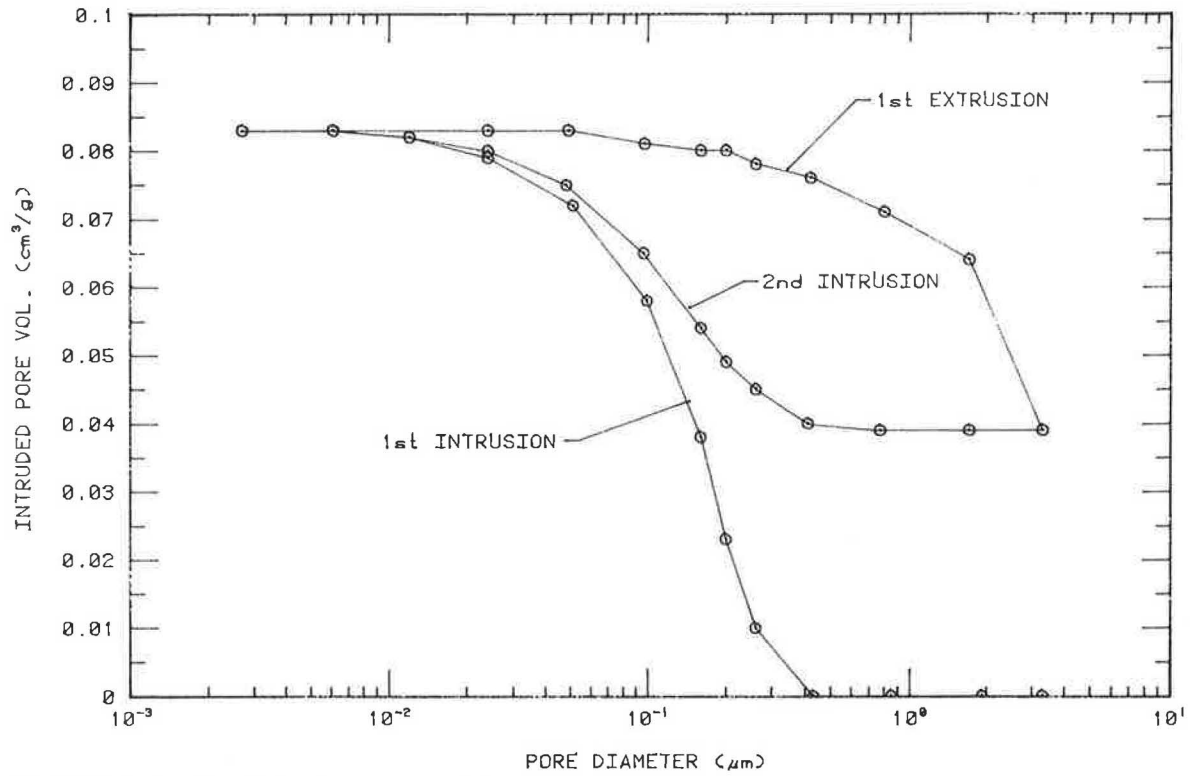

FIGURE 4 Hysteresis during mercury intrusion and extrusion.

These data indicate that scatter in results can be significantly reduced by this procedure. Thus, the number of tests required to be confident in one's results is reduced also.

There is one difficulty with this technique. The collection of smaller particles inside the porosimeter generates some interparticle porosity that is not present in the larger mass of the parent sample. As long as reasonably large particles are tested, most of this false porosity will lie in the larger pore-size range. One must subtract this extra porosity before using the results. However, if the parent material has innate porosity in this same size range, this correction cannot be made. Thus, one needs to do a certain amount of testing with large, single pieces of the material to ensure that one is justified in using this technique and to select the best crushed size fraction for the material in question.

HYSTERESIS IN PORE-SIZE DISTRIBUTIONS

The pore-size distributions derived from mercury intrusion and mercury extrusion are different for virtually all porous materials. Typically, one-third to two-thirds of the intruded mercury does not spontaneously exit the pore structure on depressurization. Lowell and Shields (*4*) have examined this hysteresis in a new way. For the distributions in Figure 4 (determined by the author for a limestone), the first intrusion and the first extrusion pore-size distributions are seen to be widely different. On repressurization (the second intrusion curve of Figure 4), the intruded pore volume returns to its previous maximum. Subsequent depressurization was found to retrace the first extrusion curve, and repressurization was found to retrace the second intrusion curve. Thus the total hysteresis, starting from the first intrusion, consists of two parts: an irreversible and a reversible portion.

Whatever the reasons for the irreversible hysteresis, Lowell and Shields found one consistent reason for the reversible part: the advancing and receding contact angles for mercury are different. Receding contact angles are typically smaller than advancing ones, and Lowell and Shields found that the reversible hysteresis loop could be completely eliminated by the selection of an appropriately smaller angle for the extrusion leg of the cycle. Figure 4 was plotted by using only the appropriate advancing contact angle of 125 degrees. However, if the extrusion curve had been plotted with a receding angle of 93.5 degrees, it would coincide with the second intrusion curve. In other words, the second intrusion curve represents both second and subsequent intrusions and subsequent extrusions, if the appropriate contact angles are invoked.

This means that the second intrusion curve is the pore-size distribution of that portion of the total pore structure that can be reversibly intruded. If this reversible distribution is subtracted from the total pore-size distribution, one obtains the irreversible pore-size distribution as well. Figure 5 shows the results of separating these two distributions from the total pore-size distribution shown in Figure 4.

The two distributions in Figure 5 are not the same. One has significantly more small pores, and the other has a greater pore volume in the size range centered around 0.1 μm. When the same sort of subdivision is performed on other distributions, the resulting distributions are frequently even more dissimilar.

It may be that one or the other better correlates with and explains other properties of a material than does the total pore-size distribution. For example, one might postulate that the reversible pore structure represents those pores that are more

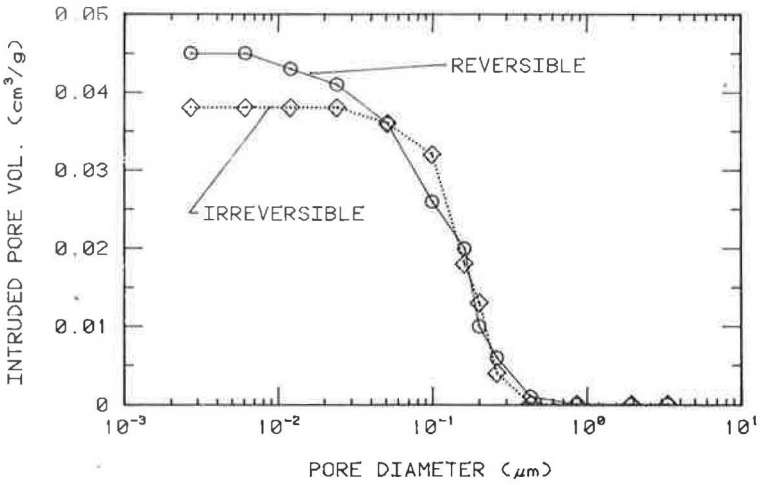

FIGURE 5 Reversible and irreversible parts of a pore-size distribution.

directly connected and accessible. It may be only this part of the pore structure that dictates the permeability of the material and not the total pore-size distribution. This approach has not been attempted. However, it appears to be a potentially fruitful extension of the technique that may lead to more informative results.

CONCLUSION

Mercury intrusion porosimetry is now a well-developed experimental procedure. However, there are applications for it that have not been much used, and there are variations on the standard uses that appear promising for obtaining additional information. It is hoped that this paper will suggest new avenues to researchers.

REFERENCES

1. *Surface and Colloid Science* (E. Matijevic and R. J. Good, eds.), Plenum Press, New York, 1984.
2. D. N. Winslow and S. Diamond. *ASTM Journal of Metals*, Vol. 5, 1970, p. 5.
3. H. M. Rootare and C. F. Prenzlow. *Journal of Physical Chemistry*, Vol. 71, 1967, p. 2733.
4. S. Lowell and J. E. Shields. *Journal of Colloid and Interface Science*, Vol. 80, 1981, p. 192.

Publication of this paper sponsored by Committee on Physicochemical Phenomena in Soils.

Measurement of Pore-Size Density Function in Sand

C. H. JUANG AND C. W. LOVELL

A study is presented on characterization of sand fabric by means of the pore-size distribution, which allows the engineer to indirectly but quantitatively examine the sand fabric. The term "pore-size distribution" is clarified so that a better link is established between the terminology used in the literature of mercury porosimetry and that used in the conventional probabilistic approaches in geotechnical engineering. A technique has been verified satisfactory for preparation of sand specimens for mercury intrusion tests, which make possible the measurement and determination of the pore-size distribution and the density function in sand. Data deduction and typical pore-size distributions and density functions for the sands studied are presented and discussed.

The characterization of soil fabric is an important aspect of soil engineering. It can lead to better understanding and prediction of engineering properties of soils. The term "soil fabric" is generally understood as "the physical constitution of a soil material as expressed by the special arrangement of the solid particles and associated voids" (*1*). Past research has shown that the fabrics of compacted clayey soils can be characterized by their pore-size distribution characteristics, and some engineering properties of clayey soils can be quantitatively correlated with their pore-size distribution parameters (*2*; *3*; *4*, pp. 839–856; *5–12*). Although engineering properties of sands are also believed to be strongly affected by their fabric characteristics (*13–16*, p. 59) a simple and rational technique to characterize the sand fabric has not yet been reported. A study is presented on characterization of the sand fabric by means of pore-size distribution. The pore-size distributions of the compacted sands studied were measured and determined by using mercury intrusion porosimetry (MIP).

MERCURY INTRUSION POROSIMETRY

The pore systems of all but the most uniform soils have an extremely complex geometry. Therefore, to characterize soil fabric by means of pore size and its distribution is a rather abstract concept. There are, however, several advantages to the use of pore-size distribution in soil engineering. For example, it allows the engineer to quantitatively examine the soil fabric; it can be measured and determined by a simple, routine laboratory test; good correlations have been established between some engineering properties and pore-size distribution parameters (*4*, *6*, *12*); it provides an equally good or even better measure to characterize the soil fabric than its counterpart—grain-size distribution—does.

C. H. Juang, Department of Civil Engineering, Clemson University, Clemson, S.C. 29634-0911. C. W. Lovell, School of Civil Engineering, Purdue University, West Lafayette, Ind. 47907.

Over the past decade MIP has been shown to be the most suitable method to measure and determine the pore-size distributions of the soils. The mercury intrusion technique is based on the Washburn model (*17*):

$$P = -(4T \cos \theta / x) \tag{1}$$

where

- P = absolute pressure being applied,
- T = surface tension of mercury,
- θ = contact angle between mercury and the pore wall, and
- x = size of pores that can be intruded at pressure P, usually called the apparent pore diameter.

For any pore size that is determined by Equation 1, a corresponding pore volume $[F_v(x)]$ is intruded and recorded. Hence, a pore-size distribution [i.e., $F_v(x)$ versus x] can be readily generated in a mercury intrusion test. The measurement of pore-size distribution with MIP may be as follows. A pore-size distribution function may be established by repeatedly determining what fraction of the total pore volume the pores have for pore sizes ranging between x and infinity. Mathematically the complementary cumulative distribution function of the pore size $[F_X(x)]$ may be expressed as

$$F_X(x) = \int_x^\infty f_X(x)dx \tag{2}$$

where f_X is the probability density function of pore size, and

$$\int_0^\infty f_X(x)dx = 1 \tag{3}$$

It may be noted that F_X, defined in Equation 2, expresses the probability that the random variable takes on realizations x equal to or greater than X. Although this is in contrast to the conventional use of the cumulative distribution function in geotechnical engineering, it is better for interpreting the measured pore-size data, and it does serve the purpose of defining the probability density function. With this viewpoint, Juang and Holtz (*18*) have derived a volumetric pore-size density function $[f_V(x)]$ as follows:

$$f_V(x) = -[d(V_t - V)/dx] \tag{4}$$

where V_t is the total volume of pores in a soil, which is a constant, and $V_t - V$ is the volume of pores with pore sizes equal to or greater than x. Integrating Equation 4 over the range from x to infinity yields

$$F_V(x) = V_t - V \tag{5}$$

The function $F_V(x)$ is a complementary cumulative distribution of the pore size in terms of pore volume, but it is often simply called the pore-size distribution in the literature of MIP. Because $F_V(x)$ is generally expressed in terms of pore volume, it is sometimes called the pore-volume distribution (ASTM D4404). It is believed, however, that the term "pore-volume distribution" could be misleading for most engineers, who have become increasingly familiar with the language of probability theory used in geotechnical engineering: the term could be misunderstood as a distribution of pore volume when in fact pore size is the random variable considered. To be consistent with the current probability terminology used in geotechnical engineering, it is suggested that the probability density function of the pore size or, simply, the pore-size density function be used and reported in the MIP test. The pore-size density function may be obtained by dividing Equation 4 by the total pore volume (V_t), which yields

$$f_X(x) = (1/V_t) \cdot \{- [d(V_t - V)/dx]\} \quad (6)$$

Because Equation 6 can be deduced directly from the mercury intrusion data and is consistent with the language of probability theory used in geotechnical engineering, it is suggested that it be used in the presentation of the MIP test data.

PORE-SIZE DENSITY FUNCTION OF SAND

Specimen Preparation

The sand tested is a uniform Ottawa sand. The grain-size distribution is shown in Figure 1. The soil classification of the sand is SP and A-1-b(0) according to the Unified Soil Classification and AASHTO systems, respectively.

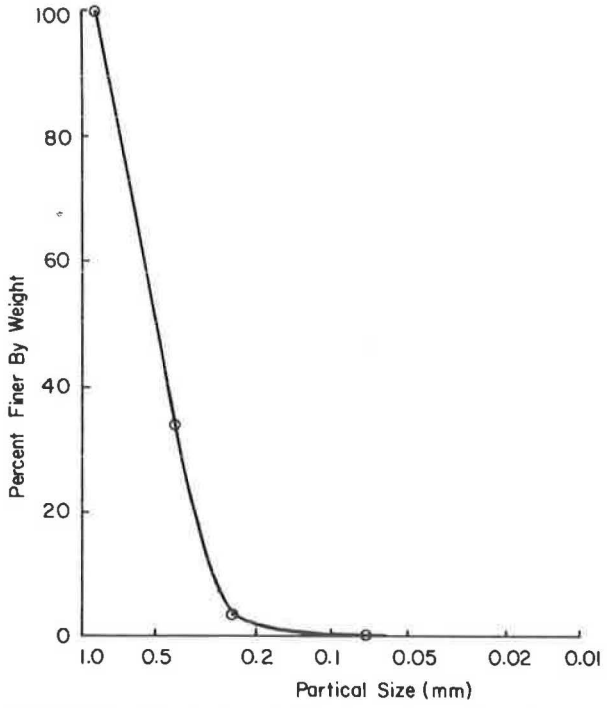

FIGURE 1 Grain-size distribution of sand tested.

Perhaps the most difficult problem in measuring and determining the pore-size distribution and pore-size density function in sand is the "sampling," that is, how to mold the soil specimen for the MIP test without destroying the sand fabric. In this study, the problem was solved by using a technique developed by Juang and Holtz (*19*). The technique involves using a resin as a bonding material. A small amount of Varcum 1364 powdered phenolic resin made by Reichold Chemicals, Inc., was mixed with sand. Pluviation was used to compact the sand sample in a standard Proctor compaction mold (ASTM D698) 102 mm in diameter and 116 mm high. After compaction the entire sample and the mold were carefully placed in the oven at a temperature of 170°C for about 1 hr. This time and temperature were sufficient to melt the resin, which surface coated the sand grains. The sample was then removed and placed in a desiccator for several hours until it cooled. The specimens for the MIP test were then trimmed from resin-bonded compacted samples. The dimensions of individual specimens were approximately 12 × 8 × 8 mm. After trimming, the specimens were placed in an oven for about 5 to 10 min in order to get rid of moisture, if any, that might have been absorbed by the specimens during trimming. The specimens were then kept in glass bottles and placed in the desiccator.

Different states of compaction of the sand studied were obtained by pluvial compaction (*14*). Figure 2 shows the pluviation scheme. The sand-resin mixture was poured from a 1000-ml flask through a nozzle made from a rubber stopper containing one hole either 6.8 or 3.8 mm in diameter. The sand-resin mixture was free to fall to the surface of the sample while

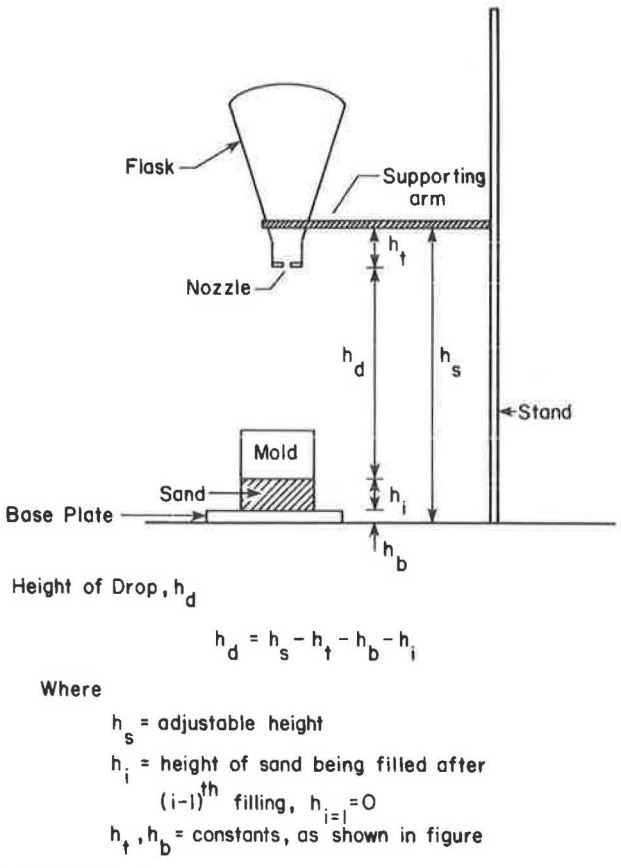

FIGURE 2 Schematic diagram of pluviation system.

the flask was rotated at a rate of approximately 15 rpm. The density of the sample obtained depended on the hole size and the drop height. In this study, the samples were made in five layers with drop height for each layer of 108 mm. In order to keep the same drop height, the flask position was adjusted for each layer. The choice of the drop height and hole size depended on the density of the compacted sample desired. For this study, they were selected by trial and error to produce a relatively dense and a relatively loose state, respectively. The results of the pluvial compaction of the sand-resin mixture are as follows (the results indicate that the desired density can be replicated by controlling the diameter of the hole and the drop height):

	State of Compaction	
Parameter	*Relatively Loose*	*Relatively Dense*
Sample no.	1–6	1–6
Diameter of hole (mm)	6.8	3.8
Drop height (mm)	108	108
No. of layers	5	5
Achieved dry density (Mg/m^3)	1.62	1.72

The minimum amount of resin that provides sufficient bonding and workability was found to be 0.5 percent by weight of sand (*18*). This percentage was used throughout the entire testing program. It must be noted that after oven drying, the compacted samples experienced about 5 percent shrinkage in volume but virtually no change in total weight. The powdered phenolic resin acted as a glue when the compacted sand was placed in the oven, and no chemical reaction between sand and resin occurred during oven drying (*18*).

The foregoing procedure has been found to be satisfactory. The fact that the results of the intrusion tests on specimens trimmed from the oven-dried samples are reproducible indicates that the procedure is an effective technique of obtaining sand specimens for the MIP test.

MIP Test

The apparatus and procedures used in this study were similar to those used by Garcia-Bengochea et al. (*4*) and ASTM D4404. However, the freeze-drying procedure was not used because the specimens had already been dried by using the specimen preparation technique described in the foregoing section. In addition, the penetrometer with intrusion capacity of 1.2 ml instead of 0.2 ml was used during the low-pressure intrusion period, because it was expected that a larger pore volume exists in sand than in clay. The low-pressure intrusion was mainly to measure the distribution of the large pores (20 to 500 m). The use of a large penetrometer (with a capacity of 1.2 mL) enhances the precision of the measurement of the distribution of the large pores. To extend the distribution curve to the range of the smaller pore size, a small penetrometer (with a capacity of 0.2 mL) was also used and the high-pressure intrusion was carried out for a separate specimen of the same sand. Thus, a combination of data measured by both penetrometers was used to obtain the distribution of the entire range of pore sizes.

RESULTS AND DISCUSSION

As mentioned earlier, the absolute applied pressures recorded in the MIP test can be used to calculate the apparent pore diameters on the basis of Equation 1. However, this step requires that the surface tension and contact angle be known. For the sand tested, the surface tension was judged to be 484 dynes/cm on the basis of Kemball's data (*20*). The contact angle of mercury on melted phenolic resin was determined to be 154 degrees following the method suggested by Winslow (*21*). Because the surface tension of phenolic resin is much lower than that of sand, the contact angle of mercury on sand was judged to be 154 degrees (D. N. Winslow, private communication). Once the two foregoing parameters have been determined, the rest of the data reduction procedures are more or less routine computations (e.g., *2*, *3*, *4*, ASTM D4404).

A graphical presentation of the complementary cumulative distribution with the intruded pore volumes per gram of specimen on the ordinate to an arithmetic scale and the apparent pore diameters on the abscissa to a logarithmic scale is a conventional way to present the MIP test data (*2*, ASTM D4404). Figure 3 shows the measured pore-size distributions of the sands at different states of compaction.

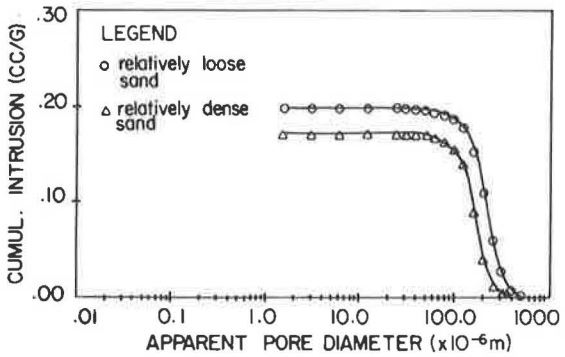

FIGURE 3 Pore-size distributions of sands tested in terms of cumulative intrusion.

As mentioned earlier, it may be desirable to present the measured data in terms of pore-size density function according to Equation 6. The pore-size density function may be obtained by using the finite difference approximation method (*19*) or by direct differentiation of a curve-fitted cumulative distribution function. The two methods generally yield approximately the same results (*6*). Figure 4 shows the pore-size density function of the sands tested.

In general, the replication of the MIP tests was satisfactory. Because of the relatively insignificant variation in the test results, Figure 4 actually represents an average of 12 data sets measured for each sand.

Finally, it has to be pointed out that in Equation 4 or 5, the term V_t implies the total pore volume that can be intruded by pressured mercury. Theoretically, it is equal to the total pore volume that exists in the soil specimen. In reality, however, a significant unintruded pore space is not unusual in an MIP test (*22*, *23*). For the sand specimens tested, however, the unintruded pore space is generally less than 5 percent. Thus, no correction measure (*24*) was taken, and the former definition

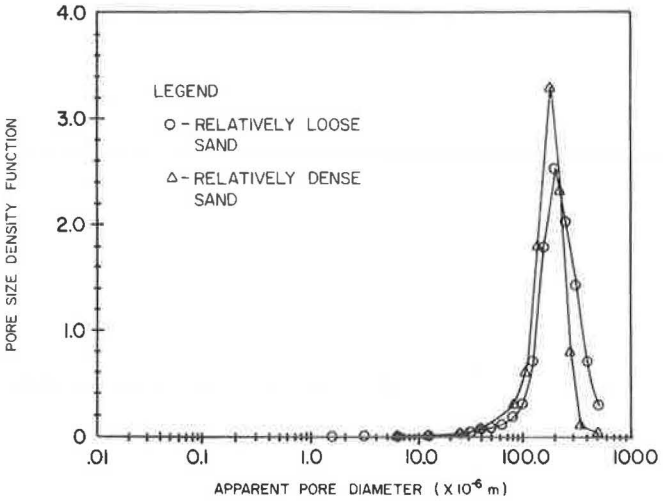

FIGURE 4 Pore-size density functions of sands tested.

was assumed in the calculation of the pore-size density function for the sands tested.

The pore-size density function curve provides some useful qualitative characteristics of the sand fabric. The curves in Figure 4 show a single mode characteristic around 200 m. As the state of compaction changes, so do the mode and its probability density (see Figure 4). This indicates that the pore-size density function may be used to characterize the soil fabric. In addition, the pore-size density function has been successfully used in, and is the core of the development of, a theoretical permeability model (*19*), which indicates that the pore-size density function is a useful quantitative measure of the sand fabric.

CONCLUSIONS

1. A technique has been verified to be satisfactory for the preparation of sand specimens for the MIP tests, which enables the measurement of the pore-size distribution and pore-size density function in sand.

2. A clarification of "pore-size distribution" has been given to provide a better link between the terminology used in the literature of mercury porosimetry and that used in the conventional probabilistic approaches in geotechnical engineering.

3. The pore-size density functions of the sands studied were found to be singly modal on a log-diameter scale. The mode occurred around 200 m, but the mode and its probability density changed as the compactive effort varied.

4. The results of this study have provided a basis for further research to investigate the sand fabric through variation in the pore-size density function. It is believed that such study could lead to better understanding or prediction of some engineering properties (compressibility, liquefaction potential, etc.) of sands.

ACKNOWLEDGMENT

The study on which this paper is based was supported by the Federal Highway Administration and the Indiana State Highway Commission through the Joint Highway Research Project at Purdue University. Also, the authors wish to thank R. D. Holtz, D. N. Winslow, and J. Lovell for their assistance in various aspects of this study.

REFERENCES

1. R. Brewer. *Fabric and Mineral Analysis of Soils*. John Wiley and Sons, Inc., New York, 1964, 482 pp.
2. S. Diamond. Pore Size Distributions in Clays. *Clays and Clay Minerals*, Vol. 18, 1970, pp. 7–23.
3. S. Diamond. Microstructure and Pore Structure of Impact Compacted Clays. *Clays and Clay Minerals*, Vol. 19, 1971, pp. 239–249.
4. I. Garcia-Bengochea, C. W. Lovell, and A. G. Altschaeffl. Relation Between Pore Size Distribution and Permeability of Silty Clay. *Journal of the Geotechnical Engineering Division, ASCE*, Vol. 105, No. GT7, 1979, pp. 839–856.
5. P. N. Gaskin and G. P. Raymond. "Pore Size Distribution as a Frost Susceptibility Criterion." *Proc., Symposium on Frost Action on Roads*, Vol. 1, Norwegian Road Research Laboratory, Oslo, 1973.
6. C. H. Juang. *Pore Size Distribution of Sandy Soils and Prediction of Permeability*. FHWA/IN/JHRP Report 81-15. Purdue University, West Lafayette, Ind., 1982.
7. T. C. Kenney. Discussion: Frost-Heaving Rate Predicted from Pore-Size Distributions. *Canadian Geotechnical Journal*, Vol. 17, No. 2, 1980, pp. 332–333.
8. G. O. Klock, L. Boersma, and L. W. DeBacker. Pore Size Distributions as Measured by the Mercury Intrusion Method and Their Use in Predicting Permeability. *Proc., American Society of Soil Science*, Vol. 33, No. 1, 1969, pp. 12–15.
9. T. J. Marshall. A Relation Between Permeability and Size Distribution of Pores. *Journal of Soil Science*, Vol. 9, 1958, No. 1, pp. 1–8.
10. R. J. Millington and J. P. Quirk. Permeability of Porous Media. *Nature*, Vol. 183, Feb. 1959, pp. 387–388.
11. A. Murota and K. Sato. Statistical Determination of Permeability by the Pore Size Distribution in Porous Media. *Proc., 13th Congress of the International Association for Hydraulic Research, Japan*, Vol. 4, Sept. 1969, pp. 183–190.
12. M. A. Reed, C. W. Lovell, A. G. Altschaeffl, and L. E. Wood. Frost-Heaving Rate Predicted from Pore Size Distribution. *Canadian Geotechnical Journal*, Vol. 16, No. 3, Aug. 1979, pp. 463–472.
13. A. Mahmood. Fabric-Mechanical Property Relationships in Fine Granular Materials. *Clays and Clay Minerals*, Vol. 22, No. 516, 1973, pp. 397–408.
14. J. K. Mitchell, J. M. Chatoian, and G. C. Carpenter. *The Influences of Sand Fabric on Liquefaction Behavior*. Report TE76-1. Department of Civil Engineering, University of California, Berkeley, June 1976.
15. M. Oda. Initial Fabrics and Their Relations to Mechanical Properties of Granular Materials. *Soils and Foundations*, Vol. 12, No. 1, 1972, pp. 1–18.
16. M. Oda. *Fabrics and Their Effects on the Deformation Behavior of Sand*. Department of Foundation Engineering, Saitama University, Japan, 1976.
17. E. W. Washburn. Note on a Method of Determining the Distribution of Pore Sizes in a Porous Material, *Proc., National Academy of Sciences*, Vol. 7, 1921, pp. 115–116.
18. C. H. Juang and R. D. Holtz. A Note on Preparation of Specimens of Noncohesive Material for Mercury Intrusion Porosimetry. *Geotechnical Testing Journal, ASTM*, Sept. 1986.
19. C. H. Juang and R. D. Holtz. A Probabilistic Permeability Model and the Pore Size Density Function. *International Journal for Numerical and Analytical Methods in Geomechanics*, Vol. 10, 1986.
20. C. Kemball. On the Surface Tension of Mercury. *Transactions of the Faraday Society*, Vol. 42, 1946, pp. 526–537.

21. D. N. Winslow. *The Pore Size Distribution of Portland Cement Paste.* M.S.C.E. thesis. Purdue University, West Lafayette, Inc., Jan. 1969.
22. R. A. Lohnes, E. R. Tuncer, and T. Demirel. "Pore Structures of Selected Hawaiian Soils." In *Transportation Research Record 512*, TRB, NRC, Washington, D.C., 1976, pp. 76–69.
23. S. Diamond and W. L. Dolch. Generalized Log-Normal Distribution of Pore Sizes in Hydrated Cement Paste. *Journal of Colloid and Interface Science*, Vol. 34, No. 1, Jan. 1972, pp. 234–244.
24. H. I. Meyer. Pore Distribution in Porous Media. *Journal of Applied Physics*, Vol. 24, 1953, pp. 510–512.

Publication of this paper sponsored by Committee on Physicochemical Phenomena in Soils.

Drained-Strength Parameters from Direct Shear Tests for Slope Stability Analyses in Overconsolidated Fissured Residual Soils

ROY H. BORDEN AND STEVEN F. PUTRICH

An experimental investigation of the drained shear strength of soils from three sites within the Durham Triassic Basin of North Carolina is described. Multistage direct shear tests conducted on specimens trimmed from block samples were utilized to evaluate the postpeak shear strength of these materials. In general, the observed reduction in strength with accumulated displacement beyond the peak strength was in good agreement with data reported in the literature for other overconsolidated soils. The residual friction angle for the soils tested was found to follow the trend of decreasing friction angle with increasing plasticity index. These results support the need for utilizing drained shear strength parameters and effective stress analyses for predicting the stability of slopes cut in overconsolidated residual soils. In a companion paper in this Record a case study is presented of a well-documented slope failure within the Durham Triassic Basin that indicates the appropriateness of using noncircular failure geometrics and suggests the applicability of utilizing postpeak strengths obtained from drained direct shear tests.

This paper is the first of two companion papers dealing with slope stability analyses in overconsolidated fissured residual soils. An experimental investigation of the drained shear strength of soils from three sites within the Durham Triassic Basin of North Carolina is described. The companion paper by Putrich et al. in this Record presents an evaluation and analysis of a documented slope failure utilizing some of the data presented here. The impetus for this study was the realization that failures were still occurring in slopes for which stability analyses based on undrained strengths had predicted stability. For example, utilizing the unconfined compressive strength in conjunction with a realistic noncircular failure surface on the basis of a field investigation after the slide, a failed slope was shown to have a factor of safety of approximately 2.5. A circular arc analysis utilizing the unconfined strength shows the slope to be even slightly safer.

It is well known that the long-term stability of overconsolidated clay slopes is governed by effective-strength parameters (i.e., drained conditions). The explanation for this behavior was originally presented by Vaughan and Walbanke (*1*) and later by Skempton (*2*), who concluded that failure of cut slopes in overconsolidated fissured clays occurred years after the excavation because of the slow dissipation of excess negative pore pressures. This study shows that the overconsolidated fissured residual soils investigated in this experimental program may be viewed in a similar manner.

R. H. Borden, Department of Civil Engineering, North Carolina State University, Raleigh, N. C. 27695-7908. S. F. Putrich, Department of Civil Engineering, North Carolina State University, Raleigh, N. C. 27695-7908. Current affiliation: Woodward-Clyde Consultants, Wayne, N. J.

GEOGRAPHIC AND GEOLOGIC BACKGROUND

Three sites have been investigated in this study; two are sites of future cut slopes that will result from construction of the East-West Freeway through Durham, North Carolina, referred to as the Anderson Street and LaSalle Street sites, and the third is the site of a previously documented slope failure in nearby Apex, North Carolina, the Railroad Underpass/US-64 site. Geographically these three sites are all located in the Durham Triassic Basin, which is the northernmost portion of the Deep River Basin. The Deep River Basin is a troughlike topographic lowland trending northeast to southwest that extends 100 mi in length and varies from 5 to 20 mi in width. Figure 1 shows the Deep River Basin deposit in relation to the Atlantic Seaboard Triassic deposits and the general locations of the three sites investigated in this study.

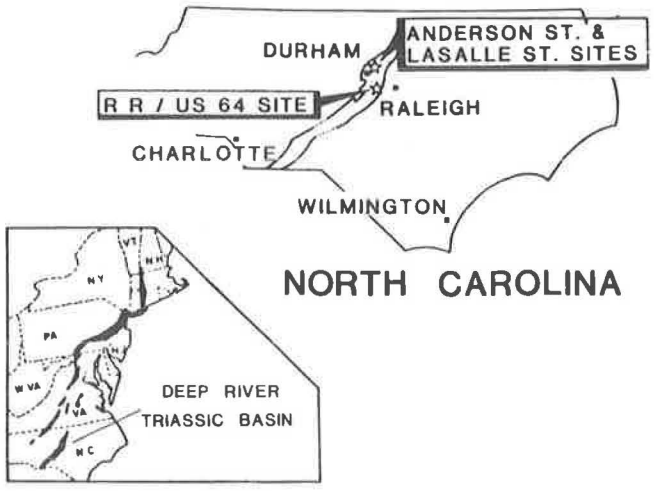

FIGURE 1 Location of Deep River Triassic Basin and test sites.

Geologically the Deep River Basin contains Triassic sedimentary rocks that are clastic deposits consisting of claystone, shale, siltstone, and sandstone. These deposits are characterized by abrupt changes in composition. The sediments of the Deep River Basin are composed largely of debris eroded from nearby pre-Triassic metamorphic and igneous rocks. In places they contain large amounts of debris derived from nearby granite intrusives. These sediments were deposited as alluvial fans, stream-channel and floodplain deposits, and lake and swamp deposits. Because of the nature of the depositional environment, a large percentage of the clays and clayey silts are fissured. Because the soils were deposited under wet conditions, subsequent drying and shrinkage caused cracks and openings classified as fissures. Soil samples from two of the three sites investigated in this study contained fissures with undulating surfaces.

Triassic sedimentary deposits are characterized by inclinations to the southeast at angles ranging from 5 to 45 degrees. This characteristic dipping of the deposits is believed to have a major impact on the stability of cut slopes in the Triassic deposits. The geometry of the failed soil mass appears to be dependent on the orientation of the soil layering. As a point of illustration, the documented slide at the Railroad Underpass/US-64 site is discussed in detail in the companion paper of this experimental study (Putrich et al. in this Record). The soil profile within the slope had layering that was inclined into the cut; therefore, the soil mass had an inherent tendency to slide into the cut. Conversely, the bedding planes on the opposite side of the railway cut dip away from the cut and the slope has remained stable (has not experienced sliding) since the end of construction more than 10 years ago. This illustrates the importance of the orientation of the layering of the subsurface profile with respect to the cut and its direct influence on the probability of slope failure, in addition to the determination of the appropriate shear strength used in the design of these slopes. As was reported by Leith and Fisher (*3*), the slope failure frequency in the Triassic Basin was anomalously high based on a statewide survey of highway cuts at that time. It can be inferred that the characteristic southeasterly dip of the Triassic sedimentary soil profile was a major factor in inducing a large number of those failures. Henkel (*4*) supports this position by stating that local geologic environment greatly influenced the stability of natural slopes, and therefore stability analyses using circular failure geometries and classical design methods developed for uniform soils are unconservative. It is critical that strength parameters determined are applicable to sliding along these bedding planes and are appropriate in the evaluation of long-term stability.

EXPERIMENTAL PROGRAM

The following is a description and rationalization of the laboratory testing program used in this study for the determination of the shear strengths of soils from three locations in the Durham Triassic Basin. Two of the three locations are sites of future bridge structures for the East-West Freeway project. The third is the site of a previous slope failure that was investigated and documented by the North Carolina Department of Transportation (NCDOT) in 1978.

Testing Equipment

The device used to evaluate shear strength in this study was a standard motor-driven direct shear device made by Soiltest Company. The device accommodates 2.5-in.-diameter samples and has a maximum displacement of 0.25 in. per run. The device was modified to enable reversing of the upper one-half of the shear box to its original position after each run. Therefore, a test can be conducted with the desired amount of accumulated one-directional displacement for each value of effective normal stress (or normal stress increment).

The reversible direct shear test was chosen as suitable for determining the shear strength of soils in this study for the following reasons:

1. The test allows for the accumulation of adequate horizontal displacement to attain postpeak shear strength considered applicable to slope stability analysis.
2. The test can be conducted as a drained shear test, where the displacement rate is adjusted to allow for drainage during the shearing of the sample. Drained-strength parameters are known to be important in the long-term stability of cut slopes.
3. Samples can be positioned and aligned in the shear box so that the plane on which shearing takes place can be selected before testing. This enables shear strength determination of seams, fissures, slickensides, and in general any plane of weakness considered susceptible to failure in the field.
4. There is a body of direct shear data accumulated from studies on a variety of soils with which the results of this study can be compared. Two such studies are those by Kenney (*5*) and by Lupini et al. (*6*).
5. The direct shear test can be conducted by using only one sample to develop a range of strength envelopes. This minimizes the number of samples necessary in the determination of shear strength.

No laboratory test is without its weaknesses. Some of the difficulties and intrinsic weaknesses in this method of direct shear testing are as follows:

1. The test is time consuming if it is to be conducted completely drained (3 to 6 working days of test time);
2. Particular attention must be given to ensure that the shearing surface is approximately planar and that the proposed plane of shearing corresponds to the actual plane of shearing (i.e., the shearing surface must be aligned with the plane of separation of the shear box); this is most important in determining the strength seams or fissures within a soil sample; and
3. Bromhead and Curtis (*7*) note in their study of residual strength determination that because of the reversing of the shear to return the box back to its original position, there is no allowance for complete particle orientation in the shear surfaces, and the reversible direct shear test therefore yields a slightly higher "residual strength" than other tests such as that for torsional shear.

Laboratory Technique

In order to develop and validate a standard laboratory technique for this series of direct shear tests, it was necessary to

identify the key variables and discuss the tests conducted to evaluate their significance.

Rate of Displacement

Since the direct shear tests must be conducted as drained tests (slow tests), it was important to select an initial displacement rate that would allow for drained behavior during shear. Using the relationship between liquid limit (W_L) and the coefficient of consolidation (c_v), as shown in Figure 2 (*8*), it was possible to determine the required time to failure in order to ensure drained behavior. Because the soils are overconsolidated, the top curve was used as a conservative estimate for c_v. Knowing c_v, one can back-calculate the time required for consolidation corresponding to a specific average percentage of consolidation [$t = (H_{dr})^2 T/c_v$] and the time to failure. ASTM D 3080 recommends a time to failure for drained shear tests as $50 \times t_{50}$, and Bishop and Henkel (*9*) recommended $10 \times t_{100}$. Both methods gave approximately the same required time to failure and subsequent suggested displacement rates of 2.2×10^{-3} in./min. The conservative nature of the relationship between W_L and c_v was confirmed by consolidation data from the Anderson Street site (on the soil having a W_L of 55) shown in Figure 3. Even the lowest c_v-value of 0.3×10^{-2} cm2/sec is only slightly lower than the projected value based on Figure 2. As a second check on the rate of displacement, one long-term test was conducted at one-third the standard displacement rate. The slower rate did not vary the shear strength developed in the faster test, and therefore confirms that the faster rate of displacement allowed drained behavior during shear. On the basis of these data, a standard displacement rate of 2.2×10^{-3} in./min was adopted for all testing.

Amount of Horizontal Displacement

In standardizing the amount of horizontal displacement for the direct shear testing in this study, two factors were considered:

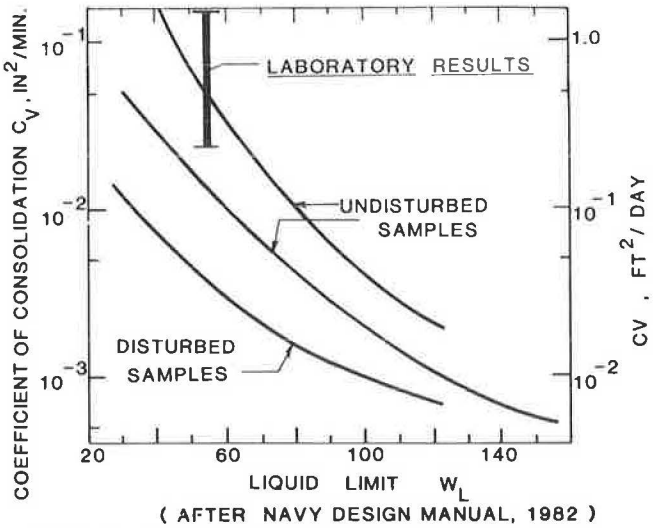

FIGURE 2 Relationship between coefficient of consolidation (c_v) and liquid limit (W_L) (*8*).

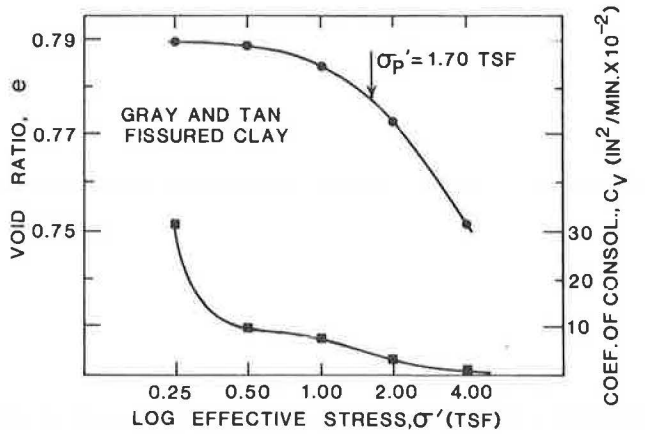

FIGURE 3 Consolidation results from Anderson Street sample.

first, the maximum one-directional displacement that the direct shear machine will allow per run (0.25 in./run) and, second, the need for adequate horizontal displacement to reach the postpeak shear strengths under consideration in this study (softened to residual strength range).

The initial estimate of required horizontal displacement was based on data from other studies involving direct and rotational shear tests (*6*, *10–14*). This body of information suggests that 0.5 in. per normal stress increment is an ample quantity to reach postpeak strengths. To evaluate this contention, one complete residual envelope was developed using a total of 1.0 in. displacement for each value of effective normal stress. This test showed a relatively small reduction in the residual strength resulting from the increase of accumulated horizontal displacement from 0.5 to 1.0 in. Therefore, 0.5 in. of horizontal displacement per normal stress increment, requiring two runs at 0.25 in./run, was adopted as standard procedure.

Test Drainage Conditions and Sample Soaking Prior to Testing

Drained shear testing means that no excess pore pressures are generated during shear as a result of free drainage. All tests were conducted "wet"; that is, the specimens being sheared were submerged throughout the duration of the test. This allowed for pore fluid to communicate freely through the upper and lower porous stones with water in the shear box reservoir surrounding the sample.

In order to evaluate the effect of sample soaking before direct shear tests were conducted, samples from both Anderson Street and LaSalle Street were soaked for 1 month and 2 weeks, respectively, under a stress approximately equal to the in situ effective stress. This extended soaking had minimal effects on the shear strength. The probable explanation for this behavior is the high degree of saturation of the samples before the long-term soaking. Without the use of back pressure, the degree of saturation would not be expected to increase substantially. For practical purposes, the standard procedure (i.e., soaking the sample overnight before testing) produced the same results as extensive soaking. This should not be considered standard behavior at other sites where soils may be desiccated due to

exposure or lowering of the groundwater and are subsequently at a low degree of saturation at the time of sampling.

Number of Specimens

Another consideration in the direct shear test procedure is the number of soil specimens needed to develop the residual shear strength envelope. The two options available are to use one specimen per normal stress increment or the same specimen for all the normal stress increments necessary to complete a strength envelope. On the basis of recommendations by Townsend and Gilbert (*15*), a single specimen is tested under various normal stresses; this is referred to as the multistage approach. This issue was investigated by conducting two test series on specimens from the same block sample. The results indicated that the use of three specimens in the second test series generated shear strength parameters considerably higher than those obtained by using one specimen under various normal stresses and significantly higher strength than that predicted based on data accumulated from other studies on similar soil. This behavior suggests less particle alignment on the failure surface as a result of the smaller accumulated displacement during the three single-shear tests as compared with the multistage tests. It was concluded that the one-specimen multistage approach to testing was an appropriate procedure, and it was adopted as standard for the remainder of the laboratory testing program.

Field Sampling

In order to secure samples for use in the laboratory direct shear tests, exploratory trenches were excavated by NCDOT personnel at both the Anderson Street and LaSalle Street sites in June 1983. Block samples were taken from specific locations within the trenches that had previously been identified as potential shear planes significant in the stability of the proposed cut slopes. Bedding planes, seams, and fissures were measured for dip and direction and recorded by NCDOT geologists. All the block samples were wrapped in plastic and tape, numbered, and returned to North Carolina State University for moisture-controlled storage.

One month before the trench sampling at the LaSalle Street and Anderson Street sites, samples were taken from the Railroad Underpass/US-64 location, also to be used in the direct shear testing. Two samples were secured by pushing 4-in.-diameter metal tubes into the soil on the face of the previously failed slope close to the existing bridge structure (i.e., the US-64 overpass). The tubes were sealed and returned to North Carolina State University for storage.

In order to catalogue the soil samples in storage, a system of numbering was developed that identified the samples according to the following criteria:

1. Type of sample—block sample (SBS) or Shelby tube sample (STS);
2. Number of sample and site name; designated sample number and letter *a*, *b*, or *r* assigned to the LaSalle Street, Anderson Street, and Railroad Underpass/US-64 samples, respectively; and
3. Location of the site where the sample was taken, for example, EB1-A (End Bent 1-A of the proposed bridge structure at the site).

These three parts are combined to give a catalogue number for each sample (example: SBS-3a, EB1-A).

Laboratory Sample Preparation Technique

Because of the difference in the nature of soils found at the three sites under investigation, different sampling and specimen preparation methods were adopted that best suited each of the materials. In all the laboratory sampling and preparation techniques employed, the objective was to obtain specimens that most accurately represented the in situ conditions of the site under question and could be aligned and positioned most easily in the direct shear device so that the plane of shearing (i.e., plane of separation of the shear box) corresponded to the plane of weakness thought most susceptible to failure in the field (i.e., fissures or seams).

For the LaSalle Street soils, the stiff siltstone with relatively soft thin clay seams was prepared for testing according to the following procedure. Block samples with the most distinct seams and adequate sample dimensions were cut into blocks 2.6 in. wide by 2.0 in. high with a hand saw. The clay seams in the brown siltstone were kept as horizontal as possible throughout the sample cutting and trimming so that the samples, once placed in the direct shear box, would fail along these seams as much as possible. These samples were trimmed further to a 2.5-in. diameter by using a motorized sampling device made by Soiltest Company and a razor blade mounted on a plexiglass strip as a trimming tool (Figure 4, *left*).

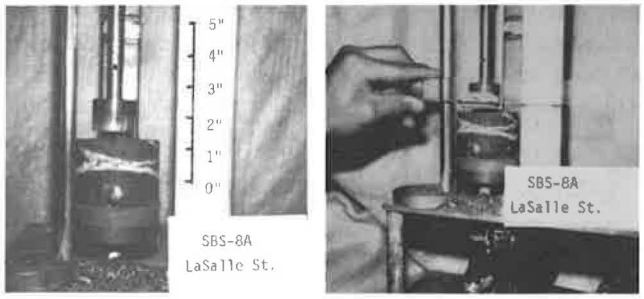

FIGURE 4 Laboratory sample preparation, LaSalle Street sample.

For the Anderson Street soils, the fissured clay was prepared for testing by using the following procedure. Block samples with the most distinct fissures and adequate sample dimensions were sawed into blocks by using a sample cutting box that was designed to accommodate a variety of sample sizes. Block samples were confined by plastic wrap and tape binding before placement in the sample cutting box. The samples were oriented in the box so that the planes of fissure were horizontal and the samples would be sheared across the apparent planes of weakness. Because the planes of fissure were undulating and discontinuous, it was often difficult or impossible to determine

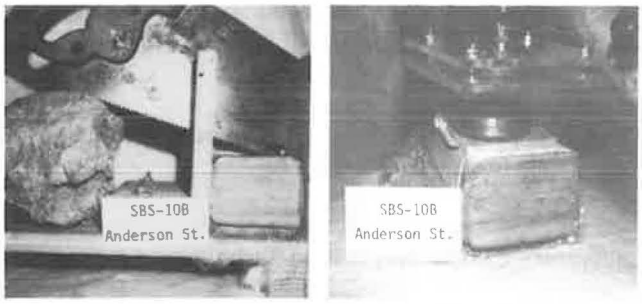

FIGURE 5 Laboratory sample preparation, Anderson Street sample.

the exact location and orientation of the fissures within the sample. Figure 5 (*left*) shows the sample cutting box; a portion of the original field sample SBS-10b and a sawed block of the same material are shown in the left and right sides of the photograph, respectively. Once the soil had been sawed into right-angle blocks, a consolidation ring with a 2.5-in. inside diameter was pressed into each block by using a modified drill press configuration. To maintain the integrity of the soil blocks and minimize soil moisture loss during the filling of the consolidation rings, the sample was bound with plastic and heavy-duty tape. After being filled with soil, the ring was recovered from the soil block and trimmed to the required 0.75-in.-high specimen. Figure 5 (*right*) shows the ring-pressure device and consolidation ring before they are pressed into the soil block.

The Railroad Underpass/US-64 soil was very similar to the Anderson Street material. The field samples were contained in small 4-in.-diameter metal tubes, which acted as lateral confinement and therefore facilitated the pressure of the consolidation rings directly into the tubes to recover a sample. No preparation was needed to trim the field sample and therefore the entire procedure of obtaining the direct shear specimen was completed in one step. Once the soil-filled consolidation ring was removed from the tube, it was trimmed to the same height as the other sample. In general, for the laboratory, field block samples are the best with which to work. Several Shelby tube samples were taken at the Anderson Street site but were not employed as a source of specimens in the direct shear testing. Field block samples are considered to be more useful than Shelby tube samples for the following reasons:

1. More soil sample is available, and therefore there is a greater degree of freedom in selecting the part of the soil mass from which the testing specimen can be taken; and
2. There is less disturbance to the soil sample (i.e., the sample must be extruded from the Shelby tube to examine it, whereas the block sample can simply be unwrapped, examined, and rewrapped with little or no disturbance).

EXPERIMENTAL RESULTS

A series of eight direct shear tests was conducted on samples from the Railroad Underpass/US-64 and the Anderson Street and LaSalle Street locations. The goal of the test program was to describe the postpeak strength parameters of materials within zones of the soil stratigraphy that had previously been identified as potential shear zones significant in slope stability analyses of cut slopes at these sites. In addition, tests of Atterberg limits and x-ray diffraction analyses were conducted to evaluate the plasticity characteristics and mineral composition, respectively, of the soils from the three sites.

Soil Description and Classification

The results of the Atterberg limits tests, natural water content determinations, liquidity index values, and the percent passing the No. 200 sieve for the soils at the three sites are compiled in Table 1. The Atterberg limits of these soils were determined by two methods:

1. The standard liquid limit and plastic limit test methods according to ASTM D423-66 and D424-59 and

TABLE 1 SOIL CLASSIFICATION DATA

Sample No.	Location	Water Content, w_n (%)	Liquid Limit, W_L (%)		Plastic Limit, W_{PL} (%)		Plasticity Index, PI (%)		Liquidity Index, LI (%)		Percent Passing No. 200 Sieve	USCS Symbol
			CP	SAT	CP	SAT	CP	SAT	CP	SAT		
1r	Railroad Underpass/US-64	31.0	49.5	50.0	20.2	19.5	29.3	30.5	0.37	0.38	82.0	CH
2r	Railroad Underpass/US-64	30.6	—	55.0	—	22.0	—	33.0	0.26	—	78.0	CH
13b	Anderson Street	33.6	63.0	57.5	20.7	27.7	42.3	30.0	0.30	0.20	91.6	CH
10b	Anderson Street	26.0	55.0	52.2	20.0	22.2	35.0	30.0	0.17	0.13	88.0	CH
10b	Anderson Street	32.0	56.4	52.8	21.4	22.0	35.0	30.8	0.30	0.32	88.0	CH
14b	Anderson Street	32.3	57.5	57.0	—	24.0	—	33.0	—	0.25	85.1	CH
2a	LaSalle Street (parent material)	16.8	34.0	—	16.4	—	17.6	—	0.02	—	76.5	CL
1a	LaSalle Street (parent material)	17.4	37.0	32.0	20.6	21.0	16.4	11.0	–0.20	–0.33	76.0	CL
2a	LaSalle Street (thin discontinuous seam material)	20.9	40.9	39.0	13.7	19.6	27.2	19.4	0.26	0.07	82.0	CL
4a	LaSalle Street (thick seam material)	32.1	56.5	55.1	20.0	22.1	36.5	33.0	0.33	0.30	88.0	CH

Note: CP = cone penetrometer determination; SAT = standard Atterberg test determination; USCS = Unified Soil Classification System.

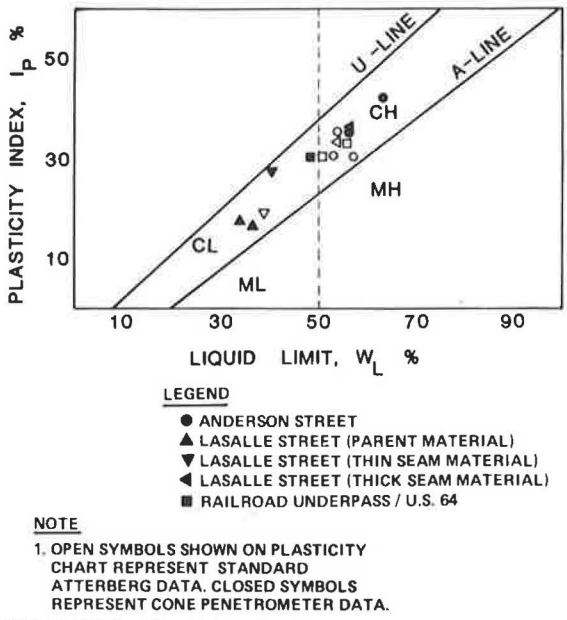

FIGURE 6 Plasticity chart.

2. The cone penetrometer liquid limit determination (British Standard No. 1377) and the plastic limit determination using two cones of different mass from a study by Wood and Wroth (*16*). Figure 6 shows the Casagrande plasticity chart with the results from all Atterberg limits test. The open symbols represent standard ASTM results and the solid symbols represent cone penetrometer results.

Railroad Underpass/US-64

The soil used in the direct shear tests was a gray and tan fissured clay with some fine sand. The term "fissured" is used here in the same way that Terzaghi used it to define a stiff, fissured clay (*17*, pp.161–165):

> When it is dropped, a big chunk of the clay breaks into polyhedric, angular and subangular fragments with dull or shiny surfaces. The diameter of the fragments may range between less than one centimeter and more than twenty centimeters.

Anderson Street

The soil used in the direct shear tests was highly plastic light gray and tan streaked fissured clay with traces of fine sand and plant roots in the fissures. The soil is classified a CH material according to the Unified Soil Classification System (USCS). This fissured clay broke into small chunks and blocks if not handled carefully. The fracture surfaces examined after breakage were distinct and appeared shiny and undulating.

LaSalle Street

From the LaSalle Street site, two types of soil were tested in direct shear. The first type of soil was a brown micaceous clayey siltstone of slight to medium plasticity (referred to in this paper as the parent material and classified as a CL material according to the USCS). The second type of soil was a medium to highly plastic light gray fissured clay that was interbedded in the siltstone in a range of thicknesses from ⅛ to 1 in. The "thin" seams (i.e., up to ⅛ in.) are classified CH according to the USCS. All seam material contained some plant roots. The water content and plasticity characteristics and the occurrence of fissures in these seams were found to be a function of the seam thickness. Field investigations by NCDOT indicated that the clay may be as thick as 1 ft.

Mineralogy Analysis

X-ray diffraction analyses were used in order to determine the type and relative quantity of clay minerals present in representative samples of soils from each of the sites. These results are given as supplemental information to enhance the data base of soil characteristics. The testing utilized modified procedures for dispersion of soil minerals and conventional x-ray diffraction analysis based on procedures by Jackson (*18*). The tests were conducted under the supervision of Sterling Weed of North Carolina State University.

The following is a summary of the clay mineral content of the soils from the three sites under study:

LaSalle Street
Parent material, brown micaceous clayey siltstone; mica (weathered) ≈ vermiculite >> montmorillonite > halloysite.
Thin gray discontinuous clay seam material; montmorillonite > halloysite > mica (weathered).
Thick gray fissured clay seam material; montmorillonite >> halloysite ≈ mica (weathered).
Anderson Street
Gray with tan fissured clay; montmorillonite >> halloysite ≈ mica (weathered).
Railroad Underpass/US-64
Gray and tan fissured clay; montmorillonite >> halloysite > mica (weathered).

DIRECT SHEAR TESTS RESULTS

The direct shear test program involved eight series of tests that resulted in the development of eight complete sets of strength envelopes (i.e., softened, residual, and lower bound residual). Of these eight series, one was conducted on soil from the Railroad Underpass/US-64 site, three on soil samples from the Anderson Street site, and four on the two soil types from the LaSalle Street site.

Shear Stress Versus Displacement Behavior

The results of the eight series of direct shear tests conducted in this study are presented in plots of shear stress versus displacement (Figure 7) and summarized in Table 2. Each of the eight series is designated by a number from 1 through 8. A list of comments that reference the eight test series and identify the procedures implemented and variables investigated follows:

Test 1: standard procedure; one sample, three normal stress levels, and two runs per increment (i.e., total one-directional displacement = 0.50 in. per increment); chosen standard rate of displacement = 2.2×10^{-3} in./min.

Test 2: three samples, standard procedure (see Test 1); three samples were used to validate the standard technique utilizing one sample to develop a complete envelope.

Test 3: standard procedure with modification of one additional run conducted on the third increment to verify the effect of reducing the rate of displacement to one-third of the standard rate (8.0×10^{-4} in./min).

Test 4: standard procedure with modification of allowing the sample to soak for 1 month before testing positioned and aligned under a stress of 0.25 tsf (i.e., approximately the existing in situ overburden).

Test 5: standard procedure with sample aligned and posi-

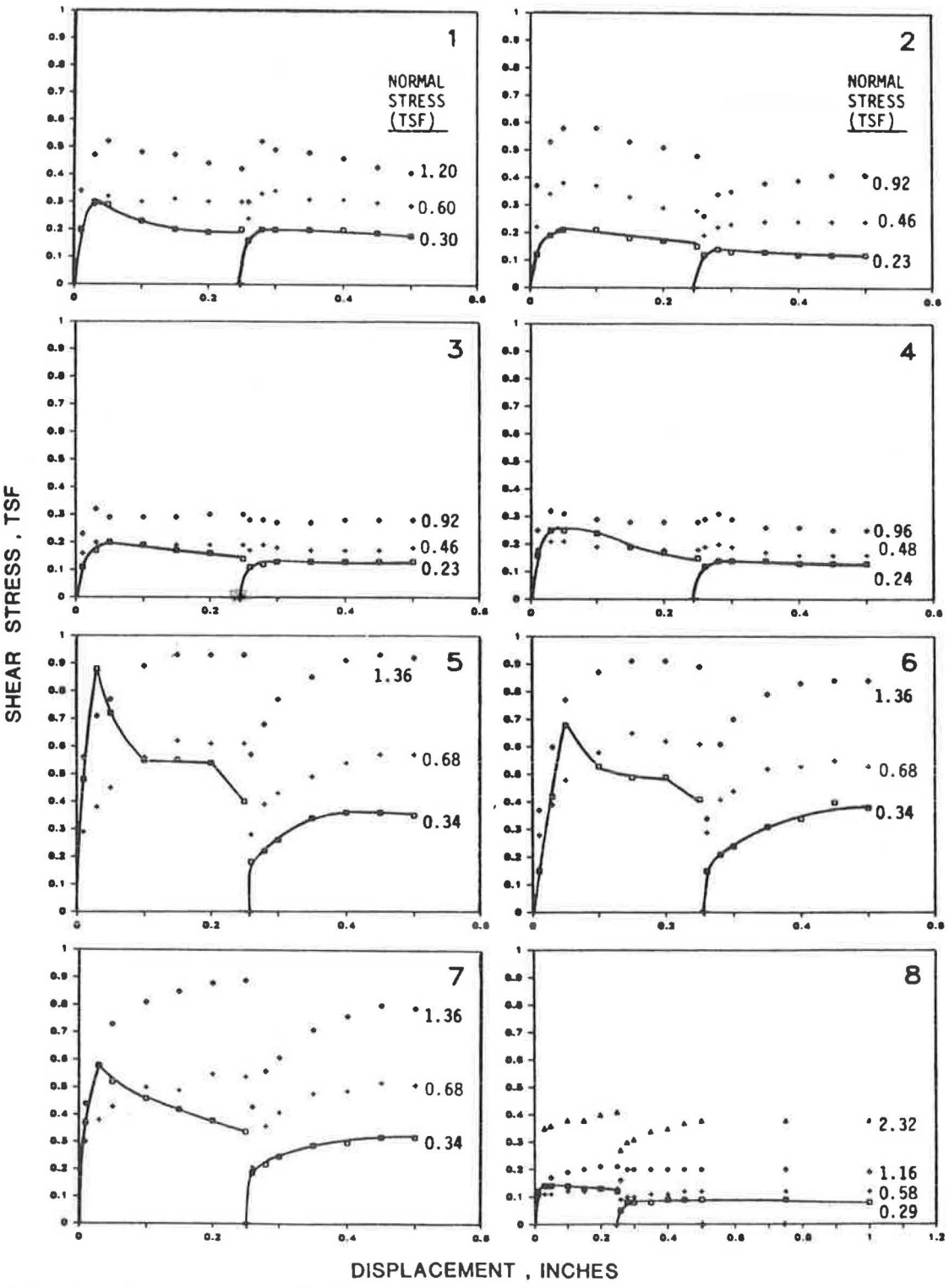

FIGURE 7 Shear stress versus displacement data: Series 1–8.

TABLE 2 SUMMARY OF DIRECT SHEAR TEST RESULTS

Test No.	Sample No.	Sample Location and Description	Shear Strength: Softened ϕ'_s (degrees)	Softened C'_s (tsf)	Residual ϕ'_r (degrees)	Residual C'_r (tsf)	Lower-Bound Residual ϕ'_{rl} (degrees)	Lower-Bound Residual C'_{rl} (tsf)
1	lr	Railroad Underpass/US-64: gray and tan fissured clay with some fine sand	19.8	0.10	14.2	0.10	19.0	0.00
2[a]	SBS-14b(1), 10b(2), 10b(3), EB1-A	Anderson Street: gray and tan fissured clay with trace fine sand and roots	25.3	0.05	22.4	0.04	24.0	0.00
3	SBS-10b(4), EB1-A	Anderson Street: gray and tan fissured clay with trace fine sand and roots	12.1	0.10	12.0	0.07	16.9	0.00
4	SBS-10b(1), EB1-A	Anderson Street: gray and tan fissured clay with trace fine sand and roots	10.3	0.10	10.1	0.08	14.4	0.00
5	SBS-1a(1), EB1-A	LaSalle Street: brown micaceous siltstone with thin gray discontinuous clay seams and trace roots in the seams	28.4	0.22	28.1	0.19	33.8	0.00
6	SBS-1a(2), EB1-A	LaSalle Street: brown micaceous siltstone with thin gray discontinuous clay seams and trace roots in the seams	24.8	0.27	23.8	0.23	31.4	0.00
7	SBS-3a(1), EB1-A	LaSalle Street: brown micaceous siltstone with thin gray continuous clay seam and trace roots in the seams	28.1	0.17	25.3	0.16	30.5	0.00
8	SBS-4a(2), EB1-A	LaSalle Street: light gray clay, thick seam material with trace roots	8.4	0.06	8.4	0.03	9.0	0.00

[a]Peak strength: ϕ'_p = 28.2 degrees, C'_p = 0.10 tsf (peak strength as determined using one sample per normal stress increment).

tioned to force failure to occur through the majority of the thin discontinuous seams.

Test 6: standard procedure (sample alignment as in Test 5) with modification of allowing the sample to soak for 2 weeks before testing positioned and aligned under a stress of 0.25 tsf (i.e., approximately the existing in situ overburden).

Test 7: standard procedure with sample aligned and positioned to force failure to occur on the thin silty clay seam.

Test 8: one sample, four normal stress levels, and four runs per increment; the fourth increment was used to define the strength envelope at a relatively large normal stress; the total displacement of 1 in. per increment was incorporated to show the effect of doubling the standard amount of displacement.

For the fissured clays found at both the Anderson Street and Railroad Underpass/US-64 sites, a peak strength value is thought to be an unconservative estimate of the available in situ shear strength with regard to stability of cut slopes in these soils. This postpeak strength phenomenon can be explained by the progressive failure theory, which states that the peak strength is passed at any one point along a failure surface within a cut slope because of fissures or discontinuities that act as stress concentrators forcing that point to pass the peak strength with a given amount of displacement. Once the peak strength has passed at one point along the failure surface, the stress is shifted to another point, causing it to pass the peak, and so on. In this way a progressive failure can be initiated and the strength along the entire length (or majority) of a slip surface will decrease as a function of displacement to a lower strength range bounded by the softened and residual strengths.

Figure 8 shows the idealized response of a stiff, fissured clay during a drained direct shear test (*19*), which illustrates the reduction in shear strength as a function of displacement that would occur at one point and eventually progress to a portion

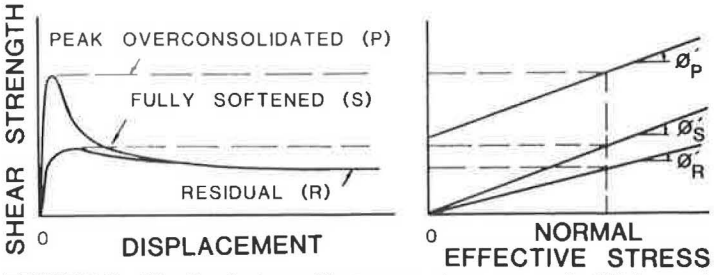

FIGURE 8 Idealized stress-displacement response of stiff fissured clay (*19*).

or the entire length of a slip surface. The curves of stress versus displacement in Figure 7 from this study are generally in agreement with the idealized response shown in Figure 8.

The softened strength and zero cohesion residual strength are generally recognized as the upper and lower boundaries for the range of in situ strength mobilized for slope failures in fissured clays. The softened strength is defined as the peak stress response for a "remolded" normally consolidated clay (i.e., critical-state condition) and is shown on the idealized stress-displacement curve of Figure 8. The residual strength value also indicated in Figure 8 is defined as that value of stress at which further accumulated displacement will not result in a lowering of strength (i.e., steady-state condition).

In this study, displacements of 0.5 in. per stress increment or an accumulated one-directional displacement of 1.5 in. for a single sample (multistage test) were used to mobilize a postpeak strength that appeared to be a relatively steady-state condition. The stress value at this condition is taken as the residual strength. Numerous studies have been conducted to date that examine techniques for determining the residual strength of clay and the amount of displacement required to achieve that minimum strength. Two of these studies, mentioned previously [LaGatta (*14*) and Lupini et al. (*6*)], specifically investigated residual strength for a variety of clay soils including Pepper shale, Cucaracha shale, and London clay. Results from these studies indicated that displacement of approximately 0.5 in. per normal stress increment would mobilize the postpeak strength, but that as much as 35 in. of displacement was needed to mobilize the true residual strength for some soils. An analysis of the data from these studies indicated that the additional accumulated displacement between 0.5 in. and that corresponding to the true residual value resulted in a reduction in shear strength ranging from approximately 6 percent to a maximum reduction of approximately 40 percent.

The objective of this experimental testing program on selected fissured clays of the Triassic Basin was not to determine the absolute lower bound shear strength of these soils, as was the case in the two studies mentioned earlier. The primary objective was to develop a reliable testing technique using the revisable direct shear device in order to establish a range of postpeak strengths thought to control instability of cut slopes in the type of soils tested, in particular, (*a*) first-time slides and the design of cut slopes in previously unfailed materials and (*b*) those somewhat lower strengths that govern the stability of a previously failed soil mass. The applicability of these results is evaluated in the case study analysis of a previously documented slope failure in the companion paper by Putrich et al. in this Record.

Shear Strength Envelopes

The shear strength envelopes (shear stress versus normal stress plots) for the eight series of direct shear tests are presented in Figure 9 and are designated 1 through 8, corresponding to the stress displacement curves in Figure 7. The softened and residual strength envelopes shown for Tests 1 and 3 through 8 in Figure 9 are determined from multistage single-sample tests. Test 2 utilized three samples, one for each load increment. This allowed for the determination of the peak strength envelope in addition to the softened and residual envelopes as shown. The range of normal stresses investigated was chosen to correspond to the in situ stress conditions anticipated on the failure planes in the cut slopes. A dashed line has been used to indicate that the shear strengths below the lowest stress increment are not known and that the dashed portion of these lines is a continuation of the slope of the strength envelopes for the stress range tested to the vertical intercept. An apparent effective cohesion (c') is given for the purpose of defining the linear equation of the envelope.

In utilizing three samples of the Anderson Street fissured clay in Test 2, comparatively higher shear strengths resulted than those in Test 3 where only one sample was used in the multistage approach. One may conclude that the accumulated displacement in the multistage single-sample test significantly reduces both the softened and residual shear strength values compared with shear strengths determined with the minimal displacement developed in the three-sample approach. In light of the fact that the displacement used in these eight series of tests was relatively small compared with the studies by LaGatta and Lupini et al., cited earlier, the lower-bound residual envelope has been introduced. A dashed line is used to indicate that this is a theoretical envelope, constructed by passing a straight line through the original, and the residual strength corresponds to the largest normal stress applied. This is a best estimate of the "practical" lower limit of shear strength of these materials. In theory, a lower shear strength could be achieved if the amount of accumulated displacement was increased by a factor of, say, 10 or more, but as will be shown by Putrich et al., this "practical" lower-bound residual strength, although greater than the "true" residual, significantly underestimates the lower-bound in situ shear strength for a landslide that occurred in these soils. Therefore, for the purpose of this study, the lower-bound residual as shown in Tests 1 through 8, Figure 9, is considered to be a reasonable first approach to describing a useful lower range of shear strength reflecting the behavior of these soils.

One of the focuses of the testing program was to evaluate the strength of somewhat continuous clay seams varying from ⅛ in. to 1 ft thick interbedded in a stiff siltstone found at the LaSalle Street site. Triassic sedimentary deposits are characterized by inclined bedding planes that dip from 5 to 45 degrees and a northeast-southwest trending strike. There had been several wedge-type failures in similar soil deposits within the Triassic Basin before this study for which stability analyses based on both undrained and drained peak strengths were predicted to be stable. These slopes were thought to fail along the sited seams of fissured clay. Therefore, there was an interest in evaluating the strength of the siltstone (referred to as parent material) and the highly plastic fissured clay seams individually. In comparing the results of Test 8 (2-in. clay seam: ϕ_r = 8.4 degrees) with those of Tests 5, 6, and 7 (parent material with the clay seams: range of ϕ_r = 23.8 to 28.1 degrees) a significant difference in shear strength is noted (as much as 300 percent greater residual friction angle for the intact parent material). It is apparent that significant differences in slope geometry would result from a design based on the results of Tests 5, 6, and 7 versus Test 8. This significantly lower shear strength would be considered in cut slope design if there was

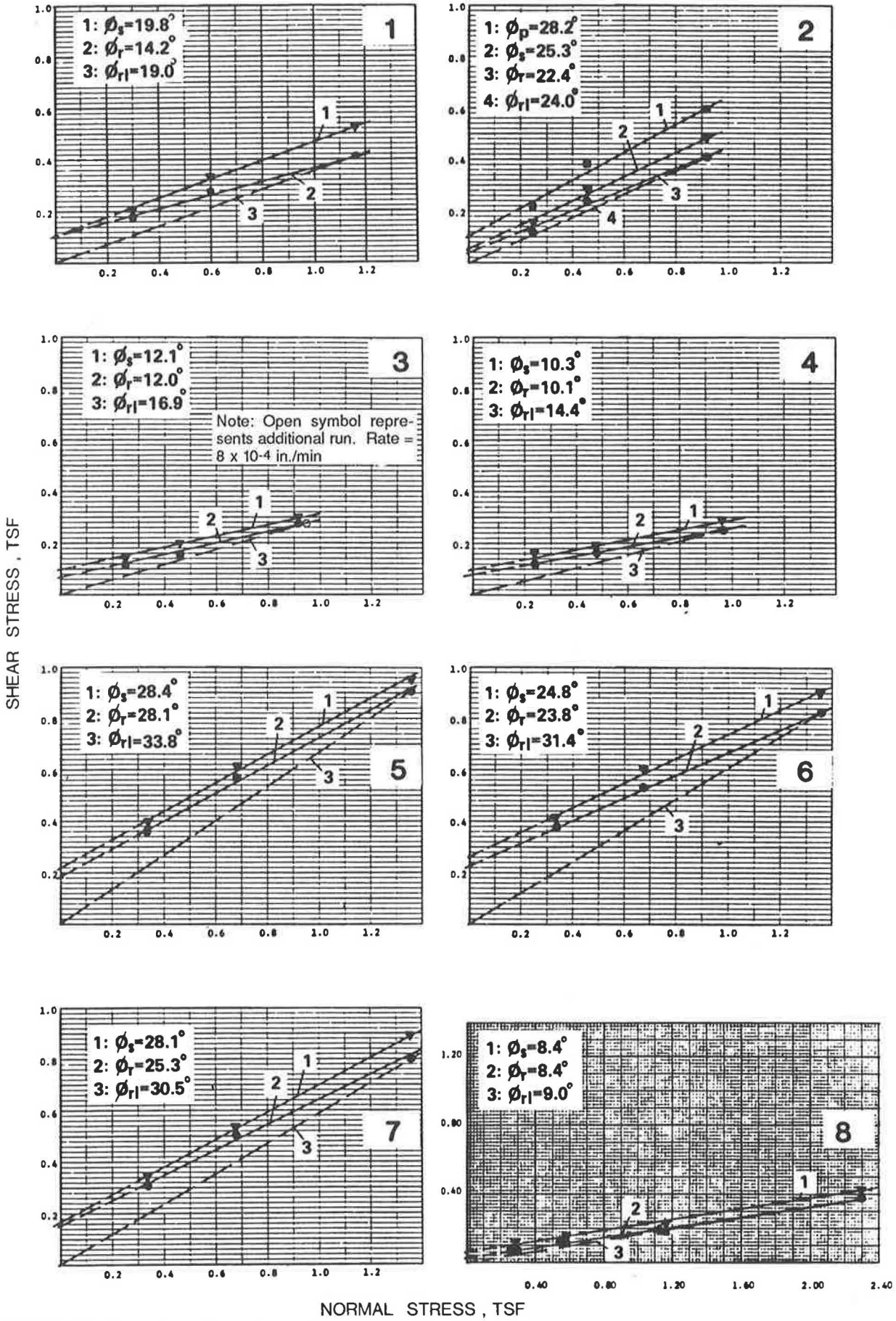

FIGURE 9 Shear strength envelopes: Series 1–8.

sufficient evidence (e.g., soil boring data, test pit excavation data, information from documented nearby slope failures) indicating that the weak seams and zones were extensive and that their orientation with respect to the planned excavation would lead to a slope failure. One can conclude that the type of sample taken from the field and the selectiveness with which the samples are tested can have a significant effect on the shear strength results. In the case of this study, special efforts were made to recover and test soil samples of the somewhat continuous interbedded clay seams and the more prevalent siltstone parent material from the LaSalle Street site.

Evaluation of Test Results

In order to evaluate the results of these direct shear tests, a summary of empirical relationships between the drained residual friction angle and the plasticity index based on the results compiled from a number of studies involving the measurement of the residual strength of soils [Lupini et al. (*6*)] is shown in Figure 10. One may conclude from these results, despite the wide range of curves, that the residual friction angle decreases with increasing plasticity index. The approximate upper and lower boundaries of the data are indicated by heavy dashed lines.

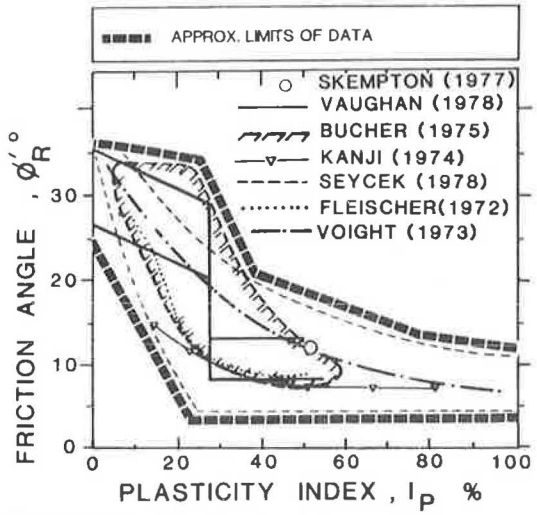

FIGURE 10 Relationship between friction angle and plasticity index (*6*).

The residual and lower-bound friction angles determined in this study are presented in Figure 11 with respect to the approximate upper and lower bounds taken from Figure 10 as a comparison. Despite the variation in the empirical relations presented in Figure 11, the test results follow the general trend of decreasing friction angle with increasing plasticity index, plot within the given limits of the range of expected results, and are in general agreement with this larger body of data.

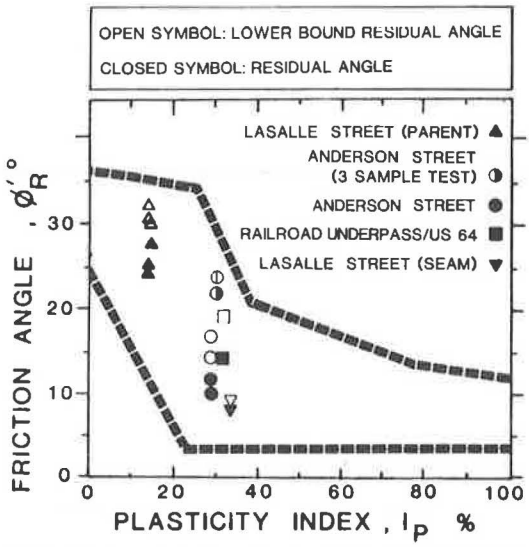

FIGURE 11 Relationship between friction angle and plasticity index including test results: Series 1–8 (*6*).

CONCLUSIONS

On the basis of the results of the direct shear tests performed in this study and the literature cited in this paper, the following conclusions are advanced:

1. The results of direct shear tests conducted on the fissured overconsolidated residual soils investigated showed a reduction in strength with accumulated displacement beyond the peak strength.
2. The amount of horizontal displacement used in the direct shear testing discussed was sufficient to mobilize postpeak shear strengths, but was probably not a sufficient amount to mobilize the "true" residual (i.e., absolute lower-bound) shear strength, on the basis of test results cited from rotational shear tests on similar soils. There is evidence to suggest, however, that the range of postpeak strengths examined in this study approximates in situ soil strengths mobilized in a documented slope failure in the same soils, and that the "true" residual strength values would greatly underestimate the in situ strength. (See paper by Putrich et al. in this Record for slide analysis of referenced slope failure.)
3. The data generated in this study were found to be in general agreement with the trend of decreasing residual friction angle with increasing plasticity index reported in the literature.
4. The type of soil samples taken from the field and the selectiveness with which the samples are tested can have a significant effect on laboratory results and the resulting slope design and stability of that cut slope. This is especially true for soil deposits with weak seams that follow the inclination of the soil bedding planes and are oriented so that planes dip into a proposed excavation. The importance of the selectiveness in sampling and testing soils is illustrated by a series of tests conducted on an intact siltstone with thin discontinuous clay seams (approximately ⅛ in.), which resulted in a residual

friction angle 300 percent greater than the same test that forced failure through a 2-in.-thick clay seam in the same siltstone material. The direct shear device allows the flexibility to evaluate the strength of seams and weak zones in soils by forcing the failure surface to pass through a specific zone of interest within a soil sample.

5. Block samples were found to be more useful than tube samples for obtaining test specimens from material containing seams or thin weakness planes because they allow for a greater degree of freedom in selecting the part of the soil mass to be tested and they are generally less disturbed by the sampling and extruding processes.

ACKNOWLEDGMENTS

The authors wish to express their sincere appreciation to the following: Dave Bingham, Fritz Koch, and Bill Moore of the North Carolina Department of Transportation for the many ways in which they assisted during this study: from trenching and field sampling to sharing their many years of experience with the stability of cut slopes in Triassic residual soils; Sterling Weed, North Carolina State University, for conducting the X-ray diffraction analyses; Phillip C. Lambe, North Carolina State University, for his assistance in various aspects of the laboratory testing; and Woodward-Clyde Consultants, Wayne, New Jersey, for their financial support in the preparation of the final manuscript.

REFERENCES

1. P. R. Vaughan and H. J. Walbanke. Pore Pressure Changes and the Delayed Failure of Cutting Slopes in Overconsolidated Clays. *Geotechnique*, Vol. 23, No. 4, 1973, pp. 531–539.
2. A. W. Skempton. "Slope Stability of Cutting in Brown London Clay." *Proc., 9th International Conference on Soil Mechanics and Foundation Engineering*, Tokyo, Vol. 3, 1977, pp. 261–270.
3. C. J. Leith and C. P. Fisher. *An Investigation of the Stability of Highway Cut Slopes in North Carolina.* Project ERD-110-U. Highway Research Program, North Carolina State University, Raleigh, 1964.
4. D. J. Henkel. Local Geology and the Stability of Natural Slopes. *Journal of the Soil Mechanics and Foundation Division, ASCE*, Vol. 93, No. SM4, July 1967, pp. 437–446.
5. T. C. Kenney. Discussion of "Geotechnical Properties of Glacial Lake Clays," by T. H. Wu. *Proc. ASCE*, Vol. 85, No. SM3, 1959, pp. 67–79.
6. J. F. Lupini, A. E. Skinner, and P. R. Vaughan. The Drained Residual Strength of Cohesive Soils. *Geotechnique*, Vol. 31, No. 2, 1981, pp. 181–213.
7. E. N. Bromhead and R. D. Curtin. A Comparison of Alternative Methods of Measuring the Residual Strength of London Clay. *Ground Engineering*, May 1983.
8. *Navy Design Manual: Soil Mechanics.* NAVFAC DM-7.1. U. S. Navy Department, May 1982.
9. A. W. Bishop and D. J. Henkel. *The Measurement of Soil Properties in the Triaxial Test*, 2nd ed. Edward Arnold Publishers Ltd., London, 1962.
10. R. B. Peck. Stability of Natural Slopes, *Journal of the Soil Mechanics and Foundation Division, ASCE*, Vol. 93, No. SM4, 1967, pp. 403–418.
11. A. W. Skempton. Long-Term Stability of Clay Slopes. *Geotechnique*, Vol. 14, 1964, pp. 77–102.
12. L. Bjerrum. Progressive Failure in Slopes in Overconsolidated Plastic Clay and Clay Shales. *Journal of the Soil Mechanics and Foundation Division, ASCE*, Vol. 93, No. SM5, 1967, pp. 1–49.
13. T. H. Wu. *Stability of Slopes in Shale and Colluvium.* Civil Engineering Department, Ohio State University, Columbus, Dec. 1981.
14. D. P. LaGatta. *Residual Strength of Clays and Clay-shales by Rotation Shear Tests.* Harvard University Press, Cambridge, Mass., 1970.
15. F. C. Townsend and P. A. Gilbert. "Effects of Specimen Type on the Residual Strength of Clay and Clay Shales." In *Soil Specimen Preparation for Laboratory Testing*, ASTM Special Technical Publication 599, ASTM, Philadelphia, Pa., 1976, pp. 43–65.
16. D. M. Wood and C. P. Wroth. The Use of Cone Penetrometer to Determine the Plastic Limit of Soils. *Ground Engineering*, April 1978, p. 37.
17. K. Terzaghi. "Stability of Slopes of Natural Clay." *Proc., 1st International Conference on Soil Mechanics*, Vol. 1, Harvard University Press, Cambridge, Mass., 1936.
18. M. L. Jackson. *Soil Chemical Analysis, Advanced Course*, 2d ed. M. L. Jackson, Madison, Wisc., 1975.
19. A. W. Skempton. First-Time Slides in Over-Consolidated Clays. *Geotechnique*, Vol. 20, No. 3, 1970, pp. 320–324.

Publication of this paper sponsored by Committee on Soil and Rock Properties.

Analysis of Slope Failure in Overconsolidated Fissured Residual Soils: A Case Study

STEVEN F. PUTRICH, ROY H. BORDEN, AND PHILIP C. LAMBE

A case study is presented of a well-documented slope failure within the Durham Triassic Basin of North Carolina that indicates the appropriateness of using noncircular failure geometrics and suggests the applicability of utilizing postpeak strengths obtained from drained direct shear tests. A companion paper in this Record presents an experimental investigation of the drained shear strength of soils from three sites within this basin.

This paper is the second of two papers in this Record dealing with slope stability analyses in overconsolidated fissured residual soils. In the first paper an experimental investigation of the drained shear strength of soils from three sites within the Durham Triassic Basin was described. Multistage direct shear tests were utilized and the results were found to be comparable with those that have been reported in the literature for other overconsolidated soils.

In this paper an analysis is presented of a slope failure that occurred in 1978 at the intersection of the Norfolk-Southern Railroad Underpass and US-64 located in the Durham Triassic Basin, the northern portion of the Deep River Triassic Basin deposit of North Carolina. Figure 1 shows the Deep River Basin deposit in relation to the series of Triassic deposits located along the Atlantic Seaboard and the general location of the site investigated in this study.

Geologically the Deep River Basin contains Triassic sedimentary rocks that are clastic deposits consisting of claystone, shale, siltstone, and sandstone. These deposits are characterized by abrupt changes in composition. The sediments of the Deep River Basin are composed largely of debris eroded from nearby pre-Triassic metamorphic and igneous rocks. In places they contain large amounts of debris derived from nearby granite intrusives. These sediments were deposited as alluvial fans, as stream-channel and floodplain deposits, and as lake and swamp deposits. Because of the nature of the depositional environment, a large percentage of the clays and clayey silts are fissured. Because the soils were deposited under wet conditions, subsequent drying and shrinkage caused cracks and openings classified as fissures.

Triassic sedimentary deposits are inclined to the southeast at angles ranging from 5 to 45 degrees. This dipping of the nonhomogeneous deposits is believed to have a major impact on the stability of cut slopes in Triassic deposits. The geometry of the failed slope mass appears to be dependent on the orientation of the soil layering. As was reported by Leith and Fischer (*1*), on the basis of a statewide survey of highway cuts, the slope failure frequency in the Triassic Basin was anomalously high. It can be inferred that the characteristic southeasterly dip of the Triassic sedimentary soil profile is a major factor in inducing a large number of slope failures.

The significance of this analysis and its application to evaluating the use of laboratory direct shear tests similar to those conducted as a portion of this study is that the Railroad Underpass/US-64 slope failure was extensively investigated and documented by the Geotechnical Unit of the North Carolina State Department of Transportation (NCDOT) in 1978. Therefore, there are sufficient field data to evaluate, with reasonable confidence, the maximum shear resistance mobilized at failure.

GEOTECHNICAL EVENTS AT THE RAILROAD UNDERPASS/US-64 SITE

The original project at this site, including the Norfolk-Southern Railroad/US-64 bridge overpass structure, was completed in late 1972 under the direction of the U. S. Army Corps of Engineers. In 1973 several slides of varying size occurred along the length of the railroad on the west side of the excavation adjacent to the bridge structure, including one relatively large, first-time slide. This slide forced the rerouting of rail traffic and posed a threat to the integrity of the bridge overpass. Several remedial measures were taken to correct the slide:

1. Clay material was trucked to the site and used to reshape the slope to its original configuration, and
2. Drain holes in the US-64 bridge deck over the Norfolk-Southern Railroad track were plugged. A 4-ft-wide concrete gutter was poured on the fill slopes beneath the drains of the bridge structure to facilitate surface drainage.

In May 1978 approximately 5 years after the original slide, a second slope failure occurred in the same general location. Figure 2 shows two views of the failed slope. In a subsequent inspection conducted in 1978 by the Geotechnical Unit of NCDOT, the following observations were made about the geometry and subsurface conditions after the failure:

1. The failed soil mass was approximately 110 ft long,

S. F. Putrich, Department of Civil Engineering, North Carolina State University, Raleigh, N. C. 27695-7908. Current affiliation: Woodward-Clyde Consultants, Wayne, N. J. R. H. Borden and P. C. Lambe, Department of Civil Engineering, North Carolina State University, Raleigh, N. C. 27695-7908.

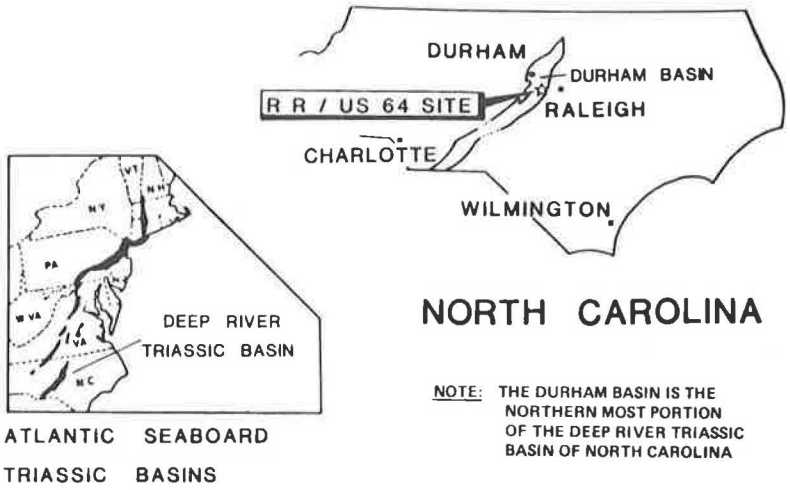

FIGURE 1 Location of Deep River Basin and Railroad Underpass/ US-64 site.

extending southward from the bent at the western end of the bridge structure. Figure 3 shows the extent of the failure and the direction of movement of the failed soil mass into the excavation. The opposite side of the excavation, in which the bedding planes dipped away from the excavation, remained stable.

2. The slope before failure was approximately 25 ft high with a 1.5 horizontal to 1 vertical slope. The location of the 1978 slide appeared to be the same as that observed in the 1973 slide at the site. Therefore this was considered a second-time slide (i.e., soil mass sliding along a previous failure surface).

3. Scarps and cracks were observed both on the surface of and within the failed soil mass.

4. Two major naturally occurring soil units were present in the cut opposite and adjacent to the failed zone (i.e., the west side of the excavation); the upper unit was a tan and gray fissured clayey sand with varying sand-clay ratios (tan unit), and the basal unit was a dark brown to maroon silty clay with irregular seams of light tan and gray fissured clay in the upper portion of the layer (maroon unit). The contact between the upper and lower units undulates and was identifiable by a thin layer of slightly clayey coarse sand.

5. As part of the postfailure investigation by NCDOT in an effort to locate the failure surface and identify the subsurface conditions, three test borings and a series of rod soundings

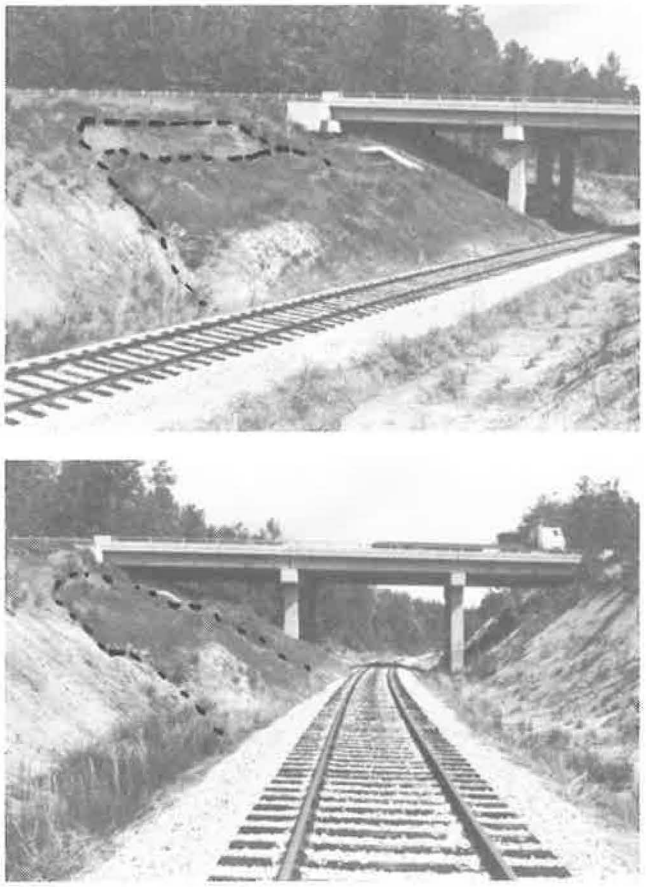

FIGURE 2 Railroad Underpass/US-64 slope failure.

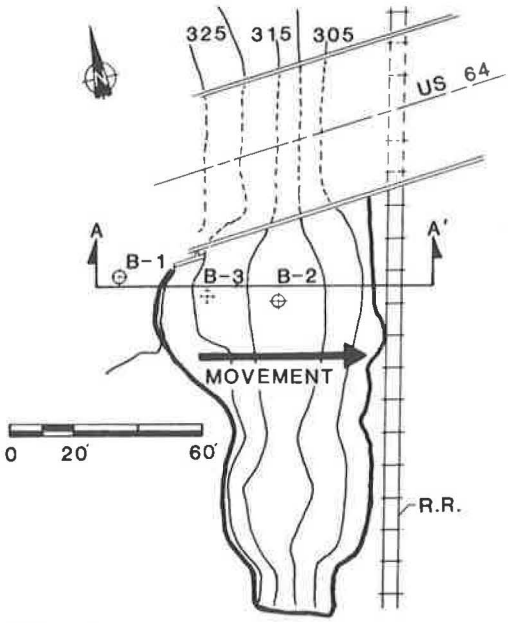

FIGURE 3 Extent of slope failure.

were made at the site shortly after failure occurred, within and adjacent to the failed soil mass. In situ vane shear tests were conducted in the vicinity of the failure surface, and soil samples were recovered in order to conduct laboratory soil classification and shear strength tests. Slope indicator pipe with attached well point was installed in two of the borings located in the failed soil mass in order to monitor further slope movement and postfailure groundwater levels.

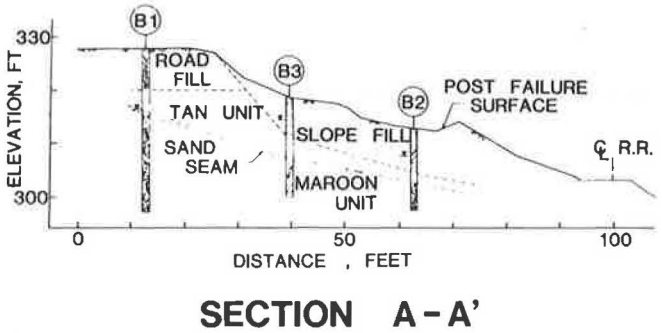

FIGURE 4 Generalized subsurface profile: Section *A–A'*.

Figure 4 shows the generalized subsurface profile (Section *A–A'*) at the Railroad Underpass/US-64 site as defined by Borings B-1, B-2, and B-3 completed by NCDOT during their postfailure investigation. The soil profile can be divided into the following soil units:

1. The top unit is fill material used to construct the existing roadway embankment in 1972. This occurs only in Boring B-1.
2. The second unit is a red clay soil brought to the site to reshape the slope after the initial failure in 1973. This red clay is the surface unit in Borings B-2 and B-3.
3. The third unit is the tan unit, previously described.
4. In between the third and basal unit is a thin layer of slightly clayey coarse sand found in Borings B-1 and B-3.
5. The basal unit is the maroon unit previously described.

The following postfailure surface water and drainage conditions were noted:

1. The perforated pipes used to drain water from beneath the bridge approach slab (part of the original bridge and roadway construction) were clogged.
2. The ditches along the toe of the failed slope were filled with soil debris from other smaller slope failures, which impeded drainage in the ditch.
3. Ditches constructed above the crest of the cut slopes designed to drain off surface water had reduced capacity due to siltation and vegetation. The surface drainage conditions at the site were considered poor.
4. There was excessive surface erosion at the site because of heavy surface runoff from precipitation. This was shown by the undermining of a pile cap supporting the bridge structure immediately adjacent to the failed slope.
5. It was noted that the original design report described the railroad excavation as a "wet" cut, with portions of the excavation below the natural groundwater table. At the time of the NCDOT investigation, groundwater was observed breaking out near the toe of the failed slope, and the face of slope was wet.

As a result of this second failure in 1978, a tie-back pile and timber retaining wall was constructed to hold the sliding mass in place and ensure the integrity of the bridge structure on the site. Figure 5 shows two views of the slope rehabilitation project with the retaining wall in its final stages of construction. Approximately 1 year after the installation of the retaining wall, water was observed seeping through the timber retaining wall at ground elevation. The face of the slope at that time was reported to be saturated and the toe ditch filled with water. These were signs that there was still a problem with on-site groundwater seepage and surface water drainage. To correct the drainage problem, a small wall was constructed back of the toe ditch so that the ditch would be free draining. In addition, 6-in. perforated pipes were installed in the slope to drain the wet slope through the new wall.

More than 10 years after the completion of the railroad and bridge structure, the west side of the railroad excavation at the site has remained stable at a slope of approximately 1 horizontal to 1 vertical. Conversely, the east side of the excavation with a slope of approximately 1.5 horizontal to 1 vertical and soil bedding planes dipping into the cut has experienced two slope failures in this same period of time. With the assumption that the soil-strength and pore-pressure regimes on both sides of the excavation are approximately equal, it can be inferred that the

FIGURE 5 Slope rehabilitation.

orientation of the subsurface profile with respect to the cut has a significant influence on the probability of slope failure in this type of soil deposit. In general, an excavation in the Deep River Triassic Basin made parallel to the direction of the dipping soil layers (i.e., northwest–southeast direction) would have the lowest probability of sliding. This statement is based on the assumption that the variables of slope geometry, soil properties, and pore pressure are constant.

The slope failures at the Railroad Underpass/US-64 site along with the anomalously high number of slope failures in highway cuts within the Triassic Basin deposit are strong evidence to support the need for designing natural slopes with consideration for local geologic characteristics. The geologic environment in the Deep River Triassic Basin deposits is characterized by inclined soil bedding planes, overconsolidated fissured soils, and abrupt changes in soil composition. It is critical that strength parameters utilized in the design of slopes be applicable to sliding along these inclined bedding planes and appropriate in the evaluation of long-term stability.

SLIDE MECHANISMS AND ANALYTICAL TECHNIQUE

The following three factors are believed to have had a major impact on the behavior of this slope:

1. Geometry (including orientation of soil layers) and soil type within the failed soil mass,
2. Soil strength in the failure zone, and
3. Pore-water pressure.

Geometry of Sliding Mass

In order to perform an analysis after the slide, one must determine the geometry, including the surface and subsurface boundaries, of the soil mass that slid. In an effort to determine the location and angle of inclination of the sliding surface, NCDOT personnel completed a series of probe soundings within and adjacent to the failed soil mass in addition to the test borings previously cited. Visual observations and surveys were used to identify the exposed boundaries of the failed slope.

Boring logs for the test borings drilled are given in Figure 6. Included in the logs are data on plasticity and percent passing the No. 200 sieve and the standard penetration values as a function of depth. As shown in the test boring logs, the standard penetration data indicate a significant increase in resistance to penetration as a function of depth into the maroon unit. These data, in conjunction with results from numerous rod soundings, suggest that the sliding surface under the failed soil mass wedge was restricted by the maroon unit. The slope geometry before and following the failure and the estimated failure surface are shown in Figure 7 and correspond to Section *A–A′* within the failed soil mass (see Figure 3 for location of Section *A–A′*).

As shown in Figure 7, the estimated failure surface for this 1978 slide is located in the vicinity of the interface of the tan and maroon soil units. On the basis of field observations, this is thought to be the sliding surface for the previous slope failure

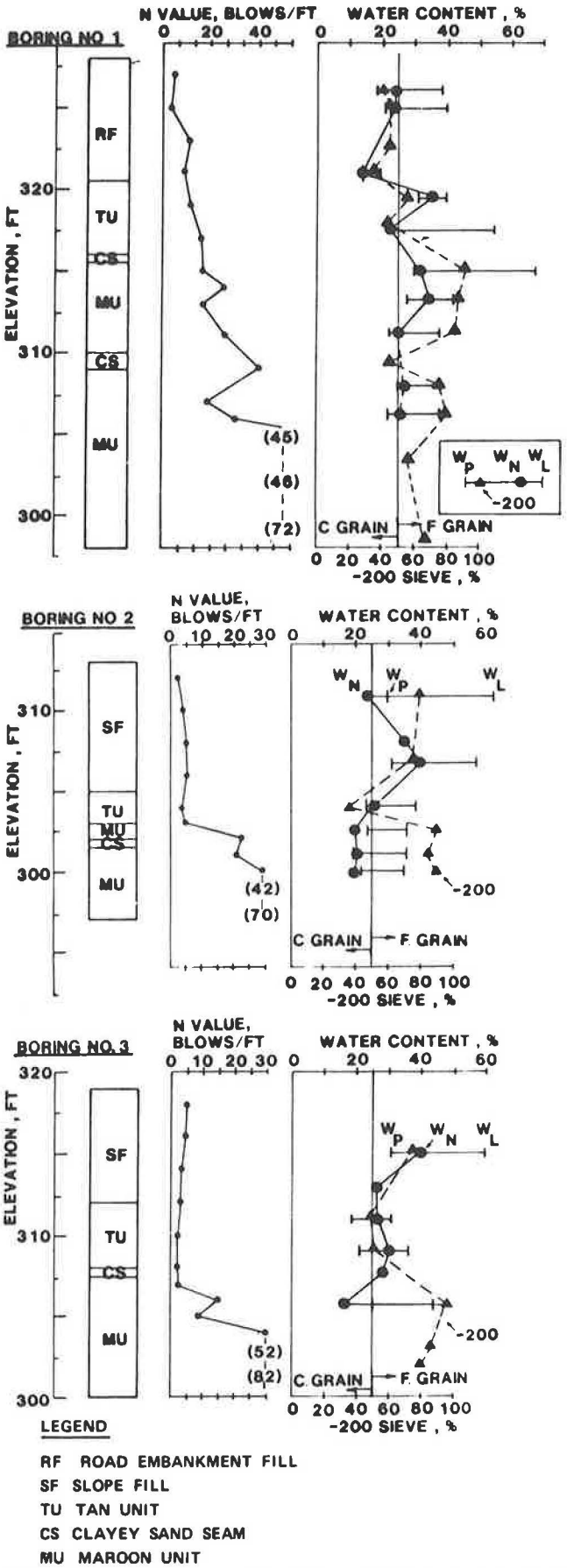

FIGURE 6 Boring logs B-1, B-3, and B-2 at Section *A–A′*.

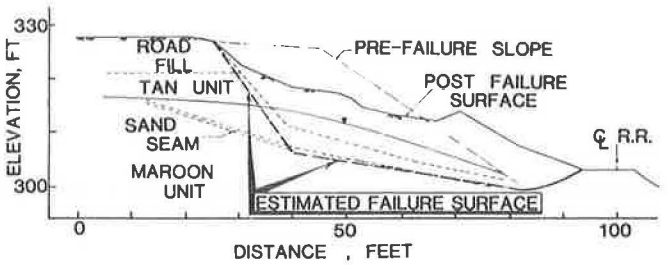

FIGURE 7 Slope geometry and estimated failure surface.

that occurred at the site 5 years earlier. Therefore, the shear strength of soil in the vicinity of this interface is of particular interest for the slide analysis.

Soil Strength

In the summer of 1983, a program of drained direct shear tests was undertaken, and the gray and tan fissured clay seam from the upper portion of the maroon soil unit was tested. The results of these direct shear tests for the Railroad Underpass/US-64 site are presented in Figures 8 and 9. The stress-versus-displacement results demonstrate that this material loses strength with continued horizontal displacement beyond the peak strength and are in general agreement with the idealized response of stiff, fissured clay during a drained direct shear test as shown in Figure 10 [after Skempton (2)].

For the fissured clays found at the referenced site, a peak strength value is an unconservative estimate of the available in situ shear strength with regard to stability of cut slopes in these soils. This post-peak-strength phenomenon can be explained by the progressive failure theory, which states that the peak strength is passed at any one point along a failure surface within a cut slope because of fissures or discontinuities that act as stress concentrators forcing that point to pass the peak strength with a given amount of displacement. Once the peak

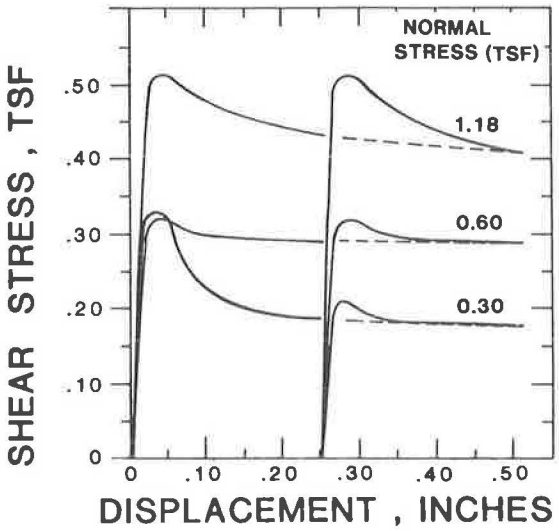

FIGURE 8 Drained direct shear test results: shear stress versus displacement.

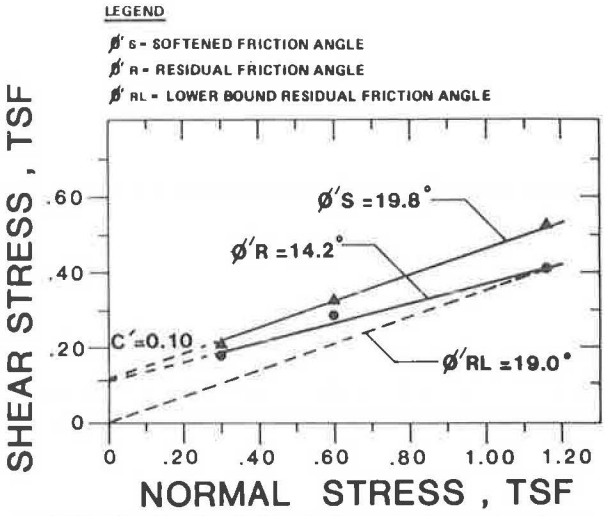

FIGURE 9 Drained direct shear test results: shear stress versus normal stress (2).

strength has been passed at one point along the failure surface, the stress is shifted to another point, causing it to pass the peak, and so on. In this way a progressive failure can be initiated, and the strength along the entire or the majority of the length of the slip surface will decrease as a function of displacement to a lower strength range bounded by the softened and residual strengths. Because this is a previously failed slope, it would be expected that a shear strength significantly less than a peak strength would be mobilized at failure. This lowered shear strength is attributed to the accumulated displacement from movements of the soil mass during the initial slide.

The softened strength and zero cohesion residual strength indicated in Figure 10 are generally recognized as the upper and lower boundaries for the range of in situ strength mobilized for slope failures in overconsolidated fissured clays. The softened strength is defined as the peak stress response for a "remolded" normally consolidated clay (i.e., critical state condition) and the residual strength is defined as that value of stress at which further accumulated displacement will not result in a lowering of strength (i.e., steady-state condition) and is generally recognized as an indication of the in situ strength mobilized in a second-time slope failure.

Shear strength envelopes corresponding to the softened, residual, and lower-bound residual conditions for the fissured clay tested are shown in Figure 9. A dashed line has been used to indicate that the shear strength below the lowest stress increment in the strength envelopes is not known. The dashed portion of these lines is a continuation of the slope of the strength envelopes for the stress range tested to the vertical intercept. An apparent effective cohesion (c') is given for the purpose of defining the linear equation of the envelope.

In light of the small amount of displacement used in this test series compared with that in studies by LaGatta (3) and Lupini et al. (4) that specifically investigated the amount of displacement required to mobilize the minimum strength of clay soils, the lower residual envelope has been introduced. This is a best estimate of the "practical" lower limit of shear strength of this fissured soil. A dashed line is used to indicate that this is a theoretical envelope. As it will be shown in the analysis of the referenced slide, the lower-bound residual significantly under-

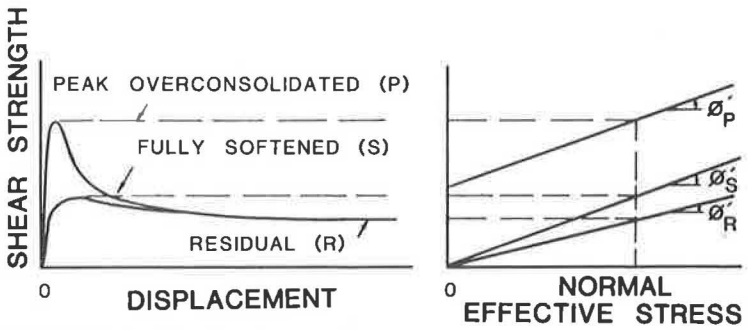

FIGURE 10 Idealized stress-displacement response of stiff fissured clay (*2*).

estimates the lower-bound in situ shear strength. In the companion paper to this analytical study by Borden and Putrich, a detailed explanation of the range of shear strength results and testing technique used for the series of direct shear tests performed in this study is given. Subsequently it will be shown how the laboratory-determined shear strength may be applied to the slope failure under consideration.

Pore Pressure

In order to conduct a slide analysis in terms of effective stresses, the pore pressure within the cut slope must be known. The pore pressure (u) is defined as the sum of the initial pore pressure before construction (u_0) and the excess pore pressure (Δu) due to changes in total stress as a result of excavating for the cut slope. In this study the initial stage is an undrained unloading followed later by drainage. Therefore, the pore pressure initially is influenced to a large degree by the changes in total stress to which the soil mass was subjected during excavation. When an excavation for a cut slope is made, the total stresses decrease, so that with time the pore pressure increases from the end-of-construction value u to $u_0 + (-\Delta u)$. These rising pore pressures result in a reduction in the factor of safety. Therefore, a cut that was designed to be safe using total stresses (undrained failure analysis) may slide after a period of time when the negative excess pore pressure decreases. This behavior is demonstrated in Figure 11 [after Bishop and Bjerrum (*5*)] and indicates that the drained condition is more critical than the undrained condition. As shown in the plot of factor of safety versus time, the factor of safety continues to decrease until the pore pressure reaches a steady-state condition ($\Delta u = 0$). Skempton (*6*) refers to this condition as the long-term stability, where the pore pressure is determined directly from the flow net. The effective stress analysis has been employed in numerous slope stability studies, including ones by Lambe et al. (*7*), Wu (*8*), Vaughan and Walbanke (*9*), and Peck (*10*).

The available data from the Railroad Underpass/US-64 postfailure investigation were used to estimate the pore pressures in the cut slope at the time of failure. The pore-pressure data from this site were obtained from well measurements (slope indicator pipe with well points attached to the bottom of the pipe) within and immediately outside the failed soil mass. These wells are not piezometers and therefore did not furnish pore-pressure data directly but gave an estimate of the groundwater level within the slope (i.e., phreatic surface). The well measurements taken immediately after the slope failure were used to evaluate the location of this phreatic surface. The pore pressures were determined directly from the location of the phreatic surface with respect to the sliding surface by assuming horizontal flow. The location of the outbreak of groundwater on the face of the failed slope observed during the NCDOT investigation was also used to estimate the position of the groundwater level. The estimated location of the phreatic surface at the time of failure is shown in Figure 7.

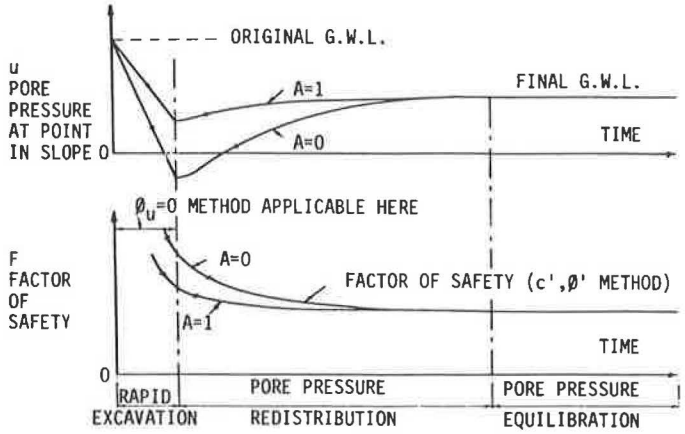

FIGURE 11 Pore pressure and factor of safety as function of time for cut slope in clay (*5*).

Excessive erosion and poor surface drainage were observed in the field investigations in 1973 and 1978 after each of the slope failures. It can be inferred that this site was subject to heavy surface runoff from precipitation. Much of this runoff was retained on the surface of the slope and allowed to infiltrate because of poor surface drainage. Sangrey et al. (*11*) state that this infiltration contributes to two factors that adversely affect the stability of slopes: increase of the unit weight of the soil mass as saturation increases and increase of the pore pressure (uplift force) on the potential sliding surface by raising the phreatic surface. Sangrey et al. further commented that a vast majority of landslides are related directly or indirectly to precipitation. This infiltration effect was indirectly accounted for in this analysis by using the well measurements taken shortly after failure. Change in the level of the phreatic surface because of surface infiltration was assumed to be reflected in the postfailure well readings.

It may be concluded that the buildup of pore pressures due to both dissipation of negative excess pore pressure induced by excavation and the infiltration of precipitation because of poor surface drainage acts as a triggering mechanism in the case of a marginally stable slope. There is strong evidence indicating that this was the case in this slope failure.

Analytical Technique

In describing the problem of an unstable slope, one may say that sliding occurs when the sum of the forces actuating movement becomes equal to the sum of the maximum forces resisting the movement. As used in this study, the term "slide analysis" refers to the situation where a slide has occurred. The slide analysis was performed by the wedge method, which uses the equilibrium factor-of-safety approach outlined in the *Navy Design Manual* (*12*).

Based on the postfailure field investigation by the Geotechnical Unit of NCDOT, the landslide would be described as a partly rotational block failure according to the movement terminology used by Varnes (*13*). Movements of the soil mass involved the sliding and partial rotation of soil blocks (wedges) as shown in Figure 12. Because the layering of the soil within the slope was inclined into the cut, the soil mass had an inherent tendency to slide into the cut. The sliding surface was planar (noncircular), oriented parallel to the inclination of the soil layering, and occurred in the vicinity of the interface between the tan and maroon units.

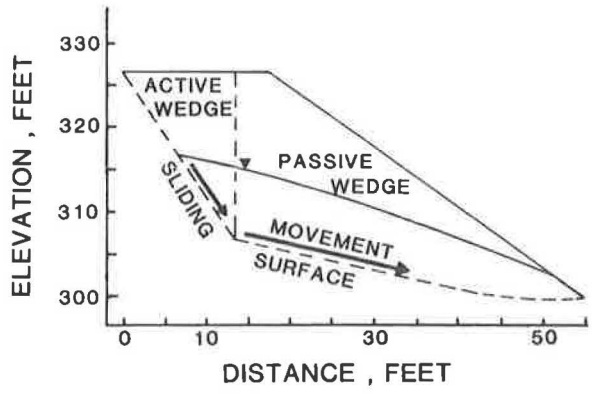

FIGURE 12 Slope failure geometry.

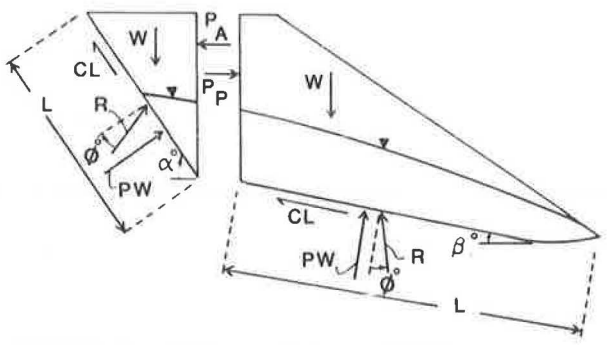

FIGURE 13 Wedge analysis model (*12*).

The failed mass may be thought of as two wedges moving downward and outward. If one imagines a wall between the two wedges, the wedge to the left of the wall corresponds to the active wedge and the wedge to the right of the wall is the passive wedge. Figure 13 shows a free-body diagram of both the active and passive wedges and a description of the forces involved. The equations used to determine the active and passive wedge forces, P_a and P_p, shown in Figure 13, are as follows:

$$P_a = [W_a - c_{am}L \sin(\alpha) - P_{aw} \cos(\alpha)] \tan(\alpha - \phi'_{am}) - [c_{am}L \cos(\alpha) - P_{aw} \sin(\alpha)]$$

$$P_p = [W_p - c_{pm}L \sin(\beta) - P_{pw} \cos(\beta)] \tan(\beta - \phi'_{pm}) + [c_{pm}L \cos(\beta) - P_{pw} \sin(\beta)]$$

where

P_a, P_p = resultant horizontal force for active and passive wedges, respectively;
W_a, W_p = total weight of soil and water in active and passive wedges above sliding surface;
c_{am}, c_{pm} = mobilized cohesion acting along sliding surface of active and passive wedges where $c_m = c/F_s$ and F_s = factor of safety;
α, β = inclination of active and passive sliding surface with respect to horizontal;
L = length of sliding surface of active and passive wedges;
ϕ'_{am}, ϕ'_{pm} = mobilized effective friction angle acting along sliding surface of active and passive wedges where $\phi'_m = \tan^{-1}(\tan\phi'/F_s)$;
P_{aw}, P_{pw} = resultant force due to water pressure on potential sliding surface of active and passive wedges; and
R_{am}, R_{pm} = result of normal and tangential forces on sliding surface considering mobilized friction angle of material.

The resultant horizontal force due to water pressure on the

interface of the active and passive wedges is not shown in these equations. These forces have been assumed equal and opposite and therefore cancel out.

The following five steps outline the procedure used to determine the resultant P_a and P_p:

1. Determine the necessary constants: weight (W_a and W_p), water pressure force (P_{aw} and P_{pw}), and the length of the sliding plane (L_a and L_p);
2. Select a set of strength parameters (ϕ' and c', or c);
3. Determine the mobilized strength parameters in terms of a trial factor of safety (ϕ'_m and c'_m or c_m);
4. Solve for P_a and P_p in terms of the mobilized parameters and the constants from Steps 3 and 1, respectively; and
5. Repeat Steps 3 and 4 for a range of trial safety factors.

Steps 2 through 5 were repeated for a range of strength values, including the unconfined compressive strength and in situ vane shear strength.

The final step in the procedure of this slide analysis was to plot curves for the factor of safety versus values of P_a and P_p as a function of shear strength acting along both the active and passive failure surfaces. A sample of this simple procedure is shown in Figure 14. The intersection of any two curves (P_a and P_p, respectively) indicates that equilibrium between the active and passive wedges has been satisfied and corresponds to a factor of safety for that set of strength parameters.

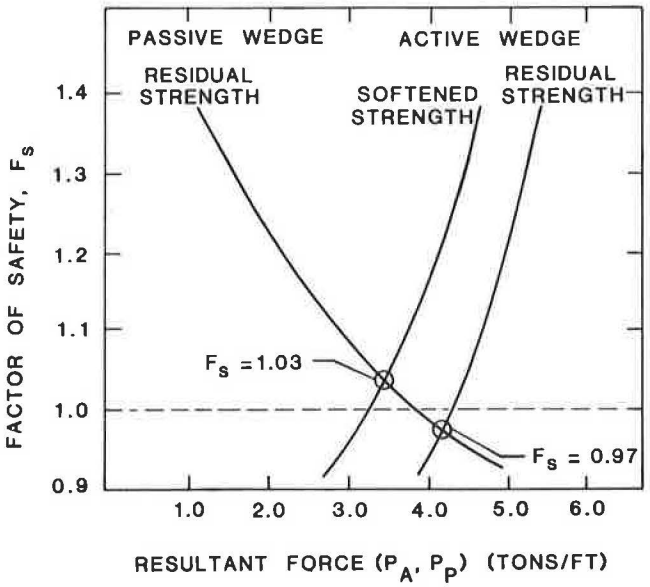

FIGURE 14 Equilibrium factor of safety.

SLIDE ANALYSIS RESULTS

Slide analyses were made for the Railroad Underpass/US-64 site by using the previously described slope failure geometry and pore-pressure conditions. Various shear strengths from drained direct shear tests conducted for this study were investigated. In addition, undrained shear strengths generated from unconfined compression tests and field vane tests completed by the NCDOT Geotechnical Unit were also evaluated.

The slide analyses were conducted by using the softened, residual, and lower-bound (zero-cohesion) residual strengths from the direct shear tests for the passive portion of the sliding surface. Only the softened and residual strengths were considered for the active portion of the sliding surface. There is evidence to suggest that the failed soil mass in the first and second slope failures of the Railroad Underpass/US-64 site slid along the bedding planes in the vicinity of the interface between the tan and maroon units represented by the passive sliding surface. Therefore a lower strength range was evaluated for the soils along the passive surface that would have accumulated more displacement than the soils on the active surface. There was no evidence to suggest that the active sliding surface was the same for both the first and second slope failures.

Table 1 gives the results of the analyses in terms of equilibrium factors of safety for the various shear strengths investigated. In evaluating the results presented in Table 1, the following observations were made:

1. The drained strength parameters govern the long-term stability of this cut slope. The logic for this behavior was described by Skempton (*14*), who concluded, on the basis of field evidence, that the failure of cut slopes in overconsolidated fissured London clays occurred years after excavation because of the slow dissipation of excess negative pore pressure. This position was stated earlier by Vaughan and Walbanke (*9*). This same pore-pressure equilibration is occurring in cut slopes in the overconsolidated residual soils of the Triassic Basin. A general indication of the overconsolidation ratio was obtained from consolidation test results on a fissured clay from a nearby site, as presented in the companion paper of this analytical

TABLE 1 EQUILIBRIUM FACTOR OF SAFETY AS A FUNCTION OF SHEAR STRENGTH

Drained Direct Shear Test			Undrained Shear Test[a]	Field Vane Test[b]
Active Wedge	Passive Wedge	Factor of Safety		
τ_s	τ_s	1.17	2.3	2.5
τ_r	τ_s	1.09		
τ_s	τ_r	1.03		
τ_r	τ_r	0.97		
τ_s	τ_{rl}	0.86		
τ_r	τ_{rl}	0.8		
τ_s[c]	—	1.25		
τ_r[c]	—	1.18		

Note: τ_s = softened strength; τ_r = residual strength; τ_{rl} = lower-bound residual strength.

Undrained shear strength values given refer to results of tests conducted by the NCDOT as a part of the postfailure geotechnical investigation completed in 1978.

The drained shear strength value used for the slightly clayey coarse sand layer (ϕ' = 32 degrees) is assumed. This value is considered a conservative estimate of shear strength based on the range of typical shear strengths for sands in overconsolidated soil deposits.

Equilibrium factor of safety values less than 1.0 indicate instability for the given slope geometry, pore pressure, and shear strength.

[a] s_u = 0.44 tsf.
[b] s_u = 0.55 tsf (0.9) = 0.49 tsf.
[c] Coarse sand layer, estimated ϕ' = 32 degrees.

study (Borden and Putrich in this Record). The maximum past effective stress was found to be 1.7 tsf, indicating an overconsolidation ratio of 3 to 4. The delay of 1 year and 5 years between the end of construction and the occurrence of the first and second slope failures at the site provides evidence that pore-pressure equilibration played a role in the failures.

2. For the failure geometry and pore-pressure regime used in these slide analyses, the residual shear strength appears to closely match the in situ shear strength mobilized for the slope failure investigated. This finding is in agreement with the general design approach for cut slopes in overconsolidated fissured clays that have experienced previous sliding.

3. The lower-bound (zero-cohesion) residual strength is considered to be the lower limit of in situ strength that would be predicted for failure in cut slopes. This is consistent with results shown in Table 1, which indicate that the lower-bound residual strength underestimated the resistance mobilized at failure, as indicated by factors of safety less than 1.

4. The analyses based on the unconfined compressive strength and vane shear strength confirm that use of the undrained strength is an unconservative approach to the analysis of overconsolidated slopes as shown in Table 1. With factors of safety greater than 2.0, it is apparent that undrained shear strength overestimates the available in situ shear strength when the slide analysis technique described is used.

5. As seen in the results of the NCDOT postfailure investigation, the contact between the upper and lower tan and maroon fissured clay units was identified by a slightly clayey coarse sand layer. The majority of the failure surface (i.e., the passive surface) was located in the vicinity and oriented parallel to the interface plane of the tan and maroon units. There was therefore an interest in evaluating the possibility that the failure surface was located in this sand layer. An analysis was conducted by using an assumed shear strength ($\phi' = 32$ degrees) considered a conservative estimate on the basis of the range of typical shear strength values for sands in overconsolidated deposits. The resulting factor of safety using this strength value for the sand layer was higher than that determined for the drained strengths for the fissured clay evaluated. Therefore, on the basis of these results, the failure surface was most likely located in the fissured clay and not in the sand layer.

EVALUATION OF TEST RESULTS

In order to verify the results of the analyses performed, the slope was evaluated for the average shear and normal stresses acting on the failure surface at failure (i.e., $F_s = 1.0$) by using the wedge analysis with a vector approach. These average stresses were then plotted on the diagram of shear versus normal stress shown in Figure 15. Included in this figure are the strength envelopes generated from the direct shear tests conducted on the fissured clay from the Railroad Underpass/US-64 site. The average stresses from both the active and passive sliding surfaces are indicated by points *A* and *P*, respectively.

Figure 15 indicates that average stresses approximately equal to or slightly greater than the residual shear strength governed in the long-term stability of the slope. This finding is consistent with the results of the wedge analysis using the equilibrium factor-of-safety approach, which indicated that the residual strength closely matched the in situ shear strength acting at failure for the previously failed slope.

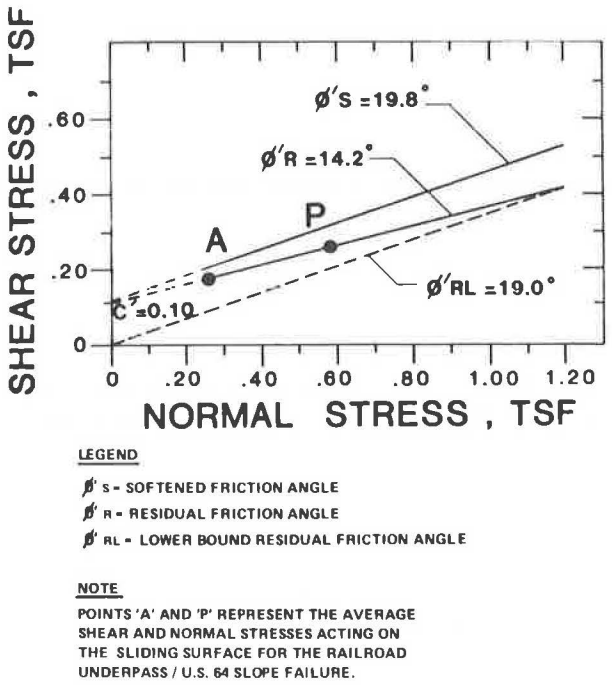

FIGURE 15 Average stress at failure for the Railroad Underpass/US-64 site.

CONCLUSIONS

On the basis of the results of the direct shear tests performed in this study, an evaluation of a well-documented slope failure at the Railroad Underpass/US-64 site, and the literature cited in this paper, the following conclusions are advanced:

1. The slide analysis performed in this study showed that the residual strength from drained direct shear tests closely approximated the average in situ strength mobilized at failure for the second-time slide at the Railroad Underpass/US-64 site. For overconsolidated fissured clays, a peak shear strength value is an unconservative estimate of the available shear strength with regard to the stability of cut slopes in these soils. In the case of a previously failed slope, a shear strength significantly less than the peak value represents the available in situ strength. This lower strength is due to the accumulated displacement associated with shearing of soil along the sliding surface during a previous slope failure.

2. In overconsolidated soils the use of the undrained shear strength was shown to be unconservative. Factors of safety greater than 2.0 resulted in the analysis of the failed slope using undrained shear strength values from unconfined compression and field vane tests. Drained strength parameters govern the long-term stability of cut slopes because the undrained strength will subsequently decrease with time as the negative pore pressures are dissipated. The delay of 1 year and 5 years between the end of construction and the occurrence of the first and second slope failures provides evidence that pore-pressure

equilibration (strength decreasing from an undrained to drained condition) played a role in the failures for the slope evaluated.

3. The infiltration of precipitation into a cut slope that is already experiencing a gradual buildup of pore pressure due to the dissipation of the negative excess pore pressures induced by excavation can act as a triggering mechanism, causing a marginally stable slope to fail. It is therefore important to evaluate the change in pore-pressure regime that will occur in the slope after the end of construction, with consideration given to surface and subsurface drainage provisions. It is very likely that the increase of pore pressure due to the infiltration of runoff acted as a triggering mechanism for the slope failures at the Railroad Underpass/US-64 site. Poor surface drainage facilitated the retaining and infiltration of runoff into the cut slope, thereby adversely affecting stability.

4. Noncircular failure geometries are most appropriate for describing slides occurring in nonhomogeneous soil deposits, which are characterized by inclined soil layers and planar seams of weak material as was the slope evaluated in this study.

5. The soil stratigraphy within the Durham Triassic Basin is characterized by bedding planes that are inclined, dipping downward in a southeasterly direction. Therefore, an excavation made parallel to the direction of the dipping soil layers (i.e., northwest–southeast direction) would have the lowest probability of sliding, with all other variables constant (i.e., slope geometry, soil properties, and pore pressure). When the orientation of excavations is otherwise, special attention must be given to the dipping of inclined layers into the cut. The importance of this issue is shown by the sliding that has occurred at the Railroad Underpass/US-64 site. The side of the excavation with the soil layers dipping into the cut has experienced two major slides in the same area, whereas on the opposite side of the excavation, the slope has remained stable since construction.

ACKNOWLEDGMENTS

The authors wish to express their sincere appreciation to the North Carolina Department of Transportation, whose assistance made this study possible. The use of field records, photographs, and post-slide investigation reports is gratefully acknowledged. Special thanks are due Dave Bingham, Geotechnical Unit, and Fritz Koch, area geologist.

The authors also wish to thank Woodward-Clyde Consultants, Wayne, New Jersey, for their financial support in the preparation of the final manuscript.

REFERENCES

1. C. J. Leith and C. P. Fisher. *An Investigation of the Stability of Highway Cut Slopes in North Carolina.* Project ERD-110-U. Highway Research Program, North Carolina State University, Raleigh, 1964.
2. A. W. Skempton. First-Time Slides in Over-Consolidated Clays. *Geotechnique*, Vol. 20, No. 3, 1970, pp. 320–324.
3. D. P. LaGatta. *Residual Strength of Clays and Clay-Shales by Rotation Shear Tests.* Harvard Soil Mechanics Series 86. Harvard University, Cambridge, Mass., 1970.
4. J. F. Lupini, A. E. Skinner, and P. R. Vaughan. The Drained Residual Strength of Cohesive Soils. *Geotechnique*, Vol. 31, No. 2, 1981, pp. 181–213.
5. A. W. Bishop and L. Bjerrum. *The Relevance of the Triaxial Test to the Solution of Stability Problems.* NR. 34. Norwegian Geotechnical Institute, Oslo, 1960.
6. A. W. Skempton. Long-Term Stability of Clay Slopes. *Geotechnique*, Vol. 14, 1964, pp. 77–102.
7. T. W. Lambe, F. Silva, and W. A. Marv. Instability of Amuay Cliffside. *Journal of the Geotechnical Engineering Division, ASCE*, Vol. 107, No. GT11, Nov. 1981, pp. 1305–1520.
8. T. H. Wu. *Stability of Slopes in Shale and Colluvium.* Civil Engineering Department, Ohio State University, Columbus, Dec. 1981.
9. P. R. Vaughan and H. J. Walbanke. Pore Pressure Changes and the Delayed Failure of Cutting Slopes in Overconsolidated Clays. *Geotechnique*, Vol. 23, No. 4, 1973, pp. 531–539.
10. R. B. Peck. Stability of Natural Slopes. *Journal of the Soil Mechanics and Foundation Division, ASCE*, Vol. 93, No. SM4, 1967, pp. 403–418.
11. D. A. Sangrey, K. O. Harrop-Williams, and J. A. Klaiber. *Groundwater Response to Precipitation with Application to Slope Stability.* USGS 9-6102-05813. Department of Civil Engineering, Carnegie-Mellon University, Pittsburgh, Pa., 1982.
12. *Navy Design Manual: Soil Mechanics.* NAVFAC DM-7.1. U. S. Navy Department, May 1982.
13. D. J. Varnes. "Slope Movement Types and Processes." In *Special Report 176: Landslides: Analysis and Control* (R. L. Schuster and R. J. Krizek, eds.), TRB, National Research Council, Washington, D. C., 1978, pp. 11–33.
14. A. W. Skempton. "Slope Stability of Cuttings in Brown London Clay." *Proc., 9th International Conference on Soil Mechanics and Foundation Engineering*, Tokyo, Vol. 3, 1977, pp. 261–270.

Publication of this paper sponsored by Committee on Engineering Geology.

Factors Important to the Development of Frost Heave Susceptibility Criteria for Coarse-Grained Soils

TED S. VINSON, FAHEEM AHMAD, AND ROSS RIEKE

Laboratory frost heave tests were performed to identify factors important to the development of susceptibility criteria for coarse-grained soils. The frost heave test results were evaluated by using the concept of the segregation potential. The results from 44 tests on mixtures of coarse-grained soils and a fines fraction consisting of silt and different types of clay were considered in the study. Correlations were established between heave rate and segregation potential and *(a)* percentage of particles finer than 0.074 mm, *(b)* percentage of particles finer than 0.02 mm, and *(c)* fines factor (an index property of the fines fraction that indirectly accounts for specific surface area and mineralogy of the fines fraction). The correlations are not strong for the 0.074-mm particles ($R^2 \approx 0.47$), good for the 0.02-mm particles ($R^2 \approx 0.72$), and very strong for the fines factor ($R^2 \approx 0.92$). On the basis of the results of the study, it appears that factors in addition to particle size must be considered in the development of frost heave susceptibility criteria for coarse-grained soils.

It is a matter of experience in cold regions throughout the world that the deformations or loadings resulting from frost heave can produce unacceptable levels of vertical movement and jacking of foundations, cracking in roads and airfields, and lateral movement of earth-retaining structures. Also important is the related problem of soil instability due to excess water when the segregated ice (associated with frost heave) thaws.

Three conditions are necessary for frost heave and the formation of segregated ice. First, ground temperatures must be sufficiently cold and prolonged that the soil water freezes. Second, the water table must be close to the freezing front in the soil mass so that water can migrate to a growing ice lens. Third, the soil must be susceptible to the formation of segregated ice. The basic approach to control frost heave is to eliminate one or more of these conditions. In the field, temperatures and available water cannot be easily controlled. Therefore, identifying and rejecting or removing a frost-susceptible soil is the most common approach used to control frost heave. As a consequence, the ability to identify a frost-heave-susceptible soil is of paramount importance to cold region engineers.

During the past 50 years since Taber's *(1)* treatise on the mechanism of ice segregation in soils and Casagrande's *(2)* frost heave susceptibility criteria, more than 100 different methods have been proposed to evaluate the frost heave susceptibility of soil. Obviously each new method presented has been developed because others available have proven to be unsatisfactory. Further, laboratory frost heave tests have been used extensively to create and evaluate susceptibility criteria. The lack of a suitable correlation between the results of frost heave tests and field observations is a significant factor contributing to differences in susceptibility criteria.

Disagreement between various frost heave susceptibility criteria is greatest when the susceptibility of coarse-grained soils is evaluated. Hundreds of thousands of dollars are spent each year when non-frost-heave-susceptible coarse-grained soils are rejected for use because of unduly conservative selection criteria.

In recognition of the need to identify factors that are most important to the development of frost heave susceptibility criteria for coarse-grained soils, a laboratory study was undertaken to determine the relative susceptibility of coarse-grained soils with varying gradational characteristics and fines contents. The results from the study are reported in this paper.

SEGREGATION POTENTIAL AND FROST HEAVE SUSCEPTIBILITY OF SOILS

It is universally recognized that frost heave is the result of growing ice lenses in a soil mass subjected to subfreezing temperatures. Water is drawn to the base of a growing ice lens because of a suction gradient that develops in response to the temperature gradient in the soil mass. Owing to the presence of dissolved ions, particle surface force effects, and the suction pressures that exist below the ice lens, the nucleation temperature T_s (expressed in degrees celsius) required to form ice at the base of the lens is colder than the normal freezing point of water T_i (≈ 0°C), the warmest temperature at which ice can grow. The condition associated with frost heave may therefore be visualized as shown in Figure 1. At the surface there is a cold-side temperature T_c. At some depth in the soil mass, the temperature is equal to the normal freezing point of water T_i. Slightly above this depth there is a growing ice lens with a base temperature of T_s, which has been termed the segregation freezing temperature. The depth corresponding to T_i has been termed the freezing or frost front *(3)*, and the zone between the base of the ice lens and the freezing front has been termed the frost fringe *(4)*. The existence of the frozen fringe in a freezing system has been established experimentally *(5, 6)*.

In the frozen fringe liquid water exists in equilibrium with pore ice at temperatures below 0°C as adsorbed films on the surfaces of soil particles. The amount of water that can flow to the base of an ice lens is a function of the thickness of the

T. S. Vinson, Department of Civil Engineering, Oregon State University, Corvallis, Oreg. 97331. F. Ahmad, Rashid Engineering, P.O. Box 100, Dhahran Airport, Saudi Arabia. R. Rieke, Hart-Crowser and Associates, Inc., 2550 Denali, Suite 900, Anchorage, Alaska 99503.

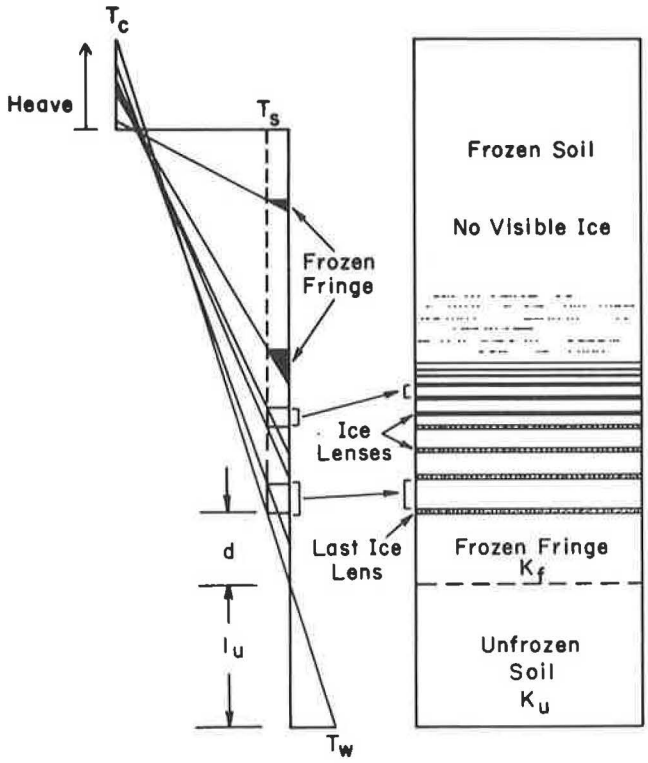

FIGURE 1 Idealization of formation of segregated ice in a soil mass [modified after Konrad and Morgenstern *(3)*].

adsorbed films, which in turn is a function of the soil particle characteristics and the temperature of the frozen fringe. Further, the amount of water that can flow to the base of the ice lens is a function of the suction gradient that exists across the frozen fringe, the suction gradient in the unfrozen soil below the frost front, and the permeability of the unfrozen soil. Indeed, frost heave may be viewed as a problem of impeded water flow to a growing ice lens *(3)*.

Under steady-state conditions, water flows to the base of the growing ice lens through the low-permeability frozen fringe and underlying unfrozen soil. The volumetric heat and latent heat, released as water is transported to the base of the ice lens and eventually forms ice, equal the heat removed when the ice lens is stationary. The frost front advances when the heat removed is greater than the latent heat released. The temperature in the frozen fringe is lowered, the permeability of the frozen fringe is reduced, and the flow of water is decreased, which in turn further reduces the latent heat released. This interrelated thermodynamic-water-flow response results in the formation of finer ice lenses near the surface of a soil column where the temperature gradient is steep and rate of heat removal is greatest. Thicker ice lenses form at greater depths in the soil column where the temperature gradient is shallow *(3)*. Also, with greater depths of frost front penetration, the thickness of the frozen fringe increases because the temperature gradient is shallower and T_s and T_i are nearly constant. The conceptual picture for the overall phenomenon is shown in Figure 1.

As the frost front slows in its advance and a near steady-state thermodynamic-water-flow condition is reached, the situation has been described mathematically by Konrad and Morgenstern *(3)* and may be summarized as follows. It is generally accepted that the Clausius-Clapeyron equation may be used to relate pressure in the liquid film at the base of a growing ice lens (u_i) to temperature; that is,

$$u_i = (L/V_w) \ln (T_{sk}/T_{ok}) = (L/V_w) \ln [1 + (T_s/T_{ok})] \quad (1)$$

where

L = latent heat of fusion of water,
V_w = specific volume of water,
T_{ok} = freezing point of pure water (°K),
T_{sk} = segregation freezing temperature (°K).
$T_s = T_{sk} - T_{ok}$.

If it is recalled that $\ln (1 + x) = x - (1/2)\,x^2 + (1/3)\,x^3 - (1/4)\,x^4 + (1/n)x^n$ and second-order terms are ignored (which is reasonable for small x), Equation 1 reduces to

$$u_i = [L/(V_w \cdot T_{ok})](T_s) \quad (2)$$

It is apparent that the first term in Equation 2 is a constant. Therefore, the suction that develops at the base of a growing ice lens, under near steady-state conditions (i.e., very slow frost penetration rate), is a function of a soil property only, namely, the segregation freezing temperature.

Now consider the two-layer system consisting of the frozen fringe and unfrozen soil beneath the last ice lens. Assuming that *(a)* there is no accumulation of water in the frozen fringe, *(b)* Darcy's law is valid for the flow regime that exists, and *(c)* the permeabilities in the frozen fringe and unfrozen soil are constant, then (by applying Darcy's law)

$$v = \Delta H/[(d/K_f) + (l_u/K_u)] \quad (3)$$

where

v = velocity of water flow to ice lens,
ΔH = total head loss between base of ice lens and base of soil column,
l_u = thickness of unfrozen soil,
d = thickness of frozen fringe,
K_u = permeability of unfrozen soil, and
K_f = permeability of frozen fringe.

l_u and d may be evaluated for a given temperature gradient, warm side temperature T_w, and a soil with a specific value of T_s.

The total head loss may be expressed in terms of the results obtained from the Clausius-Clapeyron equation; that is,

$$\Delta H = u_i + h_{ei} - u_b - h_{eb}$$

$$\Delta H = (1/\gamma_w)\,[L/(V_w \cdot T_{ok})]\,(T_s) + h_{ei} - u_b - h_{eb} \quad (4)$$

where h_{ei} and h_{eb} are elevation heads at the base of the last ice lens and soil column, respectively, and u_b is porewater pressure at the base of the soil column. Taking the base of the soil column at the water level, $u_b = 0$. Further, for a saturated soil

column with the water level close to the last ice lens, $h_{ei} \approx h_{eb}$. Thus Equation 4 reduces to

$$\Delta H = [L/(\gamma_w \cdot V_w \cdot T_{ok})]\ (T_s) \tag{5}$$

By combining Equations 3 and 5, it is apparent that the velocity of water flow to the base of a growing ice lens for a given temperature gradient is a function of soil properties only, that is, K_u, K_f, and T_s. Consequently, the rate of heave, 1.09 times the velocity of water flow, is also a function of soil properties only for a given temperature gradient.

Next consider two columns of identical soil freezing under different temperature gradients as shown in Figure 2. From Equation 5 it may be noted that the total head loss from the base of the last ice lens and soil column (ΔH) is the same for both cases. Further, the average temperature in the frozen fringe is the same for both columns, suggesting that the average unfrozen water content is the same. This implies that the average permeability (K_f) is the same in both cases. The permeability of the unfrozen soil (K_u) may also be assumed to be equal in both cases.

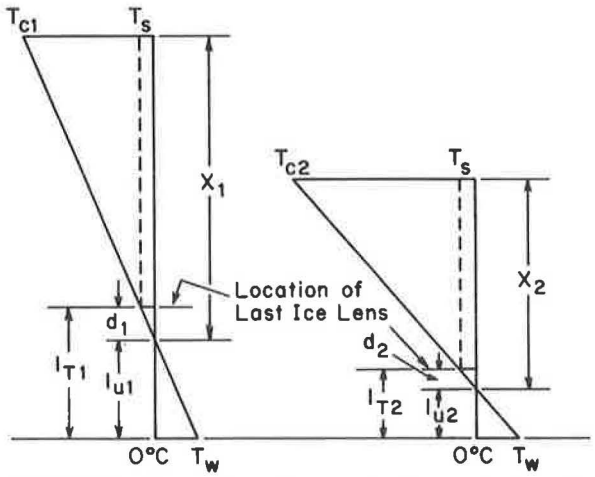

FIGURE 2 Formation of segregated ice under two different temperature gradients [after Konrad and Morgenstern *(3)*].

As a consequence of these identities and assumptions, the flow velocities for the two cases may be written as

$$v_1 = \Delta H/[(d_1/K_f) + (l_{u_1}/K_u)]$$

$$v_2 = \Delta H/[(d_2/K_f) + (l_{u_2}/K_u)] \tag{6}$$

Note that subscripts for ΔH, K_f, and K_v have been omitted, because they are equivalent for both cases.

By noting similar triangles under the two different freezing conditions,

$$T_s/d_1 = T_w/l_{u_1} \quad T_s/d_2 = T_w/l_{u_2} \tag{7}$$

$$T_s/T_w = d_1/l_{u_1} = d_2/l_{u_2} \tag{8}$$

If the ratio of velocities is taken,

$$v_1/v_2 = [(K_u \cdot d_2) + (l_{u_2} \cdot K_f)]/[(K_u \cdot d_1) + (l_{u_1} \cdot K_f)] \tag{9}$$

From Equation 8

$$l_{u_2} = (d_2 \cdot l_{u_1})/d_1 \tag{10}$$

Substituting Equation 10 into Equation 9 and factoring out d_1 and d_2,

$$v_1/v_2 = (d_2/d_1)[K_v + (l_{u_1}/d_1) \cdot K_f]/[K_v + (l_{u_1}/d_1) \cdot K_f] = d_2/d_1 \tag{11}$$

and

$$v_1 d_1 = v_2 d_2 \tag{12}$$

But

$$d_1 = T_s/\text{grad}\ T_1 \qquad d_2 = T_s/\text{grad}\ T_2 \tag{13}$$

in which grad T is the temperature gradient below the base of the ice lens. Substituting Equations (13) into Equation (12),

$$v_1/\text{grad}\ T_1 = v_2/\text{grad}\ T_2 = \text{constant} \tag{14}$$

Now the significance of Equation 14 is that if the ratio of the intake velocity and temperature gradient is a constant, it may be established from the results of tests conducted at any temperature gradient. Further, if the ratio of flow velocity to temperature gradient is known for a particular soil, the intake velocity (and hence heave rate) may be established for another temperature gradient by simple multiplication.

Konrad and Morgenstern *(3)* have termed the ratio of water intake velocity to temperature gradient the segregation potential *(SP)*. They have shown that the segregation potential is

$$SP = V/\text{grad}\ T = \left(\{[L/(\gamma_w \cdot V_w \cdot T_{ok})](T_s) - u_0\}/T_s\right)K_f \tag{15}$$

where u_0 is the suction at the base of the frozen fringe (which is close to the 0°C isotherm). The segregation potential, once evaluated at near steady-state conditions, and under the conditions previously noted (i.e., a saturated soil column with negligible overburden pressure), may be considered an index property of a soil that uniquely identifies the frost heave susceptibility considering the assumptions noted earlier. The greater the segregation potential, the greater the heave in a soil mass in response to a given set of freezing conditions.

To relate the segregation potential of a soil to field conditions, one must consider the influence of *(a)* suction at the frost front (associated with the depth to the groundwater table), *(b)* pressure applied to the warmest ice lens (associated with the weight of the soil column and surcharge loads above the lens), and *(c)* rate of cooling of the frozen fringe (associated with frost penetration rates and average temperature gradients in the frozen zone). In a series of papers, Konrad and Morgenstern *(7–11)* discussed the significance of these variables and extended the concept of the segregation potential to address frost heave prediction under field conditions. They demonstrated that only a limited number of freezing tests are required

to fully characterize the segregation potential of a soil for most field problems.

DESCRIPTION OF TEST SYSTEM

The segregation potential may be evaluated in the laboratory in a frost heave test by freezing a soil specimen and noting the intake of water into the specimen and the temperature along the specimen. Although it is desirable to apply the results of this and other laboratory investigations to actual field situations, only relative frost heave susceptibilities, as measured in the laboratory, were determined. The frost heave tests were performed under worst-case conditions to minimize the influence of variables other than gradational characteristics of the materials and the fines content. To achieve conditions that were most conducive to frost heaving, the specimen was saturated and the free water surface was maintained at approximately the same level as the frost front. No surcharge was applied to the specimen.

The frost heave cell employed in the study is shown in Figure 3. The cell, sample preparation, test procedure, and interpretation of the test results have been described in detail by Mageau and Sherman *(12)* amd Rieke *(13)*. The frost heave cell consists of a nylon barrel 30.5 cm (12.0 in.) long by 10.2 cm (4.0 in.) I.D. by 15.2 cm (6.0 in.) O.D. The specimen is placed inside the cell and an aluminum top cap and bottom plate serve as constant-temperature boundaries. The temperatures of the top cap and bottom plate are maintained at constant values by circulating constant-temperature fluids through heat exchange mazes within the cap and plate. To aid in the boundary temperature control and to prevent radial heat flow, the cell was placed in a refrigerator whose temperature was maintained at approximately 2°C. A 50-mL buret was connected to the water intake line and the flow of water into or out of the specimen during a test was noted by the change in the water level in the buret. The change in the height of the specimen during the test (reflecting frost heave) was measured with a linear variable differential transformer (LVDT). The temperature along the length of the specimen was monitored with thermistors adjacent to the soil embedded in the wall of the nylon cell barrel. Before freezing, the specimen was consolidated one-dimensionally under 50 kPa (7 psi) pressure and allowed to reach thermal equilibrium with the ambient refrigerator temperature.

The segregation potential was calculated for each frost heave test by using the measured intake of water and the temperature along the specimen as noted by the thermistors at near steady-state conditions. Near steady-state conditions usually occurred 13 to 14 hr after the test had been initiated. The temperature gradient at the end of the test was also determined and the average of the two (i.e., at 13 to 14 hr and at end of the test) was used in the calculations. The segregation potential has been shown to be independent of the temperature gradient at near steady-state conditions (see Equation 14). However, all samples were subjected to the same top-cap and bottom-plate temperatures. The heave rate for each sample at near steady-state conditions was also determined.

LABORATORY TEST PROGRAM AND MATERIALS

The soils used in the laboratory test program were mixtures of pea gravel or well-graded coarse sand with 2, 4, 5, 8, and 20 percent fines (i.e., diameter less than 0.074 mm). For the majority of the tests, the fines consisted of a mixture of 75 percent silt and 25 percent poorly crystallized kaolinite. Several tests were also conducted by mixing Hanover silt (with the plus 0.074-mm particles removed) with well-crystallized kaolinite. Grain size distributions for both types of coarse material and Hanover silt are shown in Figure 4. Specific

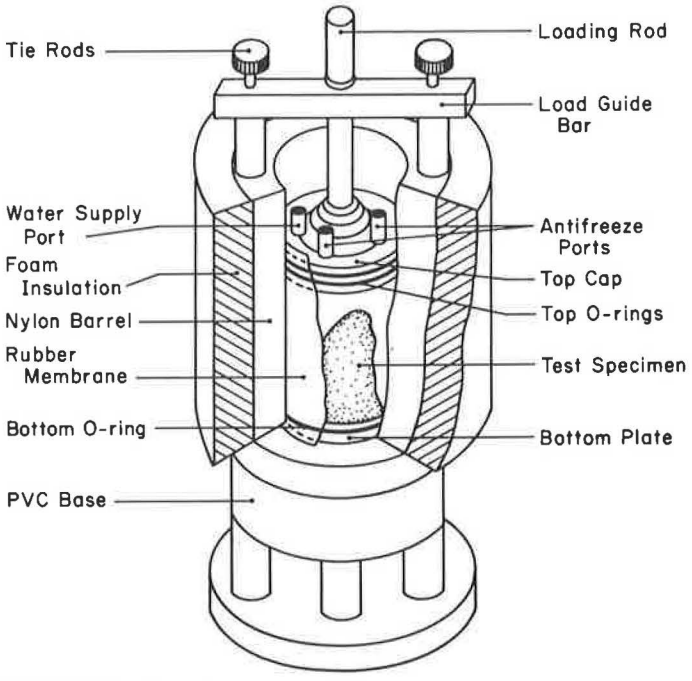

FIGURE 3 Frost heave test cell.

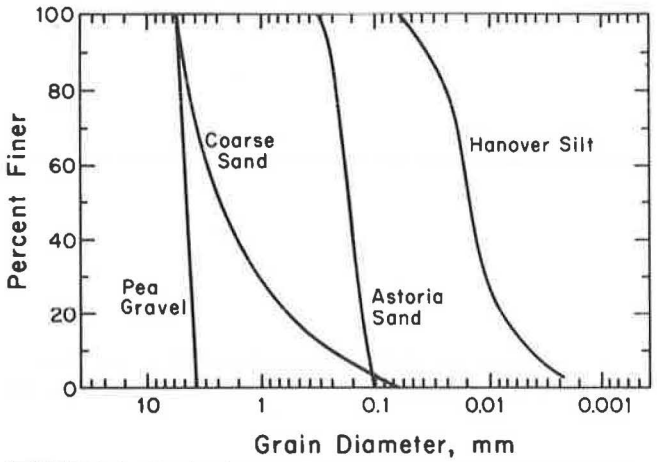

FIGURE 4 Grain size distributions for soil employed in test program.

gravity values are given in Table 1. Because it was desirable to control the effects of different clay minerals, clays with greater than 90 percent purity were required. To this end clays available from the Clay Minerals Society of America (Columbia, Missouri) were used. The diameter of the clay particles was assumed to be less than 0.002 mm.

The different components of pea gravel, sand, silt, and clay used in the soil sample mixture were weighed to ±0.5 g. Because a 2000-g sample was typically used, the resulting accuracy of the component percentages was ±0.025 percent. The components were thoroughly mixed in order to obtain a homogeneous sample. The void ratios of the samples used for the frost heave susceptibility tests ranged from 0.44 to 0.68 (porosities from 0.30 to 0.41). The void ratio was obtained by using a weighted average of the specific gravities of the soil components.

Thirteen frost heave tests were performed on various combinations of sand, pea gravel, silt, and clay. In seven of the tests, the material retained on the No. 200 sieve (0.074 mm) consisted of well-graded coarse-grained sand whereas the fines fraction consisted of mixtures of silt and different types of clay. In six tests, the material retained on the No. 200 sieve consisted of uniform pea gravel. A summary of the combinations of mixtures used in the study is given in Table 2. The percentage of material smaller than 0.02 mm, the uniformity coefficient, and the coefficient of curvature for each sample are also presented. The data base developed in the present study may be supplemented with the results from 31 tests presented by Rieke et al. *(14)* for soil mixtures consisting of a fine sand from Astoria, Oregon, and various percentages of fine soil materials previously discussed. The grain size distribution for Astoria sand is shown in Figure 4 and the specific gravity is given in Table 1.

TABLE 1 SPECIFIC GRAVITIES OF SOILS USED IN TEST PROGRAM

Soil	Clay Mineral Society Symbol	Specific Gravity
Well-graded coarse-grained sand	–	2.65
Pea gravel	–	2.68
Kaolinite		
Well crystallized	KG_a-1	2.60
Poorly crystallized	KG_a-2	2.60
Hanover silt	–	2.69
Astoria sand	–	2.75

TEST RESULTS

The purpose of this study was to identify factors important to the frost heave susceptibility of coarse-grained soils. The fines content (the percentage of particles smaller than 0.074 mm) has been identified by many researchers as an important factor. Indeed, the majority of the classification systems employed in the United States to assess frost heave susceptibility of soils are based on a percentage of material finer than 0.074 mm *(15)*. Casagrande *(2)*, however, identified the 0.02-mm fraction as being particularly important to the formation of segregated ice in a soil and stated:

TABLE 2 PERCENTAGE OF SOIL MIXTURE COMPONENTS, COEFFICIENT OF UNIFORMITY, AND COEFFICIENT OF CURVATURE OF TEST SAMPLES

Test No.	Coarse Material Percent	Coarse Material Type	Silt (%)	Clay Percent	Clay Type	Percent Finer Than 0.074 mm	Percent Finer Than 0.02 mm	C_u	C_c	Segregation Potential (mm²/°C-day)	Heave Rate (mm/day)
1	100	Well-graded sand	–	–	–	–	–	11	1.1	0.0	0.0
2	98	Well-graded sand	1.5	0.5	PCK	2	1.3	15	1.7	0.0	0.0
3	96	Well-graded sand	3.0	1.0	PCK	4	2.5	16	1.8	0.0	0.9
4	92	Well-graded sand	6.0	2.0	PCK	8	5.0	19	1.9	73	2.3
5	80	Well-graded sand	15.0	5.0	PCK	20	12.5	150	5	147	5.0
6	80	Well-graded sand	10.0	10.0	PCK	20	15.0	1350	46	232	7.8
7	95	Well-graded sand	1.0	4.0	WCK	5	4.5	17	1.8	86	3.2
8	92	Pea gravel	6.0	2.0	PCK	8	5.0	1.2	0.9	76	2.5
9	80	Pea gravel	15.0	5.0	PCK	20	12.5	370	323	203	6.7
10	80	Pea gravel	10.0	10.0	PCK	20	15.0	2900	2421	300	12.7
11	95	Pea gravel	1.0	4.0	WCK	5	4.5	1.1	0.9	67	2.5
12	91	Pea gravel	1.8	7.2	PCK	9	8.1	1.1	0.9	90	4.6
13	96	Pea gravel	3.0	1.0	PCK	4	2.5	1.1	0.9	0.0	0.8

Note: PCK = poorly crystallized kaolinite; WCK = well-crystallized kaolinite; $C_u = D_{60}/D_{10}$; $C_c = D_{30}^2/(D_{60} \times D_{10})$.

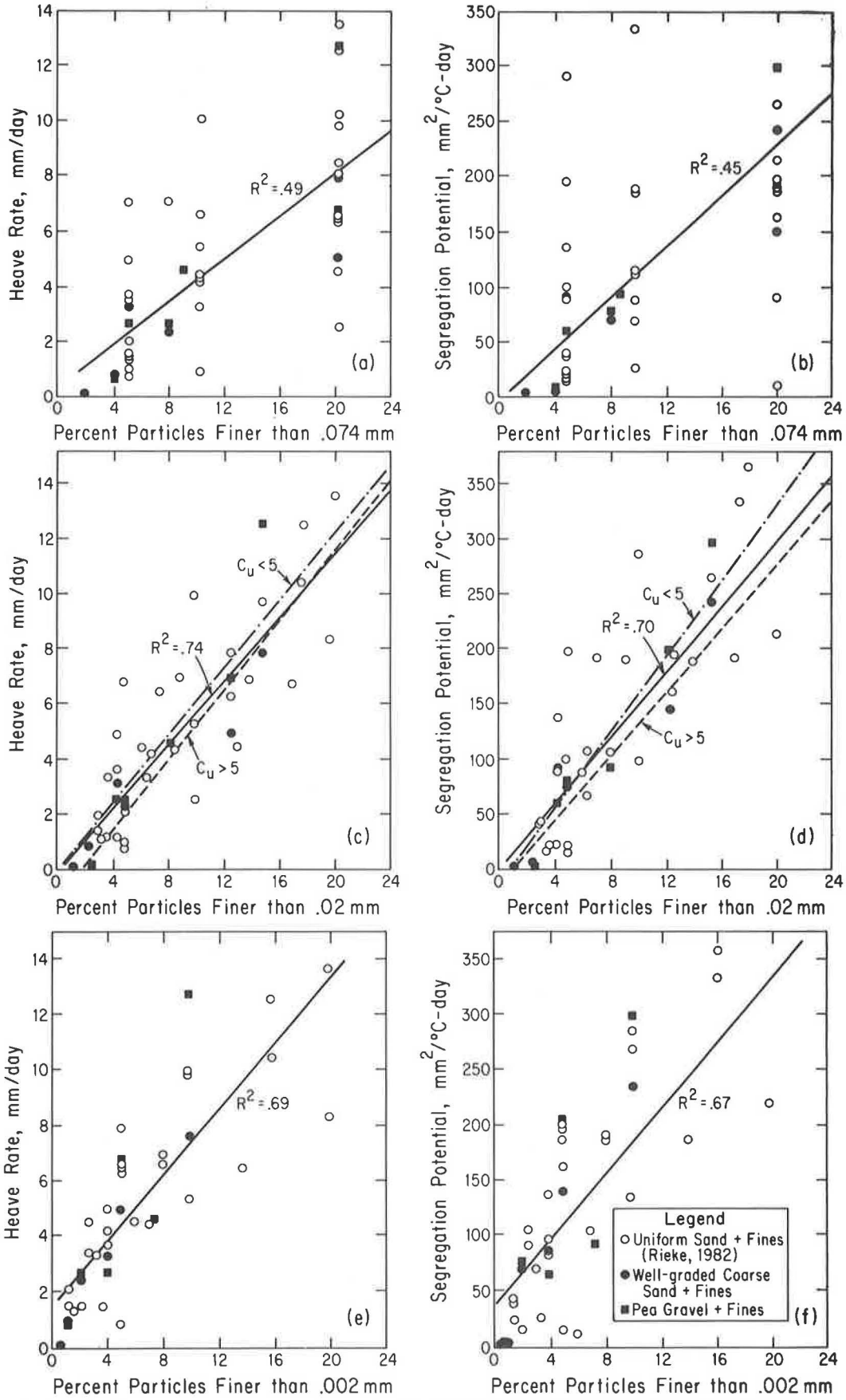

FIGURE 5 Heave rate and segregation potential versus percentage of particles finer than 0.074, 0.02, and 0.002 mm.

Under natural freezing conditions and with sufficient water supply one should expect considerable ice segregation in nonuniform soils containing more than 3% of grains smaller than 0.02 mm, and in very uniform soils containing more than 10% smaller than 0.02 mm. No ice segregation was observed in soils containing less than 1% of grains smaller than 0.02 mm, even if the ground water was as high as the frost line.

The results of the present study in terms of the heave rate and segregation potential versus the percentage of particles finer than 0.074 and 0.02 mm are presented in Figure 5. It is clear that the correlation between heave rate or segregation potential and the percentage of particles finer than 0.074 mm (see Figure 5*a* and *b*) is not strong. At a given percent finer than 0.074-mm, the heave rate or segregation potential varies by over a factor greater than 10. The poor correlation and great range in frost heave response suggest that the continued use of the 0.074-mm grain size alone as an indicator of frost heave susceptibility is not justified.

The correlation between heave rate and segregation potential and the percentage of particles finer than 0.02 mm (see Figure 5*c* amd *d*) is good. It would appear that if one is to base a classification system on particle size alone, the 0.02-mm size is an excellent choice. Further, the correlation between frost heave response and particle size is not improved if the clay size fraction (0.002 mm) is used (see Figure 5*e* and *f*). In fact, the correlation between heave rate or segregation potential and percentage of particles finer than 0.002 mm is not as strong as the correlation for 0.02 mm (but the difference in R^2-values is not great).

The uniformity of a soil is often expressed in terms of the coefficient of uniformity (C_u). If C_u is greater than approximately 5, the soil is well-graded; if the coefficient of uniformity is less than 5, the soil is uniform. The coefficients of uniformity were calculated for the soil mixtures employed in the study and the mixtures were divided into well-graded soils ($C_u > 5$) and uniform soils ($C_u < 5$). The correlation between heave rate and segregation potential and percentage of particles finer than 0.02 mm is shown in Figure 5*c* and *d*. The difference between the correlations associated with $C_u > 5$, $C_u < 5$, and the combined data set is not great.

Lambe et al. *(16)* found that the mineralogy of the clay in the fines fraction influenced the frost heave susceptibility of soils. Specifically, clays with high activities could actually decrease frost heave when added to frost-susceptible materials.

On the basis of more than 30 frost heave tests conducted on 11 distinct soil mixtures, Rieke et al. *(14)* found that the segregation potential of a soil increased with increasing percentage of fines, decreasing activity of the fines fraction, and for a specific fines fraction mineralogy, increasing liquid limit of the fines fraction. They developed a term based on empirical observations that had a strong correlation with the segregation potential of a soil, namely,

$$R_f = [(\text{percentage of fines})(\text{percentage of clay sizes in fines fraction})]/(\text{liquid limit of fines fraction})$$

where R_f is the fines factor, percentage of fines is material passing the No. 200 (0.074-mm) sieve, percentage of clay sizes is material smaller than 0.002 mm, and liquid limit (LL_f) is liquid limit of material passing the No. 200 (0.074 mm) sieve. The fines factor may be viewed as an index property of the fines fraction that indirectly accounts for the specific surface area and mineralogy of the fines fraction.

On the basis of the analysis of the fines factor, it may be demonstrated that the permeability of the frozen fringe, and hence a soil's tendency to heave, is a function of not only specific surface area but also the mineralogy of the fines fraction. It is hypothesized that fines fractions with highly active clay minerals have less mobile unfrozen water films in the frozen fringe, which results in a reduced frozen fringe permeability.

The heave rate and segregation potential versus fines factor for the soil mixtures considered in the study is shown in Figure 6. The correlation coefficients are high. Consequently, it may be concluded that factors other than particle size alone must be

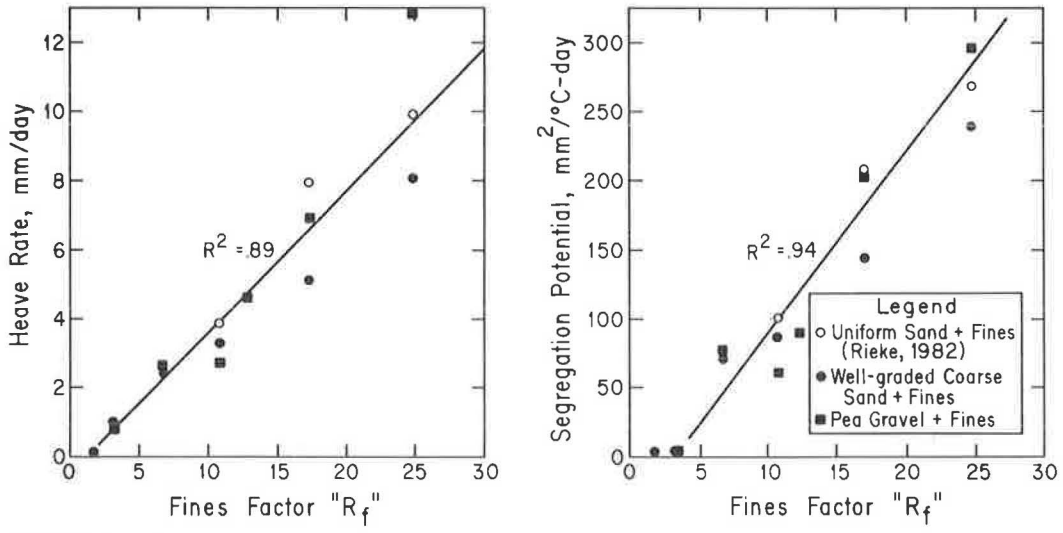

FIGURE 6 Heave rate and segregation potential versus fines factor.

considered in the development of frost heave susceptibility criteria for coarse-grained soils.

SUMMARY AND CONCLUSIONS

On the basis of the results of 44 frost heave susceptibility tests conducted on coarse-grained soils with varying percentages and mineralogy of the fines fraction, the following conclusions may be drawn:

1. The correlation between heave rate or segregation potential and the percentage of particles finer than 0.074 mm is not strong; the continued use of the 0.074-mm grain size alone as an indicator of frost heave susceptibility is not justified.
2. The correlation between heave rate or segregation potential and the percentage of particles finer than 0.02 mm is good; the difference between the correlations for the 0.02-mm particle associated with well-graded soils and those for uniform soils is not great.
3. The correlation between heave rate or segregation potential and the fines factor (a term that considers the percentage of fines and mineralogy of the fines fraction) is the strongest of those considered in the present study. It suggests that factors in addition to particle size must be considered in the development of frost heave susceptibility criteria for coarse-grained soils.

ACKNOWLEDGMENT

The studies described were supported in part by the Department of Civil Engineering, Oregon State University. The support of the department is gratefully acknowledged. John Heinicke critically reviewed the manuscript and offered many helpful suggestions. The effort of Marilyn Tubbs, who assisted in the preparation of this paper, is greatly appreciated.

REFERENCES

1. S. Taber. The Mechanics of Frost Heaving. *Journal of Geology,* Vol. 38, 1930, pp. 303–317.
2. A. Casagrande. "Discussion of Frost Heaving." *HRB Proc.,* Vol. 11, 1931, pp. 168–172.
3. J. M. Konrad and N. R. Morgenstern. A Mechanistic Theory of Ice Lens Formation in Fine-Grained Soils. *Canadian Geotechnical Journal,* Vol. 17, No. 4, 1980, pp. 473–486.
4. R. D. Miller, "Freezing and Heaving of Saturated and Unsaturated Soils." *Highway Research Record 393,* TRB, National Research Council, Washington, D.C., 1972, pp. 1–11.
5. J. P. Loch and B. D. Kay. "Water Redistribution in Partially Frozen Saturated Silt Under Several Temperature Gradients and Overburden Loads." *Journal of the Soil Science Society of America,* Vol. 42, No. 3, 1978.
6. J. P. Loch. "Influence of the Heat Extraction Rate on the Ice Segregation Rate of Soils." *Frosti Jord,* No. 20, May 1979.
7. J. M. Konrad and N. Morgenstern. "The Segregation Potential of a Freezing Soil." *Canadian Geotechnical Journal,* Vol. 18, No. 4, 1981.
8. J. M. Konrad and N. Morgenstern. "Prediction of Frost Heave in the Laboratory During Transient Freezing." *Canadian Geotechnical Journal,* Vol. 19, No. 3, 1982.
9. J. M. Konrad and N. Morgenstern. "Effects of Applied Pressure on Freezing Soils." *Canadian Geotechnical Journal,* Vol. 19, No. 4, 1982.
10. J. M. Konrad and N. Morgenstern. "Frost Heave Prediction of Chilled Pipelines Buried in Unfrozen Soils." *Canadian Geotechnical Journal,* Vol. 21, No. 1, 1984.
11. J. M. Konrad and N. Morgenstern. "Frost Susceptibility of Soils in Terms of Their Segregation Potential." In *Proc., Fourth International Conference on Permafrost,* National Research Council, Washington, D.C., 1983.
12. D. W. Mageau and M. B. Sherman. "Frost Cell Design and Operation." In *Proc., Fourth International Conference on Permafrost,* National Research Council, Washington, D.C., 1983.
13. R. D. Rieke. *The Role of Specific Surface Area and Related Index Properties in the Frost Susceptibility of Soils.* M.S. thesis. Oregon State University, Corvallis, 1982.
14. R. D. Rieke, T. S. Vinson, and D. W. Mageau. "The Role of the Specific Surface Area and Related Index Properties in the Frost Heave Susceptibility of Soils." In *Proc., Fourth International Conference on Permafrost,* National Research Council, Washington, D.C., 1983.
15. E. J. Chamberlain. *Frost Susceptibility of Soils: Review of Index Tests.* Monograph 81-2. U.S. Army Cold Regions Research and Engineering Laboratory, Hanover, N.H., 1981.
16. T. W. Lambe, C. W. Kaplar, and T. J. Lambie. *Effect of the Mineralogical Composition of Fines on Frost Susceptibility of Soils.* Technical Report 204. U.S. Army Cold Regions Research and Engineering Laboratory, Hanover, N.H., 1969.

Publication of this paper sponsored by Committee on Frost Action.

Control of Frost Penetration in Road Shoulders with Insulation Boards

HIROSHI KUBO AND TAKAYUKI SAKAUE

The replacement method for the control of frost penetration of soils is commonly used for pavements on roads with light traffic in Japan. However, because of recent concern for the protection of the natural environment and shortages of natural resources, special frost control techniques such as the insulation method now need to be developed. This method prevents frost damage from frost penetration by the use of insulation boards placed between the subgrade and subbase in road shoulder areas only. It is intended for pavement construction where narrow existing gravel roads with a sand and gravel subbase are widened. A frost control design method that combines the insulation method used for road shoulders with the replacement method used in the travel lanes is described. Estimations from calculations are compared with observed measurements of frost heave and frost penetration obtained from the test road in winter. From the results of observations on the experimental sites, this new method is found to be promising for the control of frost penetration in both the widening and the paving of existing gravel roads.

Control of frost penetration for road pavement construction is essential in severely cold regions. The replacement method, digging out frost-susceptible soils and replacing them with granular non-frost-susceptible materials such as pit-run gravel and sand, is commonly used in Japan. Because of its economy and ease of application, this method has been extensively used for low-cost road pavements and road shoulders *(1)*. However, because of recent concerns for protection of the natural environment and shortages of natural resources as well as difficulties of finding places to dump the frost-susceptible materials, special control techniques such as the insulation method, the soil-stabilization method, and the water-cut-off method must now be developed *(2, 3)*.

A design method for frost penetration control is discussed that combines the insulation method, using extruded polystyrene foam (insulation board) in the road shoulders, with the replacement method using pit-run sand and gravel subbase in roadways. The method is intended for paving and widening of narrow existing gravel roads. Estimations are also compared with observed measurements of frost heave and frost penetration obtained at the test road in winter. The test road is a part of a newly extended 75-km-long road constructed with the combined method.

H. Kubo, Research Division III, Civil Engineering Research Institute, Hokkaido Development Bureau, Toyohiraku Hiragishi 1-3, Sapporo, Japan. T. Sakaue, Faculty of Engineering, Hokkai Gakuen University, 4-1-40, Asahimachi, Toyohiraku, Sapporo 062, Japan.

APPLICATIONS OF INSULATION METHOD AND OBSERVED RESULTS

The insulation method prevents frost damage from frost penetration by the placement of insulation boards between subgrade and subbase. Generally, the engineering problems with this method are *(a)* poor bending strength under heavy wheel loads, *(b)* the possibility of decreasing insulating efficiency due to water absorption, and *(c)* the increased frequency of surface frost or ice. However, experiments on the test road over 18 years have shown no decrease of insulating efficiency and less frequency of differential icing in paved roads in Japan. Also, the problem of poor bending strength can be overcome by installing the insulation boards in the road shoulder areas, which have a very low frequency of wheel loads. The remaining problem is to determine the thickness of the sand layer above the insulation boards in order to ensure that rolling with compacting equipment will not break or crush the boards during construction.

When the depth of cover over the insulation boards is determined, the final placement depth is determined from a balance of two conflicting requirements: insulation efficiency, which requires the board to be placed near the surface, and bending strength, for which the boards should be deep in the pavement structure. In the case where insulation boards are placed only in the road shoulder, the thickness of the subbase over the insula-

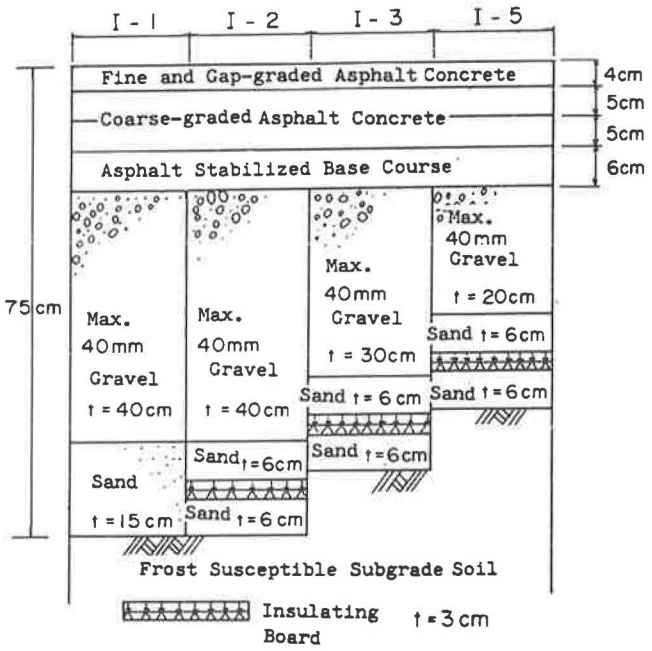

FIGURE 1 Schematic cross section of Bibi Test Road.

tion boards can be determined by considering only the bending strength necessary to avoid damage from construction equipment working on the surface, binder, and base courses.

To determine the optimum buried depth for the insulation boards in the insulation method, a test road (Figure 1) was constructed in 1973 on National Road Route 36, Tomakomai, Hokkaido. The depth of frost penetration, amount of frost heave, and bearing capacity of subbase and subgrade were measured. In Figure 1, cross section *I-1* shows the standardized pavement structure of national roads in this area. For each cross section of the test road, the amount of frost heave and depth of frost penetration were observed with the level and frost depth indicators in winter for the 6 years between 1973 and 1978.

Figure 2 shows the maximum frost heave on the road surface and the maximum frost penetration depth in the subgrade and compares them with the maximum freezing index for each year. The maximum amount of frost heave increases in proportion to the maximum freezing index in winter, and there is a high correlation between them. The amount of frost heave becomes slightly smaller when the buried depth of the insulation boards is shallow, but in general the differences in buried depth of insulation boards do not greatly affect the amount of frost heave. The amounts of frost heave observed in the cross section for the insulation method are clearly smaller than the amount in the standard section *(I-1)*. The depth of frost penetration in the subgrade becomes less with increasing buried depth of the insulation boards. This is the combined effect of the insulation board and additional depth of non-frost-susceptible materials. The depth of frost penetration observed in the cross sections with insulation is much less than the depth in the standard section for the replacement method. Considering insulation efficiency only, it may be concluded that the control of frost penetration with insulation boards is rational and reasonable in the antifrost roads.

ESTIMATES AND ACTUAL MEASUREMENTS WITH INSULATION METHOD

To estimate depth of frost penetration in road pavements in winter, the modified Berggren formula is commonly used *(4)*:

$$Z = \lambda\sqrt{[172800F/(L/k)_{\text{eff}}]^{1/2}} \tag{1}$$

$$(L/k)_{\text{eff}} = (2/X^2)\{L_1d_1(d_1/2k_1) + L_2d_2[(d_1/k_1)(d_2/2k_2)] + L_3d_3[(d_1/k_1) + (d_2/k_2) + (d_3/2k_1)] + \ldots + L_nd_n[(d_1/k_1) + (d_2/k_2) + \ldots + (d_n2k_n)]\}$$

where

$x = d_1 + d_2 + d_3 + \ldots + d_n$ = estimated depth of frost penetration (cm),
d_n = thickness of each layer down to the estimated depth of frost penetration (cm),
d = thickness of the surface layer (cm),
k_n = thermal conductivity of each layer (cal/cm•sec•°C),
Ln = volumetric latent heat of fusion of each layer (cal/cm^3),

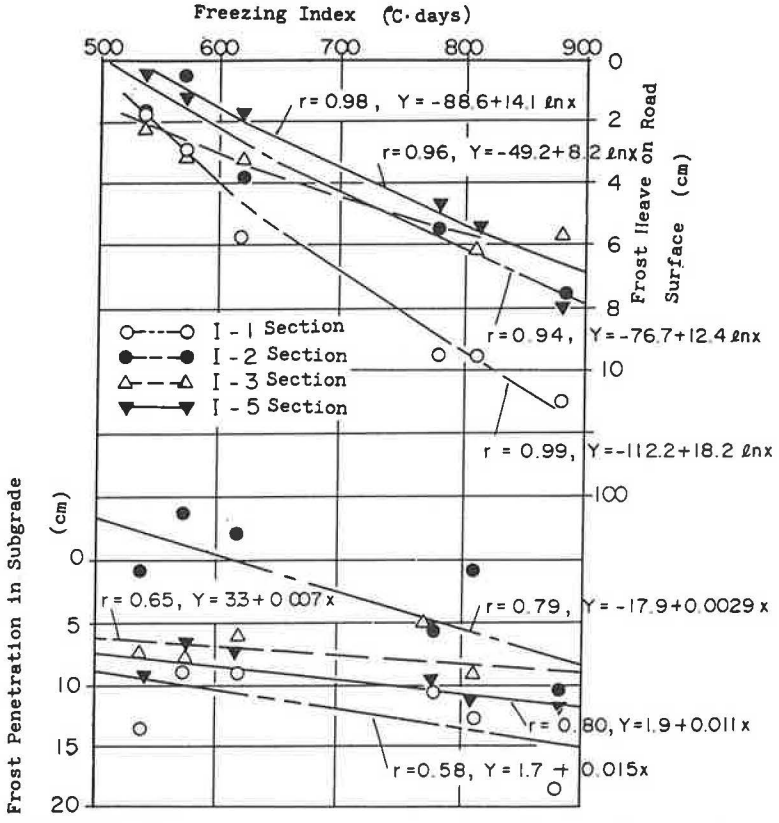

FIGURE 2 Frost heave and frost penetration of insulated test road.

F_n = freezing index (°C•days),
Z_n = depth of frost penetration (cm), and
λ = dimensionless coefficient.

The thermal conductivities of the crushed gravels, sands, and soils in the test roads shown in Figure 1 were calculated with the Kersten formula *(5)* based on the average dry density and moisture content obtained from actual measurements of national highways in Hokkaido. The values suggested by Ifukube *(6)* for the thermal coefficients of asphaltic concrete composed of surface, binder, and base courses and the insulation boards were used in the estimations. Table 1 shows the thermal coefficients used for calculating frost penetration depths in the test roads.

TABLE 1 THERMAL PROPERTIES OF MATERIALS USED IN BIBI TEST ROAD

Material	Thermal Conductivity k (cal/cm•sec•°C)	Volumetric Heat Q (cal/cm^3•°C)	Latent Heat of Fusion L (cal/cm^3)
Asphalt concrete	0.00346	0.448	0
Insulating board	0.00008	0.011	0
Gravel[a]	0.00779	0.483	5.28
Sand[b]	0.00376	0.389	9.80
Subgrade soil[c]	0.00279	0.626	50.40

[a] γ_d = 2.1 g/cm^3, w = 8 percent.
[b] γ_d = 1.75 g/cm^3, w = 7 percent.
[c] γ_d = 0.9 g/cm^3, w = 70 percent.

Figure 3 shows the relationship between estimated and observed frost penetration in the test road sections constructed with the insulation method and the replacement method, and it shows the relationship between freezing index and the estimates calculated with Equation 1. From Figure 3 it is clear that the estimated depth of frost penetration calculated with the modified Berggren formula is very close to the actual measurements, and it is possible to estimate the depth of frost penetration for the insulation method as accurately as for the replacement method.

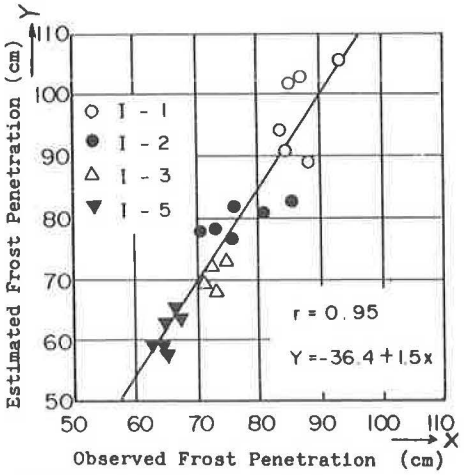

FIGURE 3 Relationship between estimated and observed frost penetration.

EXPERIMENTS

When a low-traffic road 75 km long was constructed in the Nemuro area of eastern Hokkaido, it was necessary to broaden the roadway with frost penetration control from 5.5 to 6.0 m. Winters are severe in this area and there is practically no snow until around March. Further, the soil in the road shoulder areas and subgrade has a high moisture content and is extremely frost susceptible. In this area, there are no good quality replacement materials such as crushed gravel or sand.

Under these restrictions, a new frost penetration control method combining the insulation method in the road shoulder (Figure 4) and the replacement method in the roadway (Figure 5) was introduced. With this method, it is necessary to determine the thickness and the placement depth of insulation

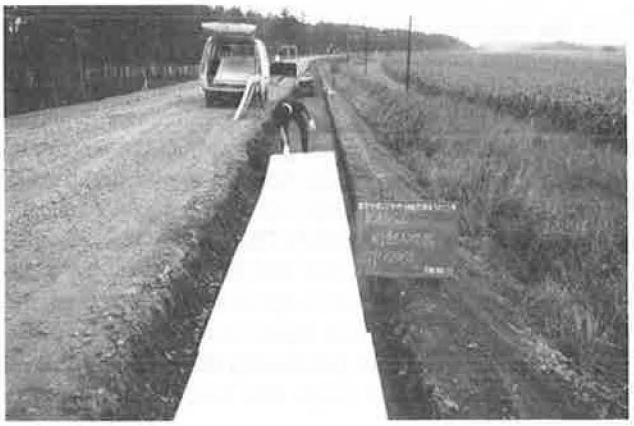

FIGURE 4 Placement of insulation boards in road shoulder.

boards used in the insulated areas. From a comparison of the cost of replaced materials for the standard pavement structures *(7)*, 25-mm-thick insulation boards were chosen for this experiment. The depth of placement of the insulation boards was determined from the difference between the frost penetration of the subgrade soil in the road shoulders and in the traveled roadway. The concept is to keep the frost penetration and heave in the shoulder and roadway the same to eliminate or minimize differential heaving. Figure 6 shows the relationship between freezing index and the depth of frost penetration calculated with the modified Berggren formula based on measured moisture content. From this figure, the replacement ratios of thickness of the replaced materials in the subgrade to the depth of frost penetration in the road shoulders and roadway, respectively, were calculated and are listed in Table 2.

From Table 2 the thickness of the sand layer on the insulation board in the road shoulder equivalent to the replacement depth in the roadway is 20 cm, and Figure 5 shows the required road pavement structure. This sand layer also satisfies the minimum thickness required for bearing the weight of the rolling equipment on the insulation boards. The insulation board was placed at a gradient of 2 percent away from the road center for drainage of water. On the test section constructed with this method, observations of frost penetration depth and frost heaving during winter were conducted for 2 years starting in 1981.

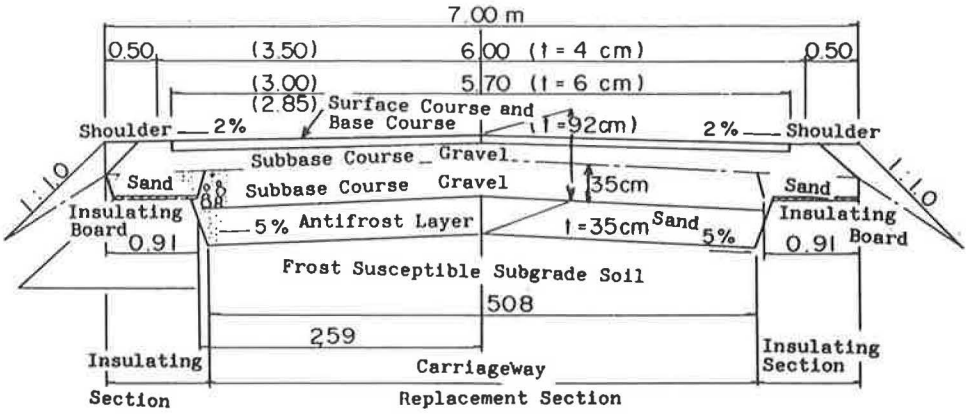

FIGURE 5 Antifrost measures with insulation and replacement methods.

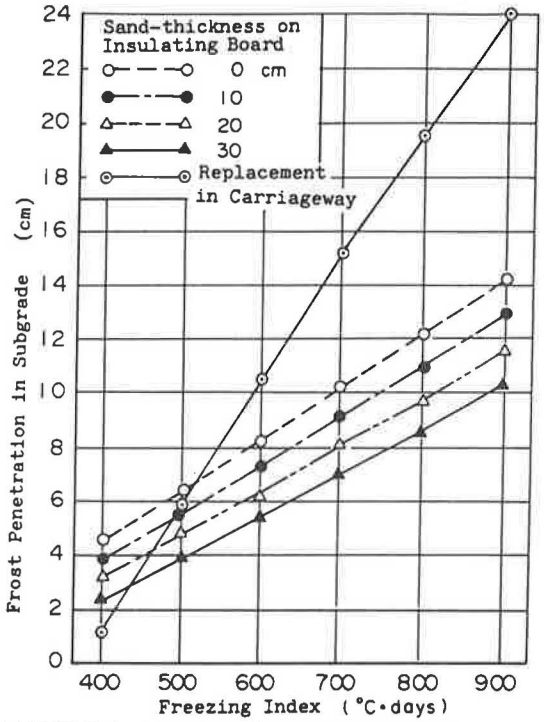

FIGURE 6 Relationship between freezing index and frost penetration in subgrade.

TABLE 2 REPLACEMENT RATIOS OF THICKNESS OF NON-FROST-SUSCEPTIBLE MATERIALS TO FROST PENETRATION IN PAVEMENT STRUCTURES

Sand Thickness in Shoulder (cm)	Replacement in Carriageway (%) by Freezing Index (°C•days)			
	600	700	800	900
0	90	86	82	79
10	85	82	79	76
20	89	86	84	81
30	92	90	88	86

DISCUSSION OF RESULTS

Figure 7 shows the depth of frost penetration and the amount of frost heave during winter in both road shoulder areas constructed with the insulation method and roadways constructed with the replacement method. From Figure 7 it was found that the maximum frost heave on the road surface in the middle of March was almost the same in both road shoulder and roadway. This suggests that the determination of the buried depth of the insulation boards was appropriate by equating the replacement rates in road shoulder and roadway.

Figure 8*a* shows changes of the frost heave transversely

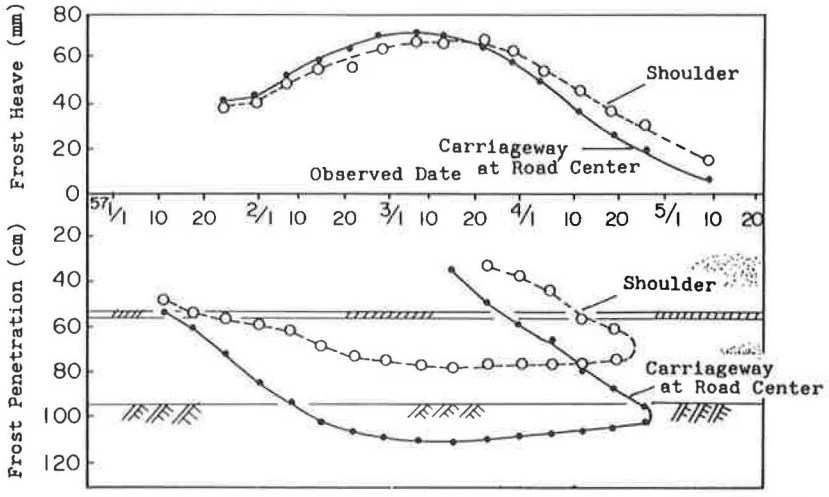

FIGURE 7 Frost heave and frost penetration in shoulder and carriageway.

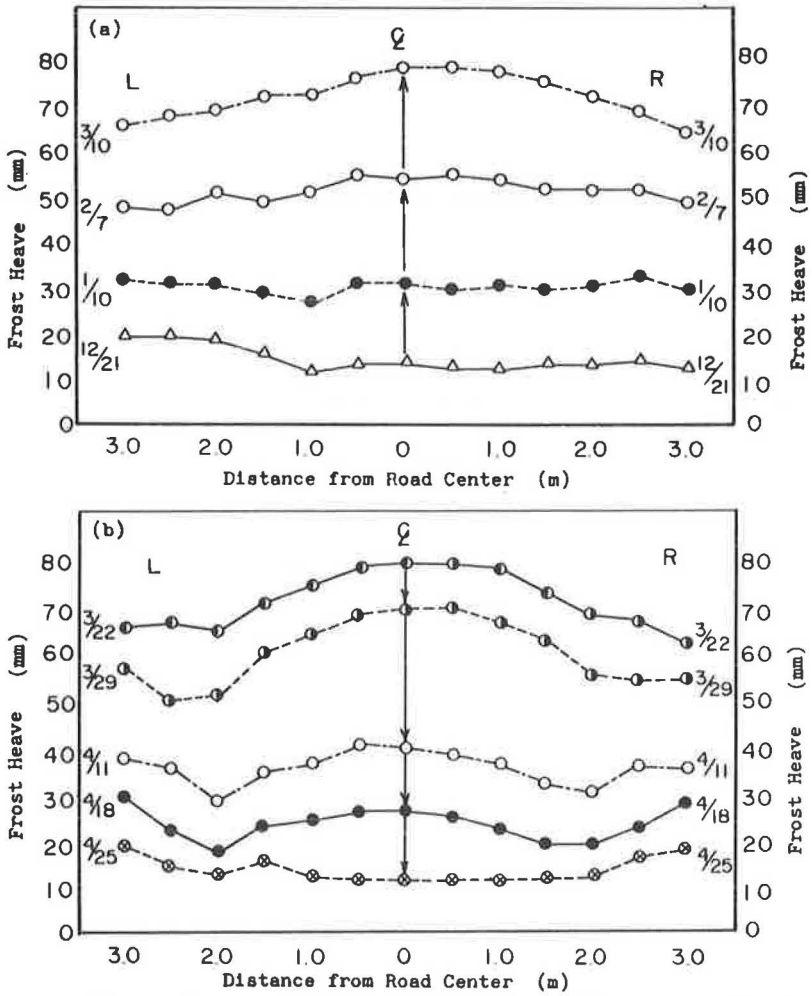

FIGURE 8 *(a)* Increase of frost heave in winter and *(b)* decrease of frost heave in spring.

across the road from December 21 to March 10 until the frost heave reaches the maximum. It shows that the amount of frost heave increases almost uniformly across the section until around February 7. However, in spring, as shown in Figure 8*b*, from the end of March to the end of April, the amount of frost heave does not decrease evenly across the section, but there is a sharp decrease at the 2-m point from the center of the roadway. This gap appears at the boundary between the road shoulder constructed with the insulation method and the roadway with the replacement method.

CONCLUSIONS

Research on a frost penetration control method that combines the insulation method in road shoulder areas and the replacement method in the roadway was conducted on roads with relatively light traffic. The results of the observation may be summarized as follows:

1. From the observations on the test road, it can be concluded that the insulation method may be practical to use for control of frost penetration in paved roads.

2. It is possible to accurately calculate the depth of frost penetration in a road constructed with the insulation method as well as that by the replacement method by using data on moisture content, dry density, and freezing index obtained with actual measurements and the modified Berggren formula.

3. Considering economy, construction, and the narrow width of the required roadway, the new method, which combines the insulation method applied in road shoulder areas and the roadway replacement method, is promising for control of frost penetration when existing gravel roads are both widened and paved. However, it is essential to consider the differences in the thawing of the frost heave that takes place in spring at the boundary between the insulation method and the replacement method.

ACKNOWLEDGMENT

Research engineers O. Sano and S. Yokochi of Dow Kako Company are gratefully acknowledged. The road pavement construction work was carried out under the Nohyochi Kaihatsu Kohdan in Hokkaido.

REFERENCES

1. H. Kubo. Prevention Measures from Frost Damages in Snowy and Cold Regions. *Journal of the Japan Society of Civil Engineers,* 1979, p. 2.
2. H. Kubo. Frost Heave in Road Pavements and Its Prevention Measures, Soil and Foundation (in Japanese). *Journal of the Japanese Society of Soil Mechanics and Foundation Engineering,* 1981, p. 2.
3. H. Kubo and T. Sakaue. "A Frost Damage Prevention Measure for Road Shoulders by an Insulating Method." Presented at 20th Japan National Conference on Soil Mechanics and Foundation Engineering, 1985.
4. H. P. Aldrich, Jr. "Frost Penetration Below Highway and Airfield Pavements." *Bulletin 135,* HRB, National Research Council, Washington, D.C., 1956, pp. 124-144.
5. M. S. Kersten. "The Thermal Conductivity of Soil." *HRB Proc.,* 1948.
6. M. Ifukube. *Studies on Frost Heave, Frost Penetration and Ratio of Replacement to Prevent Frost Damages of Roads in Hokkaido.* Civil Engineering Research Institute, Hokkaido Development Bureau, Sapporo, Japan, 1962.
7. *Manual for Design and Construction of Asphalt Pavement.* Japan Road Association, 1980.

Publication of this paper sponsored by Committee on Frost Action.

Determination of the Critical Thaw-Weakened Period in Asphalt Pavement Structures

JAMES A. MCBANE AND GORDON HANEK

Preliminary results of a soil-temperature monitoring program beneath asphalt-surfaced forest roads in northwest Montana indicate that the critical spring thaw-weakened period of a pavement structure can, in most cases, be identified by temperature alone. At all monitored locations, thawing below the pavement did not commence until the average soil temperature above a depth of 36 in., excluding the asphalt mat, had risen to approximately 30°F. Initial subpavement thawing was indicated by temperatures above the freezing point of local soilwater as measured at the asphalt–base course interface. Pavement strength values were equal to or greater than those recorded the previous fall when the depth of thaw had progressed to approximately 48 in. below the asphalt mat in areas underlain by nonplastic soils. This relationship was less clear in plastic soils. Utilizing this soil-temperature monitoring program, road managers have the means to forewarn facility users of the possible imposition of vehicle load restrictions. This program provides accurate identification of the onset of spring thaw weakening and allows an evaluation of the strength recovery as the critical period wanes.

Unseasonably warm weather in January 1984 resulted in the early development of a thaw-weakened state in the asphalt pavement structure of the Yaak 92 Forest Highway, Kootenai National Forest, Montana (Figure 1). The subsequent decision to impose vehicle load restrictions 3 to 4 weeks before the historical placement of such limits evoked adverse comments from local timber company representatives and construction contractors who regularly use the facility. Comments generally reflected an acceptance of the inevitability of spring closures; however, complaints of insufficient forewarning to allow equipment removal from the field or to plan springtime mill operations were universal. Concern was frequently expressed by the users that the road condition evaluations leading to the imposition of load restrictions were based on incorrect procedures and subjective judgments and that the shutdowns were premature.

Although the controversy lessened to a great extent when visible signs of pavement distress developed within days of the closure, it was apparent that to avoid similar problems in the future, the concerns expressed by the road users should be addressed. A program of monitoring temperature throughout the pavement structure was devised in response to the stated concerns. The system described in this paper was developed by

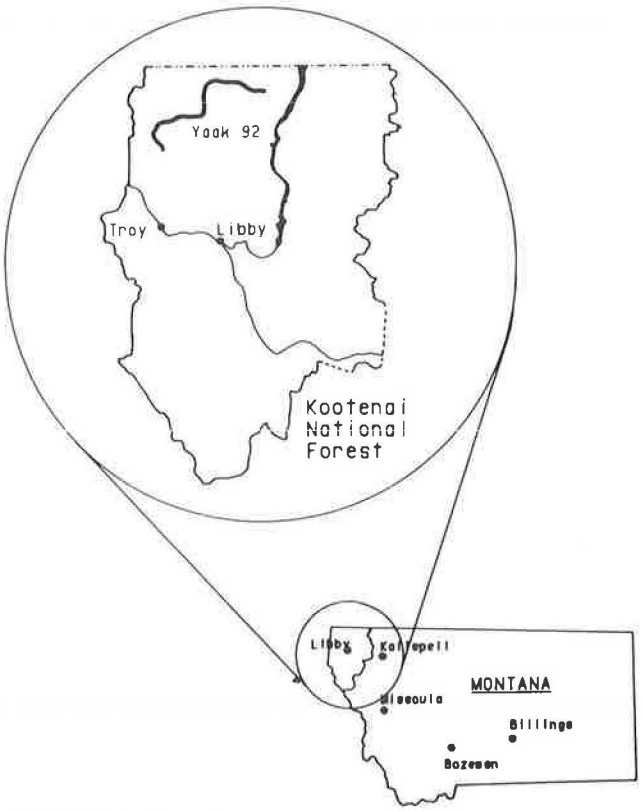

FIGURE 1 Location map.

combining the results of published research projects covering various aspects of the thaw-weakening phenomenon with the practical instrumentation and monitoring experience of agencies such as the Alaska Department of Transportation and Public Facilities. At the time of this writing, the instrumentation system had been operational on the Kootenai National Forest for one complete year.

Past research efforts aimed at developing methods for the identification of thaw-weakened conditions in pavement structures have resulted in procedures that were complex, expensive, labor intensive, or all three and that were difficult to implement in commonly encountered field settings. Public acceptance of road closure decisions based on these methods has been generally skeptical because of the lack of trust in systems not easily understood. The interrelation between temperature and thaw weakening has proven more readily apparent to most individuals than methods that must address soil moisture and excessive pore-water pressures.

The system components are inexpensive. Road networks can

J. A. McBane, Engineering Branch, Kootenai National Forest, Route 3, Box 700, Libby, Mont. 59923. Current affiliation: USAFEA-K, Building and Grounds Division, APO San Francisco, Calif. 96301-0082. G. Hanek, U.S. Bureau of Reclamation, Denver Federal Center, Box 25007, D-1542, Denver, Colo. 80225.

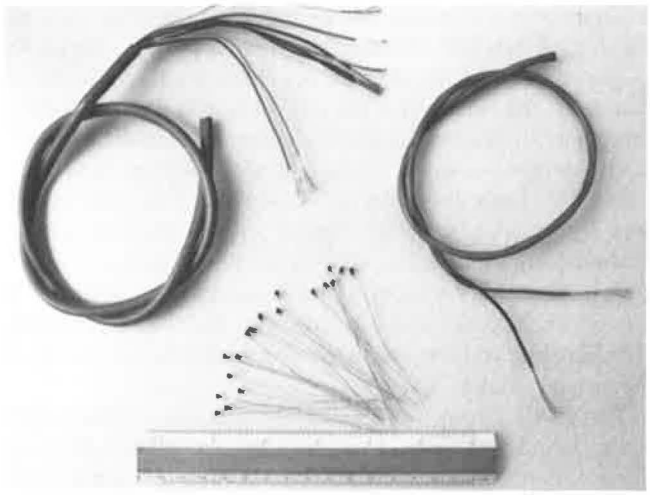

FIGURE 2 Instrumentation components: thermistors, eight-conductor cable, and two-conductor cable.

be completely instrumented at a very low cost, allowing individual road segments to be managed separately. Responsible personnel can determine whether portions of a road system may be left open to commercial use while other portions of the same system remain closed because of thaw-weakened conditions. Conversely, a road system may be reopened in segments as the instrumentation indicates strength recovery in specific areas. The duration of the closures may be shortened by the use of this system.

Finally, and most important, this system makes possible the accurate determination of the limits of the critical thaw-weakened period. Potentially destructive vehicle loads can be restricted during this more accurately defined time period, resulting in a reduction of typical spring thaw damage. A large savings in current yearly maintenance expenditures on asphalt-paved forest roads is anticipated as well as an extension of their serviceable lifetimes by years.

In short, this instrumentation system has proven to be accepted by the public and the industry and is inexpensive to install and maintain, accurate, and simple for nontechnical personnel to operate. The conservative management approach based on subjective methods can be replaced by an objective, accountable management approach easily understood by the road users. It provides increased flexibility to road managers and promises future savings in road maintenance and reconstruction expenditures.

INSTRUMENTATION

The system consists of a series of thermistors used to monitor temperature variations above, within, and below the asphalt mat. Thermistors are semiconductors consisting of epoxy-encapsulated metal oxides whose electrical resistance varies with fluctuations in temperature (Figure 2). These devices were selected because of their low cost and high degree of accuracy and interchangeability and because no special calibration or circuitry conditioning is necessary for operation. Instrumentation at each site consists of a minimum of eight sensors (Figure 3). The air temperature is monitored by a thermistor placed approximately 4 ft above the ground surface. Air probe thermistors are inserted into the center of opaque plastic tubes and mounted in the shade to prevent inaccurate readings due to direct sunlight (Figure 4). The mat temperature is obtained by a thermistor sealed within a saw cut 1.5 in. deep made in the asphalt surface. This depth represents the approximate midpoint of the new 2.5- to 3.0-in. thick hot-mix asphalt pavement recently completed on a large portion of the Yaak 92 Forest Highway (Figure 5). Each site is instrumented with a thermistor located immediately at the base of the mat. Spacing of succeeding thermistors follows a consistent sequence of 4, 9, 15, 21, and 33 in. below this sensor. At five sites, sensor strings include two additional thermistors 45 and 57 in. below the base of the asphalt. The exact depths of the temperature sensors are

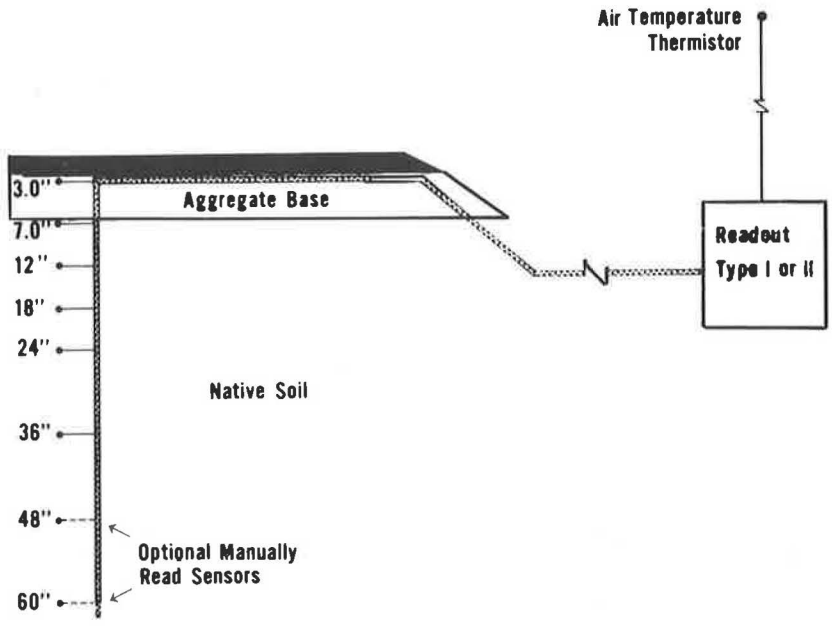

FIGURE 3 Instrumentation schematic.

FIGURE 4 Air probe, Site D2-92-38.0.

FIGURE 5 Yaak 92 Forest Highway: view south from Milepost 38.0.

governed by the thickness of the mat. Figure 3 shows thermistor depths for an idealized 3-in.-thick asphalt structure.

Ground thermistors are soldered into a multiconductor cable consisting of eight 22-gauge, multistrand, polyvinylchloride-(PVC-) insulated copper wires. One wire serves as a common ground for all sensors. Each remaining wire is connected to the second lead of the individual sensors (Figure 6). Air probe thermistors and the two bottom sensors at the five extended sites are wired into two conductor cables. The eight-conductor ground cable and the two-conductor air probe cable end at a 10-pin electrical connector placed within a junction box located near the shoulder of the road (Figure 7).

Monitoring is accomplished by removing the cover plate of the junction box and attaching the 10-pin connector (Figure 8) to one end of a switching unit. An electronic thermometer is attached to the other end of the unit (Figure 9). The thermometer operates by measuring the line resistance, converting resistance to temperature, and displaying the temperature in degrees Fahrenheit. Each thermistor on the string can be sequentially read by rotating the dial selector on the switching unit. Extended strings are equipped with two phono jacks within the junction box, one connected to the 4-ft sensor, the other to the 5-ft sensor. The electronic thermometer is detached from the switching unit and coupled to the phono jacks to monitor these thermistors (Figure 10).

The Yaak highway was divided into segments, each of which could be independently closed without significantly affecting the use of remaining segments. Within each division a minimum of two sites was selected for instrumentation. These represented areas anticipated to enter the critical thaw-weakened state early (locations exposed to direct sunlight for a large portion of the day) and areas expected to lag behind (shaded locations). In addition, instrumentation was installed in most major soil types and elevation extremes encountered along the Yaak highway. Seventeen instrument sites at an approximate density of one site every 3.5 mi were installed during the fall of 1984 along the Yaak 92 Forest Highway and adjacent paved roads.

TESTING AND MONITORING

The presence of dissolved minerals depresses the freezing point of water below the laboratory distilled value of 32°F; thus it was necessary to determine the actual soil moisture freezing point to use while the critical period was being monitored. Tests were performed on soil samples obtained from 8 of the 17 sites to determine the freezing point of local soil moisture. This testing is important because if too high a freezing value was assumed during monitoring, a significant amount of time could elapse, with thawing and associated damage to the pavement structure.

Soil samples were placed into glass test tubes. A thermistor was imbedded within the soil and the sample immersed in an ethylene glycol solution that had been cooled to +17°F. The temperature change of the soil was monitored by an electronic thermometer attached to the thermistor leads (Figure 11).

Cooling progressed through four distinct phases (Figure 12). The temperature of the sample decreased as the soil moisture

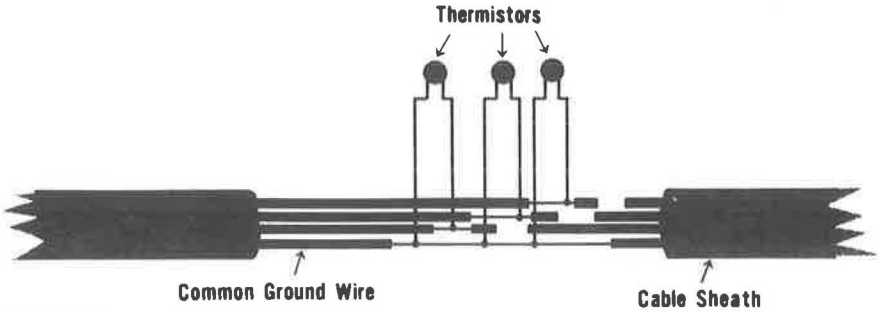

FIGURE 6 Generalized thermistor string wiring diagram.

FIGURE 7 Junction box, Site D2-92-38.0; note air probe on branch slightly above and left of junction box.

FIGURE 9 Electronic thermometer and switching box, Site D2-92-45.2.

system cooled. At the point of ice nucleation (the time when ice crystals begin to form) the temperature rose rapidly as heat was released during the phase change from water to ice. The temperature of the sample rose to a plateau where it remained constant while the moisture in the sample froze. This was recorded as the soil moisture freezing point. When all the soil moisture had been converted into ice, the temperature of the sample again decreased as the soil-ice system moved toward thermal equilibrium with the cold bath.

Test results indicated that the freezing point of soil moisture throughout the project area was 31.7 to 31.8°F. The conservative value of 31.7°F was used in all subsequent analyses.

Beginning in October 1984, air, pavement, and soil temperatures were recorded at least weekly at each site. This increased to approximately three times per week per site as ground and air temperatures rose immediately preceding the commencement of spring thaw in March. Accessibility problems caused by heavy snows and unplowed roads limited the frequency of monitoring at four of the sites to once per week throughout the winter and spring.

Pavement strength was measured by a series of Benkelman beam deflection tests (Figure 13). Testing began in late fall of 1984, ceased during the winter months, and was resumed in the spring of 1985. Deflection data were obtained at least weekly at

FIGURE 8 Ten-pin electrical connector at instrument string terminus and phono jacks for reading the 4- and 5-ft sensors, Site D2-92-23.95.

FIGURE 10 Electronic thermometer reading the 4-ft sensor, Site D2-92-45.2.

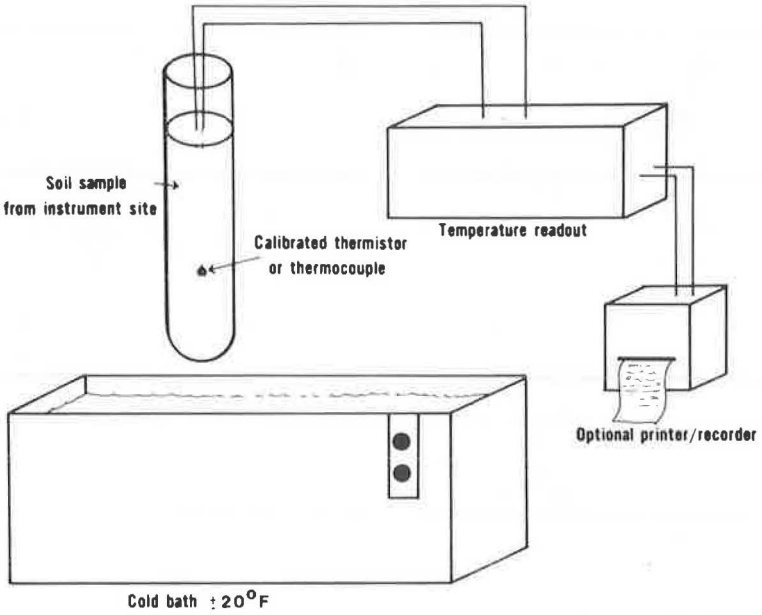

FIGURE 11 Laboratory setup for determination of groundwater freezing point.

accessible sites throughout the critical thaw-weakened period. The test vehicle was a three-axle, 8-yd^3 capacity dump truck loaded with 20,000 lb of steel railroad rails. The gross vehicle weight was 48,000 lb. A pressure of 70 psi was maintained in all ten 11.00×7-size tires. Testing was performed by placing the tip of a 12-ft-long Benkelman beam at the mid-point between the rear dual-wheel sets. Measurements were obtained at each site within the driving lane anticipated to carry the heaviest vehicle loads with a deflection reading obtained for each wheel track within that lane. Measured deflections for each given site and date were analyzed for each wheel track and then combined to obtain a site average deflection for entry into the *E*lastic *L*ayer *SY*ste*M* (ELSYM5) computer program.

The ELSYM5 computer program was used to compute stress and strain values at various points within the pavement structure from assumed and measured surface deflections. This program was selected because of its input option of up to 10 uniform loadings on the pavement, permitting deflections obtained from the nonstandard test vehicle to be analyzed. During the computer reduction of deflection measurements, four loads were input per deflection, one for each wheel load immediately adjacent to the Benkelman beam measurement point. Computer runs that included more than 4 of the test vehicle's 10 wheels as input provided results not significantly different from a four-load model and therefore were not attempted beyond the program testing. Additional program inputs include a description of the pavement structure to be analyzed (the number and thickness of layers), the material properties of each layer (modulus of elasticity and Poisson's ratio), and the spatial coordinates of points within the structure where data are desired. The program outputs values for stresses, strains, and displacements at the designated locations.

The program was used by attempting to match computer-generated surface deflections with field-measured deflections.

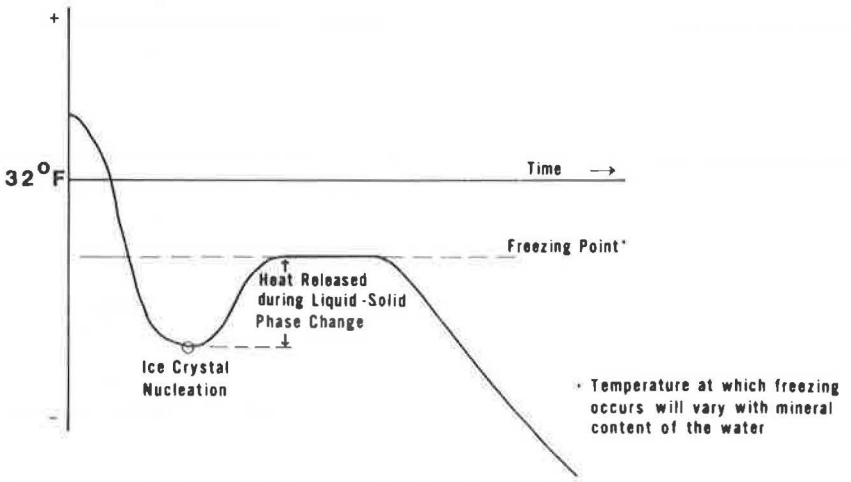

FIGURE 12 Generalized curve for freezing of water.

FIGURE 13 Benkelman beam deflection testing, Site D2-92-45.2.

The physical dimensions of the pavement structure and the material types present at each site were directly determined from drill corings. The test vehicle load magnitude and load spacing were also directly measured, leaving only the properties of the materials making up the structure as unknowns. Published values for resilient modulus and Poisson's ratio were input into the program for each structure layer to determine reasonable strength boundaries for the materials. The asphalt, base course, and subgrade soils were assumed to be drained and computer trials continued until the output deflection values matched actual deflections measured for each site in the fall.

Parametric studies performed using ELSYM5 to model a thaw-weakened pavement condition indicated that changes in the resilient modulus and Poisson's ratio of the thawing layer had the greatest effect on the calculated deflections. Variations in the asphalt parameters and the parameters of the frozen soil had very little effect. During the spring thaw period, input asphalt values were held approximately constant with only minor variations to account for differing pavement temperatures. Similarly, the frozen soil parameters varied only slightly to account for the warming ice. The thawing layer could then be incrementally analyzed for resilient modulus and Poisson's ratio values as its thickness increased throughout the critical period. When a satisfactory match was obtained between computer-generated and field-measured deflections for a given test date at a given site, the calculated horizontal strain value at the base of the asphalt mat was recorded (Table 1) and later used to develop a pavement strength parameter, the road damage factor, for presentation to the public.

The purchase of a diametral testing apparatus by the Forest Service Region I Materials Testing Laboratory early in the summer of 1985 provided the opportunity to determine the actual resilient modulus of the pavement asphalt. This allowed a comparison with the assumed values used in the computer analyses during the preceding spring thaw-weakened period. A total of 24 asphalt core samples with 3-in. diameter were obtained from 6 of the 17 sites. The cores were tested as received; no moisture conditioning was attempted. Tests were performed on samples cooled to 41°F and again at 77°F. Results are summarized in Table 2. Assumed resilient modulus values entered into the ELSYM5 program were within the range of test values obtained. Substitution of the measured values into the computer program did not affect the magnitude of resilient modulus changes calculated for the thawing layer as the critical weakened period progressed. It was the relative magnitude of the resilient modulus changes and their rate of occurrence, not the absolute values, that were of primary importance to this study.

RESULTS

The weighted average soil temperature was calculated from readings obtained from the six thermistors beginning with Thermistor 2, at the base of the mat, through Thermistor 7, located approximately 36 in. below the road surface for each site for each monitored date. The change in this average temperature from early October 1984 through late April 1985 at Site D2-92-30.6 is shown in Figure 14. This plot is representative of all noninsulated (plowed) sites. Thawing commenced when temperatures of 31.7°F occurred at the base of the asphalt. This value of 31.7°F at the base of the mat did not

TABLE 1 SAMPLE DATA: ELSYM5 INPUT AND OUTPUT, SITE D2-92-23.95, 1985

Date[a]	Pavement Deflection (in.)	Resilient Modulus (ksi)[b] by Layer 1	2	3	4	5	Strain (E-03)[c]
March 4	0.011	150	125	150	150	4.7	0.1007
March 12	0.028	100	3.5	125	150	4.7	0.6967
March 22	0.108	100	4	0.4	125	4.7	0.9913
March 29	0.086	80	7	0.83	125	4.7	0.9246
April 5	0.044	75	11	4.5	125	4.7	0.6823
April 8	0.042	60	11	6	125	4.7	0.7423
April 11	0.040	75	11.2	7	125	4.7	0.6478
April 17	0.040	75	11.2	8	10	4.7	0.6419
April 22	0.040	80	11.2	8	10	4.7	0.6267

[a]On March 4 the structure was totally frozen. On April 17 the structure was totally thawed.
[b]Layer 1 = 5.5 in. of asphalt. Layer 2 = 7.0 in. of base course [GP-GM, Unified Soil Classification System (USCS)]. Layer 3 = 15.0 in. of silt (ML USCS). Layer 4 = 22.0 in. of gravels and cobbles (GP, USCS). Layer 5 = silt (ML, USCS).
[c]Strain = maximum horizontal strain at the bottom of the asphalt mat.

TABLE 2 RESULTS OF DIAMETRAL TESTING

Site No.	No. of Asphalt Samples	Resilient Modulus (ksi) 41°F Range	41°F Avg	77°F Range	77°F Avg
92-23.95	3	–[a]	–[a]	–[a]	–[a]
92-30.6	6	394–2,557	1,274	144–367	267
92-35.55	3	1,863–2,010	1,921	234–288	254
92-38.0	3	600–855	699	315–380	355
92-45.3	3	793–1,079	936	350–400	372
92-49.4	3	447–1,089	742	304–423	373

[a]All samples failed during testing.

occur, as is shown by Figure 15, until the average soil temperature rose to approximately 30°F. This is an apparent consequence of the frozen material's efficiency in distributing incoming heat until sufficient energy has accumulated in the pavement structure to permit thawing of the base course. These initial results suggest that by developing graphs similar to Figure 14 through the late winter and early spring, it will be possible to project warming soil temperatures to determine the approximate date by which soil temperatures will reach the 30-degree threshold and predict within close limits when spring thawing will begin. The specific time can be identified by thawing temperatures recorded at the base of the asphalt. Road users can be notified in advance of impending load restrictions, and the commencement of spring thaw can be objectively demonstrated. In addition, the effects on instrumented roads of short-term weather changes such as the so-called "January thaw" of northwestern Montana can be accurately evaluated.

A relationship between depth of thaw and pavement strain was identified that allows the utilization of the soil temperature profile to monitor strength recovery near the end of the critical period. Figure 16 shows this relationship at Site D2-92-23.95. To better present strength loss and gain in a pavement structure to nontechnically oriented individuals, strain values derived from the ELSYM5 computer reduction of Benkelman beam deflection measurements were used to calculate road damage factors. A factor of 1.0 was assigned to the 18-kip equivalent axle loading value of the test vehicle when the pavement structure is in its fully recovered state, that is, in late summer. Damage factors other than 1.0 indicate the increased or decreased loading in 18-kip equivalents required under summer conditions to duplicate the calculated horizontal strain at the base of the asphalt for a given test date. The horizontal strain values were derived from the ELSYM5 computer analysis of measured Benkelman beam deflections. Values above 1.0 indicate a progressively weakening structure; below 1.0 they indicate increasing strength due to the presence of frozen ground directly beneath the mat. For example, a factor of 1.0 would indicate the relative impact on the road caused by a passing vehicle during the period of the pavement's maximum unfrozen structural strength in late summer. A factor of 10.0 indicates strength loss is such that the same vehicle has 10 times the pavement impact (damage potential) when compared with late summer values. The peak value in Figure 16 indicates that when the pavement at this specific site was at its weakest observed state, the foregoing vehicle would cause 17.6 times the impact relative to the recovered road condition. Calculations of the damage factor were based on the 48,000-lb three-axle Benkelman beam test vehicle using AASHTO 18-kip equivalent axle loads.

The rapid pavement strength loss accompanying the onset of thaw in the base course was typical for all sites tested and monitored. Within a very short time the load-carrying capacity of the pavement had dramatically decreased. The importance of placing vehicle restrictions at the beginning of base thawing is graphically illustrated by Figure 16 because even short delays will result in heavy vehicular loads traveling over a substantially weakened structure. Findings of the present study are consistent with conclusions reached in past research projects that indicated that pavement strength loss progresses swiftly as the base course begins to thaw *(1-4)*.

Strength recovery for all sites occurred with the same general pattern: an initial rapid strength gain followed by a period of more gradual improvement. At sites underlain by nonplastic soils, the change from the rapid primary recovery to the slower secondary recovery occurred when pavement strain values had returned to approximately prefrozen fall values. Thaw depths at the point of this change had progressed to between 3 and 4 ft below the asphalt mat. The conservative 4-ft value was used to

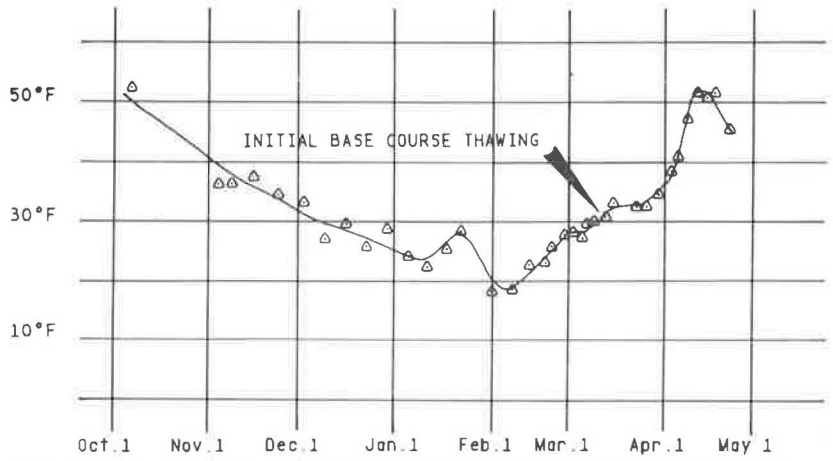

FIGURE 14 Average soil temperatures from base of asphalt to depth of 3 ft, Site D2-92-30.6.

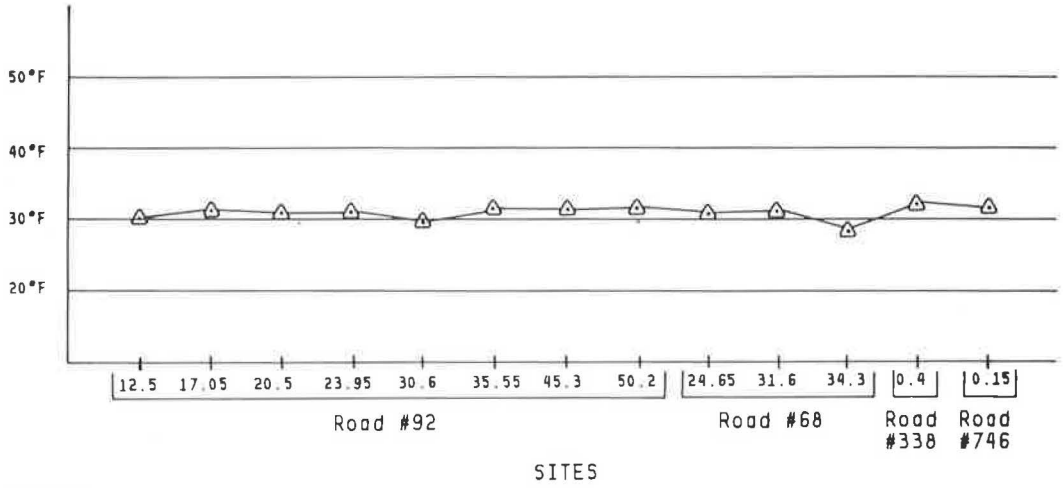

FIGURE 15 Average soil temperatures at commencement of base course thawing.

indicate recovered pavement strength for the purposes of this study (Figure 16). Data gathered after the first season of instrument monitoring strongly indicate that for pavements underlain by nonplastic soil adequate strength recovery has been achieved to allow removal of load restrictions when thawing reaches a depth of 4 ft. This is in close agreement with the results of similar studies performed by the Alaska Department of Transportation and Public Facilities (B. Connor, unpublished data).

At sites underlain by soils exhibiting plastic properties (Table 3), the change from primary to secondary recovery rates occurred at some strain value greater than the prefrozen fall value. Data to establish a reliable correlation between pavement strength recovery and depth of thaw under these conditions are currently insufficient.

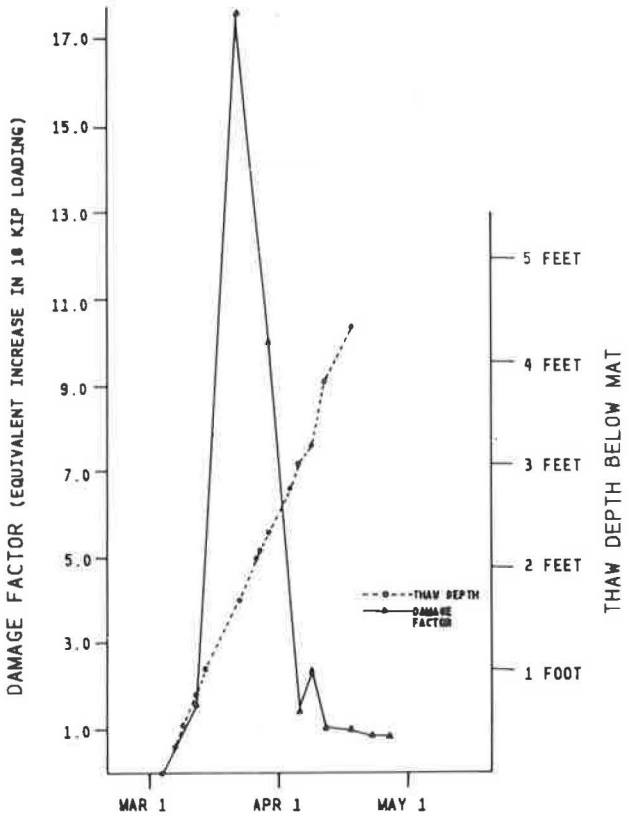

FIGURE 16 Damage potential versus thaw depth, Site D2-92-23.95.

CONCLUSIONS

Results obtained from one season of monitoring asphalt and soil temperatures as indicators of pavement structural strength during the spring thaw period suggest that road managers now possess a tool with which to address past problems involved with the imposition of seasonal load restrictions. Monitoring warming soil temperatures through the late winter and early spring allows a reasonable prediction to be made of the expected onset of pavement weakening. Road users have the opportunity to remove equipment from the field and to plan their springtime activities. Commencement of spring thaw can be accurately and objectively confirmed by the occurrence of temperatures above the freezing point of local soil moisture measured at the base of the asphalt mat. In areas of nonplastic soils the recovery of pavement strength can be indirectly determined by monitoring the depth of thaw. When thawing progresses to approximately 4 ft below the base of the asphalt mat, vehicle load restrictions can be removed. Finally, this method can be used to evaluate the effects of short-term weather fluctuations on pavement load-carrying capacity. Large decreases in annual maintenance costs and extended road ser-

TABLE 3 PROPERTIES OF PLASTIC SOILS ALONG YAAK 92 FOREST HIGHWAY, KOOTENAI NATIONAL FOREST, MONTANA

Unified Soil Classification System Symbol	Plastic Limit (%)	Liquid Limit (%)	Plasticity Index	Percent Passing No. 200 Sieve
ML-CL	22	29	7	87.5
ML-CL	20	26	6	56.5
GM-GC	21	27	6	43.0
GC	19	28	9	35.1

viceability are anticipated from the implementation of this inexpensive system. Cost of installation per site in 1984 was approximately $240, which includes all parts, equipment, and labor.

Additional work is currently under way to confirm the correlation between depth of thaw and pavement strength recovery in geographical areas outside northwest Montana, to check the reliability of projecting average soil temperature, to predict the onset of the spring-thaw period under a wider variety of climatic conditions than was possible in the present program, to test the results obtained from variations in the thermistor spacing on the instrument strings, and to evaluate the long-term survivability of the system. In addition, the relationship between thaw progression and pavement strength recovery in areas underlain by plastic soils is being investigated.

REFERENCES

1. R. N. Stubstad and B. Connor. *Prediction of Damage Potential on Alaskan Highways During Spring Thaw Using the Falling Weight Deflectometer.* Report AK-RD-83-11. Alaska Department of Transportation and Public Facilities, Juneau, 1982, 22 pp.
2. H. L. Jessberger and D. L. Carbee. "Influence of Frost Action on the Bearing Capacity of Soils." In *Highway Research Record 304,* HRB, National Research Council, Washington, D.C., 1970, pp. 14–26.
3. T. C. Johnson, D. M. Cole, and L. H. Erwin. "Characterization of Freeze/Thaw-Affected Granular Soils for Pavement Evaluation." In *Proc., Fifth International Conference on Structural Design of Asphalt Pavements,* University of Michigan, Ann Arbor, 1982, pp. 805–817.
4. T. C. Johnson, R. L. Berg, and C. W. Kaplar. *Roadway Design in Seasonal Frost Areas.* Technical Report 259. U.S. Army Corps of Engineers Cold Regions Research and Engineering Laboratory, Hanover, N.H., 1975.

Publication of this paper sponsored by Committee on Flexible Pavements.

Frost Action Predictive Techniques: An Overview of Research Results

T. C. JOHNSON, R. L. BERG, AND A. DIMILLIO

A 6-year research program has materially advanced the state of knowledge regarding frost heave and thaw weakening affecting roads and airfield pavements. The investigations included development and performance of laboratory tests, development of computer models, testing and data collection at field pavement test sites, and validation of the laboratory procedures and computer models against field data. Specific advances include development of a new freezing test to assess the frost susceptibility of soil; development and validation of a mathematical model serving to predict frost heave and thaw consolidation; development of a laboratory test procedure to determine the resilient modulus of frozen, thawed, and recovering granular soils; and conceptualization and testing of a technique for combining the frost heave and thaw consolidation model, the laboratory resilient modulus test, and a pavement response model to predict the nonlinear resilient modulus of granular soils and base course materials as variables in time and space.

Six years of intensive research have materially advanced the state of knowledge of frost action on pavement performance and its application to the prediction of such effects. The two principal adverse effects of frost are ice segregation, causing heave and transient pavement roughness, and thaw weakening of subgrade and unbound base materials, causing accelerated pavement cracking and pavement deformation. It has long been an important goal not only to improve the empirical approaches for management of these problems in designing pavements but also to develop quantitative methods for predicting the surface heave that a given trial pavement section would experience and for evaluating the seasonal changes in supporting capacity of subgrade and base materials that would affect pavement performance under traffic loads *(1, 2)*.

Having a common interest in these goals, three agencies jointly sponsored the research: FHWA, FAA, and the U.S. Army Corps of Engineers *(3)*. The research, which spanned the period from late 1978 through 1984, included equipment development, field and laboratory experiments, and development of mathematical models. The investigations were directed to four principal study areas:

1. Selection and validation of the most effective laboratory index tests to serve as indicators of the susceptibility of soils to detrimental frost action,
2. Development of a soil column device with provisions for nondestructive monitoring of changes in soil moisture content and density during freezing and thawing,
3. Improvement and validation of a mathematical model of frost heave that had been developed earlier and incorporation of processes that take place during and after thawing, and
4. Development of laboratory test methods for the characterization of seasonal changes in resilient modulus of a wide range of types of granular soil and validation of these methods by means of in situ deflection testing of pavements.

The research was performed by the U.S. Army Cold Regions Research and Engineering Laboratory (CRREL). Key investigations were conducted by consultants on certain phases of the work, and a board of general consultants who provided guidance and periodic review of the accomplished work was also assembled. The laboratory testing and analysis were conducted at CRREL's facilities in Hanover, New Hampshire, and field sites at Winchendon, Massachusetts, and Albany County Airport, New York, were used for in situ testing and data collection.

The research findings are summarized for each of the four study areas, and reference is made to other reports for details of the investigations.

FIELD TEST SITES

Field test sites were needed to serve as a source of samples of subgrade soils and base materials for roads and airfield pavements and as test beds where the performance of these soils and materials in pavement sections could be monitored and tested under varied conditions of temperature, moisture, and freeze-thaw action and under applied loads. Two sites were used for these purposes.

The first site is the Winchendon, Massachusetts, test site, constructed in 1978 by the Massachusetts Department of Public Works (MDPW) and consisting of 24 soil test sections. The six test sections used in this research consist of about 50 to 90 mm of asphalt concrete and 1.5 m of one of six test soils overlying the natural subgrade, a clean gravelly sand (see grain-size curves, Figure 1). The water table is at a depth of about 1.4 m below the pavement surface. Data were collected from each of the six test sections *(4, 5)* during the freeze-thaw-recovery seasons of 1978–1979 and 1979–1980. The data included temperatures at various depths, depth of frost, state of stress in soil moisture monitored by means of tensiometers at various depths, vertical displacement of paved surface caused by freezing and thawing, and vertical displacement of paved surface under load measured by repeated-load plate-bearing (RPB) tests and by falling weight deflectometer (FWD) tests.

The second test site is at Albany County Airport, located 9.6 km (6 mi) north of the city of Albany, New York, where two pavements were selected for field testing. Taxiway A is a new

T. C. Johnson and R. L. Berg, U.S. Army Cold Regions Research and Engineering Laboratory, Hanover, N.H. 03755-1290. A. DiMillio, FHWA, U.S. Department of Transportation, Washington, D.C. 20590.

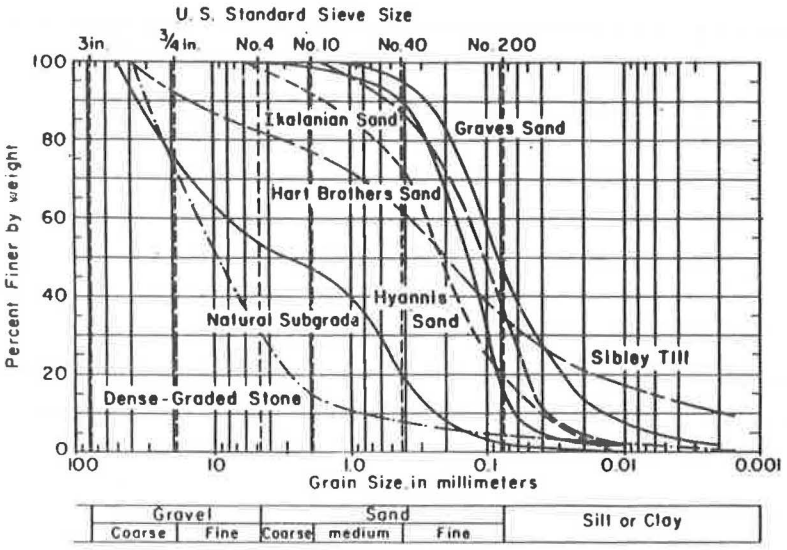

FIGURE 1 Grain-size distributions of Winchendon test soils and natural subgrade.

pavement for which the cross section consists of 330 mm of asphalt concrete, 584 mm of crushed-stone base, and 914 mm of gravelly sand subbase over a subgrade of silty fine sand (Figure 2).

Taxiway B, constructed many years ago (possibly in the 1940s), is no longer in use. The surface is uneven and the asphalt concrete is aged and severely cracked. The asphalt concrete is 76 mm thick and overlies about 102 mm of deteriorated asphalt penetration macadam stone base and 127 mm of gravel subbase. The subgrade is silty fine sand. Samples of the subbase whose composite grain-size distribution is shown in Figure 2 were taken to represent a single 229-mm base-subbase layer.

Data were collected at Albany County Airport from 1979 to 1983 of the same types noted previously for the Winchendon site. The Winchendon and Albany County Airport sites were also used as sources of samples for related laboratory tests. Core samples of the asphalt concrete of 102-mm diameter were taken, and 57-mm diameter undisturbed samples of the finer soils were obtained in the fall before freeze-up. Once frost had advanced to sufficient depth in the sections, core samples of the frozen soil were taken, except for those materials containing numerous gravel-size fragments, in which case specimens of appropriate size were frozen in the laboratory. Bulk samples of about 40 to 50 kg also were obtained from each soil and base material.

FROST SUSCEPTIBILITY INDEX TESTING

Frost susceptibility index tests allow geotechnical engineers to assess the potential for frost heave and thaw weakening of subgrade soils and unbound base and subbase materials in roads and airfields. In a survey of transportation departments throughout the world (*6–8*,pp.105–142), it was found that most agencies have developed their own unique frost susceptibility index criteria based on laboratory tests, that these criteria fail to discriminate marginally frost-susceptible material from material that is frost susceptible, and that there is little documentation of the efficacy of the adopted standards. Furthermore, most of the various tests consider only frost heave or thaw weakening rather than both, and most of those that employ laboratory freezing tests require excessive time and impose poor control of test conditions.

The objective of this study was to identify the best index test methods for fully characterizing the frost susceptibility of soils. To accomplish this task, a thorough review of frost susceptibility index tests and practices of transportation agencies was made. The index tests were categorized into three types or levels of complexity. One test from each of three types was selected for further evaluation, including the U.S. Army Corps of Engineers frost design soil classification system *(9)*, a moisture-tension–hydraulic-conductivity test, and a new freeze test including both frost heave and thaw weakening elements. For evaluation purposes these tests were conducted on the materials from the Winchendon and Albany test sites. Early results of moisture-tension–hydraulic-conductivity tests were inconclusive, however *(10)*, which led to the conclusion that this test was not suitable for routinely determining the frost susceptibility of soils. The results of the other tests were compared with field observations of frost heave and thaw weakening at the test sites and the validity of each test was determined. The procedures for the selected tests and the analysis of the data are given by Chamberlain *(10)*.

Development of New Freezing Test

From the literature review it was concluded that all freezing tests currently in use have serious faults. It was decided to develop an improved test, for which the following objectives were established:

1. The test should be as simple as possible, of short duration, and provide reliable results.
2. The test conditions must bear a relation to freezing conditions in the field and to thaw weakening.

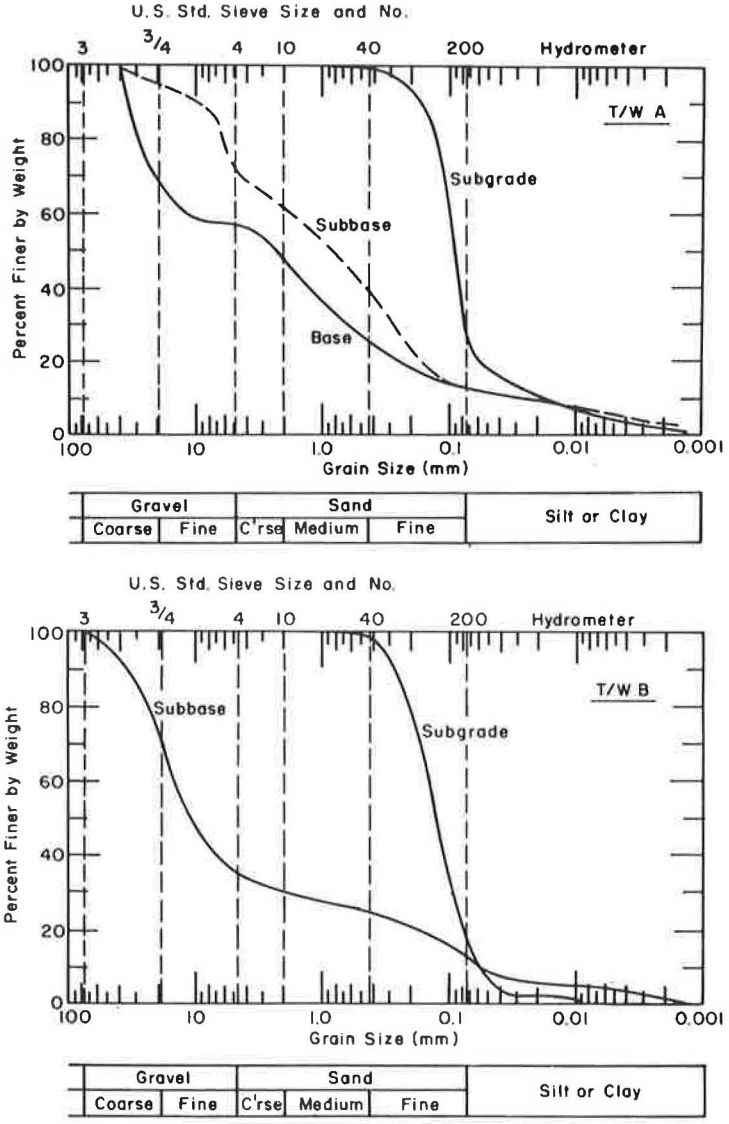

FIGURE 2 Grain-size distribution, materials from Taxiways A *(top)* and B *(bottom)*.

3. The test must accommodate the complete range of material types from granular base and subbase materials to fine-grained subgrade materials.
4. The apparatus should be inexpensive to construct and operate.

The equipment developed under these guidelines (Figure 3) includes a rubber-membrane-lined, multiring freezing cell to minimize side friction, liquid-cooled cold plates for precise top and bottom boundary temperature control, and a data acquisition and control system for automated temperature control and data processing. The test imposes two freeze-thaw cycles to account for the changes in susceptibility to frost heave caused by a prior freeze-thaw cycle, and a California bearing ratio (CBR) test is conducted after the second thaw to provide an index of thaw weakening. The test duration is 5 days. The heave rate at the end of 8 hr of freezing is used as an index of frost heave susceptibility. As will be seen, both indexes must be used to determine the frost susceptibility of a soil. Details of the test and the procedures are provided by Chamberlain *(11)*.

Results by Existing Methods

The frost susceptibility ratings according to three existing methods are shown in Table 1, ranging from *N* (negligible) to *VH* (very high). The range of frost susceptibility ratings varies widely and does not appear to be strongly related to either heave rate or pavement deflection observed in the field.

Results of New Freezing Test

Four freezing tests were conducted on each of the Winchendon soils and two on each of the Albany materials. The frost heave rates for three of the soils were significantly greater during the

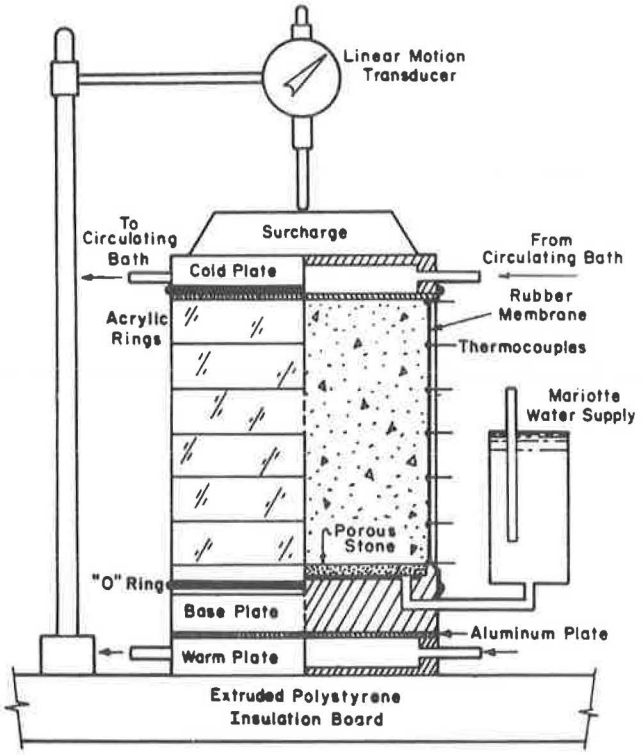

FIGURE 3 Schematic of new freezing test apparatus.

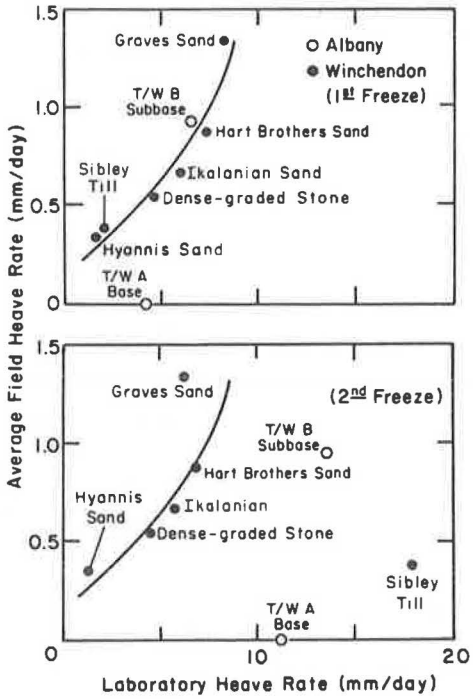

FIGURE 4 Comparison of laboratory and field heave rates during first and second freeze.

second freeze. For two of the soils [Taxiway (T/W) A base and T/W B subbase] the heave rate increased by factors of 2 to 3, whereas for Sibley till it increased by a factor of 9 from one of the lowest heave rates observed (2 mm/day) to the highest (18 mm/day). This illustrates the importance of including the second freeze-thaw cycle in this test.

Results of the tests showed that the CBR values for most of the soils were reduced by two cycles of freezing and thawing. Again the detrimental change was greatest for the Sibley till material, the reduction in CBR being by a factor of 8.5.

Discussion of Results

Comparisons of the laboratory and field frost heave rates are shown in Figure 4. With the exception of the T/W A results, there is a strong correlation between these heave rates for the first freeze-thaw cycle. The correlation is not on a line of equality, because the laboratory heave rates exceed the field values by a factor of 10 or more. However, because it was the intent of this study to use the freezing test qualitatively as an index test, not a quantitative predictor of frost heave in the field, the differences are not considered significant. When the results are plotted for the second freeze, the correlation between the laboratory and field results becomes weaker.

The correlation between the CBR after thawing and the maximum resilient pavement deflection during thawing (Figure 5) is better than the correlation between the frost heave parameters. In this case, all the average values of deflection fall close to a straight line showing inverse proportionality with CBR after thawing.

The comparisons shown in Figures 4 and 5 clearly show the

TABLE 1 SUMMARY OF FROST SUSCEPTIBILITY RATINGS ACCORDING TO ALL CRITERIA

Site and Material Type	Existing Methods: Corps of Engineers Grain Size Classification	Existing Methods: Comparison with Tabulated Data	Existing Methods: CRREL Freeze Test	New Freezing Test: 8-hr Heave Rate, First Freeze	New Freezing Test: 8-hr Heave Rate, Second Freeze	New Freezing Test: Thaw CBR	Range of Field Observations: Heave Rate	Range of Field Observations: Pavement Deflection
Winchendon								
Dense graded stone	VL-H	H	M	M	M	M	M	
Graves sand	L-H	H	H	H	M	VH	L-H	H-VH
Hart Brothers sand	VL-H	L	H	M	M	H	VL-M	H
Hyannis sand	N	N	L	VL	VL	M	N-L	M
Ikaianian sand	VL-H	L	M	M	M	H	VL-M	H-VH
Sibley till	VL-H	L-M	L-M	VL	VH	VH	N-VL	H-VH
Albany								
T/W A base	N-H	M-H	M	M	H	L	N	N
T/W B subbase	VL-H	L-M	H	M	H	M	L	H

Note: N = negligible; L = low; VL = very low; M = medium; H = high; VH = very high.

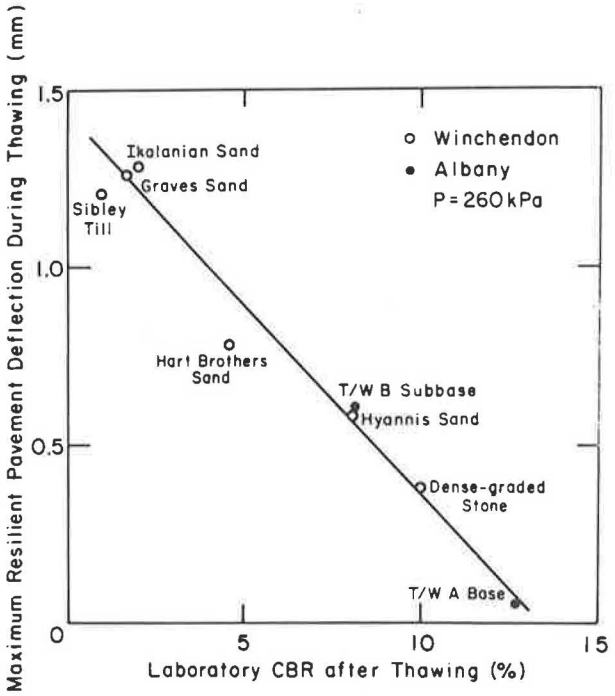

FIGURE 5 Comparison of CBR after thawing with maximum resilient pavement deflection during thawing.

need for including a thaw weakening indicator as a frost susceptibility index in the laboratory freezing test. If the heave rate from the first freeze were used alone to determine the frost susceptibility of the Sibley till soil, it would have been concluded that it was non-frost-susceptible. On the basis of results of the second freeze, the CBR after thawing, and the pavement deflection under load in the field, this soil is clearly frost-susceptible.

Preliminary frost susceptibility classification criteria for the new freezing test, based on the 8-hr frost heave rate during the first freeze and the CBR after two cycles of freezing and thawing, are as follows. Because the criteria were established on the basis of the comparison of a limited number of laboratory and field tests, they are tentative and subject to further confirmation.

Frost Susceptibility Classification	*Heave Rate (mm/day)*	*Thaw CBR (%)*
N	<1	>20
VL	1-2	20-15
L	2-4	15-10
M	4-8	10-5
H	8-16	5-2
VH	>16	<2

Conclusions Regarding Index Tests

It is clear from this study that to determine most accurately the frost susceptibility of a soil, it is necessary to conduct a freezing test. Although the Corps of Engineers soil classification method is useful for separating non-frost-susceptible soils from frost-susceptible soils, it does not discriminate well their degree of frost susceptibility, and it cannot be effectively used to predict the degree of thaw-weakening susceptibility.

The heave rate in the laboratory freezing test can be used to determine the frost heave susceptibility in the field, and the CBR value after freezing and thawing is a strong indicator of field thaw weakening leading to increased resilient pavement deflection under load.

The freezing test proposed is a workable candidate for replacing the Corps of Engineers standard freezing test because it requires much less time to conduct (5 versus 14 days), it provides much better boundary temperature control, it eliminates the side-friction problem prevalent in the current standard test, it provides an indicator of thaw-weakening susceptibility as well as an indicator of frost heaving susceptibility, and it allows the determination of the effects of repeated freezing and thawing.

SOIL COLUMN AND DUAL GAMMA SYSTEM

Design Features

It has long been known that moisture content and density change significantly when soil freezes. Changes in these variables need to be evaluated in time and space because they contain critical parameters in heat and mass transfer during freezing and thawing. A soil column and dual gamma system were constructed to generate such data from laboratory tests. The data were then used to develop, verify, and refine the mathematical model of frost heave and thaw settlement.

Figure 6 is a schematic drawing of the soil column. Three separate devices of this general type were fabricated and used. Their interior dimensions were about 50 mm in diameter, 135 mm in diameter, and 100 mm by 100 mm square, respectively. The columns consisted of segments each 300 mm long, which were stacked one on the other to provide any desired length from 900 to 1500 mm. The upper 300 mm of the column was tapered to reduce side friction that developed as freezing occurred from the top downward *(12)*. Details of the soil column, test procedures, and some early test results were given by Ingersoll and Berg *(13)*.

A dual gamma system was designed to be used with the soil column. Its primary purpose is to nondestructively monitor changes in density and moisture content with time and vertical position during freezing and thawing of soils in the soil column. The system *(14)* consists of two nuclear sources, an electronic detector to monitor gamma radiation from the sources (Figure 7), a tower to position the sources and detector vertically, and electronic equipment to control, monitor, and record data from the system.

Testing

Several tests were run on soils from the Winchendon site and other soils, and results were used as one source of data for validation and refinement of the frost heave model, a mathematical model of coupled heat and moisture flow *(13)*. During late 1984 and 1985, two special tests were conducted using the soil column and dual gamma system whose objectives were to monitor changes occurring during thaw *(15)*.

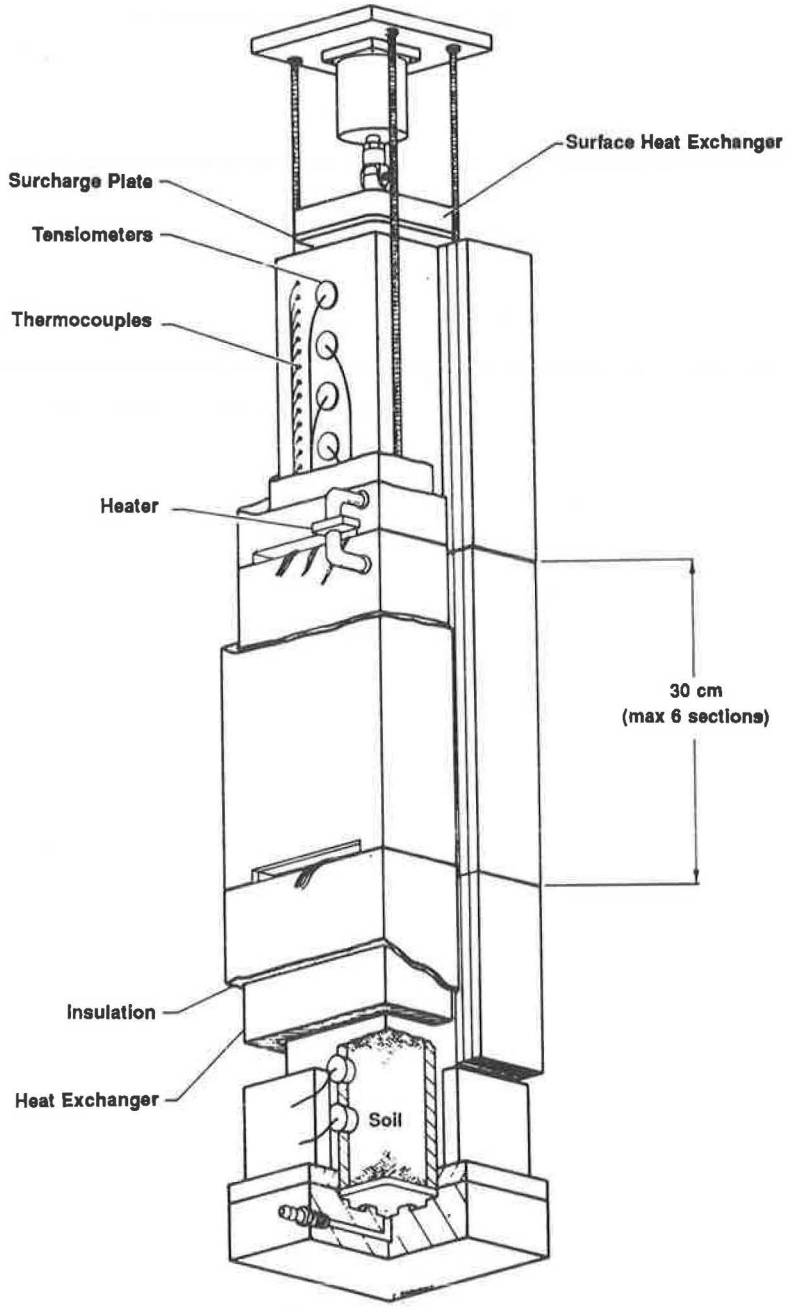

FIGURE 6 Soil column (schematic).

In addition to settlements during thawing (Figure 8), changes in temperature and moisture stress were also monitored. Slight positive pressures were observed in both tests before the entire frozen layer was thawed. When thawing was complete, water drained downward into the underlying soil. The results of the tests were used as a data set for refinement and validation of the thaw settlement portion of the frost heave model. The simulated settlements, temperatures, and moisture stress obtained by use of the model agree reasonably well with the observed values.

MATHEMATICAL MODEL OF FROST HEAVE AND THAW SETTLEMENT

Model Development

The model assumes one-dimensional vertical heat and moisture flux. Its development was reported earlier *(5, 12, 16–21)*. The model is intended for use on problems of seasonal freezing and thawing of nonplastic soils beneath pavements in which frost does not penetrate deeply into soils beneath the water table.

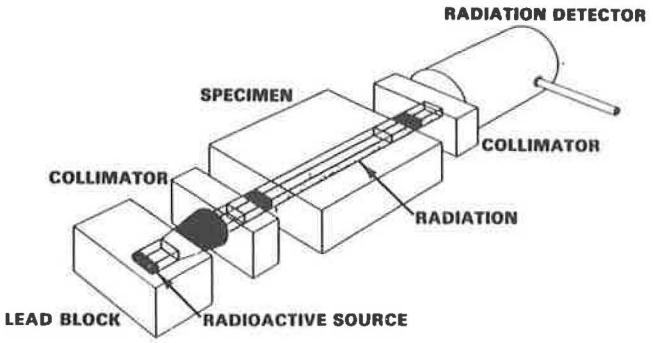

FIGURE 7 Dual gamma system (schematic).

Furthermore, it is intended for use where surcharge effects are not large (usually less than 60 kPa).

The main assumptions embodied, the governing equations, boundary and initial conditions, numerical approach to simulation as a system of finite elements, probabilistic concepts, and interim results of verification trials of the frost heave model have been presented in the reports referenced earlier. The latest version of the model has been summarized by Johnson et al. *(15)* and Guymon et al. *(22)*. The most recent development includes the incorporation of a submodel for thaw settlement. A principal objective of the submodel is the prediction of the generation and dissipation of pore-water pressures during and after thawing and the build-up of moisture tension during subsequent recovery from the thaw-weakened condition.

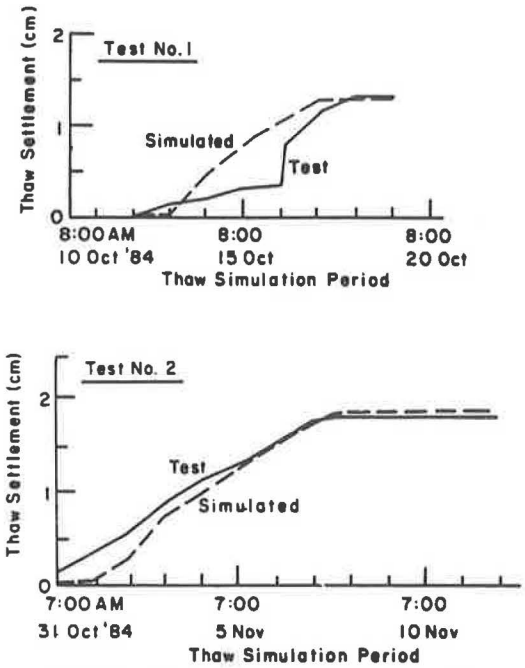

FIGURE 8 Thaw settlements observed in two soil-column tests on Graves sand.

Conceptual Basis for Thaw Settlement Algorithm

The concepts advanced by Morgenstern and Nixon *(23)* provide the framework for the thaw settlement and pore-water pressure algorithm presented here. The Morgenstern and Nixon model is based on well-known theories of heat conduction and of linear consolidation of compressible soils. Terzaghi's one-dimensional consolidation theory was applied to develop a moving boundary solution applicable to permafrost soils that thaw and consolidate under the application of load. A closed-form solution was obtained.

This application of the model is directed to layered systems of well-compacted soil. Consequently the application is restricted to winter heaving of subgrade soils and spring thaw settlement originating in those same soils with no net consolidation or change in pavement elevation occurring over a sequence of several years of freeze-thaw action.

A departure from the Morgenstern and Nixon model is the solution of the linear governing equation of excess pore-water pressure (Terzaghi's equation) numerically rather than exactly. The numerical code for this solution already exists in the frost heave model. This method allows more flexibility in handling the upper surface pore-water pressure boundary condition. A second departure of the method proposed here from that of Morganstern and Nixon is the use of a more general heat transport equation.

The equations composing the basis of the algorithm for estimation of thaw settlement and of pore-water pressure during and after thawing are given by Guyman et al. *(22)*, as are the boundary conditions and other assumptions.

Model Verification and Assessment

Model verification has been a continuing process since completion of early work on formulating the model reported elsewhere *(16)*. Details have been presented by Guymon et al. *(5, 18, 19)*, including comparison of simulations with both laboratory and field data.

The results from the model demonstrate that for different soils ranging from silts to relatively coarse-grained and marginally frost-susceptible soils, good results can be obtained with the model. To achieve such results, however, good estimates of hydraulic parameters are required. Judgment is required in assigning appropriate values, because considerable error may occur in the most carefully measured soil parameters, particularly unsaturated hydraulic conductivity.

Also, use of the model requires calibration of the hydraulic conductivity correction factor *(E)*, a phenomenological correction factor for freezing soil. Assuming that sufficient measurements were available for partly frozen soil so that hydraulic conductivity could be related to freezing temperature or ice content, it is conceivable that such data could be used instead of the phenomenological relationship.

The model also requiries an estimate of the moisture tension in the freezing zone. This is done indirectly through the selection of a residual (unfrozen) water content for the frozen zone and by calculating the corresponding pore-water tension by the

Gardner *(24)* equation. Generally values of residual water content are selected so that the moisture tension is 75 to 100 kPa. Actual values may be soil-specific and much greater or lower than this range.

It is believed that the model simulates phenomena in the freezing zone adequately for the present engineering purposes, and that it will meet the need of practicing pavement engineers to predict frost heave and some of the parameters influencing thaw weakening of pavement systems. The development of a model more closely linked to accepted concepts of soil physics awaits a more complete understanding and formulation of processes in the freezing zone, as well as justification of the additional computer time and expense required to solve a more complex formulation of the processes, and of the additional time, equipment, and expense for conducting laboratory tests to define additional soil parameters.

Output from the model includes cumulative frost heave at the surface, subsurface temperatures, and pore-water pressures. The predicted frost heave can be used directly to aid in selection of an appropriate pavement design by relating it to pavement roughness criteria. Temperatures are used to determine positions of freezing and thawing zones, and temperatures and pore-water pressures are used in empirical equations developed from laboratory tests to estimate resilient modulus values of layers within the pavement system at various times of the year.

SEASONAL VARIATION IN RESILIENT MODULUS OF GRANULAR SOILS

This phase of the research was directed to a principal underlying cause of premature distress in pavement systems containing soils that are susceptible to frost action, the reduction of the resilient modulus of subgrade soils and unbound base courses during and following spring thaws. In this context the resilient modulus is conventionally defined as deviator stress divided by resilient (i.e., recoverable) strain. The research was concerned with frost-susceptible granular soils exhibiting little or no cohesion and a high degree of nonlinear (i.e., stress dependent) mechanical behavior. The research objective was to develop laboratory methods of characterizing the seasonal changes of resilient modulus of such materials throughout a complete annual cycle. Field in situ tests were conducted to validate the laboratory methods.

Interim results have been given by Cole et al. *(25)* and Johnson et al. *(26)*. Detailed procedures, results, and analyses of repeated-load triaxial tests and of field in situ plate loading tests and the corresponding deflection basin analyses are given in a four-part report series *(4, 27–29)*. The approach developed for prediction and evaluation of resilient modulus has been presented by Cole et al. *(30)*.

Characterization by Laboratory Testing

The techniques developed here have allowed the simulation in the laboratory of the loss of stability upon thawing followed by the gradual recovery of stiffness experienced in the field after thawing as a frost-susceptible soil drains, consolidates, and desaturates.

The experimental approach called for performing repeated-load triaxial tests on all the asphalt-concrete and test soils from both test sites. Starting with samples in the frozen state, load cycles on the soils were applied by using two waveforms to simulate the loading pulses associated with the two field-testing devices used here: FWD and the RPB apparatus. At each level of confining and deviator stress used in the laboratory tests, 200 load cycles were applied, and a resilient modulus and resilient Poisson's ratio were calculated when a nominally steady-state response was achieved. Similar tests were performed on the same samples after thawing and at successive stages of recovery.

The key variable in the recovery process is soil moisture tension. As a soil drains after thawing, it first reconsolidates to a condition of zero pore-water pressure. Following this phase, gradual desaturation occurs, the moisture tension rises, and the material increases in stiffness. A system was developed that used removable triaxial cell bases equipped with tensiometers; this allowed the retesting of a given specimen several times at increasing levels of moisture tension, thus simulating the changes observed in the field work. Each specimen remained mounted on a given base throughout the testing sequence and excessive handling was thus avoided. The use of moisture tension as the primary means to describe the soil state has proven to be very effective because it strongly influences the resilient modulus and is relatively easily monitored in both the field and laboratory.

Standard statistical analysis techniques have been used in this work to generate empirical expressions for resilient modulus in terms of unfrozen water content for the frozen soil and in terms of moisture tension, applied stress, and in some cases dry density for thawed and recovering soil. In some cases, for nonfrozen material, the commonly used bulk stress model for stress dependency of a nonlinear material has been used, which is of the form

$$M_r = K_1 \theta_{K_2}$$

where K_1, K_2 are constants and θ is the bulk stress, that is, the sum of the principal stresses, also termed the first stress invariant J_1. A somewhat more complex stress function involving the second stress invariant and the octahedral shear stress has also been used:

$$M_r = K_1 (J_2/\tau_{oct})_{K_2}$$

where

K_1, K_2 = constants,
J_2 = second stress invariant = $\sigma_1\sigma_2 + \sigma_2\sigma_3 + \sigma_1\sigma_3$, and
τ_{oct} = octahedral shear stress.

This later function is unique in that it accounts for the effects on the modulus of both confining pressure and principal stress ratio in a manner appropriate for many granular materials. Figure 9 shows a plot of resilient modulus versus bulk stress for a Winchendon test soil (Hyannis sand). The bulk stress model does not account for the fact that, for certain types of soil, the

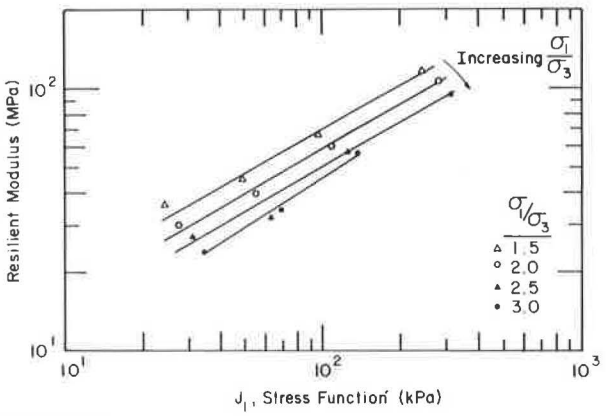

FIGURE 9 Resilient modulus of Hyannis sand versus J_1.

modulus decreases with increasing principal stress ratio. The stress function J_2/τ_{oct}, however, accounts for the influence of the stress ratio and thus linearizes the data more efficiently (Figure 10).

The laboratory testing sequence mentioned earlier generates data that allows the modeling of the post-thaw recovery process

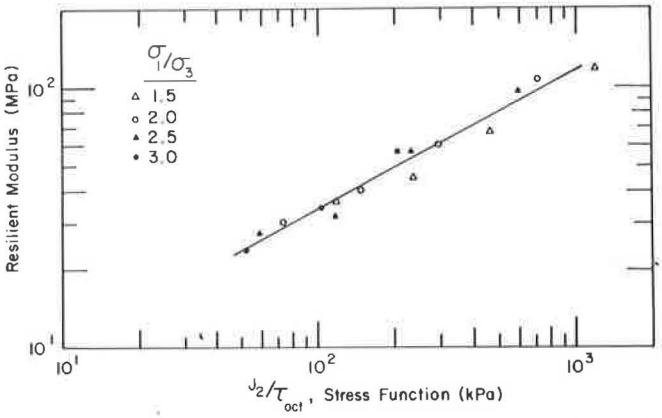

FIGURE 10 Resilient modulus versus J_2/τ_{oct} for the test data given in Figure 9.

with a single equation. The increasing stiffness associated with the recovery phase is predicted through the moisture tension term, which is a component of the coefficient K_1.

Six soils from the Winchendon test site and five from the Albany County Airport were tested in this manner and analyzed to characterize the moisture-tension-dependent nonlinear resilient modulus. For example, the results for a dense-graded crushed stone base at Albany County Airport yielded the following expression:

$$Mr \text{ (MPa)} = 1.10 \times 10^6 \, (101.36 - \psi)^{-2.40} (J_2/\tau_{oct})^{0.30}$$

where Mr is the resilient modulus and ψ is moisture tension in kilopascals.

Field Verification

For validation purposes, field tests were used to determine the surface deflection response of paved soil test sections under loads imposed by an RPB apparatus and an FWD. The tests were performed at critical times between late fall and late spring to characterize the variation in load response throughout the freeze-thaw-recovery cycle.

The validity of the laboratory results was then examined by comparing the measured deflection basins with deflection basins calculated for the test section by using the expressions for resilient modulus developed from the laboratory tests. In using these expressions, temperatures and moisture tensions measured at the time of each field loading test were applied to evaluate the resilient modulus.

Procedures for the in situ tests and for analysis of deflection basins have been given elsewhere *(25, 26)*. Measured deflections varied substantially through successive stages of the freeze-thaw cycle (Figure 11). Deflections were calculated for the same states by means of a nonlinear elastic-layer analysis for pavements (NELAPAV) (Irwin and Johnson, unpublished data). The calculated deflections generally agreed well with those measured by in situ testing (Figure 12).

The calculated resilient moduli and other results from the analysis of the test sections have been summarized elsewhere *(4, 28)*. The calculated resilient moduli of the test soils show the expected seasonal variation; extremely high values are found in the frozen condition, which decrease dramatically upon thawing and increase somewhat during the late spring, summer, and fall. An interpretation of the variation in modulus of the upper layer of each test soil is given in Figure 13 for the Winchendon test sections.

The agreement of the calculated deflections with the deflections measured under plate loading is strong evidence that the equations for nonlinear resilient modulus developed from laboratory triaxial tests represent valid characterizations of the materials in the layered pavement system. The procedures for the laboratory repeated-load triaxial tests, including testing at successive levels of moisture tension to track the recovery process in thaw-weakened soils, yield acceptable results, and such tests should provide a useful basis for structural evaluation and design of pavements affected by freezing and thawing.

This investigation has demonstrated a strong dependence of the resilient modulus on the seasonally varying environmental parameters of temperature and moisture tension. Evaluation of these environmental variables can be made by installing sensors at various depths below a paved surface and collecting data over a complete annual cycle. Alternatively, the frost heave model *(5)* can be used to predict both temperature and moisture tension as variables in time and space.

SIMULATING FROST HEAVE AND PAVEMENT DEFLECTION

Approach

In addition to its primary use for the calculation of frost heave, the mathematical model also serves the essential function of predicting the time-dependent dissipation of excess pore pres-

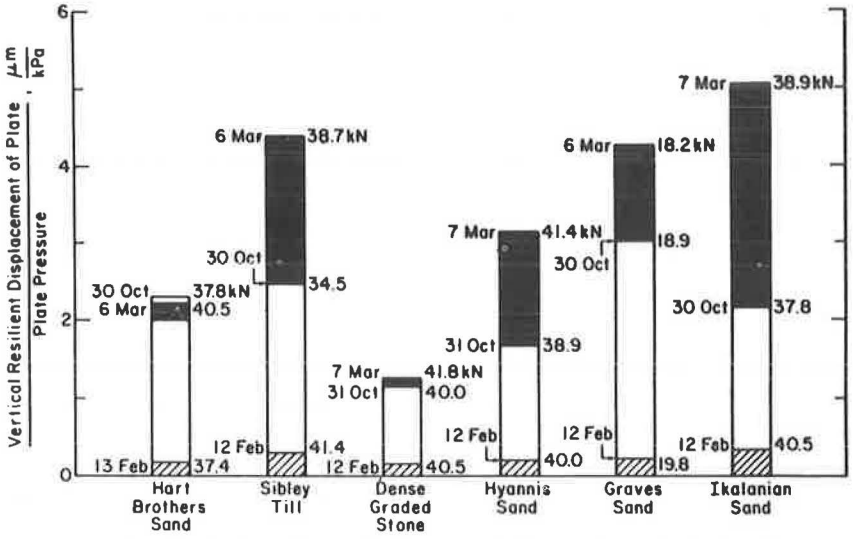

FIGURE 11 Vertical resilient displacement observed on six test sections before freezing, while frozen, and during thawing.

sure during thaw and buildup of moisture tension during recovery. To test these capabilities, the mathematical model for frost heave and thaw consolidation and the NELAPAV response model were used in concert with the results of laboratory resilient-modulus tests to simulate frost heave and pavement deflection in the field. Comparison with field observations provided the ultimate test of the modeling and laboratory testing procedures.

Calculations were made with the mathematical model to simulate the frost heave and thaw consolidation at the field test sites. The time-dependent temperature and pore pressures calculated for nodal points within the pavement profile were used to determine unique layers within the freezing or thawing system and to select equations characterizing the resilient modulus of each layer. The appropriate equations for resilient modulus were then input into the NELAPAV program along with temperatures and pore pressures (moisture tension), and the deformations and stresses at each point of interest were

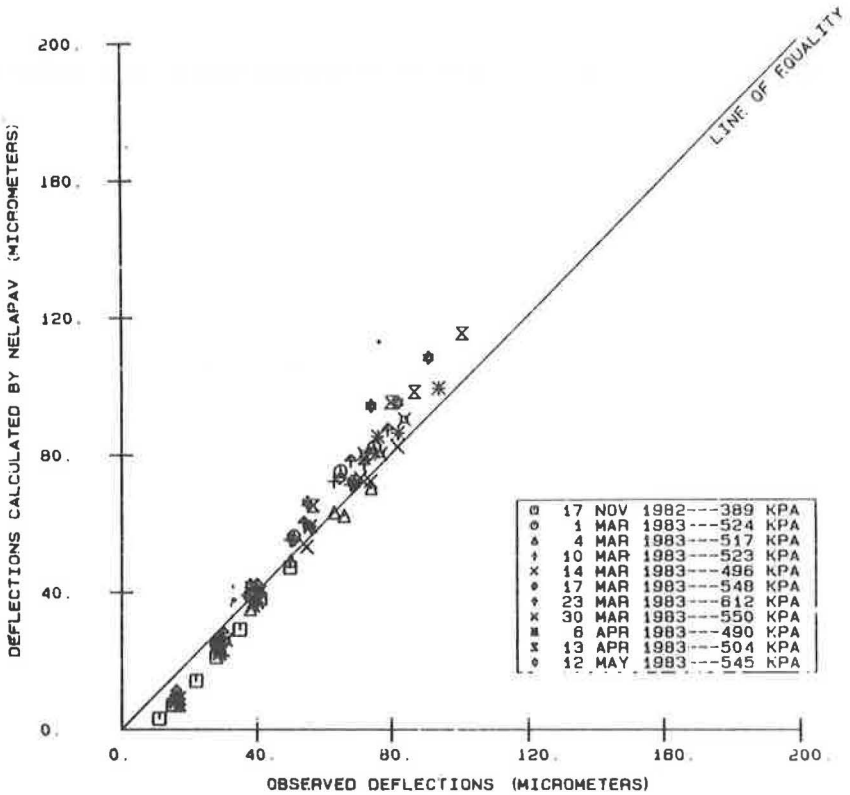

FIGURE 12 Measured surface deflections compared with deflections calculated by NELAPAV, Taxiway A, test point N2, 1982–1983.

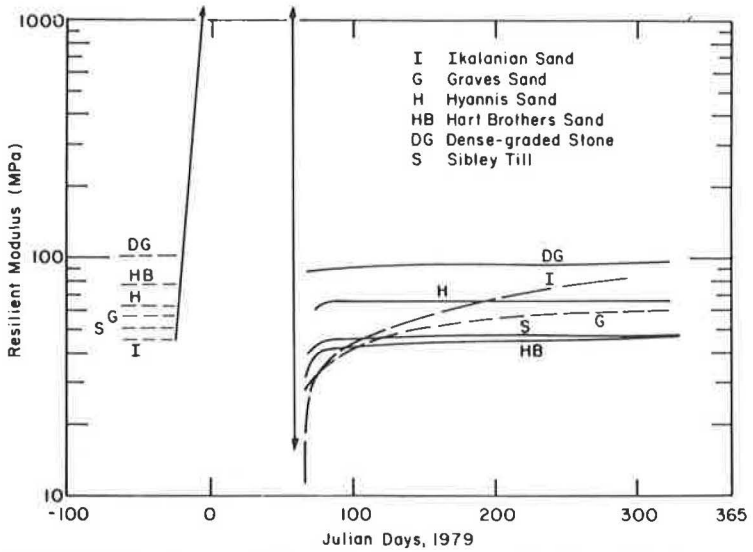

FIGURE 13 Interpretation of seasonal variation in resilient modulus of six test soils directly beneath asphalt pavement under 200 to 300 kPa plate pressure.

calculated. The test of the efficacy of the procedure required a comparison of the calculated seasonal variation of frost heave and pavement deflection under repeated loading with the observed values.

Results and Discussion

Figure 14 shows an example of the results for the Graves sand test section at the Winchendon test site. The calculated pavement deflections agree well with the measured values. The predictions made to date with this procedure demonstrate the efficacy of using the frost-heave–thaw-consolidation model and the NELAPAV response model to calculate seasonal frost heave and pavement deflection under load. The model thus provides an instrument for implementing much of the work performed under this multiphase research project.

IMPLEMENTATION OF RESEARCH FINDINGS

The investigations have produced results that can be advantageously implemented into current practice of design and evaluation of pavements in frost areas. The results of the examination of frost susceptibility index tests *(10)* have identified the Corps of Engineers frost design soil classification system and a new laboratory freeze-thaw test as two levels of testing that should be put into practice. The frost heave model can be implemented beneficially in any system for pavement design or evaluation. And finally, the laboratory repeated-load triaxial test on thawed and recovering soil can not only be implemented in mechanistic design and evaluation systems, but when used with either the frost-heave–thaw-consolidation model or with in situ measurements of moisture tension can be implemented in systems employing a cumulative damage approach.

The scope and extent of the implementation of each of the research findings and their potential impact on pavement design and evaluation depend on the type of system used for pavement analysis. The approach to implementation of each finding is shown in the form of flow charts (Figures 15 through 19).

Corps of Engineers Frost Design Soil Classification System

This frost susceptibility classification system *(9)*, based on simple classification type tests, leads to assignment of a corresponding frost group number to each soil. Its implementation (Figure 15) is limited to those pavement design and evaluation systems that are based on the frost group number.

New Laboratory Freeze-Thaw Test

This improved freezing test (Figure 16) also incorporates a CBR test on the thawed specimen. Outputs are heave rate from the freezing phase, and CBR in the thawed state; from these outputs, scales of susceptibility to frost heave and thaw weakening may be derived, as shown earlier. Frost heave susceptibility can be applied effectively to any mechanistic or empirical design and evaluation system as an indication of potential roughness. The classification of susceptibility to thaw weakening can be used as an indicator of spring loss of support for application under any empirical design and evaluation system. It is expected that the application of these indicators in developing a pavement design would be accomplished as appropriate adjustments to design thicknesses determined by other types of analyses.

Frost Heave Model

The frost heave model provides for the first time an ability to calculate with reasonable confidence the magnitude of the

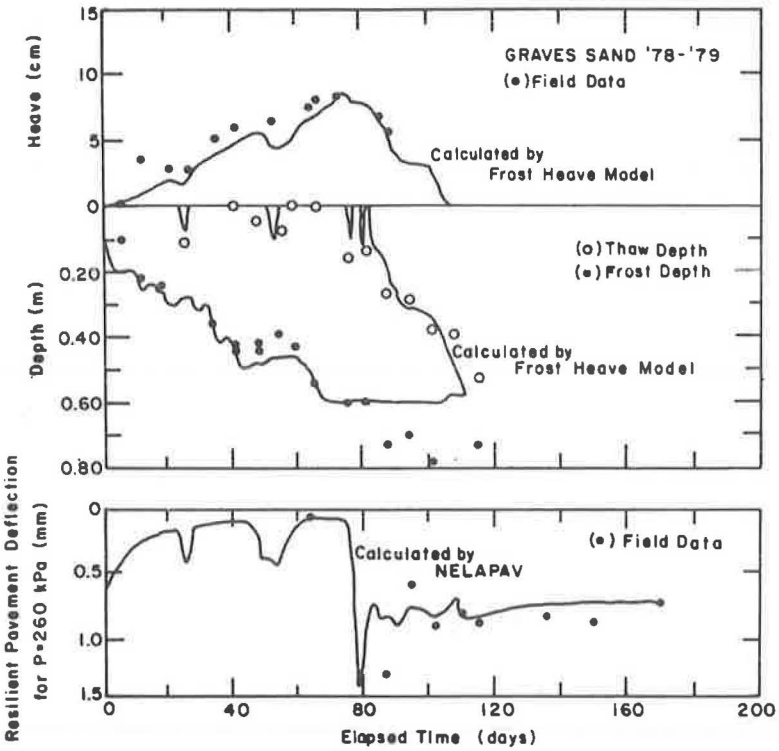

FIGURE 14 Comparison of simulated frost heave, frost and thaw depth, and pavement deflection with field observations.

heave that can be expected in a given pavement cross section under prescribed climatic, geotechnical, and hydraulic conditions. Because the outputs of depth of frost and magnitude of heave (Figure 17) are referenced to a particular point on the pavement where conditions are known, the model does not predict pavement roughness. Heave at a point can be used as an indicator of potential roughness, however, and can be implemented as an adjunct to any pavement design and evaluation system. For example, the calculated frost heave might serve as a basis for adjusting a trial design thickness if necessary to reduce the expected winter pavement roughness. The second principal output from the model, the predicted depth of frost beneath a pavement having a certain trial cross section, can be used as direct input for those design systems incorporating a dependence of the total thickness of the pavement section on the depth of frost. It can also be used as an adjunct to any design system.

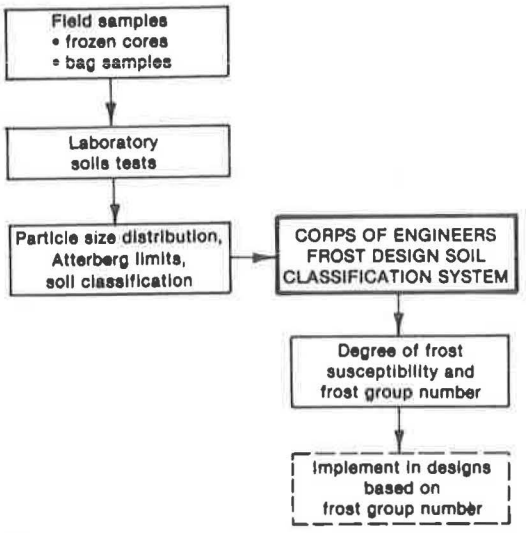

FIGURE 15 Implementation of Corps of Engineers frost design soil classification system.

Repeated-Load Triaxial Test on Frozen and Thawed Soil

The repeated-load triaxial test on frozen and thawed specimens provides a means of evaluating the resilient modulus of sub-

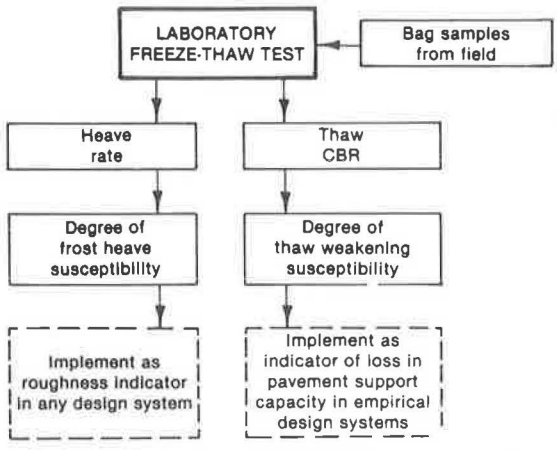

FIGURE 16 Implementation of new freeze test.

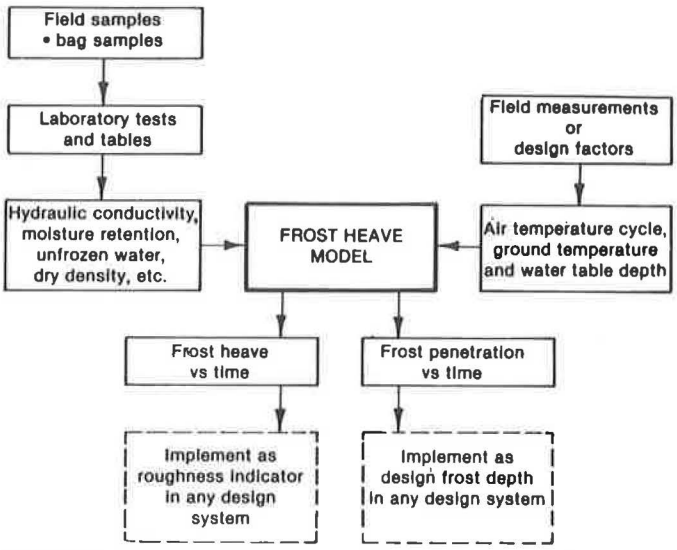

FIGURE 17 Implementation of frost heave model.

grade and base soils at various stages during the freeze-thaw-recovery cycle. The regression equations for soil in the thawed state (Figure 18) are of the greatest interest, because in many cases they represent the most critical condition showing the lowest resilient modulus and consequently the greatest potential for pavement distress. The expressions for resilient modulus can be implemented directly in any mechanistic design and evaluation system that employs a multilayered or finite-element simulation model formulated to analyze nonlinear materials.

Evaluation of Seasonal Variation of Resilient Modulus

It is unrealistic to base the design or evaluation of a pavement on only the lowest value of resilient modulus reached during the year (usually during thawing), and there is no reasonable basis for selecting any other single value to serve as an annual average representative of all the seasons. Rather, methods currently coming into greater use that include a cumulative damage approach offer the advantage of assessing in a more rigorous way the effect of the complete annual cycle of freezing, thawing, and recovery. Application of these methods requires that the resilient modulus be expressed as a function of time to make it possible to analyze the pavement performance by dividing the year into discrete intervals during which the modulus may be assumed to be constant. The evaluation of seasonal variation of the resilient modulus requires that the modulus be characterized in terms of the moisture tension and that the seasonal variation of the moisture tension be monitored or predicted. Figure 19 shows that repeated-load triaxial tests can be used to measure the resilient modulus as a function of temperature, soil stress, and moisture tension. The frost heave model and its associated thaw settlement model are used to predict the key parameters of temperature and moisture tension as variables in time and space. With this linkage, the resilient modulus at various depths is defined as a continuous function of time, facilitating the application of mechanistic analyses for pavement design and evaluation by using a cumulative damage approach.

ACKNOWLEDGMENTS

The research findings summarized here are the product of a large-scale effort that required the participation of several agencies and many persons. Particularly significant were the research contributions of Gary Guymon, University of California at Irvine, who played a key role in development of the frost heave model, and Lynne Irwin, Cornell University, who developed the pavement response model NELAPAV and made other contributions to the research on thaw weakening. The following were members of a panel of consultants who

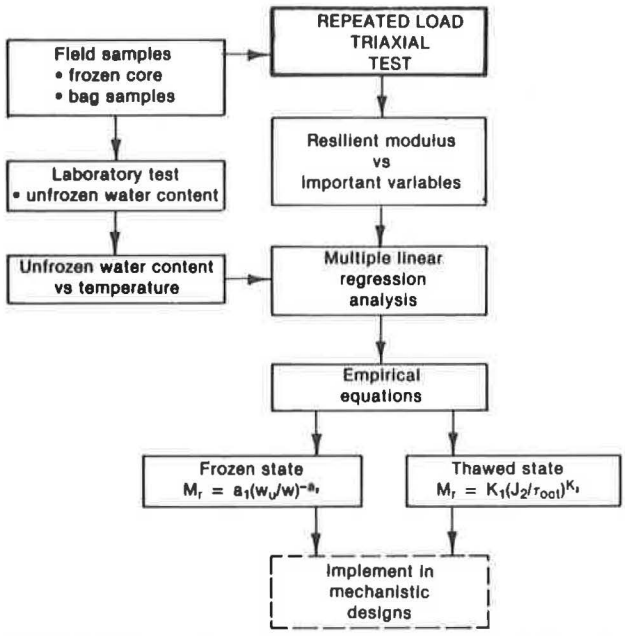

FIGURE 18 Implementation of repeated-load triaxial test for stress-strain-deflection analysis.

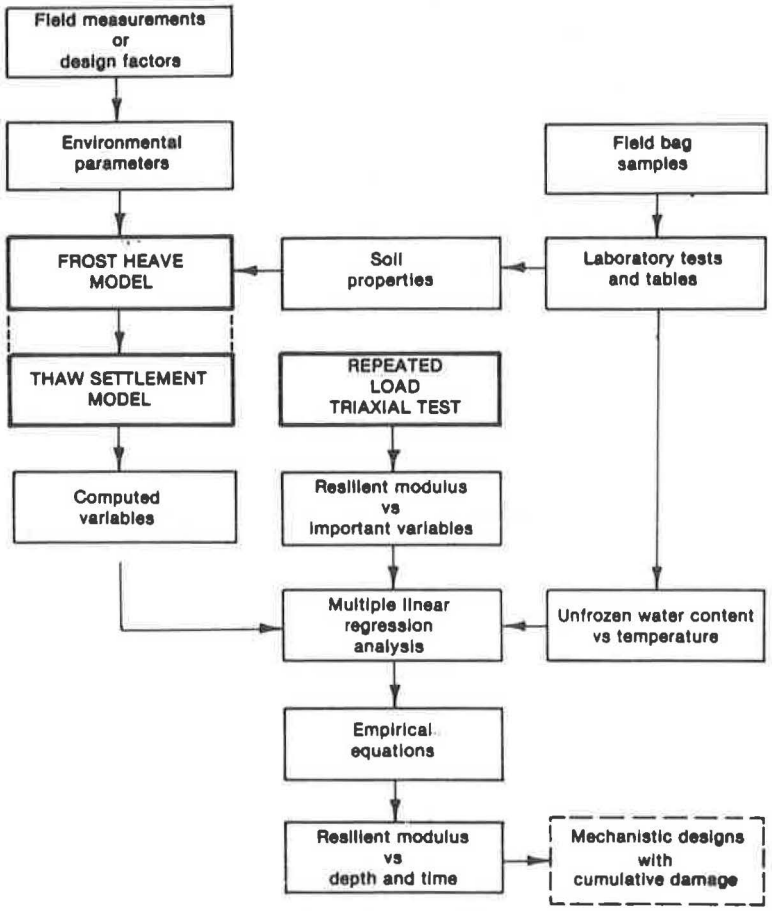

FIGURE 19 Implementation of seasonally varying resilient modulus for stress-strain-deflection analysis with cumulative damage approach.

provided guidance and periodic review of the work: B. J. Dempsey, University of Illinois (1978–1979); D. G. Fredlund, University of Saskatchewan; M. E. Harr, Purdue University; R. D. Miller, Cornell University (1981–1984); E. Penner, National Research Council of Canada; and M. W. Witczak, University of Maryland.

Many persons at CRREL participated in the research effort. Major contributions were made by E. Chamberlain and D. Cole, investigators who performed much of the research. Particularly noteworthy also are the technical contributions of D. Bentley, D. Carbee, G. Durell, J. Ingersoll, D. Keller, J. Mason, and R. Roberts.

The authors greatly appreciate the permission of the Massachusetts Department of Public Works and the Albany County Airport to use paved facilities under their jurisdiction as the test sites. Dennis Rice, then of the MDPW, and Jack Masko, Airport Manager, were especially helpful.

And finally, the project received strong support from the sponsors throughout this work. In addition to unfailing support from FHWA, the authors acknowledge the consistently helpful support received from H. Tomita and others of FAA and from A. Muller, representing the Corps of Engineers, who actively supported the research and its sponsorship by the Corps from its inception.

REFERENCES

1. T. C. Johnson, R. L. Berg, K. L. Carey, and C. W. Kaplar. *Roadway Design in Seasonal Frost Areas.* CRREL Technical Report 259. USACRREL, Hanover, N.H., 1975.
2. *NCHRP Synthesis of Highway Practice 26: Roadway Design in Seasonal Frost Areas.* TRB, National Research Council, Washington, D.C., 1974.
3. A. F. DiMillio and D. G. Fohs. The Frost Action Problem—An Overview of Research to Provide Solutions. *Public Roads,* Vol. 43, No. 4, March 1980.
4. T. C. Johnson, D. Bentley, and D. M. Cole. *Resilient Modulus of Freeze/Thaw-Affected Granular Soils for Pavement Design and Evaluation, Part II: Field Validation Tests at Winchendon Test Sections.* CRREL Report. USACRREL, Hanover, N.H., in preparation.
5. G. L. Guymon, R. L. Berg, T. C. Johnson, and T. V. Hromadka II. *Mathematical Model of Frost Heave in Pavements.* CRREL Report. USACRREL, Hanover, N.H., in preparation.
6. E. J. Chamberlain. *Frost Susceptibility of Soil—Review of Index Tests.* CRREL Monograph 81-2. USACRREL, Hanover, N.H., 1981, 121 pp.
7. E. J. Chamberlain. "Comparative Evaluation of Frost Susceptibility Tests." In *Transportation Research Record 809,* TRB, National Research Council, Washington, D.C., 1981, pp. 42–52.
8. E. J. Chamberlain, P. N. Gaskin, D. Esch, and R. L. Berg. "Survey of Methods for Classifying Frost Susceptibility." In *Frost Action and Its Control,* Technical Council on Cold Regions Engi-

neering Monograph, American Society of Civil Engineers, New York, 1984.
9. R. L. Berg and T. C. Johnson. *Revised Procedure for Pavement Design Under Seasonal Frost Conditions.* CRREL Special Report 83-27. USACRREL, Hanover, N.H., 1983, 129 pp.
10. E. J. Chamberlain. *Evaluation of Selected Frost Susceptibility Test Methods.* CRREL Report. USACRREL, Hanover, N.H., in preparation.
11. E. J. Chamberlain. *A Freeze-Thaw Test to Determine the Frost Susceptibility of Soils.* CRREL Special Report. USACRREL, Hanover, N.H., in preparation.
12. R. L. Berg, J. Ingersoll, and G. L. Guymon. Frost Heave in an Instrumented Soil Column. *Cold Regions Science and Technology,* Vol. 3, Nos. 2 and 3, 1980, pp. 211–221.
13. J. Ingersoll and R. L. Berg. "Simulating Frost Action by Using an Instrumented Soil Column." In *Transportation Research Record 809,* TRB, National Research Council, Washington, D.C., 1981, pp. 34–42.
14. A. R. Greatorex, W. N. Tobiasson, and R. L. Berg. *Design, Fabrication and Operation of a Dual Gamma System.* CRREL Report. USACRREL, Hanover, N.H., in preparation.
15. T. C. Johnson, R. L. Berg, E. J. Chamberlain, and D. M. Cole. *Frost Action Predictive Techniques for Roads and Airfields—A Comprehensive Survey of Research Findings.* CRREL Report. USACRREL, Hanover, N.H., in preparation.
16. R. L. Berg, G. L. Guymon, and T. C. Johnson. *Mathematical model to Correlate Frost Heave of Pavements with Laboratory Predictions.* CRREL Report 80-10. USACRREL, Hanover, N.H., 1980.
17. G. L. Guymon, T. V. Hromadka II, and R. L. Berg. A One-Dimensional Frost Heave Model Based upon Simulation of Simultaneous Heat and Water Flux. *Cold Regions Science and Technology,* Vol. 3, Nos. 2 and 3, 1980, pp. 253–263.
18. G. L. Guymon, R. L. Berg, T. C. Johnson, and T. V. Hromadka II. "Results from a Mathematical Model of Frost Heave." In *Transportation Research Record 809,* TRB, National Research Council, Washington, D.C., 1981, pp. 2–6.
19. G. L. Guymon, M. E. Harr, R. L. Berg, and T. V. Hromadka II. Probabilistic-Deterministic Analysis of One-Dimensional Ice Segregation in a Freezing Soil Column. *Cold Regions Science and Technology,* Vol. 5, 1981, pp. 127–140.
20. T. V. Hromadka II, G. L. Guymon, and R. L. Berg. Some Approaches to Modeling Phase Change in Freezing Soils. *Cold Regions Science and Technology,* Vol. 4, 1981, pp. 137–145.
21. T. V. Hromadka II, G. L. Guymon, and R. L. Berg. Sensitivity of a Frost Heave Model to Numerical Method. *Cold Regions Science and Technology,* Vol. 6, 1982, pp. 1–10.
22. G. L. Guymon, R. L. Berg, and E. J. Chamberlain. "A Predictive Model of Frost Heave and Thaw Weakening." Presented at 65th Annual Meeting of the Transportation Research Board, Washington, D.C., 1985.
23. N. R. Morgenstern and J. F. Nixon. One-Dimensional Consolidation of Thawing Soils. *Canadian Geotechnical Journal,* Vol. 8, 1971, pp. 558–565.
24. W. R. Gardner. Some Steady-State Solutions of the Unsaturated Moisture Flow Equation with Application to Evaporation from a Water Table. *Soil Science,* Vol. 85, 1958, pp. 223–232.
25. D. M. Cole, L. H. Irwin, and T. C. Johnson. "Effect of Freezing and Thawing on Resilient Modulus of a Granular Soil Exhibiting Nonlinear Behavior." In *Transportation Research Record 809,* TRB, National Research Council, Washington, D.C., 1981, pp. 19–26.
26. T. C. Johnson, D. M. Cole, and L. H. Irwin. "Characterization of Freeze/Thaw-Affected Granular Soils for Pavement Evaluation." *Proc., 5th International Conference on Structural Design of Asphalt Pavements,* Vol. 1, University of Michigan, Ann Arbor, 1982, pp. 805–817.
27. D. M. Cole, D. Bentley, G. Durell, and T. C. Johnson. *Resilient Modulus of Freeze/Thaw-Affected Granular Soils for Pavement Design and Evaluation, Part I: Laboratory Tests, Soils from Winchendon Test Sections.* CRREL Report. USACRREL, Hanover, N.H., in press.
28. D. M. Cole, D. Bentley, G. Durell, and T. C. Johnson. *Resilient Modulus of Freeze/Thaw-Affected Granular Soils for Pavement Design and Evaluation, Part III: Laboratory Tests, Soils from Albany County Airport.* CRREL Report. USACRREL, Hanover, N.H., in preparation.
29. T. C. Johnson, A. Crowe, M. Erickson, and D. M. Cole. *Resilient Modulus of Freeze/Thaw-Affected Granular Soils for Pavement Design and Evaluation, Part IV: Field Valuation Tests at Albany County Airport.* CRREL Report. USACRREL, Hanover, N.H., in preparation.
30. D. M. Cole, E. J. Chamberlain, and T. C. Johnson. "Prediction of Resilient Modulus During Thawing and Recovery." Presented at 65th Annual Meeting of the Transportation Research Board, Washington, D.C., 1985.

Publication of this paper sponsored by Committee on Flexible Pavements.